U. S. DEPARTMENT OF COMMERCE
Charles Sawyer, Secretary
NATIONAL BUREAU OF STANDARDS
E. U. Condon, Director

MAY 1950
VOLUME • 44
NUMBER 5

JOURNAL OF RESEARCH

of the

NATIONAL BUREAU OF STANDARDS

Contents

RP		Page
2091	Lamps and wavelengths of mercury 198. William F. Meggers and F. Oliver Westfall. (Price 10 cents)	447
2092	Heat of fluorination of cobaltous fluoride, and the heats of reaction of cobaltic fluoride with hydrogen and with bis(trifluoromethyl)benzene ($\alpha,\alpha,\alpha,\alpha',\alpha',\alpha'$,-hexafluoroxylene). Ralph S. Jessup, F. G. Brickwedde, and Martin T. Wechsler. (Price 10 cents)	457
2093	Permanence of glass standards of spectral transmittance. Kasson S. Gibson and Marion A. Belknap. (Price 10 cents)	463
2094	A 600-ohm multiple-wire delta antenna for ionosphere studies. H. N. Cones, H. V. Cottony, and J. M. Watts. (Price 10 cents)	475
2095	Mass spectra of diborane-d_6 and ethane-d_6. Vernon H. Dibeler, Fred L. Mohler, and Laura Williamson. (Price 10 cents)	489
2096	An improved apparatus for the determination of liquidus temperatures and rates of crystal growth in glasses. Oscar H. Grauer and Edgar H. Hamilton. (Price 10 cents)	495
2097	Infrared spectra of bromochloromethane, dibromomethane, tribromochloromethane, and tetrabromomethane. Earle K. Plyler, W. Harold Smith, and N. Acquista. (Price 10 cents)	503
2098	Mass spectrometric analysis of a standard sample of carburetted water-gas by laboratories cooperating with the American Society for Testing Materials. Martin Shepherd. (Price 10 cents)	509
2099	Infrared absorption spectra of hexafluoroethane and of chloropentafluoroethane. José R. Barceló. (Price 10 cents)	521
2100	Development of very-high-frequency field-intensity standards. Frank M. Greene and Max Solow. (Price 15 cents)	527
2101	Note on the Runge-Kutta method. W. E. Milne. (Price 5 cents)	549
2102	A sampling method for determining the lowest eigenvalue and the principal eigenfunction of Schrödinger's equation. M. D. Donsker and M. Kac. (Price 10 cents)	551

U. S. Department of Commerce
National Bureau of Standards

Research Paper RP2091
Volume 44, May 1950

Part of the Journal of Research of the National Bureau of Standards

Lamps and Wavelengths of Mercury 198

By William F. Meggers and F. Oliver Westfall

The production and extraction of artificial $^{198}_{80}$Hg from $^{197}_{79}$Au bombarded by neutrons is described, and the procedure in making electrodeless lamps with $^{198}_{80}$Hg is given in detail. These lamps are excited by high-frequency radio waves; they emit the mercury spectrum entirely free from isotope shifts and hyperfine structures that characterize natural mercury. Fabry-Perot interferometers and a prism spectrograph were employed for measuring, relative to Cd 6438.4696 angstroms, the wavelengths of the stronger lines in the visible spectrum of $^{198}_{80}$Hg. Preliminary values for $^{198}_{80}$Hg radiations in normal air are reported as 5790.6627, 5769.5984, 5460.7532, 4358.3377, 4077.8383, and 4046.5717 angstroms, with probable errors not exceeding ±0.0001 angstrom.

I. Introduction

In a paper entitled "On the feasibility of establishing a light wave as the ultimate standard of length", Michelson and Morley [1][1] in 1889 described the method later employed in measuring the meter and reported the first interferometer values of wavelengths for one sodium line, one lithium line, and three mercury lines. They also stated that "the brilliant *green* (mercury) line gives beautifully clear circles even with a difference of path of half a million waves, so that in all probability *this will be the wave to be used as the ultimate standard of length*". However, in 1892 Michelson [2] discovered that many spectral lines are complex and that "the green mercury line is one of the most complex yet examined". This observation disqualified radiations from natural mercury as precision standards for more than half a century, during which time the causes and cures of spectral line complexities were sought and found. The mass spectrometer disclosed [3] that natural mercury is a mixture of seven isotopes with mass numbers 196, 198, 199, 200, 201, 202, 204, and the interferometer resolved the components of complex lines so that they could be quantitatively explained [4] as resulting in part from isotope shifts and in part from hyperfine structure due to nuclear spins of ½ and ⅝ units for isotopes 199 and 201, respectively. It was obvious in 1931 that single sharp lines could be obtained from any even-mass isotope of mercury if such an isotope could be produced in sufficient quantity and purity for spectroscopic light sources. The latter requirements ruled out, at least temporarily, any physical methods of separating the isotopes of natural mercury. Fortunately another solution was found in transmutation.

Although nuclear reactions with certain elementary particles were known to transmute some elements into others, such experiments yielded only infinitesimal amounts that could not be seen or weighed. Thus, in 1934 Fermi, et al. [5] used a mixture of beryllium powder and radon as a neutron source to transmute gold into mercury, but it was wholly impracticable to make tangible amounts of mercury this way. In 1940 Alvarez boldly suggested that neutrons obtained from cyclotron operations might transmute sufficient gold into mercury to be detected spectroscopically. This experiment was successful and demonstrated that the green line of artificial mercury was devoid of complex structure [6, 7]. Attempts to produce ponderable amounts of $^{198}_{80}$Hg, required for many durable lamps, were frustrated until a more powerful source of neutrons became available. The chain-reacting uranium piles proved ideal for this purpose, and with the cooperation of the United States Atomic Energy Commission, sufficient artificial $^{198}_{80}$Hg has been made since 1945 to provide

[1] Figures in brackets indicate the literature references at the end of this paper.

several hundred satisfactory spectroscopic light sources. Now that the isotopic curse has been lifted from mercury and $^{198}_{80}$Hg has become available in abundance, there are good reasons for believing "that in all probability the brilliant *green* (mercury) line will be the wave to be used as the ultimate standard of length" [1, 8, 9, 10]. It is the purpose of this paper to describe the preparation and operation of $^{198}_{80}$Hg lamps and to report some preliminary results of measurements on wavelengths emitted by these lamps.

II. Production and Extraction of Artificial $^{198}_{80}$Hg

Gold of high purity (999.9 fine) in the form of foil or chips was first placed in a fused quartz well attached by means of a graded seal to Pyrex tubing leading to a vacuum pump through a trap immersed in liquid air. The enclosed gold was surrounded by an electrically heated furnace, maintained at 800° C for about 20 hr to remove possible contamination by natural mercury. No mercury contamination could be detected in gold foil purchased from the New York Assay Office.

This mercury-free gold was then submitted to the U. S. Atomic Energy Commission for irradiation with neutrons in a chain-reacting pile. The production of artificial $^{198}_{80}$Hg from $^{197}_{79}$Au occurs when neutrons that attach themselves to nuclei of gold atoms produce a highly radioactive isotope of $^{198}_{79}$Au, which decays (half-life 2.7 days) by β emission to become stable $^{198}_{80}$Hg; symbolically:

$$^{197}_{79}\mathrm{Au}^{0} + 1n^{0} \rightarrow {}^{198}_{79}\mathrm{Au}^{0} \rightarrow {}^{198}_{80}\mathrm{Hg}^{0} + \beta^{-1}.$$

After a period for neutron bombardment and another for radioactive decay, the gold was returned to our laboratory, where it was treated for the removal of artificial $^{198}_{80}$Hg in the same manner as formerly for extraction of natural Hg contamination. Mercury that distilled from the heated gold first condensed in tiny droplets on cooler glass walls above the furnace from whence it was driven to the liquid-air trap by flaming with a gas-air torch. To be certain that all the artificial mercury had been extracted, this procedure was continued several hours after the last visible traces of condensation could be detected above the furnace.

The yield and purity of $^{198}_{80}$Hg are both under control; the former depends on the quantity of gold and the time of exposure to a given neutron-flux density, the latter is inversely proportional to the flux density. Mass-spectrometer analyses [11] of artificial $^{198}_{80}$Hg invariably show some contamination by $^{199}_{80}$Hg, suggesting that a fraction of the $^{198}_{79}$Au atoms, before decaying to $^{198}_{80}$Hg, accrete another neutron to become $^{199}_{79}$Au, which then decays to $^{199}_{80}$Hg. Kessler [12] has demonstrated that such $^{199}_{80}$Hg contamination in impure $^{198}_{80}$Hg can be determined from the intensity of a forbidden line. A purity of 99.6 percent, or greater, can be guaranteed by choosing a low neutron-flux density, as lower yield can be compensated either by more gold or by longer exposure.

For many years it seemed hopeless to effect a large-scale production of pure isotopes by electromagnetic separation, but this outlook was changed in 1945 when the colossal calutrons constructed for separating uranium isotopes were applied to the enrichment of stable isotopes. Keim [13] reported recently that $^{202}_{80}$Hg has thus been enriched from 11 to 98 percent, $^{204}_{80}$Hg from 7 to >92 percent! Whether or not these electromagnetically separated natural isotopes will be produced in sufficient quantity and purity to compete with artificial $^{198}_{80}$Hg remains to be seen. The production and extraction of high-purity $^{198}_{80}$Hg from pure $^{197}_{79}$Au is such a simple and sure procedure that it can hardly be surpassed.

III. Manufacture of $^{198}_{80}$Hg Lamps

The first $^{198}_{80}$Hg lamp made at this Bureau in 1946 was an electrodeless Pyrex-glass tube (5-mm bore, 10-cm length) containing an invisible quantity of $^{198}_{80}$Hg and some argon gas; it was excited with a 100-Mc oscillator constructed by Wiens [7], and it emitted intense structureless lines of the mercury spectrum for about 50 hr before failing on account of clean-up [9]. Attempts to rejuvenate this lamp by heating were frustrated by the liberation of adsorbed gases whose spectra suppressed that of mercury. This experience suggested the use of fused quartz or Vycor glass (96% silica), which withstand higher temperatures than Pyrex and are therefore more easily out-gassed before $^{198}_{80}$Hg is inserted.

In 1947 about 60 mg of $^{198}_{80}$Hg of 99.9 percent purity [11] were obtained from neutron-irradiated gold, and four experimental lamps were made

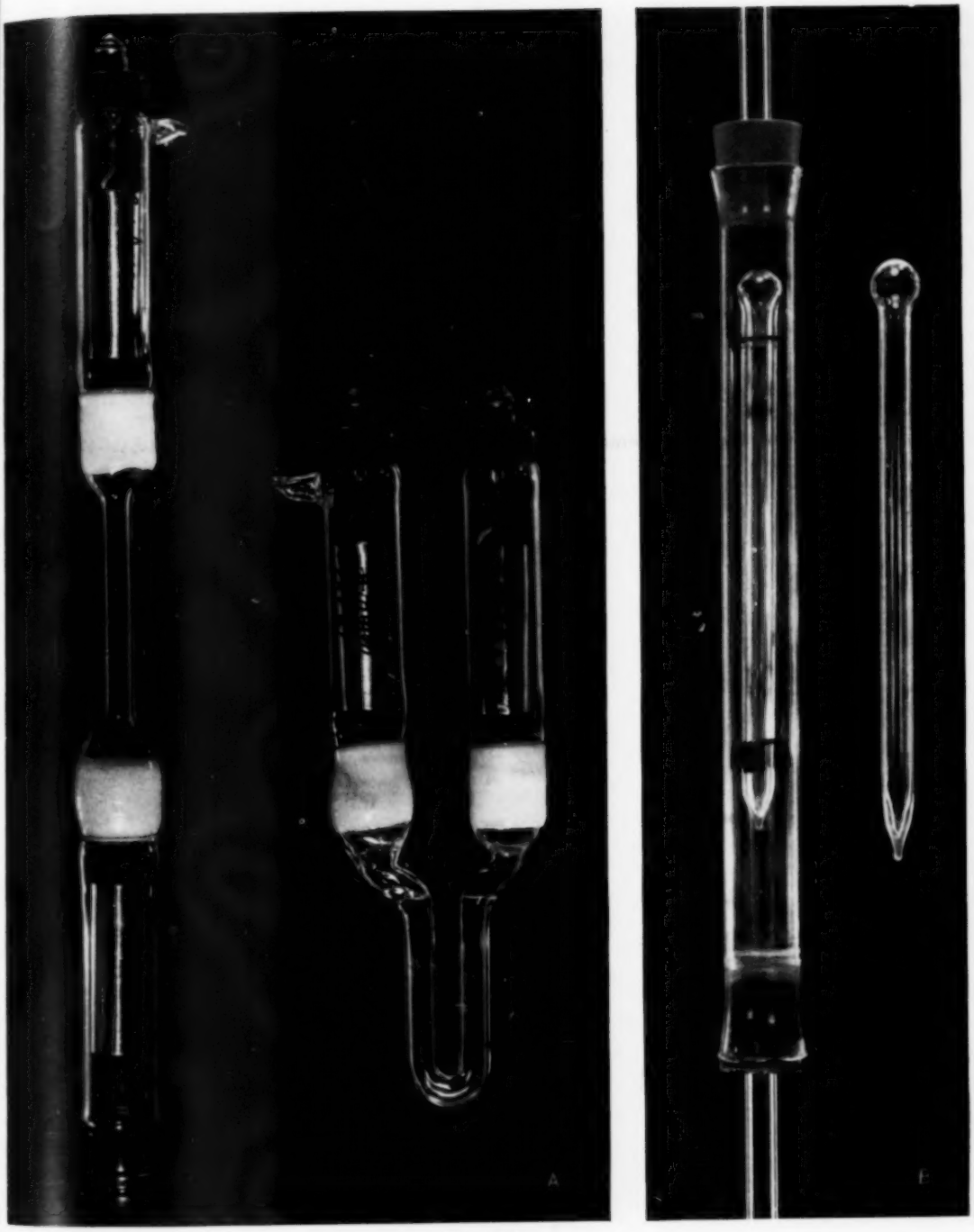

FIGURE 1.

A, Geissler-type lamps containing $^{198}_{80}Hg$. Straight lamp is 25 cm long. B, Electrodeless lamps containing $^{198}_{80}Hg$, one in water jacket. Length of lamp about 12 cm.

with 5 mg of $^{198}_{80}$Hg and 5-mm (Hg) pressure of pure argon in each. Two of these lamps were Geissler type of Vycor glass with internal electrodes of molybdenum, figure 1, A, and two were electrodeless type, one of Vycor and one of fused quartz, figure 1, B. We are indebted to N. C. Beese of the Research Division, Westinghouse Lamp Division, Bloomfield, N. J., for making the Geissler lamps and fused-quartz lamp, and for advice on their proper preparation.

The first experiments designed to measure wavelengths emitted by these lamps soon led to the abandonment of the Geissler-type on account of lower intensity and inferior sharpness of lines when compared with electrodeless lamps. The latter are the last word in simplicity and serviceability; they simplify manufacture by eliminating sealed-in wires, graded seals, and internal electrodes, thus facilitating exhausting and outgassing. In service they avoid high voltage, sparking, sputtering, and all other defects of Geissler tubes. Because these electrodeless lamps have been found to be highly satisfactory, their preparation will be described in some detail.

The essentials for making $^{198}_{80}$Hg lamps are, in addition to $^{198}_{80}$Hg, clean glass tubing, vacuum pumps, a bottle of pure argon gas, a low-range gas pressure indicator, and a gas-oxygen hand torch. Either clear fused quartz or Vycor glass is recommended because of high melting point and transparency to ultraviolet. Unless the extreme ultraviolet is desired, fused quartz should be avoided because its high transparency to Hg 1849 A radiation permits the formation of obnoxious ozone in the laboratory. Vycor is preferred because it transmits practically all Hg radiations except that forming ozone. The glass is first cleaned with hot chromic acid and rinsed with distilled water.

To eliminate the hazard of contamination with natural mercury, the use of mercury pumps and manometers should be avoided. Evacuation was effected with an oil forepump and oil-condensation pump; and for measuring the pressure of argon gas, either a calibrated dark space in an attached Geissler tube or a mechanical pressure gage was employed.

The procedure in making an electrodeless Hg lamp may be outlined with the aid of figure 2. Sections *A* and *B* are cleaned Vycor glass (5-mm bore). Section *A* is the lamp blank with constriction, *a*, and sealed upper end blown bulbous

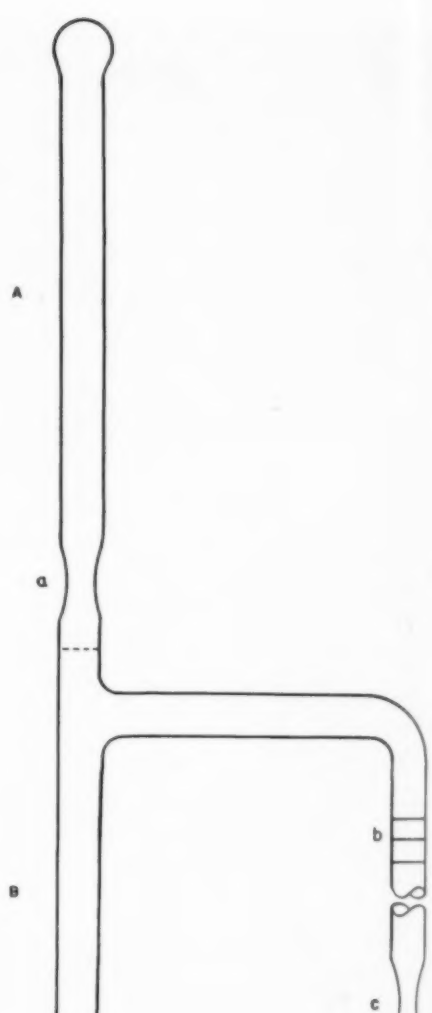

FIGURE 2. *Manufacture of electrodeless mercury lamp.*
A=lamp blank. *B*=mercury well.

so that the lamp may be viewed end-on if desired. Section *B* is the mercury well with a side tube provided with a Vycor-Pyrex joint, *b*, and constriction, *c*. A broken thermometer tube modified on the principle of the medicine dropper serves for withdrawing from the supply a measured amount of $^{198}_{80}$Hg and depositing it as a droplet, *d*, at the bottom of section *B*. This section is then

sealed to the pump (and argon flask), and section A is sealed onto section B. In making these seals, and in subsequent heating for out-gassing, accidental overheating of the droplet, d, and consequent loss of $^{198}_{80}$Hg, is avoided by wrapping the lower half of section B with wet asbestos paper. During evacuation section A and the uncovered portion of section B are heated with a gas-oxygen torch until a nonconducting vacuum has been attained. After a measured pressure of pure argon gas has been admitted, the assembly AB is sealed off at constriction, c, and inverted to roll or tap the droplet of mercury into the bulbous end of section A. Finally, section A is sealed off at constriction, a, thus completing an electrodeless lamp containing pure mercury and argon gas. The presence of argon gas retards the clean-up of mercury, increases the intensity of the mercury spectrum, and facilitates operation of the lamp when immersed in cold, circulating water.

IV. Mercury Clean-Up in Electrodeless Lamps

Experience with these lamps since 1947, and the limited supply of $^{198}_{80}$Hg, persuaded us to reduce the mercury content of future lamps to 3 mg or less. It was recognized in 1946 that gradual clean-up of mercury would limit the life of a lamp, but it was not known then that such clean-up could be retarded or corrected. Experiments were conceived and conducted to determine the minimum mercury required for a long-lived lamp. Several lamps, each containing 1 mg of natural mercury and 5 mm (Hg) pressure of argon, were prepared and life-tested at equal brightness on three different high-frequency exciter units emitting 30, 60, and 90 Mc, respectively. These units were constructed by Albert Weiss of this Bureau. We were surprised to find that, with 30 Mc, 1 mg of Hg was cleaned up in about 10 hr, with 60 Mc in 55 hr, and with 90 Mc in 2,630 hr. This experience prompted us to experiment with still higher frequencies. A lamp excited with 370 Mc for several months exhibited no trace of darkening or clean-up despite operation at a higher level of brightness. Jacobsen and Harrison [14] have recently reported high intensity and undetectable clean-up when a $^{198}_{80}$Hg lamp was excited with 3,000 Mc generated by a magnetron.

The clean-up is manifested by gradual darkening of the glass near the terminals of the high-frequency exciter until black bands are formed on the inner wall of the lamp. If the lamp is held in spring clips no darkening occurs under the clips, but only outside their boundaries. Identical effects have been observed with Pyrex, Vycor, and fused silica; blackening continues until all the enclosed mercury has penetrated the glass, whereupon the mercury spectrum vanishes and pure argon remains. Preliminary experiments with various pressures of argon indicate a marked dependence of Hg clean-up upon gas pressure. Two lamps, each containing 1 mg of Hg, were filled with 5 and 15 mm of argon, respectively, and operated at constant intensity with 30 Mc until the Hg spectrum vanished; the first lamp glowed for 45 hr and the second for 365 hr. These experiments, indicating that the rate of Hg clean-up in ultrahigh-frequency discharges decreases with frequency and with gas pressure, are being continued; they will be reported in more detail later. The mechanism of Hg clean-up is imperfectly understood, but the following facts are fixed. Hg clean-up in electrodeless discharge tubes is extremely slow if the oscillatory excitation frequency exceeds 100 Mc and if the foreign gas pressure exceeds 5 mm (Hg). In any case the clean-up is localized near the edges of the high-frequency terminals, resulting in black bands inside the lamp. This leads finally to extinction of the mercury light. In that event it is only necessary to heat the blackened portions of the lamp in a gas-oxygen flame until they glow a dull red. This treatment removes the blackening, recovers visible droplets of mercury, restores the Hg spectrum, and rejuvenates the lamp without detriment to the Vycor glass. In tests of Hg clean-up the same lamp has been resurrected several times, thus indicating that even if the clean-up cannot be entirely eliminated, successive rejuvenations guarantee practically infinite life.

V. Wavelengths Radiated by $^{198}_{80}$Hg

Superior spectroscopic light sources are of no value for length measurements until the lengths of several radiated light waves have been measured. Such measurements have been made by comparing the light waves characteristic of $^{198}_{80}$Hg with the primary standard of wavelength, 6438.4696 A, provisionally adopted [10] as the

metric value of the red radiation from Michelson's type of cadmium lamp. For this purpose we employed the method first demonstrated by Buisson and Fabry [15] and used for the past 40 years in making the most precise determinations of relative wavelengths. This method, as is well known, is based on the principle that wavelengths of monochromatic radiations are inversely proportional to the corresponding orders of interference determined from linear measurements of circular fringes produced by the Fabry-Perot interferometer. The only improvements upon the method as originally described consist of simultaneous illumination of the optical system by both light sources, and application of least squares in the reduction of measurements.

In our experiments the mercury lamp was imaged inside the cadmium lamp, and both sources were then focused upon the slit of a prism spectrograph. Both sources and lenses were initially placed on the optical axis of the spectrograph by bisecting the beam emerging from the slit when a bright light was placed at the spectrograph focus. Then the interferometer and the achromatic ring-projection lens were inserted in the beam and adjusted so that the interference fringes were accurately centered and focused on the spectrograph slit. Simultaneous observation of both sources avoids all errors resulting from slight changes in air density or optical adjustments between successive exposures to separate sources. The Michelson-type cadmium lamp was enclosed in a furnace maintained at 300 to 320° C., and the capillary was viewed end-on. The electrodeless mercury lamp was maintained at a temperature between 10° and 20° C, and was always viewed side-on.

The Fabry-Perot interferometer consisted of adjustable etalons holding a pair of crystal quartz plates separated by three invar pins. The plates were coated with evaporated aluminum having reflectance of 80 percent at 6000 A. Invar separators of 3, 5, 25, 40, 50, 67, 90, or 105 mm were employed. In order to maintain an approximately constant scale of interference fringes, achromatic lenses of different focal lengths were used with different plate spacers; 25 cm with 3 or 5 mm, 50 cm with 25, 40, or 50 mm, 75 cm with 67 or 90 mm, and 100 cm with 90 or 105 mm.

The observations reported in this paper were all made photographically with the aid of a Hilger medium spectrograph with glass prism. Four spectrograms were recorded on each 4 by 10 in. plate, but no two plates were made with identical interferometer adjustment—the orders of interference were changed slightly from plate to plate so that different configurations of fringes resulted. Beginning with low orders, associated with 3-mm separation of plates, the wavelengths published for natural mercury were accurate enough to give the correct integral orders of interference for the first approximation to wavelengths characteristic of $^{198}_{80}$Hg. These approximate values were then successively refined by observing with larger and larger orders.

In general, for any given wavelength the corresponding order of interference at the center of a Fabry-Perot pattern consists of an integer and a fraction. Because the squared values of the ring diameters are a linear function of the ring number, the fractional order is simply obtained by dividing the square of the first-ring diameter by the constant difference between squares. Furthermore, because the entire error in the comparison of wavelengths resides in this determination of fractional orders, it is desirable to reduce it by distributing it among several fringes. Finally, to derive the most probably correct values, the observations should be reduced according to the method of least squares. In all our determinations of $^{198}_{80}$Hg wavelengths we have measured for each radiation the diameters of either five or six successive rings. These measurements were made with an interference comparator, designed by K. Burns in 1913, constructed in the Bureau's instrument shop, and illustrated in an earlier paper [16]. At first the diameters of six rings were measured, and fractional orders were calculated by the procedure described and recommended by Meissner [17]. Because this procedure involves an inordinate amount of arithmetic, it was abandoned in favor of the procedure earlier described by Holt and Barrell [18]. The latter reduces to an especially simple form when five fringes are measured and all operations are simple mental arithmetic, except squaring the diameters and finding the final quotient that represents the fractional order sought. The squares were taken from Gauss [19] and the quotient from a calculating machine.

Starting with micrometered values of the plate spacers, the correct integral orders of the green and yellow waves of mercury were uniquely de-

rived from their coincidence rates and observed fractional orders as explained elsewhere [10]. The yellow pair is happily heuristic for the order of interference because coincidences can recur only at intervals of 275 waves. After the correct orders for three mercury lines had been established, the orders corresponding to other known lines, including that for red radiation from cadmium, were calculated. Finally, the wavelengths of several $^{198}_{80}$Hg lines were determined relative to Cd 6438.4696 A by taking this times its order and dividing that product by the orders of the several $^{198}_{80}$Hg lines. These are the correct relative values only if the observations have been made in standard air (pressure 760 mm Hg and temperature 15° C) and provided that the optical distance between the interferometer surfaces is the same for all wavelengths. Because, in general, neither of these conditions is present, Fabry-Perot wavelength determinations require slight corrections for normal air and for dispersion of phase change upon reflection.

The temperature of the air near the interferometer and the barometric pressure were recorded for each spectrogram, and from these data the appropriate air-density corrections to wavelengths were derived directly from tables published by Meggers and Peters [20]. The largest corrections of this type amounted to −0.0014 A for 4046 A. Corrections required on account of dispersion of phase change were deduced from systematic differences obtained for wavelengths measured with small and with large orders of interference [15, 21]. Such systematic differences observed with 5 mm and with 90 mm separations of plates are shown in figure 3. All wavelengths (except 6438 A) measured with these particular plates require a positive correction that is a function of wavelength and of order of interference. For 4046 A this correction amounts to +0.0005 A when these interferometer plates are separated 40 mm. It is obvious that these required corrections must be evaluated with some care if one desires to express wavelengths correctly within ±0.0001 A.

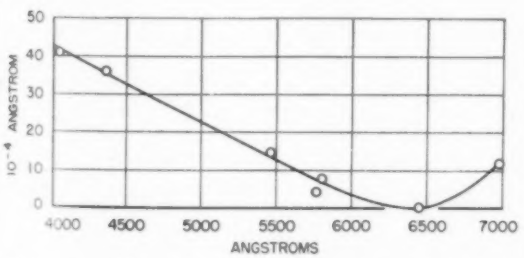

FIGURE 3. *Dispersion of phase change on reflectance in aluminum films exhibited as differences in wavelengths from 90-mm and 5-mm separations of plates.*

When these wavelength measurements were begun in 1947 a cadmium metal vapor lamp purchased from the Westinghouse Lamp Division [22] was used in lieu of the (lacking) Michelson lamp. The red radiation from this lamp was measured relative to neon standards by Meggers and Humphreys, who reported an increase of wavelength with current [8]. Such a shift in wavelength of the cadmium line emitted by Westinghouse lamps was confirmed by the present experiments after $^{198}_{80}$Hg wavelengths were compared with the primary standard emitted by Michelson-type Cd lamps, which we constructed and used during 1948. By measuring the wavelengths of certain $^{198}_{80}$Hg lines relative to the red radiation from both types of Cd lamps we arrived at the ratio of 1.000 000 23 for Cd (Westinghouse) to Cd (Michelson) when the former lamp is operated with 3 to 4 amp.

In 1949 we experimented with an "Osram" cadmium vapor lamp made by the General Electric Company of England and were satisfied that the wavelength of its red radiation is practically the same as that from the standard Michelson lamp. After innumerable discouraging experiences with Michelson lamps on account of their smallness, faintness, short life, etc., and after disappointment that the wavelength of cadmium light from Westinghouse lamps is not constant, it was a pleasure to work with the improved cadmium lamp supplied by the General Electric Company of England. Unfortunately, the latter does not conform to construction and operation specifications adopted by the International Committee on Weights and Measures [23] and by the International Astronomical Union [24].

Preliminary results for wavelengths of $^{198}_{80}$Hg visible radiations are presented in tables 1 and 2. Table 1 contains our first results based on Westinghouse cadmium lamps but now corrected to the scale of wavelengths fixed by the Michelson type of cadmium lamp. The results given in table 2 are based on Michelson cadmium lamps and are therefore preferable to those given in table 1.

580789—50——2

Only results from plate separations of 40 mm or greater are presented; those from smaller separations are naturally less accurate. Because the error of a wavelength measurement by this method lies entirely in the fractional order, it would appear desirable to hold this to a minimum and increase the integral order indefinitely. However, a limit is set by the failure of the cadmium red radiation to show sharp interference fringes beyond 400,000 waves. Even at retardations of 326,000 waves the cadmium fringes appear somewhat wide and indistinct, as shown in figure 4, and the fractional order cannot be found with the same accuracy as for $^{198}_{80}$Hg lines.

TABLE 1. *Preliminary values of* $^{198}_{80}$Hg *wavelengths relative to* Cd *6438.4696 A in normal air*

Whole angstroms	Fractional angstroms with interferometer-plate separations											
	40 mm	Observations	50 mm	Observations	67 mm	Observations	90 mm	Observations	105 mm	Observations	Means	Total Observations
5,790	0.6628	10	0.6627	10	0.6628	6	0.6627	2	0.6627	1	0.6627	29
5,769	.5982	10	.5983	10	.5985	6	.5985	2	.5983	1	.5984	29
5,460	.7532	9	.7532	10	.7533	6	.7532	3	.7532	3	.7532	31
4,916	.0697	5	.0699	2	.....	.....	.....	.....	.....	.....	.0698	7
4,358	.3377	9	.3377	8	.3376	6	.3377	3	.3375	3	.3377	29
4,347	.4959	7	.4961	5	.....	.....	.....	.....	.....	.....	.4960	12
4,339	.2248	5	.2252	2	.....	.....	.....	.....	.....	.....	.2250	7
4,077	.8383	7	.8382	8	.8381	4	.....	.....	.....	.....	.8382	19
4,046	.5718	9	.5717	10	.5717	6	.5716	3	.5715	2	.5717	30

TABLE 2. *Preliminary values of* $^{198}_{80}$Hg *wavelengths relative to* Cd *6438.4696 A in normal air*

Whole angstroms	Fractional angstroms with interferometer-plate separations							
	50 mm	Observations	67 mm	Observations	90 mm	Observations	Means	Total observations
5,790	0.6628	18	0.6627	15	0.6626	12	0.6627	45
5,769	.5985	18	.5984	15	.5984	12	.5984	45
5,460	.7532	20	.7533	15	.7531	12	.7532	47
4,358	.3378	20	.3376	15	.3377	12	.3377	47
4,077	.8383	2	.....	.....	.....	.....	.8383	2
4,046	.5718	20	.5715	15	.5717	12	.5717	47

Preliminary measurements for the wavelengths of green and yellow lines of $^{198}_{80}$Hg have been reported [25] from the National Physical Laboratory and from the International Bureau of Weights and Measures, as follows:

NPL: 5460.7531, 5769.5985, 5790.6628 A.
IBWM: 5460.7533, 5769.5986, 5790.6630 A.

In addition to the $^{198}_{80}$Hg wavelengths presented in tables 1 and 2, we have measured the wavelength of the only argon line recorded on our interference spectrograms; the average of 35 values obtained from plate separations of 40, 50, 67, 90, or 105 mm is 6965.4307 A.

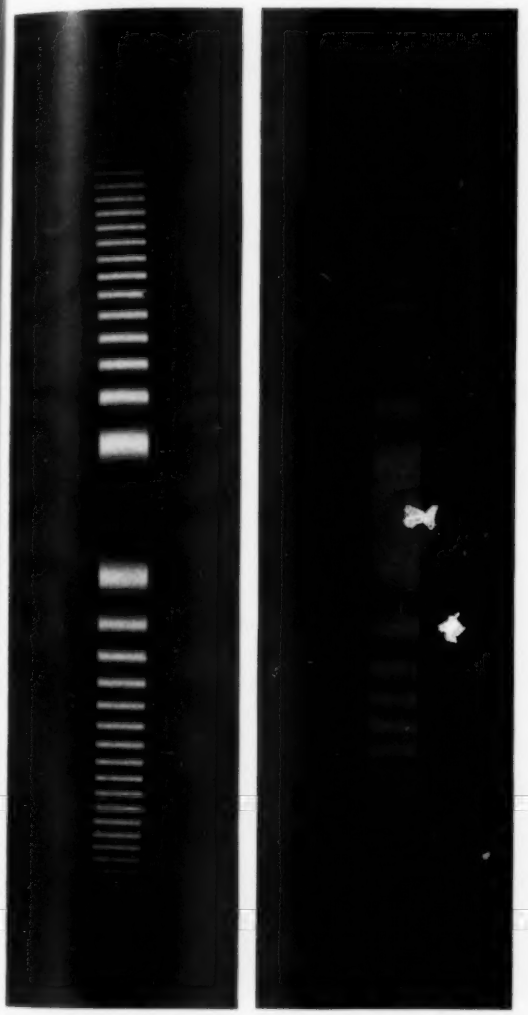

FIGURE 4. *Fabry-Perot interference fringes with total retardation of 210 mm to compare sharpness of* $^{198}_{80}Hg$ *and Cd lines.*

VI. References

[1] A. A. Michelson and E. W. Morley, Am. J. Sci. **38,** 181 (1889).

[2] A. A. Michelson, Phil. Mag. **34,** 280 (1892).

[3] F. W. Aston, Mass spectra and isotopes (Longmans, Green & Co., New York, N. Y. 1942).

[4] H. Schüler and J. E. Keyston, Z. Physik. **72,** 430 (1931).

[5] E. Fermi, E. Amaldi, O. D'Agostino, F. Rasetti, and E. Segre, Proc. Roy. Soc. **146 A,** 484 (1934).

[6] J. H. Wiens and L. W. Alvarez, Phys. Rev. **58,** 1005 (1940).

[7] J. H. Wiens, Phys. Rev. **70,** 910 (1946).

[8] W. F. Meggers, Rev. Modern Phys. **14,** 59 (1942).

[9] W. F. Meggers, J. Opt. Soc. Am. **38, 7** (1948).

[10] W. F. Meggers, Sci. Monthly **68,** 3 (1949).

[11] P. Bradt and F. L. Mohler, Phys. Rev. **73,** 925L (1948).

[12] K. G. Kessler, Phys. Rev. **77,** 559 (1950).

[13] C. P. Keim, Phys. Rev. **76,** 1270L (1949).

[14] E. Jacobsen and G. R. Harrison, J. Opt. Soc. Am. **39,** No. 12 (1949).

[15] H. Buisson and C. Fabry, J. Phys. (4) **7,** 169 (1908); C. Fabry and H. Buisson, Astrophys. J. **28,** 169(1908).

[16] W. F. Meggers and C. J. Humphreys, J. Research NBS **18,** 543 (1937) RP992.

[17] K. W. Meissner, J. Opt. Soc. Am. **31,** 409 (1941).

[18] F. H. Rolt and H. Barrell, Proc. Roy. Soc. **A122,** 122 (1929).

[19] F. G. Gauss, Tafeln für Maschinenrechnen (Konrad Wittwer, Stuttgart, 1912).

[20] W. F. Meggers and C. G. Peters, BS Sci. Pap. **14,** 724 (1918) S327.

[21] W. F. Meggers, BS Sci. Pap. **12,** 199 (1915) S251.

[22] J. W. Marden, N. C. Beese and G. Meister, J. Opt. Soc. Am. **30,** 184 (1940).

[23] Procès-Verbaux Comité Int. Poids et Mesures (2) **12,** 67 (1927).

[24] Trans. Int. Astron. Union **6,** 79 (1938).

[25] A. Pérard and J. Terrien, Compt. rend. **228,** 964 (1949).

WASHINGTON, December 18, 1949.

U. S. Department of Commerce
National Bureau of Standards

Research Paper RP2092
Volume 44, May 1950

Part of the Journal of Research of the National Bureau of Standards

Heat of Fluorination of Cobaltous Fluoride, and the Heats of Reaction of Cobaltic Fluoride with Hydrogen and with Bis(trifluoromethyl)benzene ($\alpha,\alpha,\alpha,\alpha',\alpha',\alpha'$-Hexafluoroxylene)

By Ralph S. Jessup, F. G. Brickwedde, and Martin T. Wechsler [1]

Calorimetric measurements of the heats of the following reactions have been made, with the results indicated:

(1) $2CoF_2(c)+F_2(g)=2CoF_3(c)$, $\Delta H(250°C)=-56.1\pm2.0$ kcal;

(2) $C_6H_4(CF_3)_2(g)+14CoF_3(c)=C_6F_{10}(CF_3)_2(g)+14CoF_2(c)+4HF(g)$, $\Delta H(335°C)=-409\pm20(?)$ kcal;

(3) $2CoF_3(c)+H_2(g)=2CoF_2(c)+2HF(g)$, $\Delta H(335°C)=-74\pm4$ kcal.

The values given for the heats of reactions 1 and 3 are consistent, within the assigned probable errors, with available data on the heat of formation of hydrogen fluoride. Reaction 2 was accompanied by unknown side reactions, and the value reported represents the heat of the reactions that actually took place in the calorimeter per 14 moles of CoF_3 reduced. The error in the value given for the heat of this reaction, as written, may therefore be considerably greater than that indicated by the assigned probable error.

I. Introduction

The work described in this paper was done during 1943 and 1944 at the request of the Manhattan District of the U. S. Army Corps of Engineers. At the time the work was done the need for data of moderate accuracy was urgent. For this reason, very little time could be devoted to development of apparatus, and the purity of the materials supplied for the measurements was not investigated. The results obtained are, therefore, not of high accuracy. It is believed, however, that they are of sufficient interest to justify their publication.

We were requested to measure the heats of the following two reactions:

$$2CoF_2(c)+F_2(g)=2CoF_3(c) \qquad (1)$$

and

$$C_6H_4(CF_3)_2(g)+14CoF_3(c)=C_6F_{10}(CF_3)_2(g)+14CoF_2(c)+4HF(g). \qquad (2)$$

The heat of the first reaction was determined at about 250° C and that of the second at about 335° C. According to information available to us, the reactions proceed too slowly at lower temperatures to permit accurate determination of the heat evolved, and at temperatures above 335° C, products other than $C_6F_{10}(CF_3)_2$ are formed in considerable amounts in the reaction of $C_6H_4(CF_3)_2$ with CoF_3. We were informed that, at 335° C, reaction 2 proceeded as indicated and was reasonably free from side reactions.

The value obtained for the heat of reaction 1, namely, $\Delta H=-56.1$ kcal at 250° C, differed so greatly from the value, $\Delta H=-159.2$ kcal, previously reported by Jellinek and Koop [2] for this reaction, that it was thought desirable to check the value obtained in the present investigation. This was done by determining the heat of the reaction,

$$2CoF_3(c)+H_2(g)=2CoF_2(c)+2HF(g), \qquad (3)$$

[1] Present address University of Michigan, Ann Arbor, Mich.

[2] K. Jellinek and R. Koop, Z. physik. Chem. **A145**, 305 (1929).

and comparing the experimental result with a value calculated from our value for the heat of reaction 1, and a value reported in the literature for the heat of the reaction,

$$\frac{1}{2}\,H_2(g)+\frac{1}{2}\,F_2(g)=HF(g). \qquad (4)$$

The heat of reaction 3 was measured at about 335° C with the same apparatus used for reactions 1 and 2.

II. Method, Apparatus, and Materials

The method consisted in comparing the temperature changes produced in a calorimetric system by measured amounts of chemical reaction and of electric energy.

Figure 1 is a schematic diagram of the apparatus. The calorimeter consisted of the Dewar flask, *Q*, containing liquid Aroclor No. 5460 in which was immersed the reaction vessel, *N*. A heating coil of bare nichrome wire for supplying electric energy was wound on the insulated supports, *L*, and was provided with potential leads for measuring the impressed voltage. By means of the screw propeller, *K*, the bath liquid was driven downward past the heater; through the tube, *J*; through openings in the steel support, *P*; upward between the tube, *J*, and the wall of the Dewar flask; and back into the tube, *J*, through holes located just above the propeller.

In order to reduce heat loss from the Dewar flask, it was immersed in an unstirred liquid Aroclor bath in the iron cylinder, *R*. This outer bath was heated by a 660-watt contact heater, *U*, at the bottom and by two 2,000-watt immersion heaters (not shown in fig. 1), which were coiled inside and against the iron cylinder, *R*. During a calorimetric measurement the outer bath was maintained manually at an approximately constant temperature somewhat higher than that of the calorimeter. Loss of heat from the top of the calorimeter was reduced by means of the jacket cover, *G*, of the type described by White [3] consisting of two sheets of copper separated by the asbestos board, *H*, and bent down at the edges so as to dip into the liquid in the outer bath, *R*. In spite of the precautions taken, the heat loss from the calorimeter was relatively large. This is believed to have been due principally to evaporation of the Aroclor.

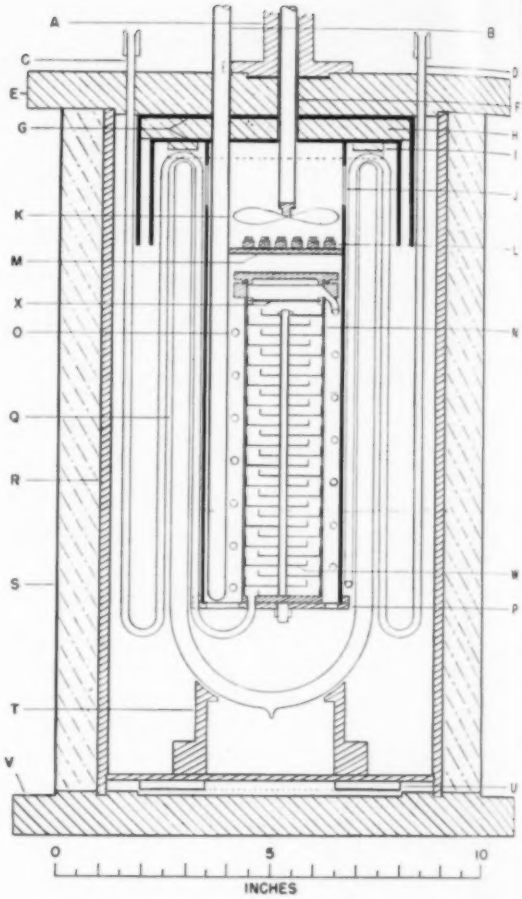

FIGURE 1. *Diagram of calorimeter.*

A, Steel support for stirring motor and shield for propeller shaft; *B*, platinum resistance thermometer; *C*, inlet tube leading through outer bath to reaction vessel in calorimeter; *D*, exit tube (continuation of tube, *O*); *E*, transite board; *F*, propeller shaft of monel metal tubing; *G*, copper shields; *H*, transite board separating shields; *I*, transite ring between top of Dewar flask and copper shield (has slots to permit passage of inlet and outlet tubes); *J*, copper baffle tube; *K*, propeller; *L*, heater supports; *M*, steel ring holding heater supports; *N*, reaction vessel; *O*, coiled outlet tube from reaction vessel; *P*, steel support for reaction vessel (permits passage of bath liquid out of baffle tube, *J*); *R*, steel container for outer bath; *S*, galvanized iron outer case (the space between *R* and *S* was filled with rock wool for insulation); *T*, support for Dewar flask; *U*, ring heater; *V*, transite base; *W*, trays for cobalt fluoride powder; *X*, nickel gauze (600-mesh).

The outer bath was insulated by a 1-inch layer of rock wool around the cylindrical wall, and by the asbestos boards, *E* and *V*, at the top and bottom, respectively. The jacket cover, *G*, and

[3] W. P. White, J. Am. Chem. Soc. **48**, 1149 (1926); The Modern Calorimeter p. 152 (Reinhold Publishing Corporation, New York, N. Y., 1928).

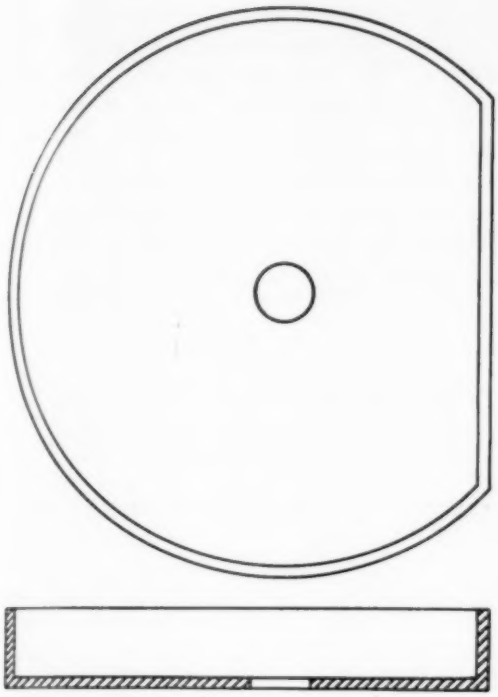

FIGURE 2.—*Tray for holding cobalt fluoride powder in reaction vessel.*

the tube, *J*, were supported from the asbestos board, *E*.

The reaction vessel, *N*, was a steel cylinder containing 29 steel trays, *W*, of the form illustrated in figure 2. A total of about 100 grams of CoF_2 was placed in the trays, the depth of the powder being about 5 mm in each tray. The trays were arranged with their flat sides staggered, as indicated in figure 1, so that the reactant gases flowed over each tray.[4] Above the trays was a 600-mesh screen, *X*, to prevent blowing of the cobalt fluoride powder from the reaction vessel.

The reactant gas entered the system through the tube, *C*, and was brought to the temperature of the outer bath before entering the calorimeter. The reactant gas was admitted to the reaction vessel at the bottom, and the product gases, if any, flowed from the top of the reaction vessel through the coiled tube, *O*, in which their temperature was reduced to that of the calorimeter before entering the tube, *D*, which was immersed in the outer bath.

The electrical energy supplied to the calorimeter in the determination of its energy equivalent was determined from measurements of current and voltage with a potentiometer, in conjunction with a volt box and standard resistor, and measurement of the time of heating, using second signals from a Riefler clock. The temperature of the calorimetric liquid was measured with a 2.5-ohm platinum resistance thermometer, *B*, and a Mueller bridge.

The fluorine, the cobaltous fluoride, and the $C_6H_4(CF_3)_2$ used were obtained by R. Rosen, then of the Kellex Corporation, from E. I. Dupont de Nemours & Co. No quantitative information concerning the purity of these materials was furnished, but it was stated that the purity was relatively high. The $C_6H_4(CF_3)_2$ was probably a mixture of isomers. The hydrogen used for the measurement of reaction 3 was prepared electrolytically at this Bureau, and was passed over hot copper and through a liquid air trap before entering the reaction vessel.

The drying of the CoF_2 powder proved to be difficult. Heating at 350° C in vacuum for 28 hours did not remove all the water. For this investigation drying was completed by fluorinating the CoF_2 at 250° C. The same filling of cobalt fluoride was used in all experiments. For use in reaction 1 it was reduced to CoF_2 by passing hydrogen through the reaction vessel at 335° C, and for use in reactions 2 and 3 it was converted to CoF_3 by passing fluorine through the reaction vessel at 250° C.

III. Details of Procedure

The energy equivalent of the calorimeter was determined before and after each determination of the heat of a reaction. The correction for thermal leakage, heat of stirring, etc. was calculated for each calorimetric experiment from measurements of rates of change of temperature of the calorimeter in "rating periods" preceding and following the "reaction period."

The amount of reaction was determined from the gain or loss in weight of the reaction vessel. The hot Aroclor corroded the steel vessel, the rate of corrosion increasing with the length of time the Aroclor had been held at the elevated

[4] The design of the reaction vessel with trays to contain the cobalt fluoride was suggested by R. D. Fowler, Johns Hopkins University.

temperatures. To reduce the error resulting from corrosion of the reaction vessel, the following steps were taken: (a) The vessel and its connecting tubes were plated with nickel and chromium; (b) the calorimeter was filled with fresh Aroclor for each measurement of the heat of a reaction; (c) the rate of corrosion of the vessel was measured, and a correction for the change in weight due to corrosion was applied to the results. The thermal effect of corrosion at a constant rate would be taken into account in the correction for thermal leakage, etc., mentioned above. The amount of reaction 3 was determined also from the increase in weight of a tube containing Ascarite (NaOH on asbestos) in which the HF generated by the reaction was absorbed, followed by a drying agent to absorb water evaporated from the Ascarite. The increase in weight of the Ascarite tube was consistent with the corrected loss in weight of the reaction vessel within 1 percent, which is within the uncertainty of the measurements.

In the measurements of the heat of reaction 2, the product gases were passed first through a tube containing Ascarite plus drying agent, and thence to a trap immersed in liquid air, and the increases in weight of the trap and of the tube containing Ascarite were determined. It was found that the sum of the losses in weight of the $C_6H_4(CF_3)_2$ container and the reaction vessel was equal (within the accuracy of the measurements) to the gain in weight of the Ascarite plus the weight of the fluorocarbon product condensed in the liquid air trap.

A small flow of helium through the reaction vessel was maintained before and after each "reaction period." While reactions 1 and 3 were proceeding, the flow of helium was stopped, the absolute pressure of the gases in the reaction vessel was held at approximately 3 atmospheres, and the outlet valve was opened slightly to permit a flow of gas from the system. This flow of gas was necessary during reaction 3 for the removal of the product gas, HF, and was found to be necessary during reaction 1 to prevent the impurities in the fluorine from accumulating in the reaction vessel.

During reaction 2 the flow of helium through the reaction vessel was maintained in order to exclude air from the system, and to carry the products of the reaction to the absorbing and condensing chambers. The $C_6H_4(CF_3)_2$ was vaporized in a metal container immersed in an oil bath at 150° C. The tube through which the vapor flowed to the calorimeter was electrically heated to prevent condensation. The rate of flow of vapor into the reaction vessel during the two measurements of the heat of reaction 2 was 0.08 and 0.03 gram per minute. In order to favor complete fluorination of $C_6H_4(CF_3)_2$, reaction 2 was stopped before half of the cobalt salt in the reaction vessel had been reduced to the difluoride.

IV. Results

There are given in table 1 the experimental values of the heats of reactions 1, 2, and 3. The reduction of the observed value for the heat of reaction 3 from 335° to 250° C, made using data on the heat capacities of hydrogen [5] and hydrogen fluoride,[6] together with the estimated values 24 cal $mole^{-1}$ deg^{-1} and 18 cal $mole^{-1}$ deg^{-1} for the heat capacities of CoF_3 and CoF_2, respectively, yielded the value $\Delta H(250°\ C) = -73.6$ kcal. A value $\Delta H(250°\ C) = -72.4$ kcal. was calculated for the heat of reaction 3 by combining our experimental value for the heat of reaction 1, $\Delta H(250°\ C) = -56.1$ kcal, with the value $\Delta H(250°\ C) = -64.3$ kcal for the heat of reaction 4. The latter value was derived from the value

TABLE 1. *Values of heat of reaction*

Reaction	Experiment	Heat of reaction ΔH	Estimated probable error [a]	Temperature to which reaction is referred
		kcal	*kcal*	°C
(1) $2CoF_2(c)+F_2(g)=2CoF_3(c)$	1	−56.0		
	2	−56.2		
	Mean	−56.1	±2.0	250
(2) $C_6H_4(CF_3)_2(g)+14CoF_3(c)=$ $C_6F_{10}(CF_3)_2(g)+14CoF_2(c)+4HF(g)$	1	−406		
	2	−412		
	Mean	−409	±20(?)	335
(3) $2CoF_3(c)+H_2(g)=2CoF_2(c)+2HF(g)$	1	−74	±4	335

[a] The estimated probable errors were derived from the agreement of the results of duplicate experiments, together with estimates of the effects of systematic errors. See text for a discussion of the probable error of the heat of reaction 2.

[5] F. G. Brickwedde, M. Moskow, and J. G. Aston, J. Research NBS 37, 263 (1946).

[6] M. Murphy and J. E. Vance, J. Chem. Phys. 7, 806 (1939).

$\Delta H(25°\ C)=-64.2$ kcal [7] for the heat of reaction 4 at 25° C, together with data on the heat capacities of hydrogen (see footnote 5), fluorine, and hydrogen fluoride (see footnote 6). Our experimental values for the heats of reactions 1 and 3 are therefore consistent with the value (see footnote 7) for the heat of reaction 4 to well within the assigned probable errors.

V. Discussion

1. Reaction 1

As stated in section 1, the value $\Delta H=-56.1$ kcal, obtained in the present work for the heat of reaction 1 at 250° C, is in violent disagreement with the value $\Delta H=-159.2$ kcal at 260° C, reported by Jellinek and Koop (see footnote 2). The latter value was derived from measurements of the equilibrium concentrations of HF and H_2 in contact with CoF_2 and CoF_3 over a temperature range from 470° to 595° K, together with a value reported in the literature for the heat of formation of HF. In view of the consistency of the values obtained in the present work for the heats of reactions 1 and 3 with the value, $\Delta H(250°\ C)=-64.3$ kcal, for the heat of reaction 4, it is believed that the value reported by Jellinek and Koop must be seriously in error. It may be noted that the value for the heat of reaction 3, calculated using the value reported by Jellinek and Koop for reaction 1 and the value (see footnote 7) for the heat of reaction 4, is of opposite sign to the value for reaction 3 found experimentally in the present work.

An experimental value, $\Delta H=-52\pm3$ kcal, for the heat of reaction 1 has been reported by Fowler, et al.,[8] who also state that the value reported by Jellinek and Koop leads to values for heats of fluorination of hydrocarbons with CoF_3 that are inconsistent as to sign with their laboratory experience.

It is of interest to calculate the equilibrium pressure of F_2 over CoF_2 and CoF_3. An accurate calculation of this pressure is not possible, because the low-temperature heat capacities of CoF_2 and CoF_3 are not available for a calculation of their absolute entropies. An approximate calculation, taking

$$\ln p_{F_2}=\frac{\Delta F^\circ}{RT}\cong\frac{\Delta H}{RT},$$

indicates that p_{F_2} is of the order of 10^{-20} atmosphere at 250° C. In view of this extremely low value for the equilibrium pressure of F_2, the reduction of CoF_3 in reactions 2 and 3 must involve immediate contact of the gaseous reactant molecules with the CoF_3 crystals.

2. Reaction 2

The value given in table 1 for the heat of reaction 2 is subject to considerable uncertainty, because of the fact that the exact nature of the reaction between CoF_3 and $C_6H_4(CF_3)_2$ in the calorimeter is not known. There is evidence, which indicates that, under the conditions of our experiments, reaction 2 is accompanied by unknown side reactions. Thus, Fowler et al (see footnote 8) report that the reaction of CoF_3 with $C_6H_4(CF_3)_2$ under optimum conditions (similar to those in our experiments) gave a crude yield of 97 percent, and a yield of pure $C_6F_{10}(CF_3)_2$ of 83 percent. For the same reaction, Benner et al.,[9] report a crude yield of 91 percent, and a recovery of HF of 80 percent of theory.

In our measurements of the heat of reaction 2, the amount of $C_6H_4(CF_3)_2$ passed into the reaction vessel was found to exceed that chemically equivalent to the loss in weight of the cobalt fluoride. In the first experiment, in which the cobalt fluoride was initially completed fluorinated, the excess of $C_6H_4(CF_3)_2$ was 10 percent, while in the second experiment, after partial reduction of the cobalt fluoride, the excess was 20 percent, although the rate of flow of $C_6H_4(CF_3)_2$ was much lower in the second experiment than in the first.

It is believed that the value given in table 1 for the heat of reaction 2 represents the heat produced per 14 moles of CoF_3 reduced in the reaction, or reactions, which actually took place in the calorimetric experiments, within the limits indicated by the assigned probable error. This quantity would be useful in connection with the design of equipment for fluorinating $C_6H_4(CF_3)_2$, and data for this purpose were of primary interest when the work

[7] Selected Values of Chemical Thermodynamic Properties, National Bureau of Standards, Washington, D. C. Table 9-1.

[8] R. D. Fowler, W. D. Burford, III, J. M. Hamilton, Jr., R. G. Sweet, I. S. Kasper, and I. Litant, Ind. Eng. Chem. **39**, 292 (1947).

[9] R. G. Benner, A. F. Benning, F. B. Downing, C. F. Irwin, K. C. Johnson, A. L. Linch, H. M. Parmelee, and W. V. Wirth, Ind. Eng. Chem. **39**, 329 (1947).

was undertaken. Because of the uncertainty indicated above as to what reactions actually took place in the calorimetric experiments, the true value for the heat of reaction 2 may differ from the value reported in table 1 by considerably more than might be inferred from the assigned probable error.

Benner et al (see footnote 9) reported the value $\Delta H = -460$ kcal for the heat of reaction 2. This value was estimated from the observed heat-transfer rates, in their fluorination apparatus, during fluorination of CoF_2 with gaseous fluorine, and during fluorination of $C_6H_4(CF_3)_2$ by passing it over CoF_3. They used a preliminary value, $\Delta H = -58$ kcal, from the present work for the heat of reaction 1. Using our final value for the heat of reaction 1, their value for reaction 2 becomes $\Delta H = -445$ kcal. This value is subject to the same uncertainty as ours with respect to the nature of the reaction to which it applies.

WASHINGTON, January 17, 1950.

U. S. Department of Commerce
National Bureau of Standards

Research Paper RP2093
Volume 44, May 1950

Part of the Journal of Research of the National Bureau of Standards

Permanence of Glass Standards of Spectral Transmittance

By Kasson S. Gibson and Marion A. Belknap

Shortly after the introduction of commercially available photoelectric spectrophotometers, the National Bureau of Standards began issuing calibrated disks for checking the photometric scale of spectrophotometers. At the time these standards were selected no precise information was available regarding their permanence. The present paper presents data showing that the glass standards kept in the files for 16 years with only occasional use have not changed. Data are also given showing the nature of the changes occurring in glasses similar to the standards when exposed under glass to south skylight (including sunlight) for periods up to 3 years.

I. Introduction

One of the essential parts of a spectrophotometer is the photometric equipment, and the accuracy of the photometric scale is one of the major items with which both the manufacturer and the user of the spectrophotometer should be concerned. This photometric scale may be based on optical principles and devices, as in all visual spectrophotometers and the Hardy or General Electric recording spectrophotometer, or it may be based on electrical principles and devices, as in many of the other photoelectric spectrophotometers. Whatever the method, the user of the spectrophotometer should have some means available to insure that the instrument is giving reliable results or to warn him that something is wrong.

On a visual spectrophotometer this can be done by means of rapidly rotating sectored disks, whose apertures can be mechanically calibrated with high accuracy. On photoelectric spectrophotometers, however, for one reason or another, such a procedure is not generally feasible. An acceptable alternative, and one that is in general much more convenient, is the use of solutions or glass disks whose spectral transmissive properties are accurately known over the desired spectral range.

At first thought one might wish for a series of filters whose respective transmittances do not vary with wavelength, which will not displace the beam, which do not reflect strongly, and for which the transmittances can be independently determined with high accuracy. Such filters would enable a test of the photometric scale to be made that would be independent of all other sources of error, and if available they would probably be useful. They are not available, however, and in fact would probably not be as useful as the series of moderately selective filters that are discussed in the present paper. This is because the nonselective filters would not enable the detection of wavelength errors no matter how great; they would give no information regarding the effects of wide slits; nor would they detect the presence of stray spectral energy. The selective filters, on the other hand, will often yield valuable information about these things in addition to affording the desired check of the photometric scale over most of its range.

Shortly after the appearance of commercially available photoelectric spectrophotometers in 1930, this Bureau began the preparation and issuance of glass standards of spectral transmittance. These were described at a meeting of the Optical Society of America in 1933 [1].[1] They have been noted in other Bureau publications since that date [2, 3, 4], and they have been listed in past and present Bureau test fee schedules. To date about 170 of these filters have been issued.[2]

[1] Figures in brackets indicate the literature references at the end of this paper.

[2] Solution standards of spectral transmittancy are described, with data, in NBS Letter Circular LC929 [3] and in NBS Circular C484 [4].

At the time that decision was made on the types of filters to use, little quantitative information was available as to the permanence of colored glasses. Manganese glasses were known to be unstable, and the spectral transmittances of many glasses were known to vary in the ultraviolet upon exposure to strong ultraviolet radiant flux. On the other hand it can be assumed that many kinds of colored glass have high stability in the visible spectrum, else cathedral windows would have paled or otherwise deteriorated to a notable degree through the centuries of exposure.

Since no evidence was available that the common types of colored glass other than manganese would change, the selection of the filters was made wholly from the standpoint of suitable spectral transmittances in suitable thicknesses. Of necessity it was assumed that these glasses would remain constant until sufficient time had elapsed that changes could be ascertained even though small. The kinds of glass selected are described in the next section. For each type two glasses were selected for initial measurement, and these have been kept in the Bureau files, unused except for occasional measurement. These remeasurements were not systematic but were sufficient to show that no important changes were taking place.

Naturally there were often differences in the third decimal between the original and the repeat values of transmittance, but these were usually slight and always within the combined experimental uncertainties. Nevertheless, consideration of these small differences made it seem desirable to carry out some kind of accelerated exposure test in order to find out the nature of any real changes that might be expected. This was accordingly carried out over a 3-year period.

The purpose of the present paper is to show the nature and extent of the changes produced under this accelerated exposure and to indicate the degree of certainty within which the Bureau standards (not so exposed) have or have not changed. It is believed that this information will be of interest to most of the users of these standards.

II. The Standards

1. Description

Four types of glass were finally chosen for these standards: (1) A "cobalt blue" glass from the Corning Glass Works, designated by them formerly as G55A and at present as 5551. This has been used mostly in 3-mm thickness. (2) A "carbon yellow" glass from the Corning Glass Works, designated by them formerly as HT (high transmission) Yellow, and at present carrying their number 3307. This has been used mostly in 2-mm thickness. (3) A Jena "copper green" glass, supplied by the Fish-Schurman Corporation, and carrying the Jena number BG14. This has been used mostly in 2-mm thickness. (4) A Jena "selenium orange" glass, supplied by the Fish-Schurman Corporation, and carrying the Jena number OG3. This has also been used mostly in 2-mm thickness.

When it is desired not to be specific, these glasses will be referred to by the color names given above, but without quotes—namely, cobalt blue, carbon yellow, copper green, and selenium orange.

The usual procedure in preparing the standards has been to secure a supply of each kind of glass (all pieces from the same melt) and prepare as many disks (29.8 mm in diameter) as possible from the supply at hand. From these disks one or two would be selected and retained as Bureau standards. The others would be kept as standards to be issued. In this paper reference may be made to the "Bureau standards" or the "issued standards" where it is desired to differentiate between them, or simply to the "standards" or to the "glasses" if such differentiation is unimportant.

The general types of transmittance curves for these glasses are shown in figure 1. For each type are shown curves for the pair of glasses originally selected as Bureau standards in 1933 and a third curve for the Bureau standard selected from the glasses now being used. In general, the spectral transmittances of the issued standards are similar to but not identical with the values illustrated in figure 1. The broken-line curves, below 390 and above 750 mμ, show the spectral transmittances of these glasses in the ultraviolet and near infrared, when these have been measured.

The wavelengths used in reporting values of transmittance for these standards (shown in table 1) are often the wavelengths of lines in the mercury or helium spectra. These were chosen originally with the intention of making the photometric measurements at these wavelengths with

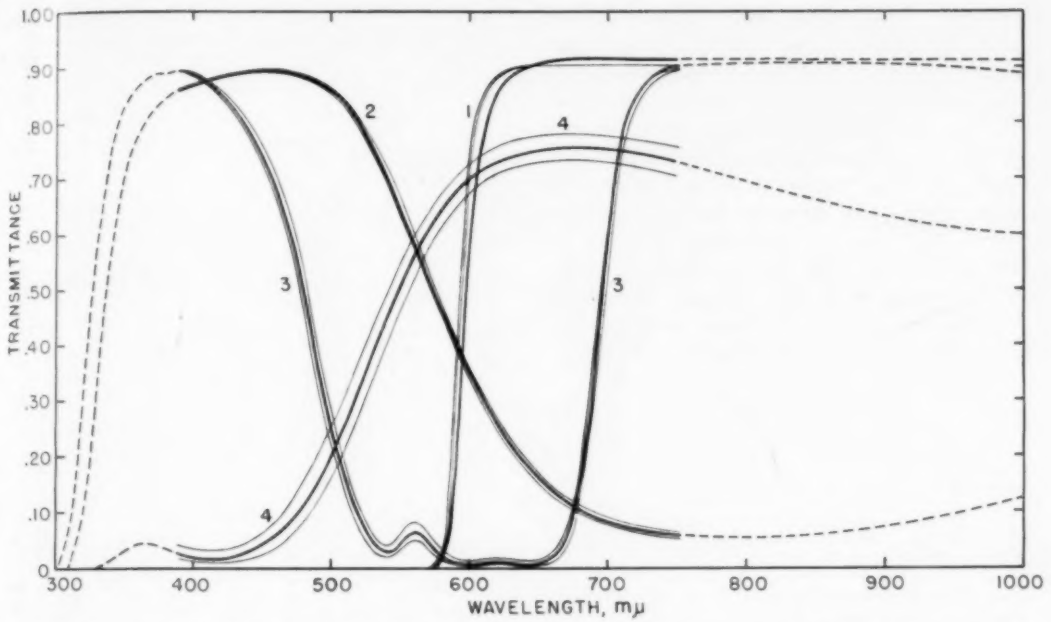

FIGURE 1. *Spectral transmittances of the four types of glass standards: 1, selenium orange; 2, copper green; 3, cobalt blue; 4, carbon yellow*

Light lines: standards of different thickness prepared in 1933. Heavy lines; standards now in use. The standards are issued primarily for the range 390 to 750 mμ. The broken lines show the ultraviolet and near infrared spectral transmittances of the present standards.

these sources, and the Hg 404.7, 435.8, 546.1, and 578.0 (577.0 and 579.1 doublet) lines and the He 501.6 and 587.6 lines have been extensively used for such purpose. The advantage of this, as often pointed out, is that values are obtained that are independent of any possible wavelength and slitwidth errors. After extensive trial it was found, however, that the intensities at the other Hg and He wavelengths were so low that accuracy was lost rather than gained by their use. Although incandescent sources are now used at most of these other wavelengths in the standardization measurements, there is still some advantage in retaining these wavelengths instead of going to an adjacent even number (for example, 471.3 instead of 470) because of slightly greater certainty possible in wavelength calibrations. Furthermore, much of the value of earlier work at these Hg and He wavelengths would have been lost by starting anew at an adjacent wavelength.

2. Temperature Effects

It is probable that the spectral transmittance of all glasses changes at all wavelengths if the temperature change is sufficiently large (for example, from −180° C to +450° C). Illustrations of such changes for a considerable number of types of glasses have been collected and published in NBS Circular 484 [4]. In many instances such changes are important even for the usual room temperature variations. For use as a standard of spectral transmittance, accordingly, it is necessary that the values be obtained and certified for some selected temperature and that a formula be given enabling the user of the glass to compute the spectral transmittance of the glass at room or instrument temperatures other than that specified.

Room temperatures in laboratories, if not air-conditioned, often vary from around 20° C on winter mornings to above 30° C in summer weather. A temperature of 25° C was therefore selected as the most useful temperature for the standardization measurements, and the spectral transmittances of all issued standards are certified at this temperature.

In addition measurements were made at 40° C on the Bureau standards in 1933 and at 55° C on three of the four newly selected Bureau stand-

ards in 1946. These more recent measurements were not only made at about twice the temperature interval used in the former measurements, but were also made with greater instrumental precision. They were thus considered more reliable than the earlier ones and have superseded them for certificate use. The two sets of values were wholly consistent within the uncertainties of measurement.

As already noted, at the start of the work standards of different thicknesses were used. A suitable way of reporting these temperature "coefficients", d, was therefore taken simply from the relations:

$$-\log_{10}T_{25}=ba_{25}+k$$

$$-\log_{10}T_{40}=ba_{40}+k$$

$$-\log_{10}T_{\theta}=ba_{\theta}+k,$$

where T is the transmittance at the subscript temperature, a is the absorbance index [5], b is the thickness in millimeters, and k is a constant ($=-\log_{10}0.92$, approximately).

We define d as equal to

$$a_{40}-a_{25}=\frac{-\log_{10}T_{40}-(-\log_{10}T_{25})}{b}$$

and assume that

$$a_{\theta}-a_{25}=\left(\frac{\theta-25}{15}\right)d.$$

From this we get

$$-\log_{10}T_{\theta}=-\log_{10}T_{25}+bd\left(\frac{\theta-25}{15}\right),$$

as given in the certificates sent out with the issued standards. These values of d are given in table 1 for the four types of standards. The assumption of linearity in the variation of a_{θ} with θ is justified by the small temperature changes involved and by the uncertainties of measurement of d; the values of d are mostly small and are generally reported to but one significant figure.

3. Use of Standards

In addition to the values of transmittance at 25° C and the values of d, the Bureau reports values of uncertainty at the respective wavelengths. These uncertainties are the "huge errors" [6], taken as 4.9 times the probable errors.

TABLE 1. *Values of d, the temperature coefficient, for the four types of glass used as standards of spectral transmittance.*

[For definition of *d*, see text.]

Wavelength	Temperature coefficient, *d*, of glasses designated as—			
	Cobalt blue	Carbon yellow	Copper green	Selenium orange
$m\mu$				
390	0.000	−0.0005	0.000	.....
404.7	.000	−.0025	.000	.....
420	.....	−.0025	.....	.....
435.8	.000	−.0015	.000	.....
471.3	.000	+.001	.000	.....
491.6	+.0005	.....	.....	.....
501.6	+.001	+.0035	.000	.....
520	+.0005	+.0035	.....	.....
530	.....	+.003	.000	.....
540	−.003	.....	.....	.....
546.1	−.004	+.0025	.000	.....
560	−.003	+.002	.000	.....
578	−.004	+.0015	−.0005	+0.17
587.6	.....	+.0015	.....	+.11
600	−.005	+.001	−.0005	+.022
620	−.003	+.0005	−.001	+.002
640	−.005	+.0005	−.001	.000
660	.....	.000	.....	.000
667.8	+.004	.....	−.001	.....
680	+.006	.....	.....	.....
690	+.004	.000	.....	.000
706.5	+.002	.....	.....	.....
710	.....	.....	−.001	.....
720	+.0005	−.0005	.....	.000
750	.000	−.0005	−.0005	.000

These huge errors have been computed twice, once in 1933 from the values obtained on the six original glasses of each type when computed to common thickness, and again in 1945–46 from values obtained from repeated determinations on the same glasses with three different types of instruments [2].

While the number of determinations entering into the computations of the huge error was too small in either case to give a highly significant result, there was satisfactory agreement in the two sets of data, and there has been no evidence that the values reported in the respective certificates do not cover the over-all uncertainty of measurement. These reported values of uncertainty are usually close to those given in figures 2 to 4.

The method of obtaining the values of transmittance for the issued standards has varied somewhat over the years, changing with instruments

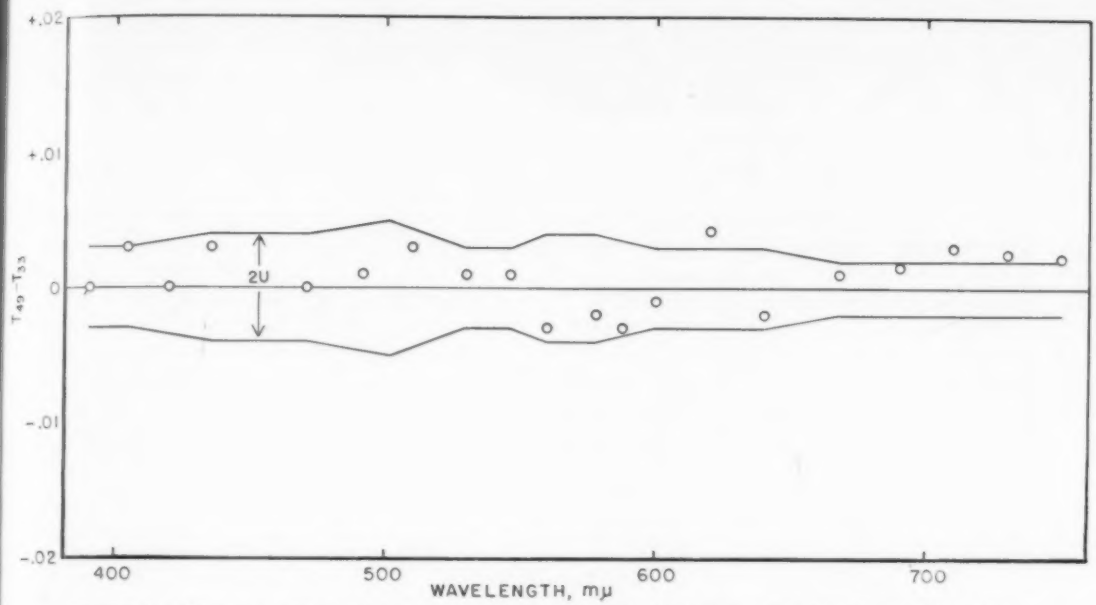

FIGURE 2. *Permanence of a copper green glass standard kept in the Bureau files with only occasional use.*

The circles represent differences between values of transmittance obtained in 1949 on the Beckman photoelectric spectrophotometer and values adopted in 1933 from measurements made on the König-Martens visual and the Gibson photoelectric spectrophotometers. The boundaries designated as $2U$ represent the over-all uncertainties, $\pm U$, pertaining to the adopted values. It is concluded that the standard has not changed.

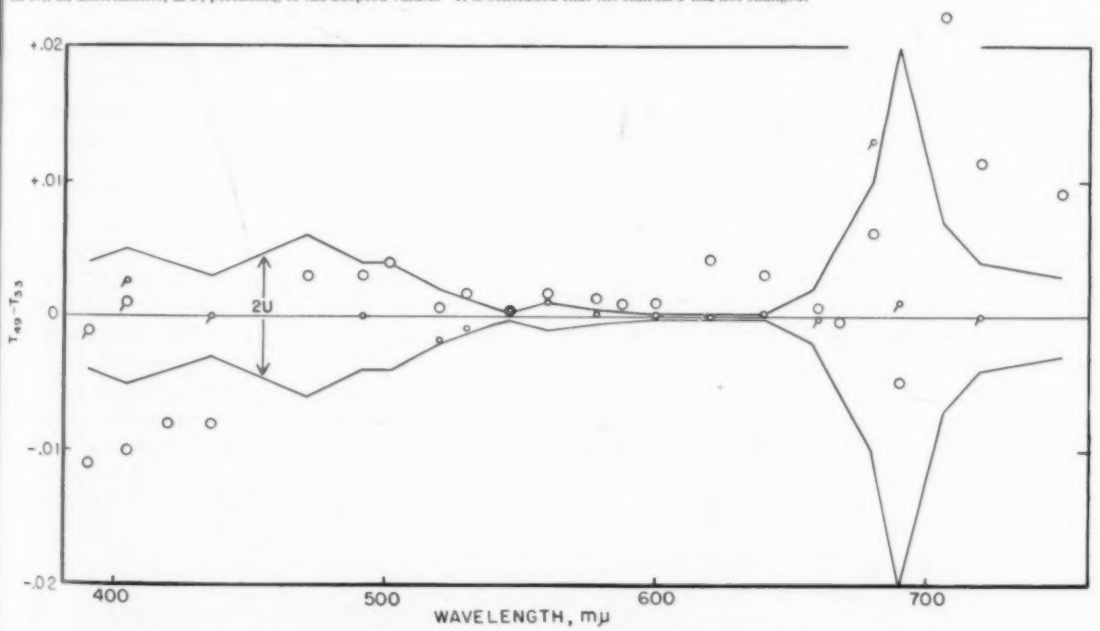

FIGURE 3. *Permanence of a cobalt blue glass standard kept in the Bureau files with only occasional use.*

The circles represent differences between values of transmittance obtained in 1949 on the Beckman photoelectric (large circles) and the König-Martens visual (small circles) spectrophotometers and values adopted in 1933 from measurements made on the König-Martens and the Gibson spectrophotometers. Circles with diagonal lines attached were obtained by use of stray energy filters in the 1949 measurements. The boundaries designated as $2U$ represent the over-all uncertainties, $\pm U$, pertaining to the adopted values. It is concluded that the standard has not changed.

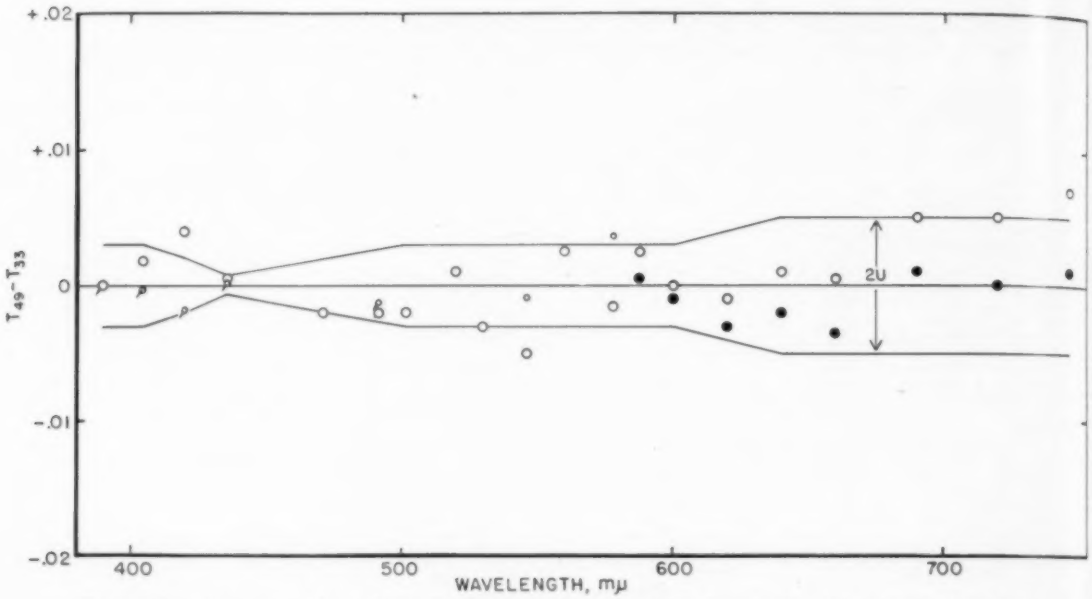

FIGURE 4. *Permanence of a carbon yellow glass standard kept in the Bureau files with only occasional use.*

The open circles represent differences between values of transmittance obtained in 1949 on the Beckman photoelectric (large circles) and the König-Martens visual (small circles) spectrophotometers and values adopted in 1933 from measurements made on the König-Martens and the Gibson spectrophotometers. The solid circles represent values of $T_a - T_o$, the adopted values having undergone slight revision in 1940. The boundaries designated as $2U$ represent the over-all uncertainties, $\pm U$, pertaining to the adopted values. It is concluded that the standard has not changed.

and personnel. At present the values for the issued standards are measured on the Beckman spectrophotometer [2, 7] by direct comparison with the carefully calibrated Bureau standards of the same type. The uncertainty of this comparison is very small, and the uncertainties as reported in the certificates are always large enough to cover this final step. In addition, an absolute determination of transmittance is usually made on each issued standard on the König-Martens visual spectrophotometer [8] at a few wavelengths, this serving continually also as an indirect check on the stability of the Bureau standards.

The intent in the use of the issued standards by those receiving them should be not to correct the photometric scale of the spectrophotometer but to check it. If the instrument gives values on the standard that are in agreement with those reported, within the combined uncertainties, the instrument presumably is functioning correctly and can be expected to give reliable results. If the values obtained are outside of the combined uncertainty, the user should attempt to eliminate the cause of the error. The issued standards are hardly adequate to use as a means of correcting the photometric scale, a possible exception to this occurring for low values of transmittance. For example, the error found by use of the standards might be caused by stray radiant energy, wide slits, or wavelength errors. If important, one should attempt to eliminate the cause, not attempt to correct the photometric scale, which may be wholly reliable.

Regarding selection of these standards by those who wish to check the photometric scale of their spectrophotometers, it is generally found that two are sufficient, (1) the carbon yellow and (2) either the cobalt blue or the copper green, depending on the desires of the user. The cobalt blue is useful for checking the photometric scale near the values $T=0.01$ or $-\log_{10}T=2.00$. The selenium orange has not proved useful for this purpose and its purchase is not recommended. Only a few have been issued.

III. Permanence of Unexposed Samples

The pairs of glasses originally selected for retention as Bureau standards have been kept mostly in the files, with only occasional use and

with no excessive exposure to radiant flux. In 1933 these glasses had been carefully measured on the König-Martens visual and Gibson photoelectric [9] spectrophotometers at the various selected wavelengths from 390 to 750 mμ, and values of spectral transmittance adopted at that time. After the intervening 16 years, one of each of these pairs of glasses was remeasured in 1949, and the comparison of these results with those adopted in 1933 is given in this section.

The glasses selected for this comparison are designated as Corning G55A α^{11} (cobalt blue), Corning HT Yellow α^{7} (carbon yellow), and Jena BG 14^{1} (copper green). The spectral transmittances of these glasses are shown in figure 1 (the upper of the two light-weight curves in each case). (As noted above, the Jena OG3 glasses have proved to have little use as spectrophotometric standards, and no investigation of their permanence has been made.) The most certain test of permanence would have been to remeasure these glasses on the same instruments and under the same instrumental conditions as were used in the original measurements. The older methods are slower, however, particularly the visual, and in the hopes of expediting the work the three samples were measured on the more rapid Beckman spectrophotometer. These measurements were on an absolute basis, not relative to any other standard, and were made with the samples at 25° C as in the previous measurements. They did, in fact, show that the samples had in all probability not changed, but it proved necessary also to make some additional measurements on the König-Martens for greater certainty, particularly at the low transmittances.

The results could be illustrated in various ways, but the most suitable appears to be that used in figures 2, 3, and 4. In these figures there are shown the differences between the values of spectral transmittance measured on the Beckman or König-Martens spectrophotometers in 1949, and as adopted in 1933 from the measurements made on the König-Martens and Gibson spectrophotometers. These differences are designated as $T_{49}-T_{33}$ and are plotted as circles. In the same figures there are shown the over-all uncertainties, $\pm U$, that are usually reported on the issued standards and that would apply closely to the adopted values. If the 1949 values fall within these uncertainties there would be no certainty of change in the transmittance having occurred. Furthermore, at least an equal over-all uncertainty should be assumed for the 1949 values, so that deviations up to twice the plotted uncertainties would not give certain indications of change.

As may be seen, the values of $T_{49}-T_{33}$ in most cases fall within the over-all uncertainties plotted. In those instances where the values fall outside, the evidence, such as it is, is nullified by the other measurements shown.

With special reference to figure 4, Corning HT Yellow α^{7}, the values adopted in 1933 were revised slightly in 1940 at the longer wavelengths on the basis of some measurements made at that time, and in figure 4 the values of $T_{49}-T_{40}$ are also shown. It is not believed that the sample changed between 1933 and 1940, but it was felt in 1940 that the revised values were slightly more accurate than the 1933 values. Note, however, that the values of $T_{49}-T_{33}$ exceed the uncertainties only at 750 mμ.

It seems fair to conclude that the spectral transmittances of these standards have not changed over this 16-year period.

IV. Accelerated Exposure Tests

It was desired that the accelerated exposures should be made under conditions not too widely different from ordinary indoor conditions. The samples were accordingly placed in a small box with a plate glass cover, which was kept outside of a south window on the fourth floor. The samples were thus exposed to daylight, including sunlight, from the south half of the sky, in all kinds of weather. However, the plate glass and box kept the samples dry at all times. The plate glass further served to keep the solar ultraviolet radiant flux of the shortest wavelengths from the glasses, since conditions would otherwise not have been comparable with those indoors. Small holes in the box permitted circulation of air in and out of the box and helped to prevent condensation of moisture on the plate glass cover.

These exposure tests were made with carbon yellow, copper green, and cobalt blue glasses similar to the respective standards. No corresponding tests have been made of the selenium orange glass. Measurements on the three glasses were made prior to the start of the exposures and further measurements have been made after the

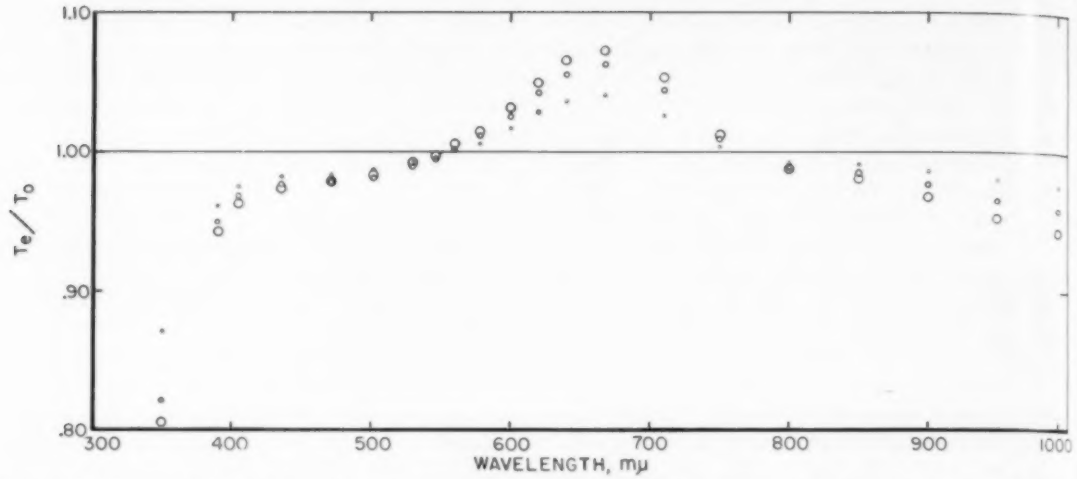

FIGURE 5. *Change of spectral transmittance of a copper green glass (similar to the standards) upon exposure under glass to south skylight (including sunlight).*

T_e/T_o is the ratio between the transmittance after exposure (T_e) and the transmittance before exposure (T_o). The small circles are for an exposure of 3 months, the intermediate circles for 1 year, 8 months, and the large circles for 2 years, 8 months. At 334.2mμ the respective ratios are 0.39, 0.25, and 0.21.

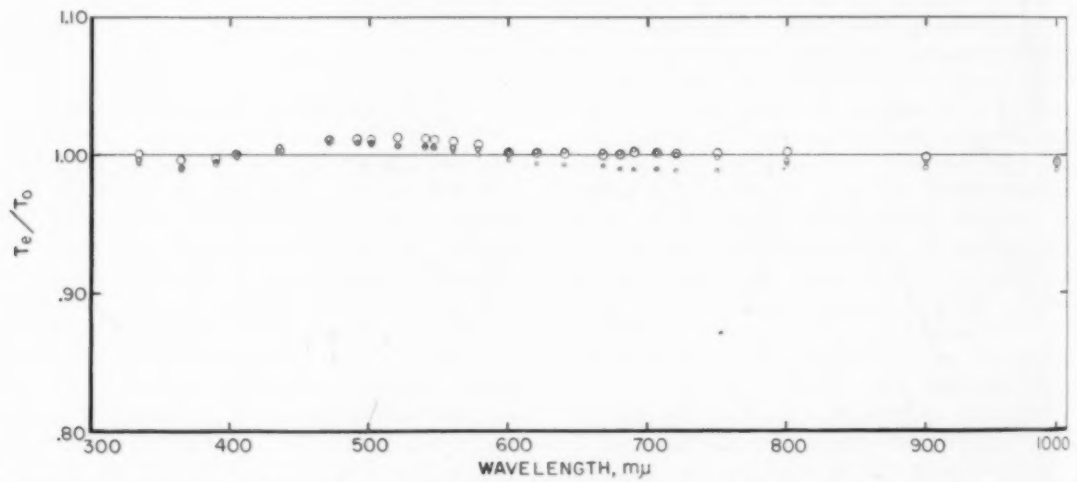

FIGURE 6. *Change of spectral transmittance of a cobalt blue glass (similar to the standards) upon exposure under glass to south skylight (including sunlight).*

T_e/T_o is the ratio between the transmittance after exposure (T_e) and the transmittance before exposure (T_o). The small circles are for an exposure of 3 months, the intermediate circles for 1 year, 8 months, and the large circles for 2 years, 8 months. The "changes" barely exceed the uncertainties of measurement.

periods indicated. All measurements were made at 25° C.

The results are illustrated in figures 5, 6, and 7. Differing from figures 2 to 4, the ordinates of these figures are plotted as ratios rather than differences. These ratios are the values of transmittance measured after the indicated exposures divided by the respective values of transmittance before the exposures began. Since all of these measurements, initial and after exposure, were made on the Beckman spectrophotometer relative to a closely similar reference glass, the precision of measurement was higher than obtainable in figures 2 to 4, in which the measurements were

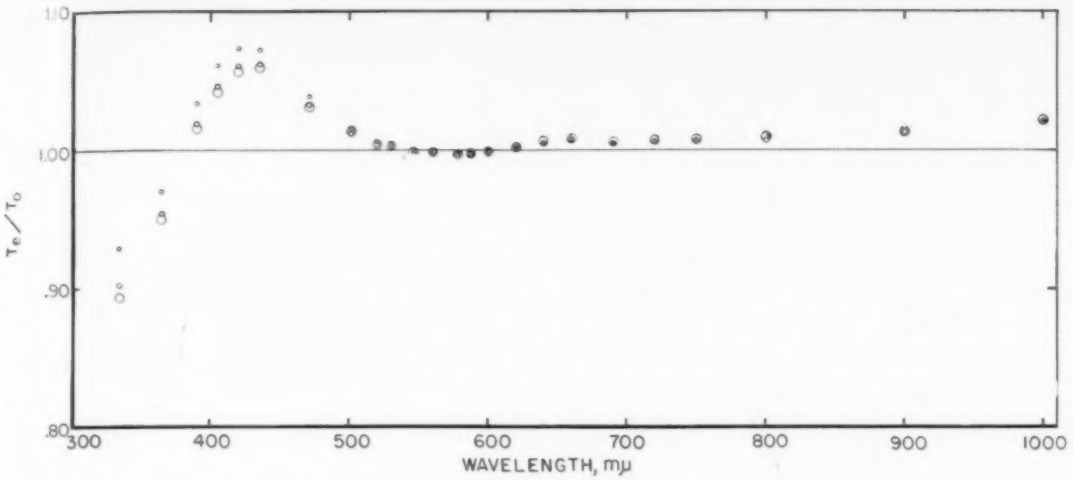

FIGURE 7. *Change of spectral transmittance of a carbon yellow glass (similar to the standards) upon exposure under glass to south skylight (including sunlight).*

T_e/T_o is the ratio between the transmittance after exposure (T_e) and the transmittance before exposure (T_o). The small circles are for an exposure of 3 months, the intermediate circles for 1 year, 8 months, and the large circles for 2 years, 8 months. Note that between 400 and 500mμ the values of T_e/T_o are greatest for the shortest exposure.

made on an absolute basis, no reference standard being involved.

It is probable that all changes indicated in figures 5 to 7 outside the value 1.00 ± 0.01 are certain, and in fact the consistency of the data in some cases indicates that the changes are real even though less than 1 percent.[3]

Perhaps the most important conclusion to be drawn from figures 5 to 7 is that, in view of the small changes that occurred between 390 and 750 mμ, the wavelength range for which the issued standards are customarily certified, one would not expect the issued standards to show changes with ordinary laboratory use. In this respect the data of figures 2 to 4 and 5 to 7 may be said to be consistent, and thus the assumption made, or perhaps we should say the result hoped for, in 1933 has been corroborated.

A few details relating to figures 5 to 7 may be noted.

1. In the ultraviolet between 334.2 and 400 mμ the copper green glass, figure 5, shows a large solarization effect of the usual type, the carbon yellow glass, figure 7, a small one, and the cobalt blue glass, figure 6, none at all. It is possible, of course, that the cobalt blue glass might solarize at shorter wavelengths. Those interested in this effect should read the papers by Coblentz and Stair, who made an extensive study of the ultraviolet solarization of window glasses and other materials [10, 11].

2. The changes in the cobalt-blue glass, figure 6, are small throughout, with extremes barely exceeding 1 percent. While some of the changes shown are probably real, further work would be necessary to indicate whether the rather erratic behavior shown by the curves are significant. The changes, if real, are certainly not important for this purpose, and no further measurements are contemplated.

3. The changes in the copper green glass shown by the curves of figure 5 are undoubtedly real, but again are of little importance (above 390 mμ) in view of the extent of the exposure necessary to bring them about.

4. The major changes shown by the carbon yellow glass of figure 7 are also undoubtedly real. Again these would not be judged of much importance in this connection except for the fact

[3] It may be noted that the ratios shown in figures 5 to 7 must be multiplied at each wavelength by the respective values of transmittance shown in figure 1 to obtain values of ΔT comparable with those shown in figures 2 to 4. For example, in figure 5 at 680 mμ the ratio, T_e/T_o, for 3 months exposure is 1.041. From figure 1, $T_o = 0.115$ (for a different sample of the same type). $T_e - T_o = (T_e/T_o)T_o - T_o = 1.041 \times 0.115 - 0.115 = 0.120 - 0.115 = 0.005$. From figure 2 the value of ΔT at 680 mμ $= \pm 0.002$. That is, *after 3 months of exposure*, the change produced is only 2½ times the uncertainty in absolute measurement shown in figure 2. A further illustration is given later in this paper for the carbon yellow glass.

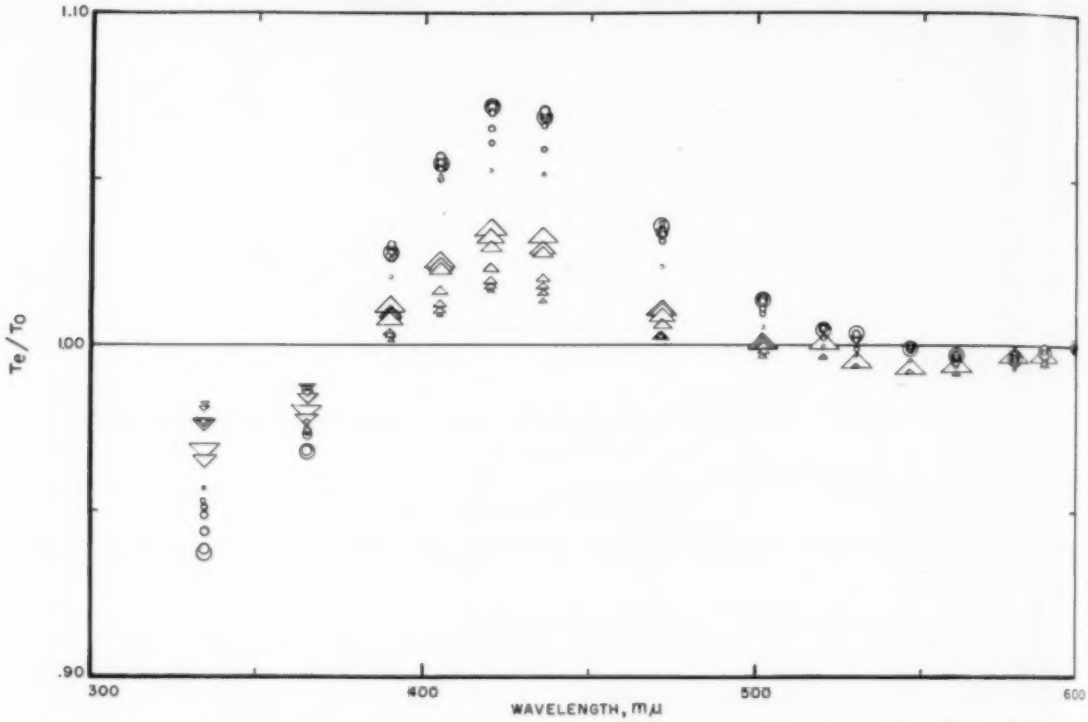

FIGURE 8. *A repetition of figure 7 over the range from 300 to 600 mμ, with other similar carbon yellow glasses and shorter exposures.*

Small to large circles represent exposures of 10, 17, 27, 32, 38, 45, and 53 days. Small to large triangles represent exposures of 1, 2, 3, 4, 5, 6, and 7 days. Note that below 500 mμ there is a definite change upon exposure to sunlight of only one day.

that all of the change occurred during the first summer of exposure, there being in fact a slight recovery shown by the later measurements. Another sample was accordingly selected and measurements made at the intervals shown in figure 8. These results show that the large change between 400 and 500 mμ starts immediately upon exposure and is half completed within 8 days after start of the exposure. One would therefore recommend that this glass not be left around where sunlight or other strong radiant flux might irradiate it. At that, however, only at 435.8 mμ do the changes shown in figures 7 and 8 greatly exceed the over-all uncertainties shown in figure 4.[4]

[4] This is shown by three examples: (1) The transmittance of this glass at 435.8=0.040. 1.07×0.040=0.0428. 0.0428−0.040=0.0028, which is four times the tolerance shown in figure 4 at 435.8 mμ. (2) At 420 mμ T=0.035 and the resulting change in T=0.0025 compared with an uncertainty of 0.002 in figure 4. (3) At 501.6 mμ T=0.254 and the resulting change in T=0.004, compared with an uncertainty of 0.003 in figure 4.

Acknowledgment is made to various individuals who have cooperated in this work. Most of the original measurements were made by Geraldine Walker Haupt and Mabel E. Brown, as indicated by reference [1]. Recordings of the spectral transmittances of the standards were made at various times by Harry J. Keegan. Recent calibrations of new standards of the same type of glass were made by Margaret M. Balcom and Lois Peterson Gloster, as indicated in reference [2]. Miss Peterson also made new and more precise determinations of the change of transmittance with temperature than had been possible with the previous instruments, and made the initial measurements on the exposure tests.

V. References

[1] K. S. Gibson, G. K. Walker, and M. E. Brown, Filters for testing the reliability of spectrophotometers, J. Opt. Soc. Am. **24**, 58 (1934).

[2] K. S. Gibson and M. M. Balcom, Transmission measurements with the Beckman quartz spectrophotometer, J. Research NBS **38,** 601 (1947) RP1798; J. Opt. Soc. Am. **37,** 593 (1947).

[3] Standards for checking the calibration of spectrophotometers, NBS Letter Circular, LC929 (1948).

[4] K. S. Gibson, Spectrophotometry (200 to 1,000 millimicrons), NBS Circular C484 (1949).

[5] Terminology and symbols for use in ultraviolet, visible, and infrared absorptometry. NBS Letter Circular, LC857 (1947).

[6] M. Merriman, A textbook on the method of least squares, 8th ed., rev. (John Wiley & Sons, Inc., New York, N. Y., 1911).

[7] H. H. Cary and A. O. Beckman, A quartz photoelectric spectrophotometer, J. Opt. Soc. Am. **31,** 682 (1941).

[8] H. J. McNicholas, Equipment for routine spectral transmission and reflection measurements, BS J. Research **1,** 793 (1928) RP30.

[9] K. S. Gibson, Direct-reading photoelectric measurement of spectral transmission, J. Opt. Soc. Am. & Rev. Sci. Instr. **7,** 693 (1923).

[10] W. W. Coblentz and R. Stair, Data on ultraviolet solar radiation and the solarization of window materials, BS J. Research **3,** 629 (1929) RP113.

[11] W. W. Coblentz and R. Stair, Ultraviolet transmission changes in glass as a function of the wavelength of the radiation stimulus, J. Research NBS **13,** 773 (1934) RP744.

WASHINGTON, December 20, 1949.

U. S. Department of Commerce
National Bureau of Standards

Research Paper RP2094
Volume 44, May 1950

Part of the Journal of Research of the National Bureau of Standards

A 600-Ohm Multiple-Wire Delta Antenna for Ionosphere Studies

By H. N. Cones, H. V. Cottony, and J. M. Watts

This paper describes the design and the performance of a multiple-wire delta antenna developed for use with high output impedance, vertical-incidence ionosphere sounding equipment. Graphs are presented showing the terminal impedance of this antenna over the separating frequency range (1 to 25 megacycles), using various lengths of open-wire transmission line. The results of pattern measurements using model techniques are given, showing the expected radiation characteristics of the full-scale antenna. A practical test of the comparative merits of the antenna is described in which ionosphere records obtained by the use of this antenna are compared with those obtained by the use of a larger antenna developed previously.

I. Introduction

During the past 20 years the technique of vertical-incidence ionosphere soundings by the use of pulse transmitters scanning over a wide frequency range has been adopted internationally for recording the virtual height of ionosphere layers and their degree of ionization. These are to be used in predicting the conditions for communication in the high-frequency band. One of the latest developments in the equipment employing this technique is exemplified by the model C-2 automatic ionosphere recorder. This instrument was developed at the Central Radio Propagation Laboratory of this Bureau. It scans through the frequency range of 1 to 25 Mc in an interval of time as short as 7½ secs. The performance requirements imposed by the equipment on the antenna system, including the associated transmission lines, which are to hold over the entire frequency range of 1 to 25 Mc, are as follows: (1) The impedance of the antenna system must be relatively uniform and, for purposes of maximum power transfer, as nearly equal to the output impedance of the transmitter (of the order of 1,000 ohms) as possible; (2) the radiation must be substantially in the vertical direction; (3) the antenna must be as efficient a radiator as possible. In addition to the operating requirements above, the physical dimensions of the antenna should be moderate, at least in the vertical dimension.

Numerous experimenters have worked on the problem of the design of antennas suitable for ionospheric recorders. Systems of several antennas, each operating over a fairly narrow frequency range and switched automatically by the equipment, have been tried. Some systems obtained satisfactory operation over a fairly wide frequency band by employing low-Q cage antennas. Even antennas that changed their dimensions in the course of operation are known to have been tried. The most generally satisfactory results have been obtained by the use of nonresonant antennas, such as rhombic and vee antennas. These are particularly suitable for use with the model C–2 ionosphere recorder because of their inherently high input impedances. Experimental work has been carried out at this Bureau looking toward the development of an effective antenna system for ionosphere sounding. Some of the results of this work have already been published.[1] Here, the results of the work performed since the date of that paper are described.

[1] H. N. Cones, Impedance characteristics of some experimental broadband antennas for vertical-incidence ionosphere sounding, J. Research NBS 43, 71 (1949) RP2006.

II. Instrumentation

As mentioned previously, the important aspects of the antenna to be considered are its impedance, its radiation pattern, and its radiation efficiency. The last factor may be defined as the ratio of the power radiated in space by the antenna to the power delivered to it by the transmitter. This factor is of particular significance in a nonresonant, terminated antenna where actually more power is likely to be dissipated in the terminating resistor than radiated in space.

For measurements of antenna impedance, a balanced recording impedance meter developed at this Bureau was used. A description of this instrument was presented at the Winter 1946–47 IRE Convention in New York City.[2] Figure 1 is the block diagram of the instrument. Briefly, it is a beat frequency generator including a 57-Mc fixed-frequency oscillator beating with a variable frequency oscillator covering the band from 57 to 82 Mc. The difference frequency of 0 to 25 Mc is passed through a wide-band amplifier designed to have a constant current output. The output voltage is, therefore, directly proportional to the absolute magnitude of impedance connected across the output terminals. A voltage stabilizing circuit is incorporated for the purpose of maintaining reasonably constant output current. This voltage is rectified, amplified, and applied to a recording milliammeter. The recording milliammeter and the variable frequency oscillator are mechanically coupled, so that the impedance is plotted as a function of frequency. No direct indication of the phase angle of the impedance has thus far been provided. The instrument is calibrated by making several frequency sweeps using fixed noninductive resistors across the measuring terminals.

For measurement of the radiation pattern of the antenna, a model antenna technique has been employed. The principles of this technique consist briefly of constructing a model antenna having the configuration of the full-sized antenna under study, but with the linear dimensions reduced by some scaling factor n. The radiation pattern of this antenna is then measured in a conventional manner at a frequency n times the operating frequency of the full-sized antenna. It thus becomes possible to bring the target transmitter much closer physically to the antenna under test and still maintain a spacing of several wavelengths at the scaled-up frequency. The dimensional analysis of this technique shows that in addition to scaling the linear dimensions down by a factor n, and the frequency up by n, the conductivity should be increased by the same factor n. This scaling factor should be applied to all elements of the radiating system. The radiating system is not merely the antenna itself, but also the ground and, insofar as the conductivity is concerned, the scaling factor should, properly, be applied to both the material of the antenna (copper) and the soil. It is patently not possible to select a material having conductivity exceeding that of copper by any scaling factor n. However, at least in the present case where copper losses may reasonably be expected to be small compared with the radiated power and the terminal resistor losses, no significant error should be introduced by the failure to scale the conductivity.

In the case of the ground, the conductivity should be scaled if strictly accurate results are to be obtained. However, no completely satisfactory method for scaling the ground constants was available. Furthermore, since the ground constants change from one location to another, and, in general, will also change to some extent in a given location with time, no attempt was made in course of these tests to scale the ground constants. Instead, the ground was covered by a wire netting that effectively provided perfect reflector conditions at all frequencies. This, of course, is an approximation of the actual operating conditions. The principles of model technique are now well known and are described in the technical literature.[3] [4]

The actual model range employed in these tests consists of a level gravelled surface, covered by a ½-in. wire mesh. In practice the model of the antenna was used as the receiver, while a target transmitter, powered by self-contained batteries, was swung about the antenna in an arc approximately 13 ft in radius. To simulate the frequencies of 9 to 25 Mc, a scaling factor of n equal to 30 was employed, the target transmitter operating between 270 and 750 Mc. To simulate operation

[2] H. V. Cottony, A method of rapid continuous measurement of antenna impedance over a wide frequency range, paper presented before IRE Convention (New York, N. Y., March 6, 1947).

[3] Ernest A. Jones, Final report on investigation of model techniques for determination of the characteristics of low-frequency antennas, Ohio State University Research Foundation (Columbus 10, Ohio).

[4] George Sinclair, Theory of models of electromagnetic systems, Proc. IRE **36**, No. 11, 1364 to 1370 (Nov. 1948).

between 5 and 9 Mc, a scaling factor of 85 was employed.

Figure 2 illustrates the terminology employed with reference to the radiation patterns presented in this paper. It is convenient, for reference purposes, to locate the antenna under test in the *X-Z* plane. That plane and the *Y-Z* plane at right angles to it are the principal planes of the antenna, and all radiation patterns were taken in one or the other of the two planes, and are so identified. In making the patterns of the antenna in the *X-Z* plane (path *X-Z-X'*), the plane of polarization of the target transmitter was always coincident with the *X-Z* plane, and its equatorial magnetic plane always passed through the *Y-Y'* axis. For patterns in the *Y-Z* plane, (path *Y-Z-Y'*), the *X-X'* axis was always in the plane of polarization, whereas the equatorial magnetic plane was coincident with the *Y-Z* plane.

No direct measurements of radiation efficiency were made. However, a measure of over-all performance of the antenna (including its radiation efficiency) was obtained in a series of tests, in which the antenna under discussion was compared with an earlier type of antenna and with a number of simple doublets. In these tests an ionosphere recorder was alternately switched from the multiple-wire delta to a double-*W* antenna (see footnote 1). In each test a number of records were obtained and the results compared with each other. This method does not permit measurement of small differences but is a useful check of relative effectiveness of the antennas.

III. Design of the Antenna

Nonresonant antennas, which are sometimes referred to as terminated or traveling-wave antennas, are, in general, of three types: (1) Beverage, (2) vee, and (3) rhombic. Of these, the Beverage antenna is suitable primarily for low-angle radiation. Of the vee and the rhombic antennas, the vee antenna can be shown to be more uniformly effective as a radiator over the frequency range than the rhombic antenna. However, the conventional-type vee antenna with the input terminals at the apex and the terminating resistors at the open end of the vee presents certain mechanical difficulties when designed to radiate in the vertical direction. It requires two full-height poles for its installation, and additional wires must be furnished for termination to ground. For these reasons rhombic antennas have frequently been used for ionosphere sounding.

A variation of a vee antennna commonly known as a delta was devised several years ago by J. W. Cox of the Baddow Research Laboratories of the British Marconi Co. Its principal features are that the termination is made at the vertex of the vee, and the extremities of the vee are brought together by two horizontal wires extending a few feet above ground. The radiation due to these horizontal wires is minimized by their proximity to the ground, and the radiation pattern should be approximately that of a vee antenna.

Practical considerations require a delta antenna to be designed for a much lower height than one having theoretically optimum size and proportions. To be very efficient a nonresonant antenna should be several wavelengths long. Since the equipment operates at frequencies down to 1 Mc, and since the desired direction of radiation is straight up, the antenna must necessarily be short (measured in the desired direction of propagation) as compared to the wavelength except at the upper end of the operating frequency band. This height was limited by the lengths of the readily available telephone poles to 70 ft. In addition, it was highly desirable that the antenna be capable of being connected to the equipment by transmission lines that might differ in length for each ionosphere station according to local conditions. In order that the transmission line need not accentuate the ratio of maximum to minimum impedances of the antenna proper, it is necessary that the geometric mean of these impedances be very close to the characteristic impedance of the line. The geometric mean of the impedance of a simple single-wire delta antenna is of the order of 800 ohms. An open-wire transmission line having this value of surge impedance has awkwardly large wire spacing. A 600-ohm transmission line is, on the other hand, a very common one for which standard commercial spacers are available. Furthermore, 600 ohms is a suitable load impedance for the type C–2 ionosphere recorder. It was, therefore, decided to reduce the mean impedance of the antenna to 600 ohms. Such reduction of impedance is readily accomplished without affecting either the radiation pattern or the mechanical construction by the use of multiple-wire elements. The use of multiple-wire construction offers the additional

880789—50——3

advantage of being able to reduce the impedance variations over the frequency range by varying the spacing of the wires that compose the individual elements.

The height of the apex having been set by practical considerations at 70 ft, it is possible to compute the base width of the antenna so that it is wide enough to give useful radiated power at 1 Mc and yet not so wide as to have the first null or minimum within the operating frequency range of the equipment. Guided by such computations, a number of scaled-down antennas having various base widths were constructed and tested on the model range. The final design selected was one with the largest base width, which had no nulls or minima in the vertical direction at any point in the frequency range. The width so selected was 130 ft measured corner-to-corner.

Following the determination of the major dimensions of the antenna, the task remaining consisted of adjusting the minor configuration of the antenna construction, so that the mean terminal impedance of the antenna would be as nearly 600 ohms as possible and that the impedance of the antenna would be as uniform over the whole frequency range as possible. The approach to this task was largely empirical. By using multiple-wire construction, the impedance was lowered; increasing the spacing between the wires provided an additional control of impedance. Further uniformity of impedance was obtained by varying the spacing between the wires along the length of the antenna. The principle of reducing the reflection along the electric path by varying the spacing between electrically paralleled conductors is well known, and the technique of its application is strictly empirical.

The end result of the experimental work is a 600-ohm multiple-wire delta antenna. Figure 3 shows the principal dimensions of this antenna. For comparison purposes a "double-W" antenna (see footnote 1), developed previously, is illustrated in figure 4.

IV. Performance of the Antenna System

The performance of the antenna system was evaluated by measuring its terminal impedance with three different lengths of 600-ohm transmission line; by measuring the radiation patterns of a model antenna constructed to scale; and by using the antenna in conjunction with a model C-2 automatic ionosphere recorder for making ionosphere records.

Figure 5 presents the terminal impedance of the multiple-wire delta antenna system with three lengths of 600-ohm transmission line, and, for comparison purposes, the terminal impedance of the double-W antenna including the exponential line transformer. As can be observed, the mean impedance of the antenna for all lengths of transmission lines is approximately 600 ohms, and the variations of impedance are between approximately 400 and 1,000 ohms. The performance of the doube-W antenna from the standpoint of terminal impedance is substantially the same; the mean impedance is also very nearly 600 ohms, and the impedance variations are between approximately 400 and 900 ohms. The greater number of impedance variations in the case of the double-W antenna is caused by the longer transmission-line system of that antenna. The exponential line transformer used in the latter is approximately 288 ft in length.

Figure 6, a and b, illustrates the expected radiation patterns of the multiple-wire delta antenna between the frequencies of 5 and 25 Mc, as obtained on the model antenna range. In the frequency range from 5 to 9 Mc a scaling factor of 85 was used, and in the frequency range from 9 to 25 Mc a scaling factor of 30 was used. At 9 Mc the results obtained by the two scaling factors can be checked against each other. It should be noted that the patterns shown are normalized, i. e., the gain of the pattern plotter was adjusted for each frequency to give a full-scale deflection at the point of maximum gain.

Examination of the radiation patterns shows that no significant side lobes are developed in the patterns for frequencies below 11 Mc. Some lobing is observed at the frequencies near 14 Mc. The maximum of the major side lobe is at 54° to the horizontal. It is believed that this lobe is caused by radiation from the horizontal wire.

On the basis of the model measurements, serious lobe splitting would not be expected below 23 Mc. Above this frequency the patterns should rapidly deteriorate. However, even at 25 Mc there can be expected to be considerable useful radiation in the vertical direction.

No patterns have been taken at frequencies corresponding to 12 and 13 Mc because no target

transmitter was immediately available to operate at corresponding scaled frequencies. The patterns obtained at frequencies corresponding to 9 Mc (765 Mc using scaling factor of 85 and 270 Mc for that of 30) agree reasonably well. It should be noted that this is the point of least satisfactory operation for the model range since at a frequency of 270 Mc the target transmitter is only three and one-half wavelengths away from the antenna model under test.

Upon completion of the scale model tests, a practical test of antenna performance was attempted by comparing actual ionospheric records made using the various antenna systems. The comparison was principally between the multiple-wire delta and the double-*W* antennas, both used for transmission; initially horizontal doublets of various lengths were used for reception. A check was also made of the relative merit of the delta antenna as compared with a doublet when used for reception and of the effect of the length of the transmission line on the effectiveness of a multiple-wire delta antenna.

Unfortunately, the reflecting characteristics of the ionosphere may vary in a period of seconds, so that measurements made by comparing received pulse amplitudes by switching from one antenna to another are subject to error. However, it was considered that a series of as many as ten consecutive records using one antenna could be compared with two other series using another antenna—one recorded immediately before and the other immediately afterward. Both receiving antennas and transmitting antennas were compared separately by switching only one of the antennas at a time. Figures 7 through 11 show some of the ionosphere records made for these comparisons. All of the records for each comparison were made with the same receiver gain setting unless otherwise noted.

Figure 7 shows the multiple-wire delta compared with the double-*W* antenna when used for transmission. The records were made in the early morning hours so that observations on low frequencies would be more likely. A long receiving antenna was also used to favor the low frequencies. From the appearance of these records it is concluded that the multiple-wire delta is substantially equal in performance to the double-*W* antenna for transmission between 1.5 and about 3.5 Mc.

Figure 8 compares the same antennas as the previous figure, except that it is intended to compare the double-*W* and multiple-wire delta antennas at higher frequencies. This comparison was made with a shorter antenna for receiving and during a daytime period when critical frequencies were high. The conclusion is that these two antennas are also practically equivalent at frequencies between 3.0 and 12.0 Mc.

Figure 9 is the same as figure 8, except that a long receiving antenna was used. Both sets of records exhibit weaknesses that are primarily a characteristic of the receiving antenna. No conclusions were drawn from these records, but further tests illustrated by figure 10 were suggested by them.

Figure 10 shows the difference between the single-wire delta and a 500-ft doublet for receiving. The receiver gain setting was the same for each run. It may be noted that much greater pickup of both ionospheric signals and noise is obtained with the delta.

Figure 11 is a comparison between the effect of using long and short transmission lines to connect the transmitter to the multiple-wire delta. For receiving, a single-wire delta was erected in a plane perpendicular to that of the transmitting antenna. The records made with a 200-ft line and with a 20-ft line are substantially alike, and the slight differences observable are no greater than the variations from record to record caused by changes in the ionosphere.

V. Conclusions

On the basis of the preceding discussion the following conclusions were reached:

1. The impedance of the multiple-wire delta antenna is reasonably flat in its characteristics over the operating frequency range of 1 to 25 Mc. the ratio of maximum to minimum impedance being of the order of 2.5. This compares satisfactorily with the double-*W* antenna.

2. The mean impedance of the multiple-wire delta antenna is sufficiently close to 600 ohms to permit satisfactory operation with a 600-ohm transmission line of any moderate length. This is also confirmed by the service tests using the ionosphere recorder.

3. The model antenna study of the multiple-wire delta indicates that the radiation pattern to be expected from this design is such that the

direction of maximum intensity of radiation will be at the desired zenith angle over all of the operating frequency range below 23 Mc. However, even at 25 Mc. a substantial proportion of power is radiated in the vertical direction.

4. The ionosphere records obtained by the use of the automatic recorder indicate that, within the limits of the accuracy of this method of comparison, there is little difference in the effectiveness of the multiple-wire delta antenna when compared with the double-*W* antenna, either at the lower or the middle frequency portion of the operating frequency range.

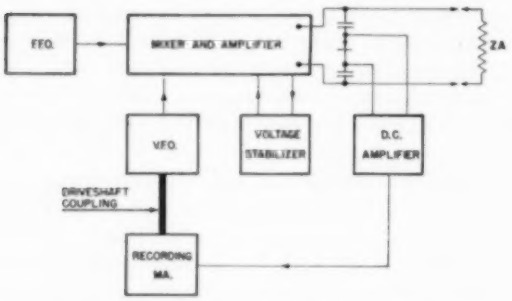

FIGURE 1. *Block diagram of impedance meter.*

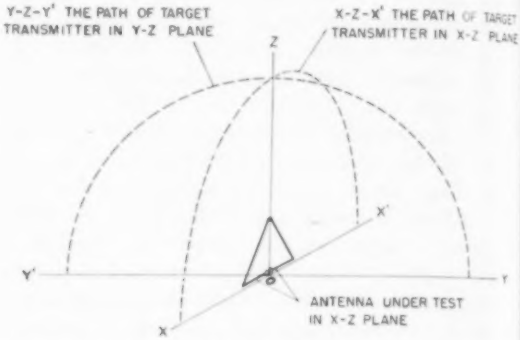

FIGURE 2. *Diagram of the model range showing the paths of the target transmitter with reference to the antenna under test.*

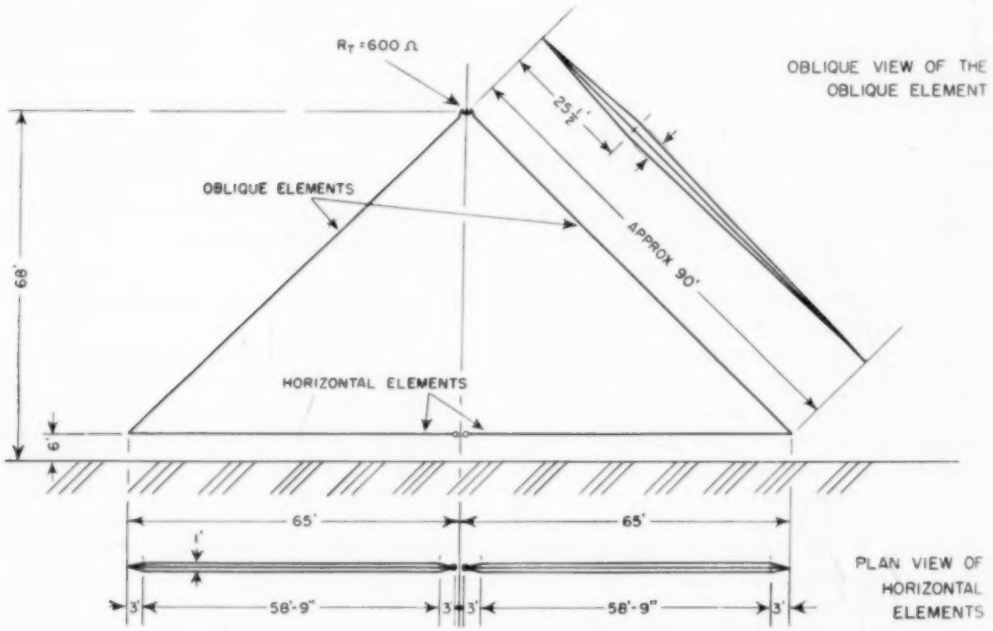

FIGURE 3. *Simplified diagram of the 600-ohm multiple-wire delta antenna.*

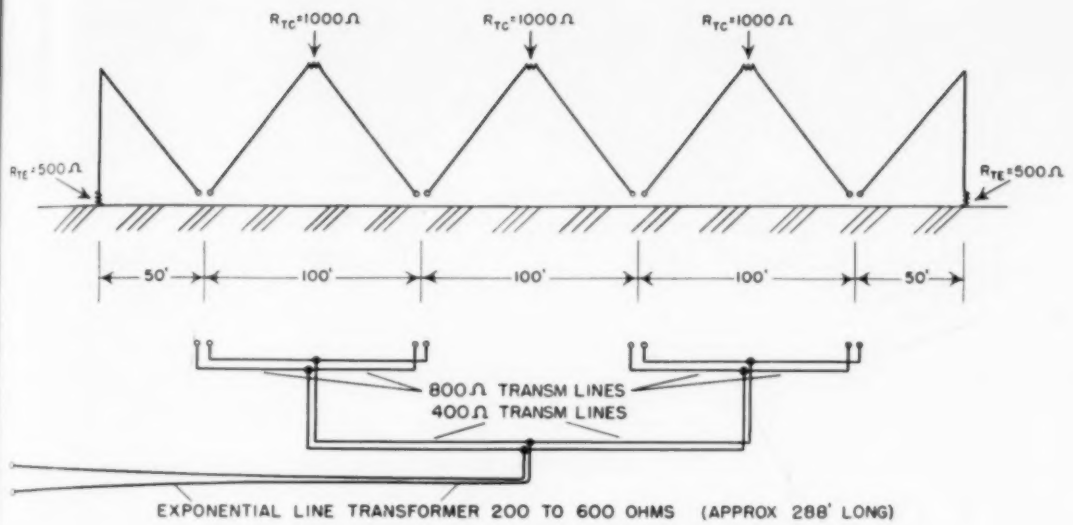

FIGURE 4. *Simplified diagram of the double-W antenna.*

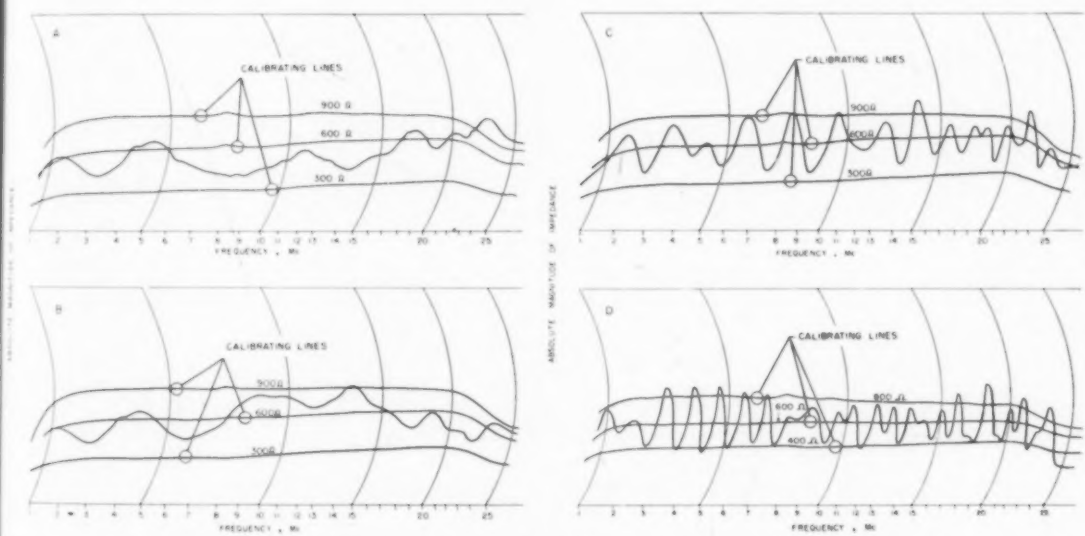

FIGURE 5. *Impedance of 600-ohm multiple-wire delta using three different lengths of 600-ohm transmission line and that of single-wire double-W antenna including exponential line transformer.*

A, Impedance of multiple-wire delta antenna when used with a 4-ft length of 600-ohm transmission line. R_t=600 ohms. *B*, Impedance of multiple-wire delta antenna when used with a 20-ft length of 600-ohm transmission line. R_t=600 ohms. *C*, Impedance of multiple-wire delta antenna when used with a 200-ft length of 600-ohm transmission line. R_t=600 ohms. *D*, Impedance of double-*W* antenna for optimum termination of 1,000 ohms.

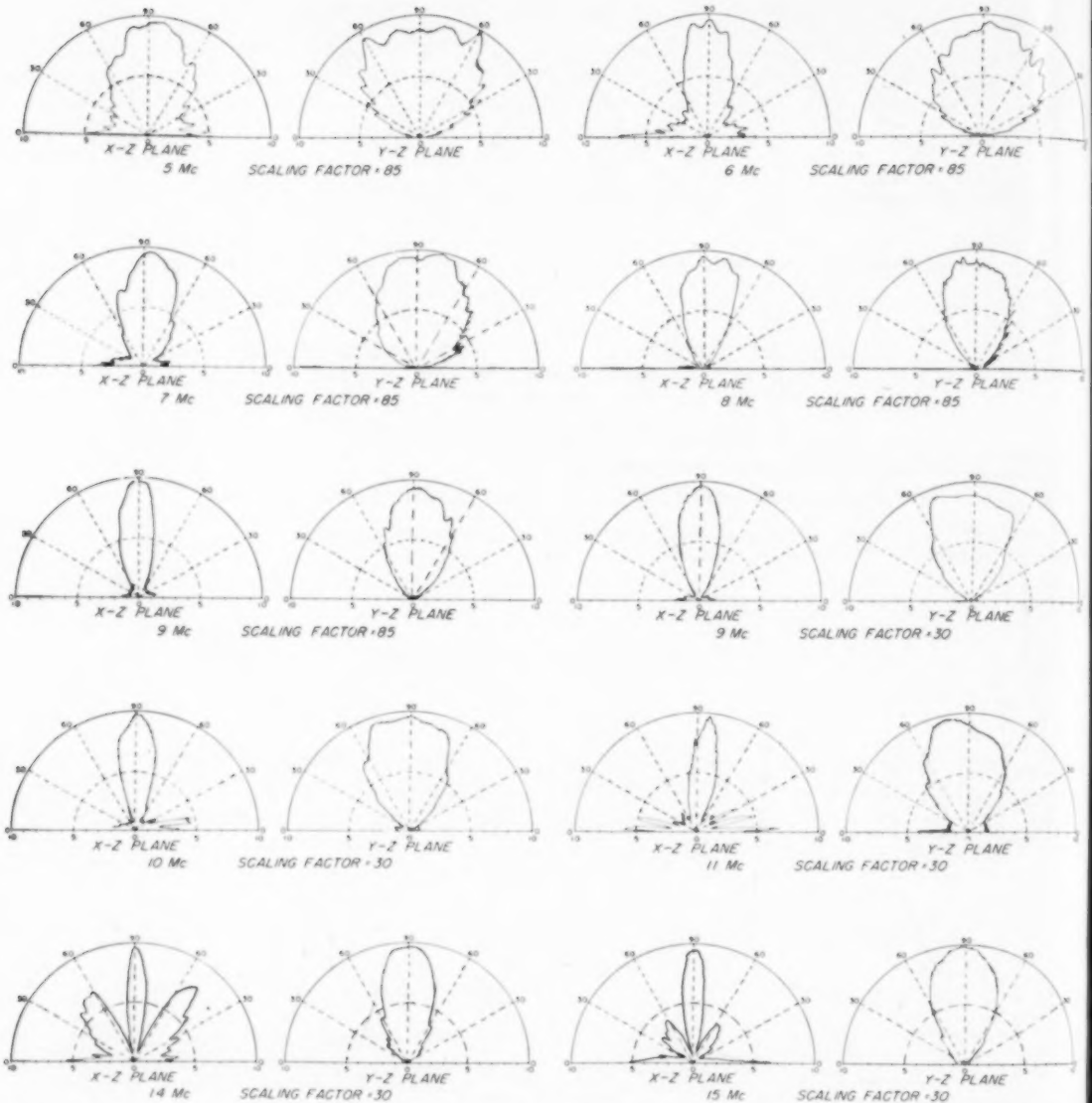

FIGURE 6a. *Normalized radiation patterns in space for multiple-wire delta antenna as obtained by the use of model antenna technique.*

The scaling factor is equal to 30 or 85, as noted at each pattern. The antenna is in the X-Z plane. The radial displacement is linear with power.

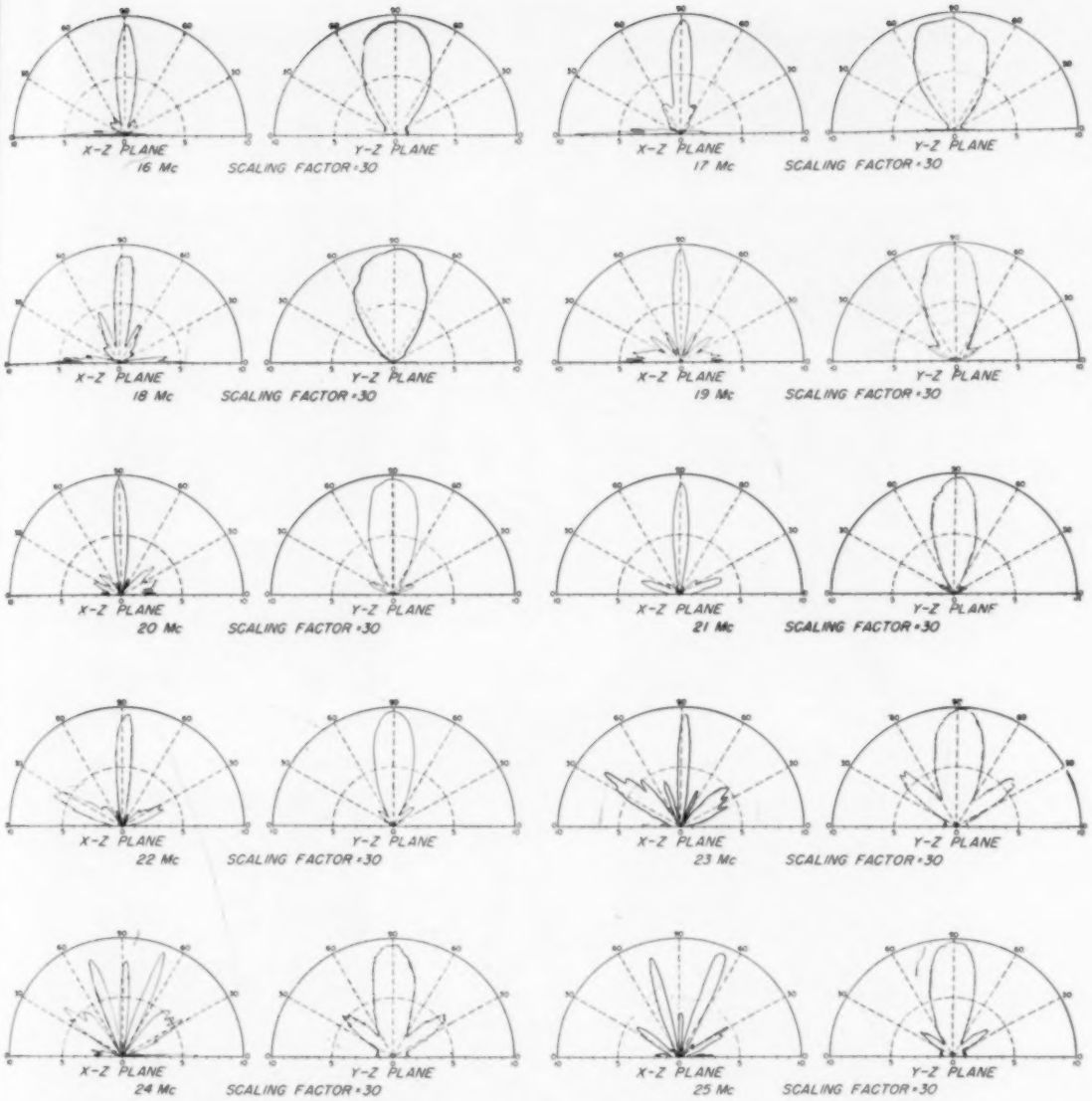

FIGURE 6b. *Normalized radiation patterns in space for multiple-wire delta antenna as obtained by the use of model antenna technique.*

The scaling factor is equal to 30. The antenna is in the *X-Z* plane. The radial displacement is linear with power.

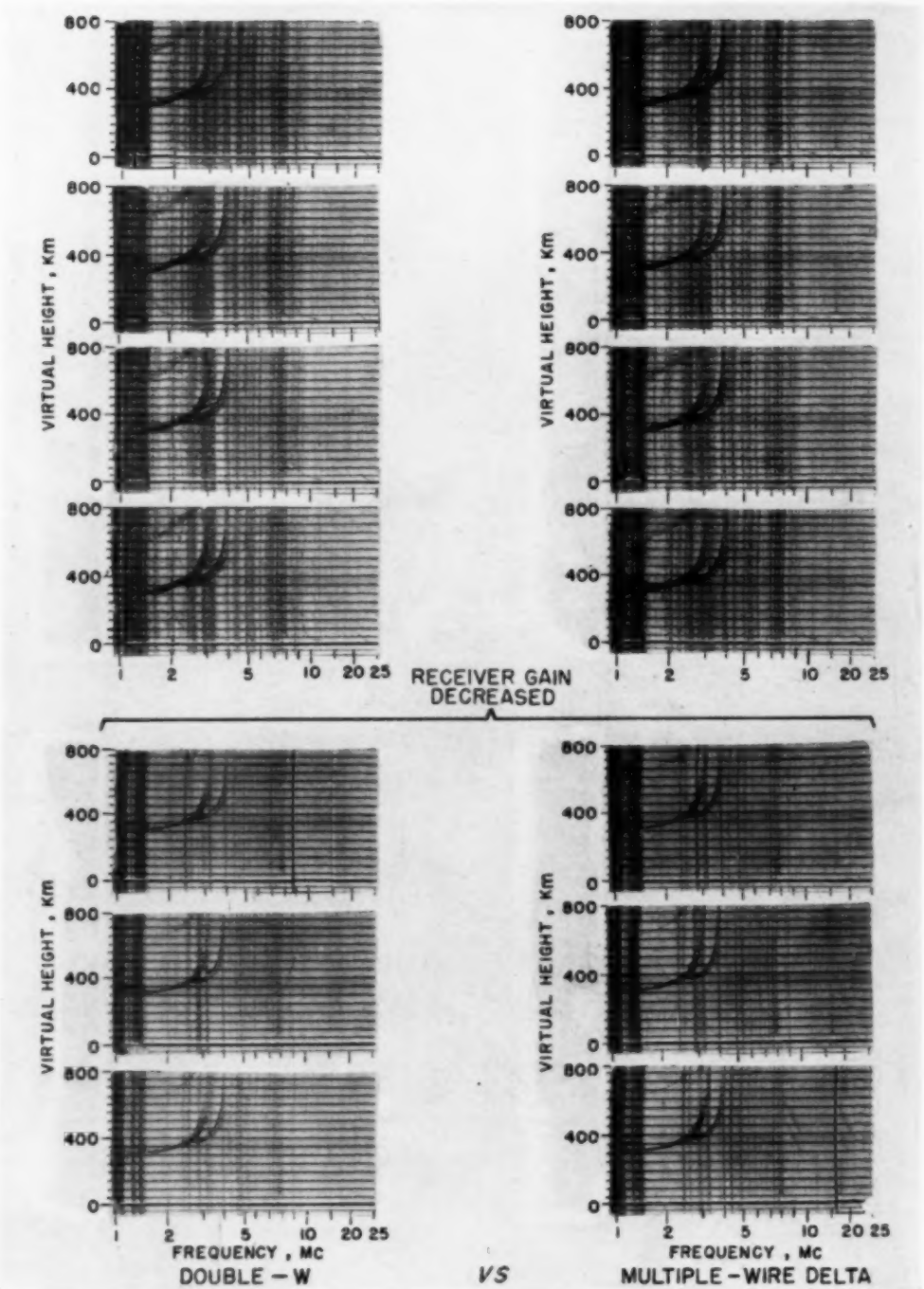

FIGURE 7. *Nighttime comparison of multiple-wire delta with double-W antenna, each used for transmission.*

A 500-ft horizontal doublet, 25 ft above ground was used as a receiving antenna.

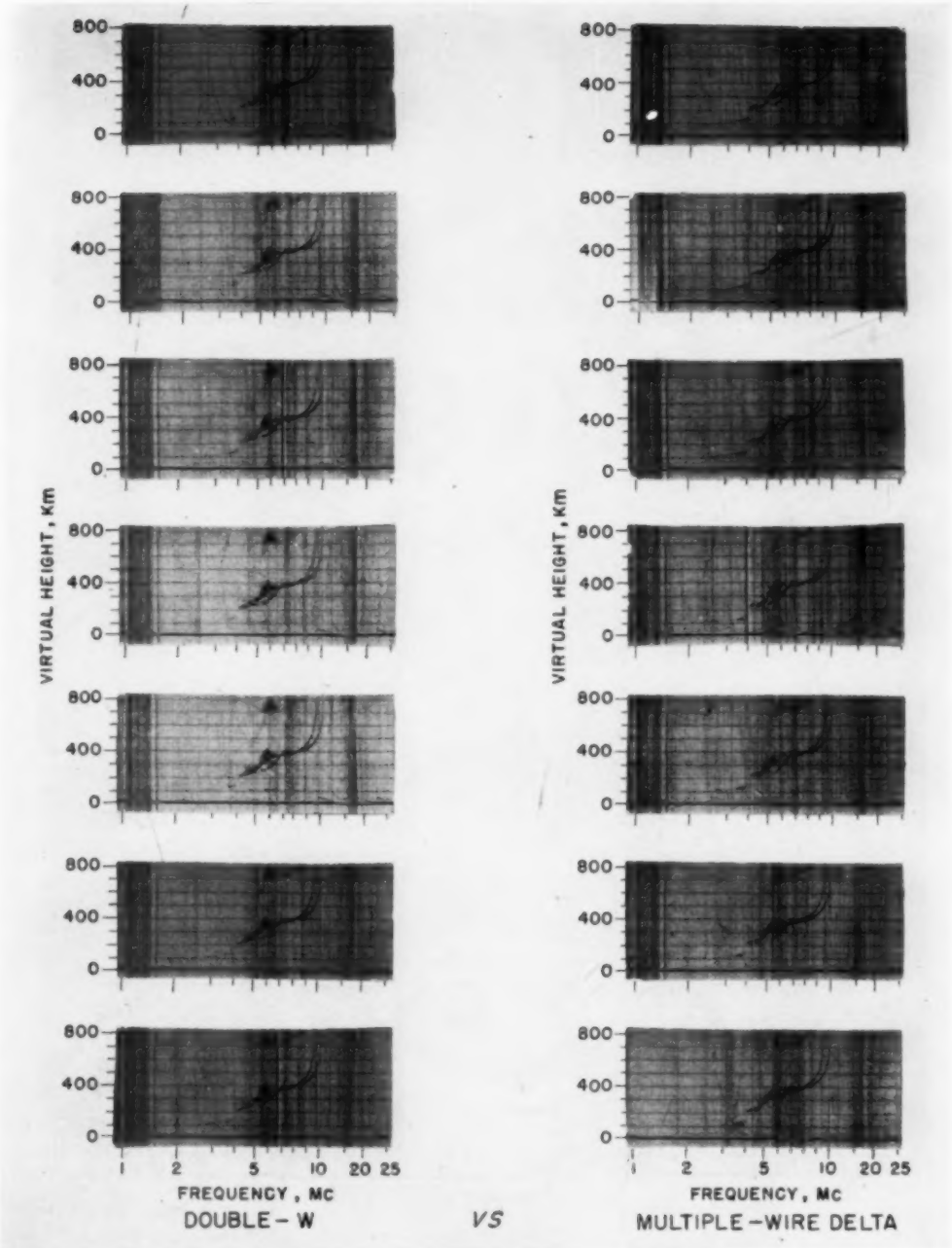

FIGURE 8. *Daytime comparison of multiple-wire delta with double-W antenna, each used for transmission.*

A 150-ft horizontal doublet, 7 ft above ground was used as a receiving antenna.

880789—50——4

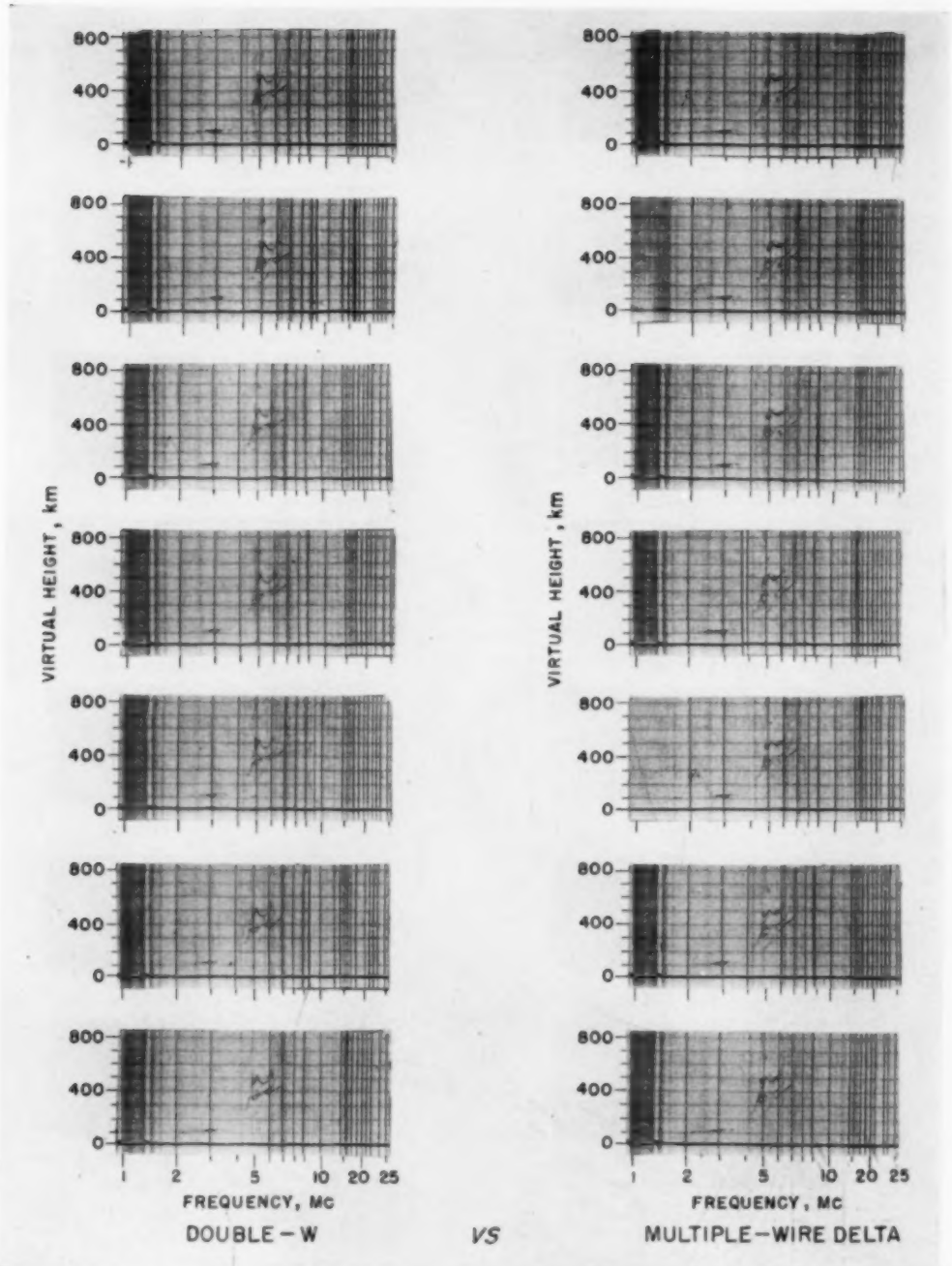

FIGURE 9. *Daytime comparison of multiple-wire delta with double-W antenna, each used for transmission.*

A 500-ft horizontal doublet, 25 ft above ground was used as a receiving antenna.

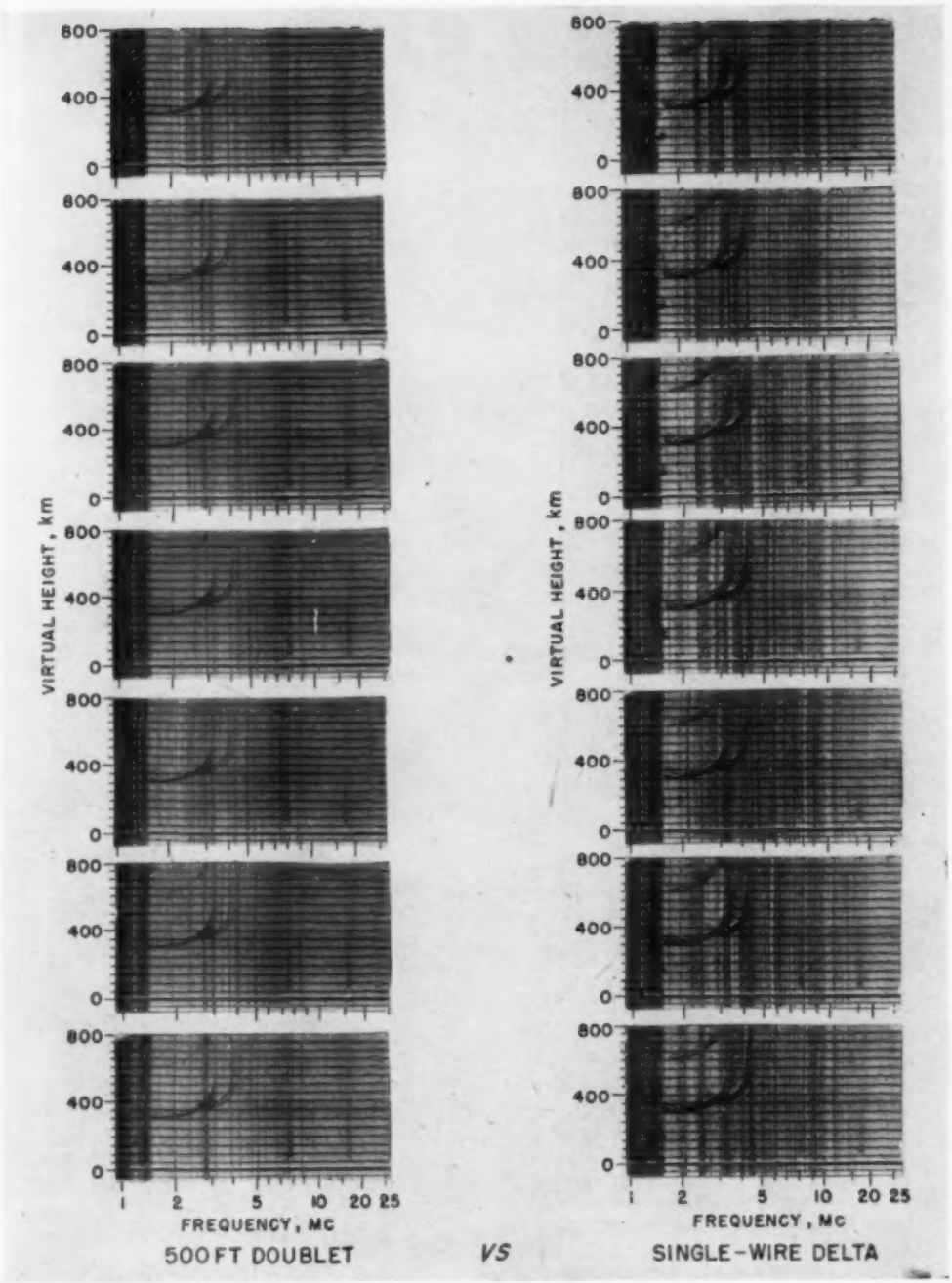

FIGURE 10. *Comparison of single-wire delta antenna with 500-ft doublet each used for reception.*

The multiple-wire delta antenna was used for transmission.

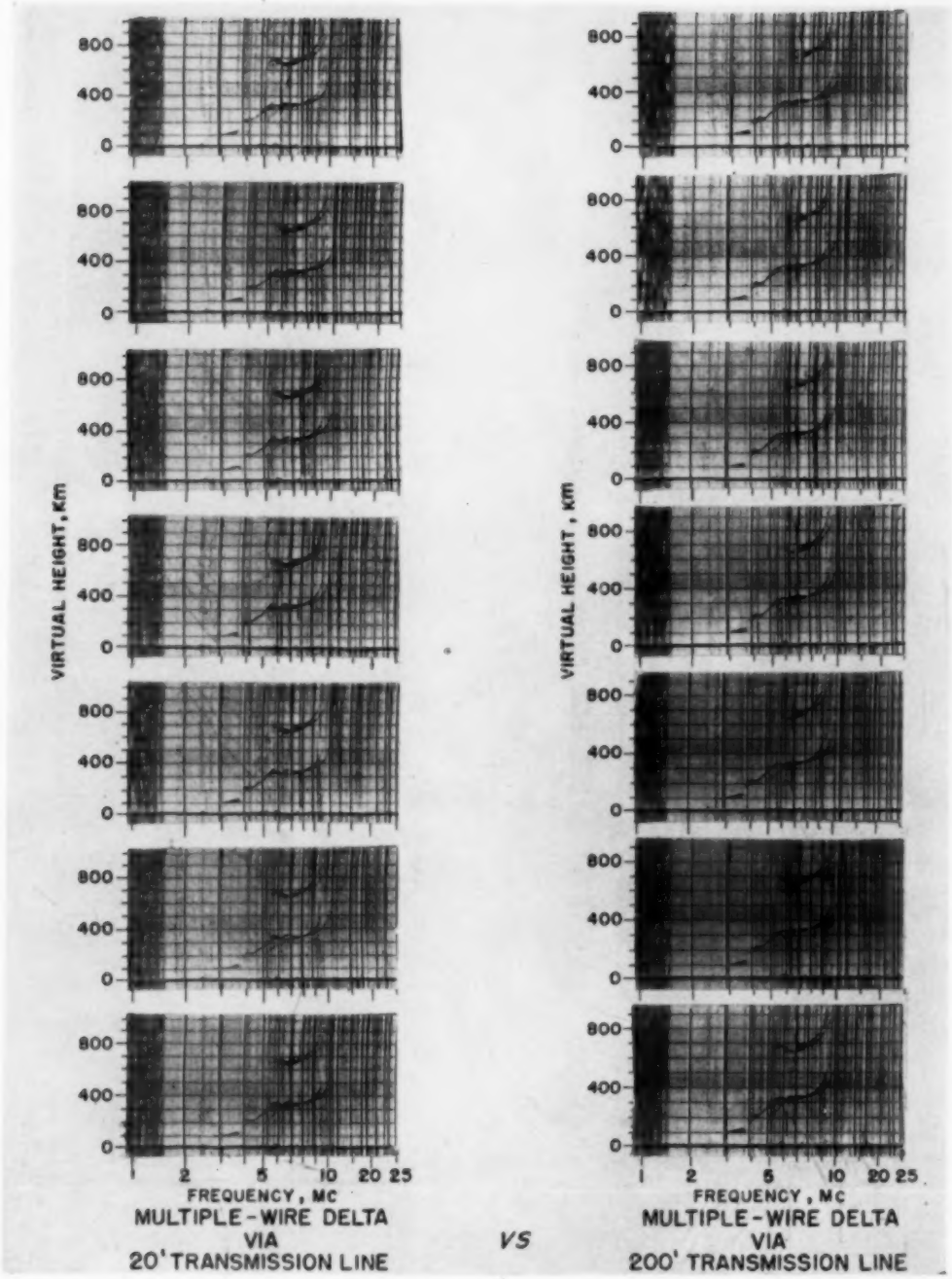

FIGURE 11. *Comparison of multiple wire delta antenna with 20- and with 200-ft lengths of 600-ohm transmission line, in each case used for transmission.*

A single-wire delta was used for receiving.

WASHINGTON, September 20, 1949.

U. S. Department of Commerce
National Bureau of Standards

Research Paper RP2095
Volume 44, May 1950

Part of the Journal of Research of the National Bureau of Standards

Mass Spectra of Diborane-d_6 and Ethane-d_6

By Vernon H. Dibeler, Fred L. Mohler, and Laura Williamson

The complete mass spectra of B_2D_6 and C_2D_6 and the partial spectrum of B_2D_5H have been obtained for ionizing voltages of 50 volts and 70 volts. An analytical procedure is given for deriving the contribution of all ions containing a hydrogen atom from the poly-isotopic spectrum of a mixture of B_2D_6 and B_2D_5H. A comparison of spectra of B_2D_6 and B_2H_6 and of C_2D_6 and C_2H_6 indicates that substitution of deuterium for hydrogen has only a slight effect on the dissociation probabilities in diborane and ethane. An exception is the occurrence of a metastable transition in B_2D_6 that does not occur in B_2H_6 viz $B_2D_5^+ \rightarrow B_2D_3^+ + 2D$.

Simple statistical considerations, based upon the assumption of equal probabilities for the removal of a deuterium or a protium, give a dissociation pattern that differs by more than experimental error from that observed.

I. Introduction

A number of theories have been proposed [1] [1] on the structure of electron-deficient molecules, particularly the hydroborons. Of these, the hydrogen bridge model and "protonated double bond" model have received support from recent measurements of the infrared absorption spectrum of diborane [2] and the mass spectra of diborane [3] and pentaborane [4]. In the case of diborane, a possible structural correspondence with ethane is ruled out and the presence of an ethylenic linkage is indicated. It is also apparent from the mass spectra of diborane and pentaborane that not all hydrogens are bound in the molecule by equivalent bonds.

In the present investigation, we have obtained the mass spectrum of diborane-d_6 for comparison with normal diborane to obtain information on the stability of the molecule ion as well as the effect of deuterium substitution on dissociation processes in diborane.

It is convenient at this time also to report the mass spectrum of ethane-d_6. This spectrum is compared with normal ethane to demonstrate the effect of complete deuterium substitution in hydrocarbons. Similar data for methane and methane-d_4 have been published by Turkevich, Friedman, Solomon, and Wrightson [5].

II. Experimental Details

Mass spectra were obtained with a type 21–102 Consolidated mass spectrometer. The temperature of the ionization chamber was controlled at 245° C. Ionizing electron energies were nominally 50 and 70 v.

The B_2D_6 was synthesized according to Finholt, Bond, and Schlesinger [6]. Approximately 0.3 g of 98-percent lithium aluminum deuteride [2] [7] were dissolved in 25 ml of anhydrous dibutyl ether contained in a flask provided with a reflux condenser and connections to a vacuum system. Solution was accomplished after several hours of stirring under an atmosphere of nitrogen at a temperature just below the boiling point of the ether. The solution was frozen with liquid nitrogen, the flask evacuated, and approximately 1.5 g of boron trichloride distilled onto the frozen solution. The flask and contents were allowed to warm slowly to room temperature, stirring when possible. The reaction was moderate, and after completion, the volatile material was drawn off

[1] Figures in brackets indicate the literature references at the end of this paper.

[2] The deuteride, deuterium gas, and deuterium oxide used in the preparations of B_2D_6 and C_2D_6 were obtained through the Isotopes Branch of the USAEC.

by a Toepler pump through a trap at −120° C. A mass spectrometric analysis showed no hydroborons heavier than diborane, although approximately 7 percent of B_2D_5H was present. The BCl_3 originally obtained from Kahlbaum in 1906 was quite yellow and probably contained some HCl. This may account for the more than expected amount of protium in the product. The rate of decomposition of B_2D_6 to give deuterium gas and heavier hydroborons is apparently slow even at room temperature, as a sample showed no appreciable increase in noncondensibles or heavier hydroborons over a period of several weeks. Before admitting a sample to the mass spectrometer, however, the precaution was always taken to pump off possible noncondensibles at liquid nitrogen temperature.

The ethane-d_6 was kindly supplied by L. A. Wall of this Bureau. It was made by the catalyzed reduction of acetylene-d_2. Mass spectrometric analysis indicated impurities of approximately 1 percent of deuteromethane, 2 percent of deuteropropane, and 1 percent of deuterobutane, in addition to approximately 1 percent of C_2D_5H. The isotopic purity of nearly 99 percent is exceptionally good for a compound containing six deuterium atoms.

III. Results

The computation of the monoisotopic spectrum of B_2D_6 is complicated by the presence of B_2D_5H. The method used, however, is similar to that already described for B_2H_6 [3]. By trial approximation, the abundance ratio, $B^{10}/B^{11}=0.250$, was found to give the best fit. This is in agreement with the ratio obtained for normal diborane (0.251) and pentaborane (0.250). Using the ratio 0.250, one derives the abundance ratios

$$B^{10}B^{11}/B_2^{11}=0.500 \text{ and } B_2^{10}/B_2^{11}=0.0625.$$

With these values it is possible to calculate the spectrum of ions containing only deuterium and of ions containing 1 protium atom. As relatively few molecules contain protium atoms, the first spectrum is to a first approximation the B_2D_6 spectrum, and the second spectrum is the partial spectrum of B_2D_5H accounting for all ions that contain protium. There is no basis for distinguishing between ions from B_2D_6 and from B_2D_5H with protium removed.

Table 1 shows the B_2 portion of the B_2D_6 and B_2D_5H mixture spectra at 70 v ionizing voltage and summarizes the calculations of the complete monoisotopic spectrum of B_2D_6 and the partial spectrum of B_2D_5H. Column 1 lists the mass numbers of the recorded ions; column 2 gives the mixture spectrum with the ion intensities relative to the maximum peak at $m/e=32$ taken as 100. The monoisotopic spectra are separated by starting at the heavy mass end and applying the abundance values calculated above to determine the contribution of each B_2 ion to each value of m/e. The peak at $m/e=34$ comes entirely from

TABLE 1. *Summary of the monoisotopic spectrum calculations for the* B_2 *group of* B_2D_6 *and* B_2D^5H *for 70-v electrons*

m/e	Mixture spectrum	B_2D_6 *				B_2D_5H *			
		$B_2^{11}D_x$	$B^{10}B^{11}D_x$	$B_2^{10}D_x$	ΣB_2D_x	$B_2^{11}D_xH$	$B^{10}B^{11}D_xH$	$B_2^{10}D_xH$	ΣB_2D_xH
20	0.10	.....	.....	0.10	2.55	.....	.....	.....	.....
21	.82	.....	0.82	.....	.....	.....	.....	.....	.....
22	1.92	1.63	.....	.29	7.22	.....	.....	.....	.....
23	2.43	.....	2.31	.....	.....	0	.....	0.12	3.09
24	9.79	4.62	.....	4.18	104.47	.....	0.99	.....	.....
25	35.49	.....	33.43	.....	.....	1.98	.....	.08	1.97
26	68.97	66.86	.....	1.48	36.89	.....	.63	.....	.....
27	13.25	.....	11.80	.....	.....	1.26	.....	.19	4.64
28	28.09	23.61	.....	2.91	72.66	.....	1.48	.....	.....
29	26.64	.....	23.25	.....	.....	2.97	.....	.42	10.62
30	56.15	46.50	.....	6.25	156.24	.....	3.40	.....	.....
31	56.80	.....	50.00	.....	.....	6.80	.....	.....	.....
32	100	99.99	.....	0.01	0.26	.....	.....	.....	.....
33	0.07	.....	0.08	.....	.....	.....	.....	.....	.....
34	.17	0.17	.....	.....	.....	.....	.....	.....	.....

* x assumes integral values from 0 to 6.

the $B_2^{11}D_6^+$ ion; therefore, the $B^{10}B^{11}D_6^+$ ion ($m/e=33$) $=0.17\times0.50=0.08$ and the $B_2^{10}D_6^+$ ion ($m/e=32$) $=0.17\times0.0625=0.01$. The difference between the calculated and observed values at $m/e=33$ is in the region of experimental uncertainty, since this peak is very small. The $B_2^{11}D_5^+$ ion is $100-0.01=99.99$. The principal contribution is from B_2D_6 but with a small contribution from B_2D_5H. The $B^{10}B^{11}D_5^+$ ion ($m/e=31$) is $99.99\times0.50=50.00$, and the $B_2^{10}D_5^+$ ion ($m/e=30$) is $99.99\times0.0625=6.25$. We now have a measure of the $B_2^{11}D_4H^+$ ion, which is the difference $56.80-50.00=6.80$. From this value we compute the contributions of the $B^{10}B^{11}D_4H^+$ and $B_2^{10}D_4H^+$ ions as before. The $B_2D_4^+$ ion is now obtained by subtracting the contributions of $B_2^{10}D_5^+$ and $B^{10}B^{11}D_4H^+$ from the 30 peak; i. e., $56.15-(6.25+3.40)=46.50$. The $B^{10}B^{11}D_4^+$ and $B_2^{10}D_4^+$ ions are computed and the cycle continued until all contributions to all peaks are obtained. There are two checks on the calculations. The abundance of the 21 and 20 peaks is calculated to be 0.82 and 0.10, respectively, in exact agreement with the observed abundance.

Table 2 is a summary of the monoisotopic spectra calculations of the B_1 group for ionizing electron energies of 70 v. Starting with the heaviest mass in that group, $m/e=17$ is assumed to be entirely the $B^{11}D_3^+$ ion. Therefore, the $B^{10}D_3^+$ ion ($m/e=16$) is $0.84\times0.250=0.22$. By subtraction, the $B^{11}D_2H^+$ ion is $0.29-0.22=0.07$ and the $B^{10}D_2H^+$ ion ($m/e=15$) is 0.02. After all contributions are obtained, the single check point is $m/e=10$. The observed discrepancy is considerably larger than the experimental uncertainty, requiring a B^{10}/B^{11} ratio of approximately 0.26 to obtain a zero residual. A similar effect was noted and discussed in a previous paper [4]. The B_2D_6 and B_2D_5H dissociation patterns are obtained by summing the contributions of all ions with the same number of deuterium atoms regardless of boron isotopic species. The most abundant ion of B_2D_6 ($B_2D_5^+$) and of B_2D_5H ($B_2D_4H^+$) are taken as 100. Other values of ion abundance are relative to the maximum peak. The complete spectrum of B_2D_6 and the partial spectrum of B_2D_5H for 50- and 70-v electrons are given in table 3. The spectrum of B_2H_6 is included for comparison. Sensitivities (ion current in arbitrary units per unit of sample pressure) are given for the maximum peaks of B_2D_6 and B_2H_6.

TABLE 2. *Summary of the monoisotopic spectrum calculations for the* B_1 *group of* B_2D_6 *and* B_2D_5H *for 70-v electrons*

m/e	Mixture spectrum	B_2D_x *			B_2D_5H *		
		$B^{11}D_x$	$B^{10}D_x$	ΣBD_x	$B^{11}D_xH$	$B^{10}D_xH$	ΣBD_xH
10	5.54		5.37	26.85			
11	21.53	21.48				0.05	0.25
12	3.94		3.74	18.71	0.20		
13	15.19	14.97				.22	1.09
14	7.63		6.76	33.81	.87		
15	27.07	27.05				.02	.09
16	.29		.21	1.05	.07		
17	.84	.84					

* x assumes integral values from 0 to 3.

TABLE 3. *Monoisotopic dissociation patterns of* B_2D_6, B_2H_6, *and the partial pattern of* B_2D_5H *for 50 and 70-v electrons*

B_2D_6			B_2H_6			B_2D_5H		
Ion	50 v	70 v	Ion	50 v	70 v	Ion	50 v	70 v
B^+	17.7	17.3	B^+	21.7	21.5	B^+	.....	.....
BD^+	12.0	12.1	BH^+	10.2	10.6	BH^+	2.5	1.4
BD_2^+	22.8	21.8	BH_2^+	19.9	19.5	BDH^+	10	10
BD_3^+	.68	.67	BH_3^+	.58	.65	BD_2H^+	.8	.8
B_2^+	1.56	1.63	B_2^+	2.84	3.22	B_2^+	.....	.....
B_2D^+	5.27	4.62	B_2H^+	8.46	7.72	B_2H^+	0	0
$B_2D_2^+$	69.2	66.9	$B_2H_2^+$	76.2	74.6	B_2DH^+	30	29
$B_2D_3^+$	24.3	23.6	$B_2H_3^+$	29.6	28.8	$B_2D_2H^+$	19	18
$B_2D_4^+$	46.9	46.5	$B_2H_4^+$	53.2	52.9	$B_2D_3H^+$	42	44
$B_2D_5^+$	100	100	$B_2H_5^+$	100	100	$B_2D_4H^+$	100	100
$B_2D_6^+$	.18	.17	$B_2H_6^+$	.34	.31	$B_2D_5H^+$	.....	.....
Sensitivity	23.6	24.3	Sensitivity	23.0	23.7	Sensitivity	.....	.....

Omitted from the B_2D_6 spectrum in table 2 is a small peak at $m/e=12.5$ amounting to 0.36 percent of the maximum at 50 v and 0.40 percent at 70 v. This peak is due to the double charged ion, $B^{10}B^{11}D_2^{++}$. The two isotope peaks expected coincide with large peaks at $m/e=12$ and 13. A similar doubly charged peak appears in B_2H_6 at $m/e=11.5$, amounting to 0.39 percent of the maximum at 50 v and 0.43 percent at 70 v. This doubly charged ion of mass 23 was ascribed [3] to either $B_2^{11}H^{++}$ or $B^{10}B^{11}H_2^{++}$. It is very likely $B^{10}B^{11}H_2^{++}$ corresponding to the $B^{10}B^{11}D_2^{++}$ peak in the B_2D_6 spectrum.

Also omitted from the B_2D_6 spectrum are the four small peaks listed in columns 2 and 3 of table 4. These are the result of dissociation of ions after they have traversed the electric field [8]. The peaks at 21.6 and 22.6 are isotopic as indicated by their relative abundance and are due to the transitions $B^{10}B^{11}D_4^+ \rightarrow B^{10}B^{11}D_2^+ + 2D$ and $B_2^{11}D_4^+ \rightarrow B_2^{11}D_2^+ + 2D$. The peaks at $m/e=23.6$ and 24.6 are also isotopic and are a result of the transitions $B^{10}B^{11}D_5^+ \rightarrow B^{10}B^{11}D_3^+ + 2D$ and $B_2^{11}D_5^+ \rightarrow B_2^{11}D_3^+ + 2D$. The transition $B_2^{10}D_5^+ \rightarrow B_2^{10}D_3^+ + 2D$ may also contribute to $m/e=22.6$, but the contribution is very small and below the threshold of observation. The two metastable transitions observed in diborane are also given in table 4. These are also isotopic and result from the transitions $B^{10}B^{11}H_4^+ \rightarrow B^{10}B^{11}H_2^+ + 2H$ and $B_2^{11}H_4^+ \rightarrow B_2^{11}H_2^+ + 2H$. The apparent mass of each metastable ion is calculated from the usual relation $m_a=(m_f)^2/m_i$, where m_i and m_f are respectively the ion masses before and after metastable dissociation. The calculated and observed values agree within 0.1 mass unit.

TABLE 4. *Percentage abundance of metastable ions relative to the maximum peak in* B_2D_6 *and* B_2H_6

m/e	B_2D_6		B_2H_6	
	50 v	70 v	50 v	70 v
21.1			0.05	0.06
21.6	0.07	0.09		
22.1			.13	.15
22.6	.16	.17		
23.6	.07	.08		
24.6	.13	.14		

Table 5 gives the dissociation patterns of ethane and ethane-d_6 at 50 and 70 v. The sensitivities of the maximum peak in each compound are also given. The peaks at the odd mass numbers in the C_2D_6 spectrum have been corrected for carbon isotope and represent contributions from an estimated 1.5 percent of C_2D_5H in the sample. The two peaks indicated by the footnote very probably include contributions due to the doubly charged ions $C_2D_3^{++}$ and $C_2D_5^{++}$. Analogous doubly charged ions appear in C_2H_6 at $m/e=13.5$ and 14.5. The relative abundance of these ions is given in the C_2H_6 spectrum. Three metastable ions not included in table 5 are observed in the C_2D_6 spectrum. One appearing near mass 24.5 amounting to 0.19 percent of the maximum peak at 50 v and 0.18 percent at 70 v is a result of the transition $C_2D_4^+ \rightarrow C_2D_2^+ + 2D$. Another, near $m/e=26.5$, of 0.19 percent at 50 v and 0.17 percent at 70 v, comes from the transition $C_2D_5^+ \rightarrow C_2D_3^+ + 2D$. The third, near $m/e=28.4$, of 0.08 percent at 50 v and 0.09 percent at 70 v, comes from the transition $C_2D_6^+ \rightarrow C_2D_4^+ + 2D$. Analogous transitions are observed for ethane at $m/e=24.1$, 25.1, and 26.1. They are 0.10, 0.17, and 0.30 percent, respectively, of the maximum peak at 50 v and 0.12, 0.17, and 0.30 percent at 70 v.

TABLE 5. *Monoisotopic dissociation patterns of* C_2D_6 *and* C_2H_6 *for 50 and 70 v electrons*

C_2D_6				C_2H_6			
m/e	Ion	50 v	70 v	m/e	Ion	50 v	70 v
12	C^+	0.54	0.67	12	C^+	0.52	0.6
13	CH^+						
14	CD^+	1.27	1.47	13	CH^+	1.11	1.3
15	CDH^+	*.04	*.08	13.5	$C_2H_5^{++}$	.05	.0
16	CD_2^+	3.44	3.71	14	CH_2^+	4.27	4.6
17	CD_2H^+	*.33	*.54	14.5	$C_2H_5^{++}$	.56	.7
18	CD_3^+	4.29	4.45	15	CH_3^+	4.67	4.9
19	CD_3H^+	.03	.02				
20	CD_4^+	.04	.04	16	CH_4^+	.08	.1
24	C_2^+	.32	.44	24	C_2^+	.56	.8
25	C_2H^+						
26	C_2D^+	2.28	2.61	25	C_2H^+	3.73	4.3
27	C_2DH^+	.04	.04				
28	$C_2D_2^+$	17.9	18.4	26	$C_2H_2^+$	22.9	23.3
29	$C_2D_2H^+$	.12	.11				
30	$C_2D_3^+$	24.4	24.4	27	$C_2H_3^+$	32.3	32.7
31	$C_2D_3H^+$	.82	.83				
32	$C_2D_4^+$	100	100	28	$C_2H_4^+$	100	100
33	$C_2D_4H^+$	.23	.21				
34	$C_2D_5^+$	15.3	16.4	29	$C_2H_5^+$	18.7	18.8
35	$C_2D_5H^+$	.28	.23				
36	$C_2D_6^+$	19.1	19.9	30	$C_2H_6^+$	23.7	23.1
Sensitivity.		45.8	46.4	Sensitivity.		44.1	45.1

* Includes contributions from the doubly charged ions $C_2D_3^{++}$ and $C_2D_5^{++}$.

IV. Discussion

As evidenced by table 3, the mass spectra of diborane and diborane-d_6 are quite similar. The 34 peak in B_2D_6 is considered a good measure of the $B_2D_6^+$ ion as an impurity on this peak is unlikely in diborane. The lower value of the relative abundance of the $B_2D_6^+$ ion (0.18) compared to the $B_2H_6^+$ ion (0.34) is perhaps not significant. The latter value suggests that a trace of nitrogen impurity may contribute to the 28 peak of normal diborane. Although the molecule ion is very unstable, it is evidently not completely absent from the mass spectrum as first supposed [9]. The sensitivities of the maximum peaks of both compounds agree within 3 percent, which is the estimated uncertainty, demonstrating the nearly equal probability of dissociating a deuterium from B_2D_6 and a protium from B_2H_6. In the B_2 group the relative probabilities of dissociating successive deuterium atoms from B_2D_6 and successive protium atoms from B_2H_6 are similar but always somewhat less for the deuterated compound. In the B_1 group the probabilities are roughly equal. This compares reasonably well with the similarities previously reported [5] and those observed for ethane and ethane-d_6 discussed below.

Metastable transitions with the loss of mass 2 are by far the most frequent type found in hydrocarbons [10]. It is not surprising, therefore, to find this transition readily occurring in deutero- and normal diborane. An interesting difference between B_2D_6 and B_2H_6, however, is the occurrence of a metastable dissociation of the $B_2D_5^+$ ion in diborane-d_6, whereas the analogous transition is absent in normal diborane. As observation of a metastable ion indicates a delay of roughly 10^{-6} second in the dissociation process, it is evident that substitution of deuterium for protium in diborane has materially changed the mean life of the transition involved. The other metastable dissociations are similar and have nearly equal probability in diborane and diborane-d_6.

The formula $B^{10}B^{11}D_2^{++}$ is unambiguously assigned to the ion appearing at $m/e=12.5$ in the diborane-d_6 spectrum. The similarity of relative abundance of this peak and the doubly charged ion appearing in diborane at $m/e=11.5$ suggests an unique interpretation of the latter that is not possible from the B_2H_6 spectrum alone. From the foregoing, it is probable but not certain that the doubly charged peak in B_2H_6 has the formula $B^{10}B^{11}H_2^{++}$ analogous to the doubly charged ion in B_2D_6.

The part of the B_2D_5H spectrum that contains protium atoms has been included in table 3. The method of computation and the small magnitude of the residuals from which the pattern is derived give a relatively large uncertainty for this pattern. As expected, the pattern is not like the patterns of either B_2D_6 or B_2H_6. One would predict that the abundance of the ions $B_2D_5^+$ plus $B_2D_4H^+$ from B_2D_5H should be compared with the abundance of the $B_2D_5^+$ ion from B_2D_6; the abundance of $B_2D_4^+$ plus $B_2D_3H^+$ should be compared with the abundance of $B_2D_4^+$ from B_2D_6, and so forth. If the probability of removing a dueterium or protium atom is merely a statistical matter, then the abundance ratio $B_2D_4H^+/B_2D_5^+$ from B_2D_5H would be 5 to 1. From table 1 the $B_2D_4H^+$ peak is 6.8 percent of the $B_2D_5^+$ peak, and on the above basis, B_2D_5H contributes 1.36 percent to the $B_2D_5^+$ peak. As the $B_2D_5H^+$ ion is immeasurably small, there is no check on this. The probability of removing a deuterium rather than a protium from $B_2D_4H^+$ is 4 to 1, and it might be expected that the pattern coefficient of $B_2D_3H^+$ from $B_2D_4H^+$ is 4/5 of the pattern coefficient of $B_2D_4^+$ from $B_2D_5^+$. The value thus calculated (37) is not in agreement with the observed value of 44. The probability of removing two deuteriums rather than a deuterium and a protium from $B_2D_4H^+$ is $3/4\times4/5=3/5$, and one would predict a pattern coefficient of 14 compared with 18 observed. Similarly, for B_2DH^+ one would predict $0.4\times66.9=27$ instead of 29, and for BDH^+, 8.8 instead of 10. For B_2H^+ one would expect 0.9 instead of zero, and for BH^+, 2.4 as observed. Analysis of the mass spectra of simple hydrocarbons containing one deuterium atom [5, 11] indicates that removal of the deuterium and protium atoms is not equally probable but in a ratio of about 0.5 to 1 for these molecules. It is not surprising, therefore, that purely statistical considerations fail to account for the B_2D_5H spectrum. The case of diborane, however, is more complicated as, according to recent theory [1], the six hydrogen atoms are not equivalent, but two of the atoms are bound loosely to an ethylene-type structure.

Insofar as the statistical method roughly accounts for the spectrum, the following conclusions can be drawn. The amount of B_2D_5H in the mixture is about 8.5 percent. The contribution of this to most peaks in the B_2D_6 pattern amounts to a few tenths of a percent of the $B_2D_5^+$ peak. (The B_2D_6 pattern is normalized with $B_2D_5^+$ taken as 100, therefore only differential effects enter as errors in the pattern.) The peaks resulting from the ions $B_2D_5H^+$ and B_2H^+ are very small and near the threshold of observation, and it is not unexpected to observe a pattern coefficient of zero for these peaks.

From table 5, the mass spectra of C_2D_6 and C_2H_6 are also quite similar. The sensitivities of the most abundant ion in both compounds agree to about 3 percent, which is the approximate uncertainty of the measurements. The similarity of the spectra extends to the doubly charged ions and the metastable transitions. The amount of C_2D_5H present is too small to permit conclusions concerning the dissociation of this molecule compared to ethane-d_6. The abundance of the molecule ion in ethane permits an estimate of the amount of C_2D_5H assuming only equality in sensitivity of the two ethanes. The 35 peak indicates approximately 1.5 percent C_2D_5H in the mixture. The dissimilarities of C_2H_6 and B_2H_6 spectra are already noted [3]. The same observations are applicable to C_2D_6 and B_2D_6, namely, the low abundance of the molecule ion and the BD_3^+ ion in the latter molecule compared to the analogous ions in ethane-d_6. In addition, a metastable transition of the $B_2D_5^+$ ion observed in diborane-d_6 has no analog in ethane-d_6.

V. References

[1] K. S. Pitzer, J. Am. Chem. Soc. **67,** 1126 (1945); R. E. Bundle, **69,** 1327 (1947); and A. B. Burg, **66,** 747 (1947).

[2] W. C. Price, J. Chem. Phys. **15,** 614 (1947).

[3] V. H. Dibeler and F. L. Mohler, J. Am. Chem. Soc. **70,** 987 (1948).

[4] V. H. Dibeler, F. L. Mohler, L. Williamson, and R. M. Reese, J. Research NBS **43,** 97 (1949) RP2010.

[5] J. Turkevich, L. Friedman, E. Solomon, and F. M. Wrightson, J. Am. Chem. Soc. **70,** 2638 (1948).

[6] A. E. Finholt, A. C. Bond, Jr., and H. I. Schlesinger, J. Am. Chem. Soc. **69,** 1201 (1947).

[7] Metal Hydrides, Incorporated, Beverly, Mass.

[8] J. A. Hipple, R. E. Fox, and E. U. Condon, Phys. Rev. **69,** 347 (1946).

[9] J. A. Hipple, Phys. Rev. **57,** 350 (1940).

[10] E. G. Bloom, F. L. Mohler, J. H. Lengel, and C. E. Wise, J. Research NBS **40,** 437 (1948) RP1888.

[11] M. W. Evans, N. Bauer, and J. Y. Beach, J. Chem. Phys. **14,** 701 (1946).

Washington, October 21, 1949.

U. S. Department of Commerce
National Bureau of Standards

Research Paper RP2096
Volume 44, May 1950

Part of the Journal of Research of the National Bureau of Standards

An Improved Apparatus for the Determination of Liquidus Temperatures and Rates of Crystal Growth in Glasses[1]

By Oscar H. Grauer and Edgar H. Hamilton

The liquidus temperature of a glass is the highest temperature at which equilibrium can coexist between the molten glass and the primary crystalline phase. An improved temperature-gradient apparatus is described for the rapid determination of liquidus temperatures and rates of crystal growth in glasses. In this method the use of small glass fragments confined in the cells of a platinum alloy holder largely eliminates the errors inherent in previous gradient methods. The procedure is simple and rapid. Liquidus temperatures in the range from 950° to 1,225°C were determined to a precision of 4 degrees C.

Rates of crystal growth were found to be linear. The usefulness to the glass technologist of data obtained by this method is indicated.

I. Introduction

Crystallization or devitrification is the most important limitation to the development of new glasses. The significance of this fact has been recognized by many investigators including Littleton [1][2] in 1931 and Preston [2] in 1940, who emphasized the need for further study of devitrification in glass. Any such study must take into account two factors: (1) the liquidus temperature or maximum temperature at which equilibrium coexists between the glass and the primary crystalline phase; and (2) the rates of crystal growth at various temperatures. Such data are an important aid not only in the development of new glasses but also in the manufacturing processes of melting, forming, and annealing.

Most of the data that could be used in devitrification studies are expressed as phase equilibria diagrams, such as those compiled by Hall and Insley [3], which indicate the liquidus temperatures for various compositions but which present no information as to rates of crystal growth. The classical method for obtaining the liquidus temperature is the quenching method, which was used at the Geophysical Laboratory of the Carnegie Institution of Washington in phase studies of silicate systems. In this method a small powdered sample of glass or crystals, encased in a suitable container, usually a platinum foil envelope, is heated at a given temperature until equilibrium is attained and then quenched in air or some suitable liquid. The sample is examined with the petrographic microscope for crystals, and the process repeated at other temperatures until the highest temperature is found at which crystals persist.

In 1914 Tammann [4] determined the maximum rate of crystal growth of glass rods that had been heated in a known temperature gradient. Zschimmer and Dietzell [5] determined rates of crystal growth by placing a piece of glass on a platinum plate in a furnace and maintaining a given temperature for a specific time interval. After the sample was removed from the furnace, it was sectioned and the crystal size measured with a micrometer microscope. This procedure was repeated for each temperature at which data were desired, and from a graph of temperature and crystal size the temperature of maximum devitri-

[1] Presented at the meeting of the Glass Division of the American Ceramic Society, Bedford Springs, Pa., October 9, 1948.
[2] Figures in brackets indicate the literature references at the end of this paper.

fication was determined. Tabata [6] used a similar procedure to indicate relative rates of crystallization. Swift [7] used the same method with a modification for determining the rates of growth at temperatures immediately below the liquidus temperature. For these cases, the sample was placed over a small hole in a platinum foil, which permitted direct observation with a microscope after each heat treatment.

Farmelee and Monack [8] set up criteria for evaluating devitrification in glasses based on prescribed cooling cycles for small experimental melts.

A gradient method to determine liquidus temperature was developed by Silverman [9]. In this method a sample of powdered glass was placed in a platinum-alloy boat, which was inserted in a furnace in which a known temperature gradient was maintained. Preston [2] used the same method to determine both liquidus temperatures and rates of crystal growth.

In a previous investigation at this Bureau [10] the Silverman method was found to give good results except for those glasses that were very fluid at temperatures in the region of their liquidus temperatures. Such glasses had a tendency to flow when the boat was removed from the furnace, frequently resulting in erroneous values.

In the present investigation an improved apparatus has been developed that permits a rapid determination of liquidus temperatures and rates of crystal growth.

II. Apparatus and Procedure

The apparatus used for holding the glass sample is illustrated in figure 1. It consisted of an inserted channel-shaped piece of platinum–10-percent-rhodium alloy, 5½ in. long by ½ in. wide. Open cells for containing small fragments of glass were spaced along the length of the holder.

The cells were tapered from a 2-mm-diameter opening at the top to a 1-mm-diameter opening at the bottom and extended 1 mm below the surface. At one end of the channel the cells were spaced in two parallel rows 3/16 in. apart. In each of the parallel rows the cells were separated by ⅛ in. from center to center, but since one row offset the other by 1/16 in., the distance along the channel between centers of succeeding cells was 1/16 in. This interval was found to correspond to a temperature difference of about 5 deg C in the temperature gradient. At the other end of the apparatus the cells were spaced ¼ in. apart between centers in a single row along the length of the strip, corresponding to a 20 deg C temperature difference. In actual operation, the holder was so positioned in the temperature gradient that liquidus temperatures could be determined within the region of the closely spaced cells of the parallel rows and measurements of crystal sizes within the cells of the single row.

The horizontal tube furnace consisted of two concentric, spirally grooved alundum cores, insulated from each other and encased in a steel shell packed with diatomaceous earth. The inner core was wound with platinum–20-percent-rhodium wire along a central zone for a distance of 6 in. and the outer core with a nickel-chromium alloy wire along 20 in. of its length.

A fairly linear temperature gradient was obtained by adjusting the current in both windings with small variable transformers. The maximum temperature of the furnace was maintained constant to within ±2 deg. C by means of a commercial-type electronic controller operating from a platinum–platinum-10-percent-rhodium thermocouple located in the hot zone. As a result, a stable gradient was maintained in the remainder of the furnace.

Temperatures in the gradient were measured with a movable platinum–platinum-10-percent-rhodium thermocouple in conjunction with a potentiometer. The thermocouple was encased by a double-bore clay insulating tube except for the last half inch at the hot junction.

In making liquidus temperature determinations and measurements of rates of crystal growth in glass, the following procedure was used. A small piece of glass or of glass-crystal mixture, about 1 cm in each dimension, was crushed in a hardened-steel mortar, and the fragments were transferred to a sheet of black paper or black glass to facilitate the selection of particles of the desired size. Pieces about 2 mm long and 1 mm wide were loaded into the cells of the platinum holder, which was then inserted and positioned accurately in the furnace. The sample holder was left in the gradient furnace for the desired time, usually 20 to 60 min. for experimental glasses. A temperature probe at ½-in. intervals was then made of the gradient with the movable thermocouple, and the

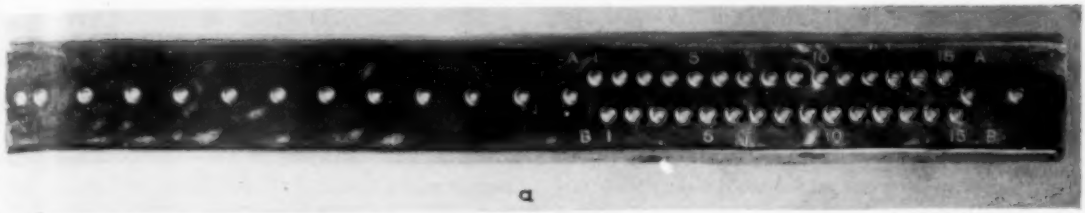

a

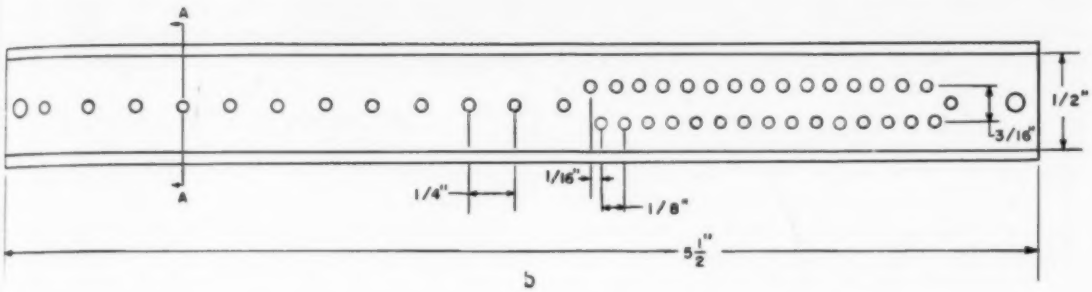

b

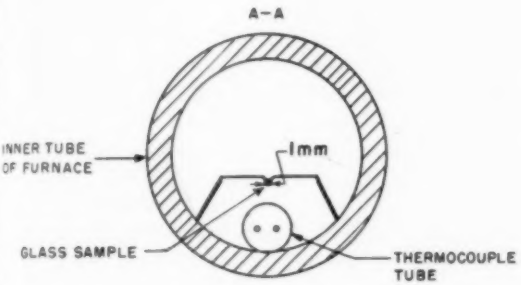

c

FIGURE 1. *Platinum alloy specimen holder.*

a, Photograph of holder; b, line drawing, plan view; c, section through A—A of view (b) showing position in furnace in relation to inner furnace tube and movable thermocouple.

holder was removed immediately (air-quenched) from the furnace by means of a long wire hook.

Since the cells confined the glass, no displacement due to flow occurred when the holder was removed rapidly from the furnace. Surface tension prevented the glass from flowing out of the lower opening. After air quenching, the holder was placed on the microscope stage, and the contents of the cells were examined with a petrographic microscope. The opening in the bottom of each cell permitted direct examination of the enclosed sample using transmitted light, thereby obviating the necessity of breaking away the glass from the holder. The last cell that contained crystals was considered to locate the position in the temperature gradient corresponding to the liquidus temperature. The temperature of the cell was obtained by linear interpolation between the two nearest points of the temperature probe.

In general, each fragment of glass tended to take the shape of the platinum cell when the temperature was above the softening point and to assume a somewhat lenticular appearance. For photomicrography it was desirable to avoid the optical distortion and uneven illumination due to the curved surfaces. This was effected by placing cover glasses at both surfaces of the sample and interposing a drop or two of a liquid having the same index of refraction as the glass sample. A cover glass with an appropriate liquid sufficed for the visual measurement of crystal sizes.

In determining the crystal size, Preston's

method of making measurements of the semimajor axis of the crystal or of the radius of spherulitic crystals was used. Corrections were made for the foreshortening effect of those crystals that did not lie in the plane perpendicular to the optical axis of the microscope. A microscope, containing a filar micrometer eyepiece, was focussed sharply on one end of the crystal or of the radius of the spherulite. The crosshair was brought into coincidence with the image, and the readings of the micrometer and the microscope fine adjustment scale were noted; the microscope was refocussed on the other end of the crystal or on the radiant point of the spherulite; the crosshair was repositioned; the new readings of both scales were observed. The horizontal projection of the crystal or of the radius was obtained from the difference of the micrometer scale readings, and the vertical projection from the product of the difference of the microscope scale readings and the index of refraction of the glass. From these data the true size of the crystal was determined by the geometrical relationship as indicated in figure 2. An average of four measurements of different spherulites was used for the data. The reproducibility of the measurements was about 2 percent.

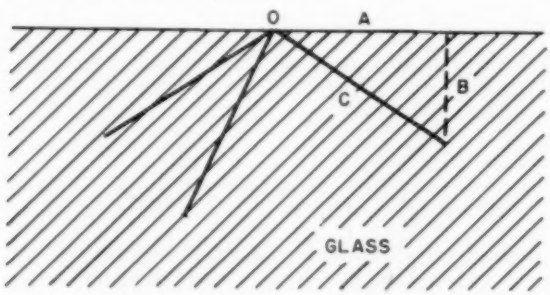

FIGURE 2. *Geometrical solution of spherulitic radii.*

The radius C is determined by the equation $C=\sqrt{A^2+(BN)^2}$, where A is the horizontal projection, B is the vertical projection, and N is the index of refraction of the glass.

Measurements by Preston [2] indicated that the rate of crystal growth in glass was linear with time only during the first stages. A more recent investigation by Swift [7] showed that the rate of crystal growth in glass was constant until the crystallization zones from opposite surfaces met. In the present investigation the linearity of crystal growth was also observed from measurements made on various types of glasses.

Thus, both the rates of crystal growth at various temperatures and the liquidus temperature could be obtained after only one treatment. However, in those cases where the rate of crystal growth was very rapid, a short treatment of 5 or 10 min was desirable so that the crystals in the region of maximum devitrification would not interfere with each other and depart from linearity in their rates of growth. In these few instances a separate determination was made of the liquidus temperature.

III. Results and Discussion

1. Liquidus Temperature Determinations

Liquidus temperature determinations were made for five different glasses using the classical quenching method, the Silverman method, and the new method. The results are listed in table 1 and the compositions of the glasses in table 2. The values of duplicate determinations with the new method show less scatter than those with the Silverman method. Considering the values obtained by the quenching method as the standards for comparison, the average deviation of the values obtained by the new method is 3.6 deg C as compared to 7.2 deg C for the Silverman method. The greatest deviation between duplicate determinations for the new method was 6 deg C compared to 23.4 deg C for the Silverman method.

TABLE 1. *Liquidus temperature determinations*

Glass	Classical quenching method	Silverman method				New method			
	°C	°C	°C	°C	°C(Avg)	°C	°C	°C(Avg)	
E 1105	958.5	960	954	.....	957	957	953	955	
E 994	1,011.0	1,001	1,010	.....	1,006	1,017	1,017	1,017	
E 1067	1,079.0	1,072	1,078	.....	1,075	1,074	1,079	1,076	
E 955	1,170.0	1,159	1,167	1,167	1,164	1,165	1,172	1,168	
E 1055	1,223.4	1,200	1,209	.....	1,204	1,218	1,221	1,220	

TABLE 2. *Compositions* [a]

Glass	SiO_2	B_2O_3	BaO	BeO	CaO	La_2O_3	Na_2O	Al_2O_3	Ta_2O_5	ZnO
	wt %	wt %	wt %	wt %	wt %	wt %	wt %	wt%	wt %	wt %
E 1105	70.09	.....	.....	.....	10.0	.....	20.0	.....	.....	.....
E 994	23.2	17.0	54.2	2.2	.....	.....	.....	3.4	.....	.....
E 1067	14.0	16.2	33.1	1.2	.....	24.4	.....	.....	11.1	.....
E 955	14.6	16.9	31.9	1.3	.....	33.9	.....	.....	.....	1.4
E 1055	12.7	16.5	33.8	1.3	.....	33.1	.....	2.6	.....	.....

[a] All compositions calculated from batch proportions.

It is among the glasses that are very fluid at their liquidus temperatures that the results obtained by the Silverman method are erratic, due to the flow of the molten glass in the boat upon removal from the furnace.

In the new method flow is practically eliminated by confining the specimens to the small cells of the holder. Due to the small mass of the sample and its intimate thermal contact with the platinum alloy cell, equilibrium is more quickly attained, and cooling of the sample on removal approaches the quenching method in its rapidity.

2. Rates of Crystal Growth

Figure 3 gives the values of crystal size and temperature for glass E 1105, for heat treatments of 13, 26, and 60 min. It indicates that the maximum size for each holding period occurs at about the same temperature, 895° C. Up to 1 hr the rates of crystal growth (at a given temperature),

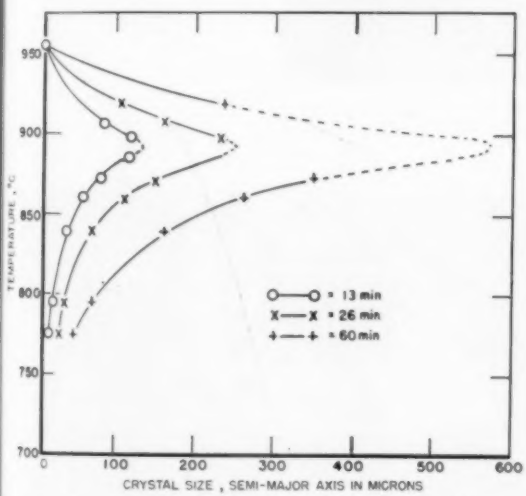

FIGURE 3. *Effect of temperature on crystal size for treatments of 13, 26, and 60 min.*

which are the slopes of the curves in fig. 4, were found to be linear. When rates of crystal growth are plotted against temperature, the curve in fig. 5 is obtained. In this curve the rate of crystal growth is zero at the liquidus temperature, and the maximum rate occurs at about 895° C. Figures 6 and 7 are photomicrographs of devitrite crystals that were grown in glass E 1105 (Na_2O, 20%; CaO, 10%; SiO_2, 70%) at 860° C for 13 and 26 min, respectively.

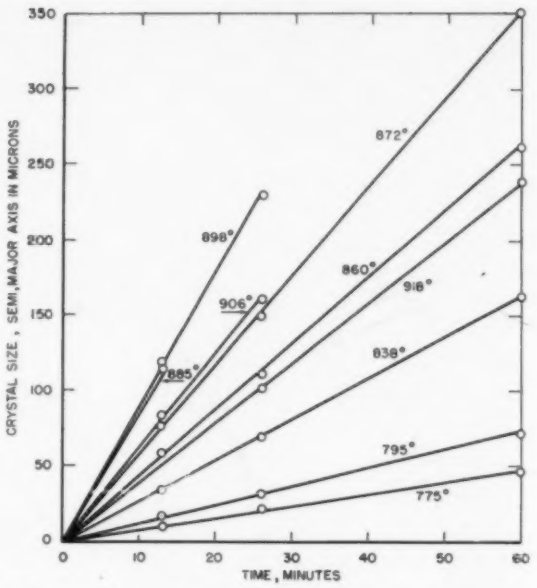

FIGURE 4. *Effect of duration of treatment at constant temperature on crystal size.*

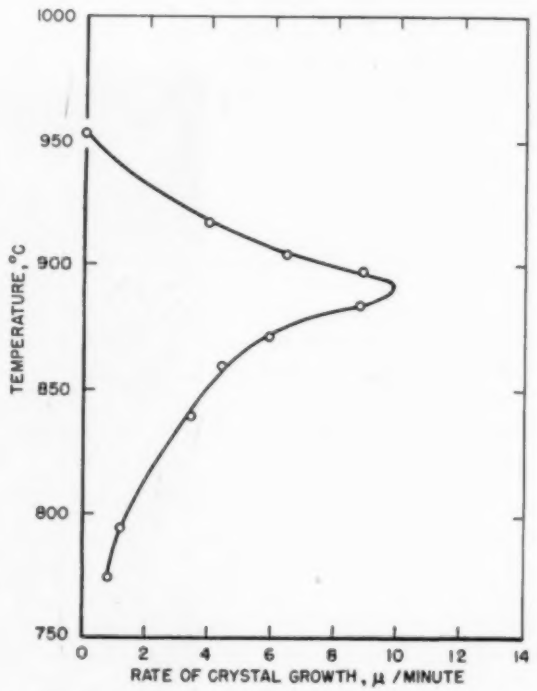

FIGURE 5. *Rate of crystal growth versus temperature.*

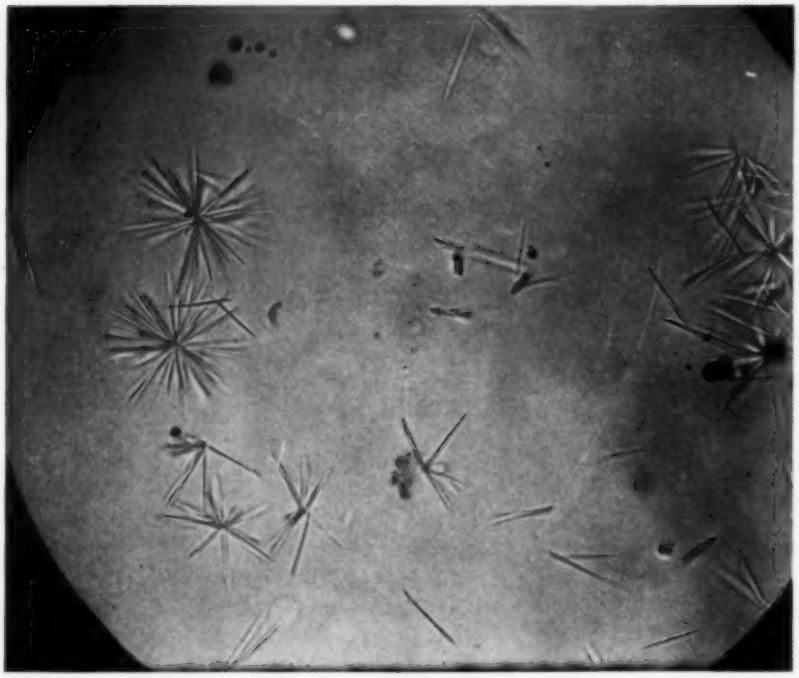

FIGURE 6. *Photomicrograph of devitrite crystals ×20 after 13 min treatment a 860 C.*

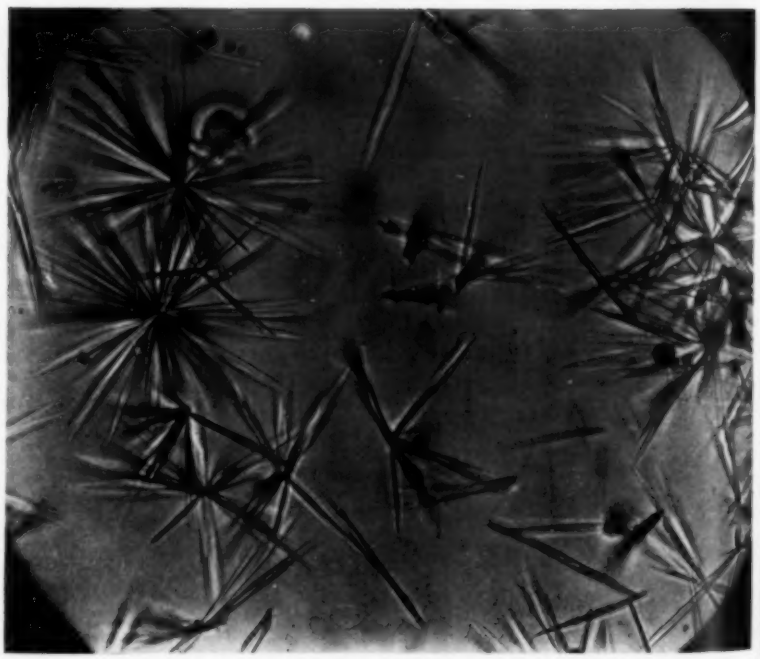

FIGURE 7. *Photomicrograph of devitrite crystals ×200 after 26 min treatment at 860° C, focus at center of crystals.*

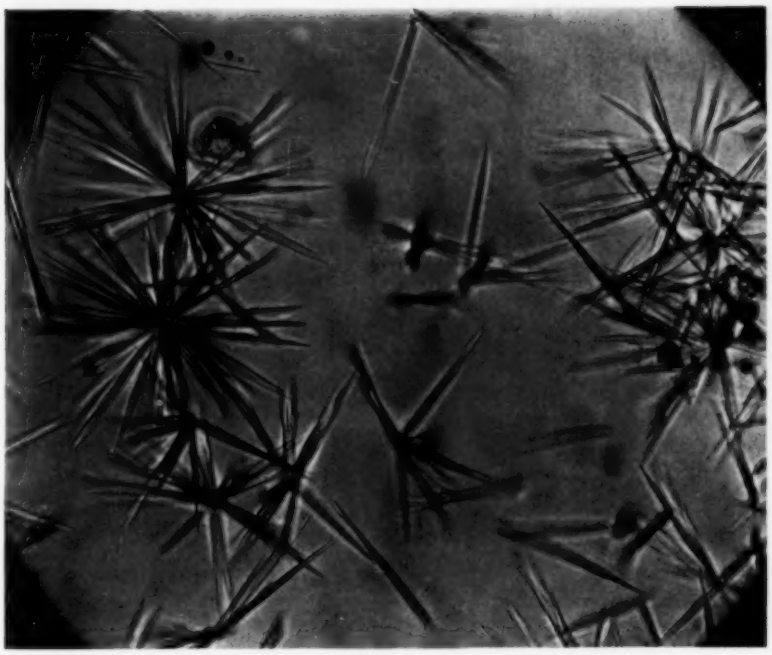

FIGURE 8. *Photomicrograph of same devitrite crystals as figure 7 with microscope focused at ends of crystals.*

The photomicrograph shown in figure 7 was obtained with the microscope focused on the centers of the spherulites. It can be seen that the end of the spherulites are out of focus, indicating varying degrees of inclination. The photomicrograph shown in figure 8 was obtained when some of the ends of the same spherulites had been brought into focus; this time the centers are out of focus. Values of maximum rates of crystal growth for two glasses are given in table 3. Other determinations of crystal growth as an indicator of devitrification have been made with this apparatus. From these results, suitable time-temperature schedules have been derived for the slumping of large interferometer plates and other large disks of various types of optical glasses without the usual devitrification.

TABLE 3. *Rates of crystal growth for glass forming and nonglass-forming materials*

Material	Maximum rate of crystal growth	Temperature
	μ/min	°C
Glass E 1105	9.8	895
Glass E 1222 [a] (devitrifies readily).	63.3	890
Picric acid [b] (nonglass-forming).	860,000	85
Phosphorus [c] (nonglass-forming).	60,000,000	[d] 25

[a] A low-dispersion, high-index experimental glass.
[b] A. Bogojawlensky, Z. physik. Chem. **77**, 585 (1898).
[c] M. D. Gernez, Compt. rend. **95**, 1278 (1882).
[d] Not maximum.

IV. Viscosity and Crystal Growth

Various attempts [7, 11, 12, 13, 14] have been made to find a relationship between the rate of crystal growth and the temperature. Below the liquidus temperature, the stable state of a system consists of crystals or a mixture of glass and crystals. The glassy phase at ordinary temperatures is unstable; even at a temperature below the softening point of the glass, the viscosity may be sufficiently low so that crystals may grow at a measurable rate.

In reviewing the kinetics of crystallization, the familiar hump-shaped curve of rate of crystal growth and temperature can be considered as the result of two opposing forces: a driving force that increases as we depart from the liquidus temperature and a resisting force related to the viscosity, which increases exponentially and plays the dominant role as the temperature is diminished. The

rate of crystal growth has been shown to be inversely proportional to the viscosity: by Frenkel [11] on the basis of the classical activation theory, by Richards [12] using the concept of thermal relaxation time, and by Leontjewa [13], empirically in a series of Na_2O-SiO_2 glasses. The latter used the equation,

$$v = K/\eta + K_0 \log \eta,$$

where v is linear speed of crystallization, η is the viscosity, and K and K_0 are constants, K_0 being very small.

Swift [9] used the semiempirical equation of Preston,

$$R = K \frac{(T_{liq} - T)}{\eta},$$

where R is the rate of crystal growth, T_{liq} is the liquidus temperature, T is the temperature during holding period, η is the viscosity, and K is a constant. A plot of this equation fitted one set of his data fairly well but not others.

From a consideration of the difference in vibrational energy between condensation and melting at a plane glass-crystal boundary, Cox and Kirby [14] derived an equation for the rate of crystal growth of the form,

$$R = A^{-E_1/KT} 1 - (r+1)^{E_1 - E_2},$$

where E_1 is the vibrational energy needed to make the ions in the glass mobile, E_2 the energy that is necessary to make the ions in the crystal mobile, r the ratio of the surface densities of crystal and glass, T the absolute temperature, and A and K are constants. While this equation gave a fair fit for most of their data, there was poor agreement at temperatures immediately below the liquidus temperature for the two borosilicate-type glasses that they used.

A comparison of the rates of crystal growth in glass-forming and nonglass-forming materials (table 3) shows the tremendous differences in their rates of growth. As the rate of crystal growth increases it becomes increasingly difficult to produce glass.

V. Summary

An improved apparatus for the rapid determination of liquidus temperatures and rates of crystal growth has been developed.

The simplified technique required with this apparatus makes it possible for an inexperienced operator to determine quickly data that formerly required much time and skill.

A rapid means is provided the glass technologist for assessing the effects of changes in composition upon the devitrification characteristics of glasses.

The authors express thanks to William R. Eubank for his aid in determining liquidus temperatures by the quenching method, to Charles P. Saylor for aid in preparing the photomicrographs, and to Clarence H. Hahner for helpful suggestions.

VI. References

[1] J. L. Littleton, J. Soc. Glass Tech. Trans. **15,** 262 (1931).
[2] E. Preston, J. Soc. Glass Tech. **24,** 139 (1940).
[3] F. P. Hall and H. Insley, J. Am. Ceram. Soc. **30,** No. 11, part 2 (1947).
[4] G. Tammann, J. Soc. Glass Tech. **9,** 166 (1925).
[5] E. Zschimmer and A. Dietzel, Sprechsaal **60,** 110, 129, 165, 186, 204 (1927).
[6] K. Tabata, Researches Electrotechnical Laboratory, Japan, No. 191 (1927).
[7] H. R. Swift, J. Am. Ceram. Soc. **30,** 165 (1947).
[8] C. W. Parmelee and A. J. Monack, J. Soc. Glass Tech. **13,** 322 (1929).
[9] W. B. Silverman, J. Am. Ceram. Soc. **22,** 378 (1939).
[10] E. H. Hamilton, O. H. Grauer, Z. Zabowsky, and C. H. Hahner, J. Research NBS **40,** 361 (1948) RP1881.
[11] J. Frenkel, Physik. Z. Sowjetunion **1,** 498 (1932).
[12] W. T. Richards, J. Chem. Phys. **4,** 449 (1936).
[13] A. A. Leontjewa, Acta Physicochim. URSS, **14,** 245 (1941).
[14] S. M. Cox and P. L. Kirby, Nature **159** [4031] 162 (1947).

WASHINGTON, February 13, 1950.

U. S. Department of Commerce
National Bureau of Standards

Research Paper RP2097
Volume 44, May 1950

Part of the Journal of Research of the National Bureau of Standards

Infrared Spectra of Bromochloromethane, Dibromomethane, Tribromochloromethane, and Tetrabromomethane

By Earle K. Plyler, W. Harold Smith, and N. Acquista

The infrared spectra of bromochloromethane, dibromomethane, tribromochloromethane, and tetrabromomethane have been measured from 2 to 36 microns. By the use of the results of other workers in Raman spectra it has been possible to classify all the strong bands that have been observed. Many of the weaker bands were classified as combinations and overtones. Only a few of the bands of tetrabromomethane were observed, on account of the breaking down of the compound in solutions of carbon disulfide and carbon tetrachloride. The intense bands of dibromomethane and tetrabromomethane were measured in the vapor state. The infrared absorption bands of these compounds had not previously been measured over an extended range of wavelengths, and these measurements were undertaken to determine the positions of weak bands so that a more complete classification of the spectra of these molecules could be made.

I. Introduction

Other workers have measured the vibrational bands of a number of substituted methanes in the infrared region, and also the frequencies have been determined by Raman spectra. From theory it has been determined that molecules of the type of CX_4 show two active and two inactive fundamentals. Where interaction occurs the inactive frequencies also appear in the infrared spectrum. When the substituted atoms are of more than one species, the degeneracy is removed and nine fundamentals are present in the spectrum. In a molecule of the type CXY_3, the degeneracy is only partly removed and six fundamentals are found in the spectrum.

The four substituted methanes, bromochloromethane, dibromomethane, tribromochloromethane, and carbon tetrabromide, represent the the three types of molecules that give nine, six, and two active fundamentals in the infrared spectrum. The infrared bands of these compounds had not previously been measured over an extended range of wavelengths, and these measurements were undertaken to determine the positions of the weak bands so that the combination bands could be classified.

II. Experimental Observations

A Perkin-Elmer spectrometer was used for all measurements with lithium fluoride, potassium bromide, sodium chloride, and thallium bromide-iodide prisms to cover the wavelength range of 2 to 36 μ. In the spectral region of 2 to 24 μ, cell thicknesses of 0.2, 0.1, and 0.05 mm were used to bring out most of the bands. For very strong bands the compounds were diluted either in carbon tetrachloride or in carbon disulfide, or liquid films with a thickness of 0.01 mm or less were formed between two potassium bromide windows. In the thallium bromide-iodide region between 24 and 36 μ it was necessary to use cell thicknesses of 1.5 mm to bring out the weaker absorption bands. The method of measurement and the reducing of data have been described in a previous paper [1].[1] Bromochloromethane, dibromomethane, and tribromochloromethane were obtained from the Dow

[1] Figures in brackets indicate the literature references at the end of this paper.

Chemical Company and tetrabromomethane from the Eastman Kodak Company.

Purification consisted of treatments until an examination of the products indicated satisfactory agreement with accepted physical constants. To avoid any effect of oxygen, the infrared measurements were made as quickly as possible after purification.

Figure 1 shows the absorption spectra of the four halogenated methane derivatives in the region from 2 to 15 μ. The cell thicknesses and other conditions of the measurements are given on the figure and in the captions. The intense bands were observed by use of a cell that contained a thin layer of the material. The cell was made by placing a small quantity of the liquid on a plate of potassium bromide and then pressing another plate on the top without the use of a shim. The thicknesses of the cells made in this manner were not measured, but it is estimated that they were of the order of 0.005 mm. This estimate of the thickness was made on the basis of the percentage absorption that was observed in a 0.1-mm cell when the compound had been diluted with a transparent solvent. The reason that the thin cell was employed was to locate the position of the band accurately for the pure liquid in regions of intense absorption. In figure 1 the portions of the absorption curves represented by broken lines indicate that small details could not be accurately determined on account of the absorption of the solvents or the absorption of atmospheric bands.

As tribromochloromethane and tetrabromomethane are solids at room temperature, their spectra were determined in solutions of carbon tetrachloride and carbon disulfide. There was a tendency for the solutions of tetrabromomethane to darken on standing, and the absorption spectrum was

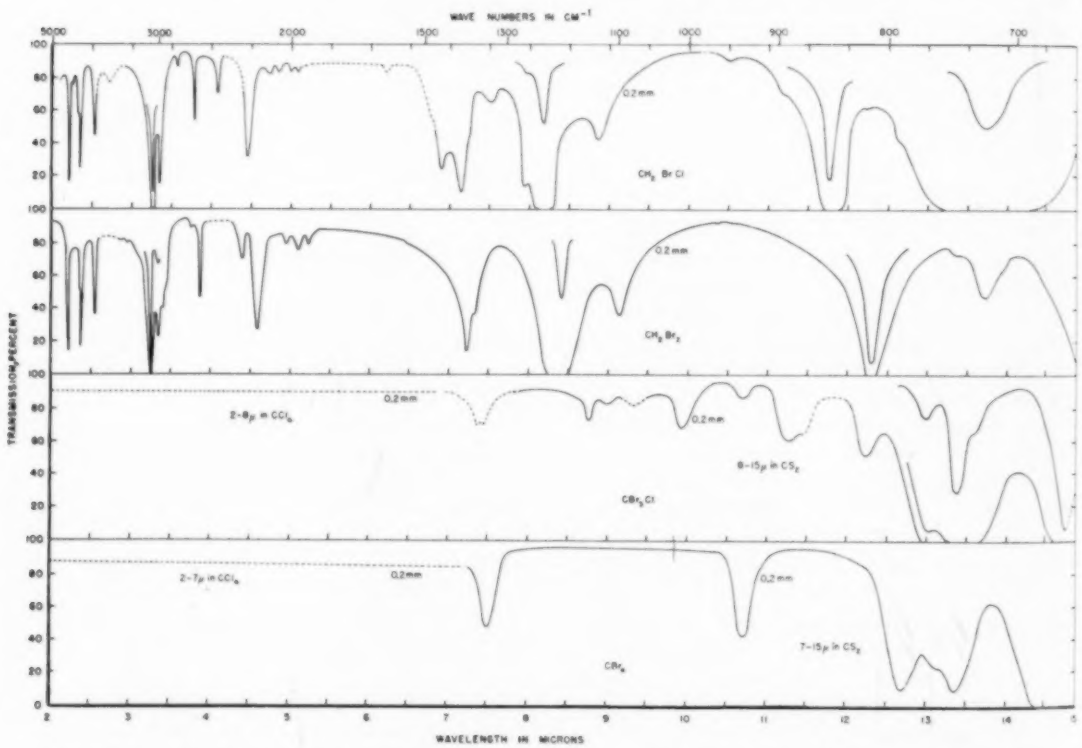

FIGURE 1. *Infrared absorption spectra of bromochloromethane, dibromomethane, tribromochloromethane, and tetrabromomethane.*

Tribromochloromethane and tetrabromomethane were dissolved in carbon tetrachloride and carbon disulfide. The solution concentration of tribromochloromethane in carbon tetrachloride is 3.1 g/ml, and in carbon disulfide, 2.4 g/ml for the observations in 0.2-mm cell. For the insert bands the concentration is 0.14 g/ml. Saturated solutions of tetrabromomethane were prepared in each solvent.

measured immediately after their preparation. The observations were repeated several times and the same bands were always found. Since it was possible to account for all the observed bands as combinations, overtones, or fundamentals, it does not seem probable that any of the observed bands were produced by products of decomposition or oxidation in the solution.

Figure 2 shows the long wavelength spectra of the four substituted methanes from 14 to 36 μ. Some general absorption was observed in the spectra of bromochloromethane and dibromomethane from 28 to 36 μ, but no definite bands could be found in this region. For the measurement of tribromochloromethane in the region of 24 to 36 μ, a saturated solution in methylcyclohexane was used. The methylcyclohexane has a high transmittance in this region, and its spectrum shows only one absorption band when a cell 1.5 mm thick is used.

In figures 3 and 4 are shown some of the absorption bands of dibromomethane and tetrabromomethane measured in the vapor state. The substances were placed in the bottom of a cell 40 cm long, which was not evacuated, and allowed to remain in the cell for several hours. On repeating the measurements 6 hours later, it was found that the bands did not increase in intensity. It is probable that the vapors were at a saturated condition in the air of the cell at 25° C.

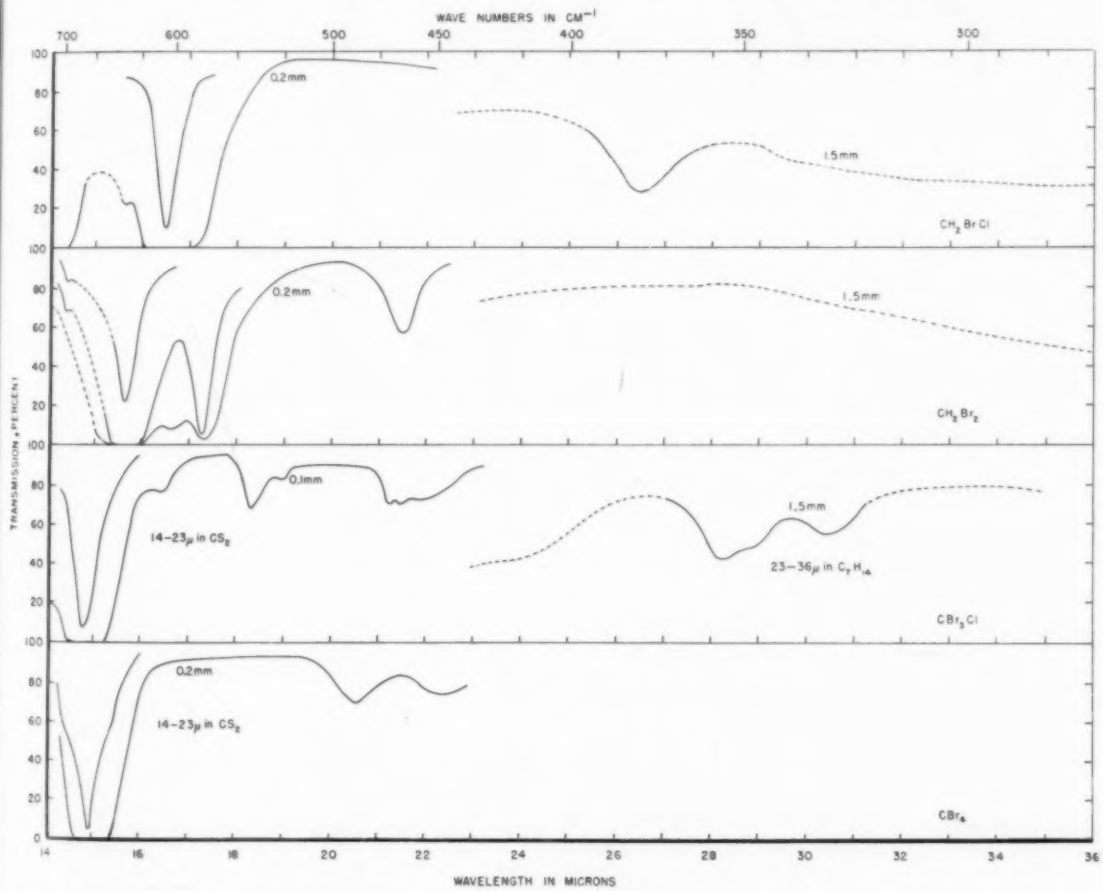

FIGURE 2. *Absorption spectra of bromochlo omethane, dibromomethane, tribromochloromethane, and tetrabromomethane in the region from 14 to 36 μ.*

A solution concentration of 4.0 g/ml in carbon disulfide was used for tribromochloromethane with the 0.1-mm cell. A concentration of 0.14 g/ml was used in the 0.05-mm cell. A saturated solution in methylcyclohexane was used in the region of 24 to 36 μ.

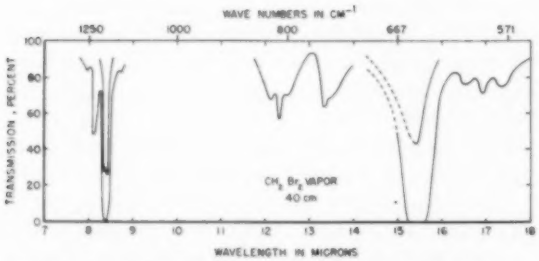

FIGURE 3. *Absorption spectrum of dibromomethane vapor from 7 to 18 μ.*

The more intense absorption is for the saturated vapor (45 mm of Hg at 25° C).

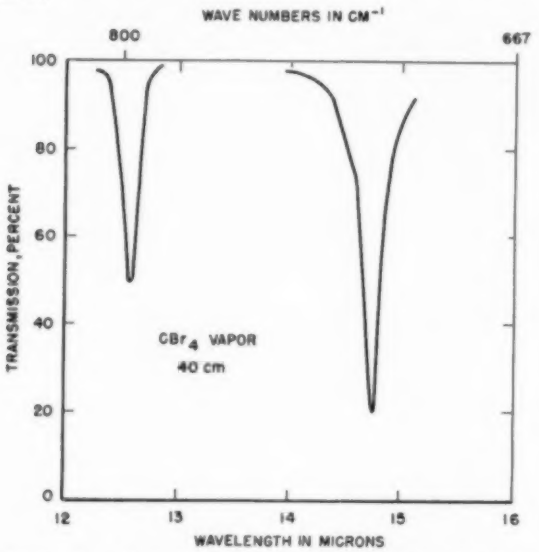

FIGURE 4. *Absorption bands at 12.6 and 14.9 μ for saturated vapor of tetrabromomethane at room temperature.*

III. Discussion

In table 1 are given the wavelengths and frequencies of the observed bands. These bands have been interpreted as fundamentals, combinations, and harmonics. The numbering of the levels is in accordance with that adopted for correlation of a large number of molecules of different symmetries, as will be discussed in a forthcoming paper by Plyler and Benedict. Eight of the infrared active fundamentals of bromochloromethane have been observed, and the other, occurring at 226 cm^{-1}, was outside the range of the thallium bromide-iodide prism. In the determination of the combination bands for this compound the Raman value was used from the work of W. Bacher and J. Wagner [2]. The other fundamental bands, as determined by Raman spectra, check within a few wavenumbers with infrared measurements given in table 1, except ν_7, which was estimated by them at 724 cm^{-1} from Raman

TABLE 1. *Observed frequencies of the infrared bands of bromochloromethane, dibromomethane, tribromochloromethane, tetrabromomethane, and their assignments*

Classification	ν	λ
	cm^{-1}	*Microns*
BROMOCHLOROMETHANE		
ν_4	* 226(R)	44.2
ν_2	606	16.51
ν_9	728	13.73
ν_7	852	11.76
ν_5	1,130	8.85
ν_8	1,225	8.16
ν_3	1,402	7.13
ν_1	2,987	3.348
ν_6	3,060	3.268
$\nu_2-\nu_4$	377	26.5
$\nu_7-\nu_4$	638	15.65
$\nu_4+\nu_9$	950	10.52
?	1,261	7.93
$\nu_2+\nu_7$	1,331	7.51
$2\nu_9$	1,453	6.88
$\nu_5+\nu_8$	1,969	5.08
$\nu_2+\nu_5$	2,004	4.99
$\nu_5+\nu_6$	2,006	4.84
$\nu_3+\nu_9$	2,119	4.72
$\nu_3+\nu_7$	2,242	4.460
$2\nu_8$	2,450	4.082
$\nu_3+\nu_8$	2,639	3.789
$2\nu_5$	2,803	3.568
$\nu_1+\nu_9$	3,751	2.665
$\nu_6+\nu_7$	3,939	2.539
$\nu_1+\nu_8$	4,228	2.365
$\nu_5+\nu_6$	4,502	2.221
DIBROMOMETHANE		
ν_4	* 174(R)	57.5
ν_2	579	17.27
ν_9	639	15.66
ν_7	813	12.29
ν_5	1,096	9.12
ν_8	1,190	8.40
ν_3	1,385	7.22
ν_1	2,988	3.347
ν_6	3,065	3.263
$\nu_2-\nu_4$	466	21.5
?	729	13.71
$\nu_5-\nu_4$	922	10.85
$\nu_4+\nu_9$	1,366	7.32
$\nu_3+\nu_7$	1,912	5.23
$\nu_3+\nu_2$	1,961	5.10
$\nu_3+\nu_9$	2,020	4.95
$2\nu_5$	2,179	4.59
$\nu_3+\nu_8$	2,587	3.866
$\nu_9+\nu_7$	3,909	2.558
$\nu_1+\nu_5$	4,195	2.384
$\nu_1+\nu_6$	4,488	2.228

Classification	ν	λ
	cm^{-1}	*Microns*
DIBROMETHANE VAPOR		
?	1,233	8.11
ν_8	1,195	8.37
ν_7	810	12.34
?	745	13.42
ν_9	648	
ν_2	591	
TRIBROMOCHLOROMETHANE		
ν_{25}	* 141(R)	70.9
ν_{19}	* 214(R)	46.7
ν_4	215(calc.)	46.5
ν_1	329	30.4
ν_{18}	675	14.81
ν_7	747	13.39
$\nu_{25}+\nu_{19}$	355	28.2
$2\nu_4$, $2\nu_{19}$	436	22.9
$\nu_1+\nu_{25}$	467	21.4
$\nu_1-\nu_4$	525	19.01
$\nu_7+\nu_{19}$	545	18.35
$\nu_1-\nu_{25}$	608	16.44
?	735	13.61
$2\nu_4+\nu_{25}$	769	13.00
$\nu_{18}+\nu_{25}$	817	12.23
$\nu_{19}+\nu_{18}$	872	11.47
$\nu_{18}+\nu_4$	886	11.28
?	933	10.69
$\nu_{18}+\nu_1$	1,006	9.94
$\nu_1+\nu_7$	1,068	9.33
$\nu_1+\nu_{25}+\nu_{19}$	1,114	8.98
$\nu_7+\nu_{25}+\nu_{18}$	1,141	8.76
$2\nu_{18}$	1,350	7.40
TETRABROMOMETHANE		
ν_{25}	* 123(R)	81.3
ν_{19}	* 183(R)	54.6
ν_3	* 267(R)	37.4
ν_{18}	669	14.95
$\nu_{18}+\nu_3+\nu_{19}$	748	13.38
$\nu_{25}+\nu_{18}$	787	12.70
$\nu_7+\nu_{18}$	934	10.71
$2\nu_{18}$	133	7.50
TETRABROMOMETHANE VAPOR		
$\nu_{25}+\nu_{18}$	796	12.57
ν_{18}	678	14.75

* (R) indicates Raman value obtained from literature.

spectra, and has been observed by us in the infrared spectra as a strong band at 852 cm^{-1}.

All of the fundamental bands of dibromomethane have been observed in the infrared spectrum except ν_4 at 174 cm^{-1}. This value has been determined by Dadieu and Kohlrausch and several other workers in Raman spectra [3]. The Raman spectra for the remaining eight fundamentals check well with these observations, except that ν_7 and ν_8 are found at 813 and 1,190 cm^{-1}, respectively, in the infrared as compared to 723 and 1,133 cm^{-1}, respectively, in the Raman spectrum as reported by Dadieu and Kohlrausch. The other observed bands, except for a few weak ones, have been classified on the basis of the nine fundamentals.

A close similarity between the spectrum of dibromomethane and of bromochloromethane is observed. The effect of replacing the chlorine in bromochloromethane by the heavier atom bromine is to shift corresponding vibrations to longer wavelengths. The shift is observed for all frequencies except those involving primarily C—H stretching vibrations. As can be seen from table 1, the values of ν_1 and of ν_6 for the two compounds fall within 5 cm^{-1} of each other. This difference in wavenumber is almost within the limit of experimental error for this region of the spectrum.

The spectrum of dibromomethane was also determined in the vapor state for some of the intense bands, so that a comparison could be made with the liquid state. The type of bands at 1,195 and 648 cm^{-1} could not be determined with the prism instrument available. For the band at 1,190 cm^{-1} in the liquid state there is a small shift to 1,195 cm^{-1} in the vapor state. The other band shifted from 639 to 648 cm^{-1}. Two of the remaining bands located at 810 and 591 cm^{-1} show definite zero branches when measured in the vapor state. These bands have shifted from 813 and 579 cm^{-1}, respectively, as measured in the liquid state. The vapor band at 745 cm^{-1} is shifted 16 cm^{-1} from the liquid band at 729 cm^{-1} and may have a zero branch. The comparison of the positions of the bands in the liquid and in the vapor states shows that there is a small change in the frequencies when measured in the two different states.

Of the six active infrared fundamentals of tribromochloromethane, only three bands, ν_1, ν_{68}, and ν_3, were observed in the infrared region that was covered in these measurements. The other three fundamentals fall beyond the range of the thallium bromide-iodide prism. Calculations show that two of these bands, ν_{79} and ν_4, should have frequencies at 214 and 215 cm^{-1}, respectively. The calculated values are in good agreement with the wavenumber of a single Raman line determined by Lecomte and coworkers [4].

For the classification of the combination and harmonic bands, the Raman values 141 and 274 cm^{-1} have been used. The three fundamentals observed in the infrared checked within 5 cm^{-1} with the Raman values of Lecomte. The differences between the infrared and Raman values may be attributed to the effect of the solvent carbon disulfide on the tribromochloromethane in producing a small shift in the bands, and also to the presence at 667 cm^{-1} of the absorption band of atmospheric CO_2, which made it difficult to locate accurately the position of the band at 675 cm^{-1}. The two absorption bands at 735 and 933 cm^{-1} could not be accounted for on the basis of the fundamentals.

In comparing the fundamentals of tribromochloromethane and tetrabromomethane, it is seen that the substitution of the bromine atom for the chlorine atom reduces the number of fundamentals from six to four. Only the two threefold degenerate vibrations, ν_{168} and ν_{479}, are infrared active. The remaining two appear in combination. One of these bands, ν_{168}, with frequency 669 cm^{-1}, was observed in the rocksalt region. This is 4 cm^{-1} greater than the Raman value as determined by Dadieu and Kohlrausch [5]. This difference can probably be attributed to error of observation caused by the presence at 667 cm^{-1} of the absorption band of atmospheric CO_2. The other bands in the observed spectrum, which are of low intensity, can be interpreted on the basis of the four fundamentals. Three of the fundamentals listed in table 1 are the Raman values determined by Dadieu and Kohlrausch.

The classification of the bands as given in table 1 accounts for most of the observed bands. The band observed at 729 cm^{-1} in dibromomethane was not classified and may have arisen from a small amount of bromochloromethane that was present as an impurity. There was observed an intense band in this region for bromochloromethane. When the vapor of dibromomethane was measured, the ratio of intensities of the bands at 735

cm^{-1} and 813 cm^{-1} were much different than in the liquid, and also a band at 1,233 cm^{-1} appeared. This is near the location of another intense band of bromochloromethane at 1,225 cm^{-1} as measured in the liquid state. Another sample of dibromomethane was measured that also contained these bands. According to mass spectrograph determinations it contained about 1 percent of chlorine. It is probable that a small amount of bromochloromethane is present in the dibromomethane and produces the bands that do not fall in the classification scheme. On further purification of dibromomethane it was found that the band in the region of 13.6 μ (729 cm^{-1}) disappeared when the compound was measured in cells 0.1 mm thick.

Without a study of the rotational structure of these bands the molecular constants cannot be obtained. Unpublished observations made with a different instrument show resolution of some of the near infrared bands of dibromomethane and bromochloromethane into a series of lines approximately 1.5 cm^{-1} apart. The spacing interval is less for dibromomethane than for bromochloromethane.

The authors thank W. S. Benedict of this Bureau for his discussions on the classification of the bands of these compounds.

IV. References

[1] E. K. Plyler, R. Stair, and C. J. Humphreys, J. Research NBS **38,** 211 (1947).
[2] W. Bacher and J. Wagner, Z. physik Chem. (B) **43,** 191 (1939).
[3] A. Dadieu and K. W. F. Kohlrausch, Mh. Chem. **53,** 58 (1930); **57,** 488 (1931).
[4] J. Lecomte, H. Volkringer, and A. Tchakirian, J. phys. radium **9,** 105 (1938).
[5] A. Dadieu and K. W. F. Kohlrausch, Mh. Chem. **57,** 488 (1930).

Washington, November 18, 1949.

U. S. Department of Commerce
National Bureau of Standards

Research Paper RP2098
Volume 44, May 1950

Part of the Journal of Research of the National Bureau of Standards

Mass Spectrometric Analysis of a Standard Sample of Carburetted Water-Gas by Laboratories Cooperating With the American Society for Testing Materials

By Martin Shepherd [1]

The mass spectrometer was used for the analysis of a standard sample of carburetted water-gas by laboratories cooperating with Subcommittee VII of Committee D–3 of the American Society for Testing Materials. The results of the cooperative analysis show the reproducibility and, in certain respects, the accuracy of this powerful new apparatus for gas analysis. The heating value and the specific gravity of the sample calculated from the analytical data were compared with the known values. Some very creditable work is reported, but the need for improvement and standardization with respect to the determination of hydrogen, carbon monoxide and nitrogen is evident.

I. Introduction

This report is the fifth of a series of cooperative analyses of standard gas samples [2] conducted to furnish basic information for the development of standard methods for the analysis of fuel gases. The development of these standards is a task assigned to Subcommittee D–3–VII of the ASTM, and the method of this development has been outlined in four previous reports.[3]

The 27 laboratories that cooperated in the present work were widely distributed geographically, but most of them were associated with the petroleum industry. There was some representation from the chemical industry and Government laboratories. In general, all the laboratories followed the operating procedures prescribed in the manuals furnished with the instruments. Departures from the prescribed course were few and of such nature that no significant change was expected or observed. The greatest variation was in the method of computation. Thus, with respect both to apparatus and methods of operation, this series of cooperative analyses was conducted with a preliminary standardization that was unofficial but none the less real; and, while this may or may not have been a factor in the accuracy achieved, it must have affected the over-all reproducibility. The need for further standardization, particularly in calculating methods, is evident.

II. Standard Carburetted Water-Gas Sample ASTM D–3–VII–5

The preparation of the standard sample of the carburetted water-gas type, identified as ASTM D–3–VII–1, which was used in the cooperative analysis by volumetric chemical methods, has been described in detail in Research Paper RP1704 (see footnote 3). That account will serve to establish the history of the present sample, ASTM D–3–VII–5, which was analyzed by the mass spectrometer, since the No. 1 and No. 5 samples were identical, except for oxygen, which had been mostly removed from sample 5. This information was not disclosed when sample 5 was issued, and accordingly it was analyzed as a blind sample.

[1] Chairman of Subcommittee VII (Analysis of Gaseous Fuels) of Committee D-3 (Gaseous Fuels), American Society for Testing Materials.

[2] These samples are not to be confused with the regular Standard Samples prepared and offered for sale by this Bureau. They are mixtures prepared especially for these cooperative analyses and are issued to laboratories cooperating with the American Society for Testing Materials on this project.

[3] Martin Shepherd, Analysis of a standard sample of the carburetted water-gas type by laboratories cooperating with the American Society for Testing Materials, J. Research NBS **36**, 313 (1946) RP1704; Analysis of a standard sample of *natural* gas by laboratories cooperating with the American Society for Testing Materials, J. Research NBS **38**, 19 (1947) RP1759; Cooperative analysis of a standard sample of natural gas with the mass spectrometer, J. Research NBS **38**, 491 (1947) RP1789; Analysis of a natural gas by volumetric chemical methods and by mass spectrometer, Anal. Chem. **19**, 635 (1947).

880789—50——5

In general, it did not find its way into the same laboratories that had performed the chemical analyses, although, in a few cases, this did happen.

Sample ASTM D–3–VII–5 was issued in the same type of cylinder as that used for the sample 1, and the instructions for transferring it to the spectrometer without contamination were essentially the same. This information will, accordingly, not be repeated here.

Chemical and physical methods were thus put into direct competition. The part of the story concerned with the analysis by the mass spectrometer is given in this paper. A comparison of the two methods will be given in another paper.

III. Analytical Results

All of the analytical data submitted have been tabulated, together with the average values derived from each laboratory's analyses; but the study of these data for a long time would not serve to reveal what may be seen at a glance when these same data are presented in a series of frequency-distribution plots. These plots, which amount to actual pictures of the analytical results, will enable the reader to arrive at the obvious conclusions.

In the plots, each circle represents a value derived from a single determination of the substance indicated in the legend. The abscissas are values derived from the analyses; and these values are plotted equidistant on the ordinates and so indicate the frequency with which these values occur. For example, the frequency-distribution plot for carbon dioxide (fig. 1) shows that 4 determinations gave the value 4.0 percent, 8 determinations gave 4.1 percent, 4 gave 4.2 percent, 10 gave 4.3, 18 gave 4.4, and so on. The plots are divided into two sections, one of which shows the laboratory averages, the other all of the determinations. Thus a laboratory to laboratory comparison may be made, but the study of accuracy and reproducibility may be referred to the plot giving all determinations. This system is carried throughout the group of plots, and with this in mind, they can be studied. The analyses for each component will be considered.

Carbon Dioxide (fig. 1). All of the determinations for carbon dioxide are given in figure 1. The greatest frequency is indicated at 4.5, in agreement with the arithmetical average (determined

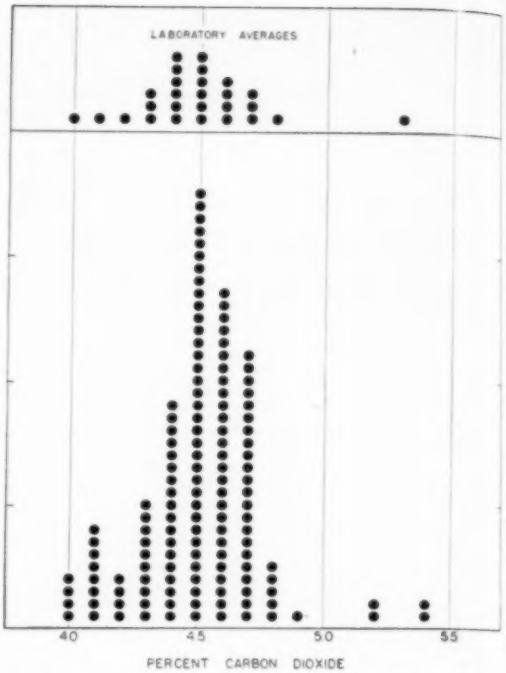

FIGURE 1. *Frequency-distribution plot for percentage of carbon dioxide.*

with four high values dropped), 4.49 ±0.14 (average deviation), and with the median, 4.5. These values agree with the most probable value, 4.44 ±0.04, previously determined (RP1704). The laboratory average is 4.49 ±0.17—or, with one high value dropped, 4.46 ±0.14. Accuracy and reproducibility are thus satisfactory.

Oxygen (fig. 2). Oxygen occurred in this sample in an amount less than 0.05 percent, so that rounded off values indicate its absence in 66 percent of the determinations. After dropping the three high values, the arithmetical average becomes 0.03. Highest frequency and median are found at 0. Laboratory average (without the three high rogues) is 0.03. Most of the determinations of this gas are satisfactory.

Carbon Monoxide (fig. 3). The spectrometer was not altogether comfortable with respect to this determination. Some analysts calculated from the over-populated though most sensitive 28 peak; a few others used the less sensitive 12 peak. In one case CO was completely confused with N_2. The plot shows no adherence to the Gaussian pattern. The arithmetical mean com-

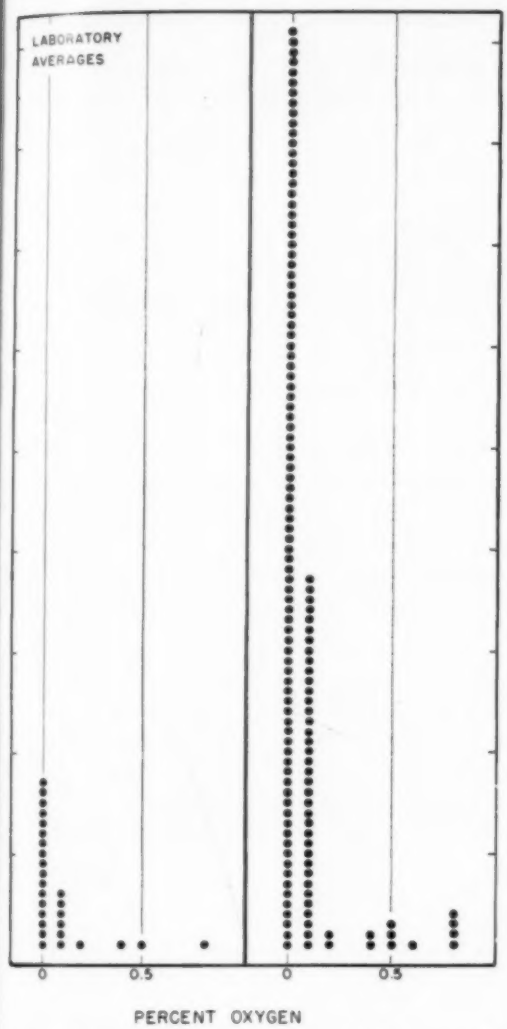

FIGURE 2. *Frequency-distribution plot for percentage of oxygen*

puted from values between 28.4 and 32.3, inclusive, is 30.3 ±0.9, which is in reasonable agreement with the chemical determination of 29.41 ±0.18, even though its derivation included a wide variety of values. No highest frequency is apparent; the median is 30.35. The laboratory averages range from 19.3 to 33.5 (dropping one zero); their average is 29.8 ±1.5. Need for improvement is evident.

Hydrogen (fig. 4). The spectrometer is not altogether happy with this determination, as shown by the far flung values and disregard for the Gaussian shape. The mean, computed from values between 33.0 and 37.8, inclusive, is 35.1 ±0.8. The median is 35.1. These values agree well with the chemical determination of 35.0, even though the derivation was from scattered values. Improvement is needed, and, indeed, some has been achieved since these data were taken. Laboratory averages range from 31.9 to 38.6; their average is 35.2 ±1.1.

Methane (fig. 5). While some difficulty was experienced with carbon monoxide and hydrogen in this sample (and more difficulty will occur with nitrogen), the spectrometer is at home in dealing with the hydrocarbon fractions of this gas. The change is evident in the methane plot. The mean (with three low values dropped) is 8.0 ±0.4; the median is 8.0; and the highest frequency occurs at 8.1. Laboratory averages range from 6.2 to 9.3; their average is 7.9 ±0.4. In general, the values are satisfactorily clustered, and a Gaussian pattern is now evident.

Ethane (fig. 6). A clean-cut analysis for ethane is shown in this plot. The highest frequency occurs at 3.3. The mean is 3.3±0.15, and the median is 3.3. Laboratory averages range from 2.8 to 3.5, with an average of 3.3±0.15. The answer seems to be 3.3.

Ethylene (fig. 7). Determination of the ethylene was not achieved in the decisive manner shown in the determination of the ethane. (In general, this is true of the unsaturated hydrocarbons.) Nevertheless, the determination for ethylene was satisfactory. The plot shows a block-like structure of values centered about 13 percent. The mean is 12.9±0.4, and the median is also 12.9.

Other hydrocarbons reported in small amounts are shown at the right of the plot for ethylene. There are not many, but out of 138 analyses, propane was reported 15 times, propylene 18 times, *n*-butane 6 times, butenes 6 times, "C_3" three times, C_3+ heavier hydrocarbons 12 times, and acetylene 3 times.

Nitrogen (fig. 8). The values for nitrogen are sufficiently diverse to be statistically inconvenient from the analyst's viewpoint. The laboratory averages vary from 4.3 to 13.8 (dropping eight values at 36.+), with an average of 6.4±0.1. The mean for all determinations is 5.9±0.8, if values from 4.2 to 8.2, inclusive, are accepted. The pattern is not molded along classical lines. The

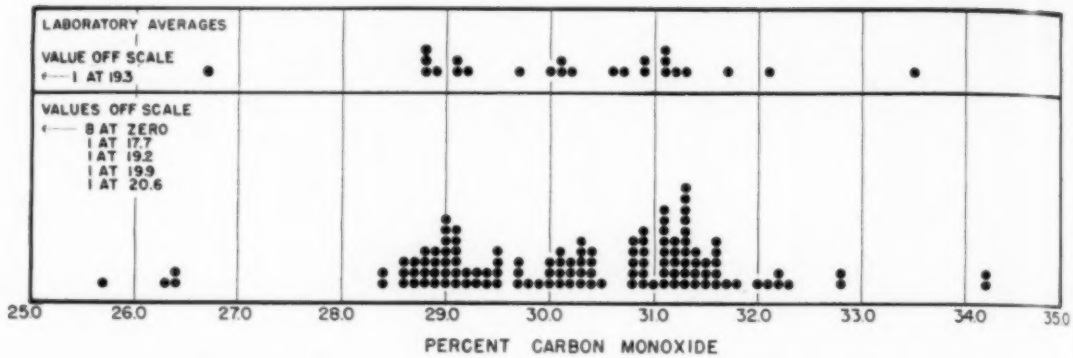

FIGURE 3. *Frequency-distribution plot for percentage of carbon monoxide.*

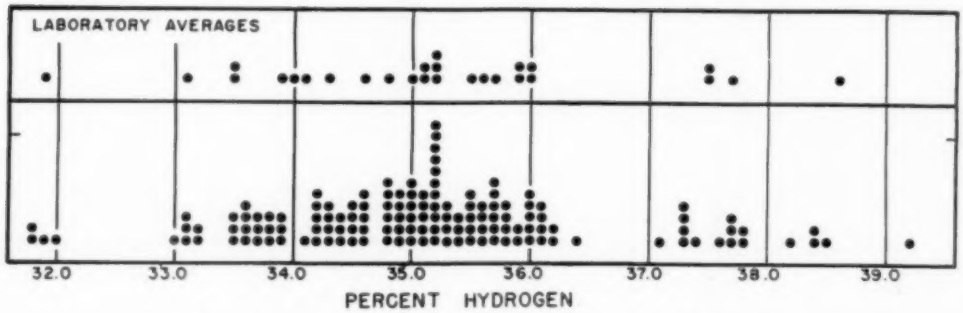

FIGURE 4. *Frequency-distribution plot for percentage of hydrogen.*

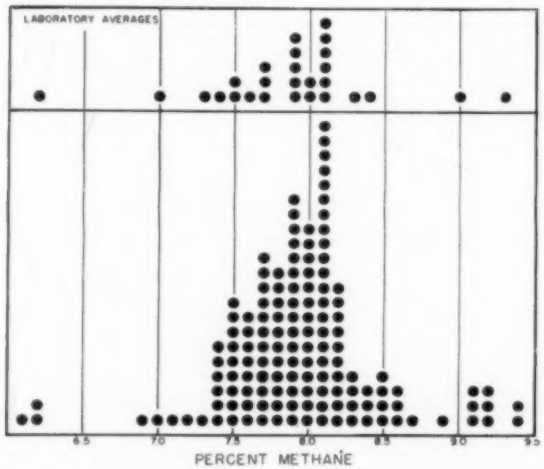

FIGURE 5. *Frequency-distribution plot for percentage of methane*

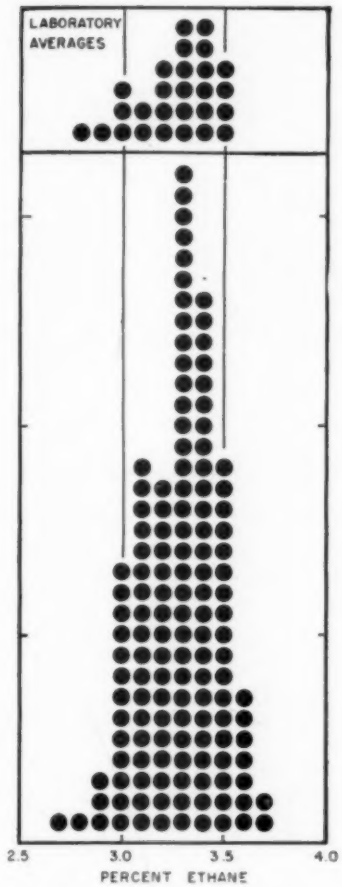

FIGURE 6. *Frequency-distribution plot for percentage of ethane.*

median is 5.8, dropping eight values at 36.+. The median is nearer the best chemical value of 5.74±0.06. Certainly this determination must be improved for this type of gas.

Calculated Specific Gravity (fig. 9). Specific gravity calculated from the mass spectrometric analyses show rogues to both right and left of center. The mean of all values between 0.626 and 0.677 is 0.650±0.007; the median is 0.651. The Gaussian pattern is distorted, with maxima suggested at 0.644 and about 0.651. Laboratory averages range from 0.617 to 0.676,with an average of 0.648±0.009. The actual measured value for this sample is 0.6475.[4] It should be remembered that calculated specific gravity is a direct over-all measurement of the accuracy of the analysis.

Calculated Heating Value (fig. 10). The plot again shows no decisive Gaussian pattern. The mean of values from 529 to 566 is 550±7, and the median is 551. Laboratory average is 547+8, dropping the value 458. The measured value is 549.[5]

IV. The Tabulated Data

No attempt has been made to set forth all of the statistical inferences that can be derived from the data given in this report. The whole object of the report is to present a general integrated picture of the real state of analysis of this kind without, for the moment, distracting particulars. This is not to say that a statistical study will not prove of equal or greater value, but it should be presented separately. To tempt someone to do this, the data are given in table 1 at the end of this paper.

The table is self-explanatory except for the column "Operator-Spectrogram-Calculator Key." The experiment was designed to show the effect of these three factors—the operator of the spectrometer, the instrument itself as indicated by the spectrogram it produced, and the calculator who derived the final answer from the spectrogram. Each laboratory was asked to produce four spectrograms of the standard sample, using two instrument operators and two calculators. The complete pattern for each laboratory should have been

O1–S1–C1
O1–S1–C2
O1–S2–C1
O1–S2–C2
O2–S3–C1
O2–S3–C2
O2–S4–C1
O2–S4–C2

where O means operator, S designates spectrogram, and C, the calculator. The O–S–C key of the table is thus explained. The table discloses only seven complete patterns, while others are partially complete, or not clearly defined.

Before passing these data along to competent statistical talent, a few observations may be briefly made. If the complete patterns for

[4] The specific gravity was measured by Carrol Creitz at this Bureau. The method used is described in NBS Miscellaneous Publication M177 (1947).

[5] The heating value was measured by John Eiseman and Ralph Jessup at this Bureau.

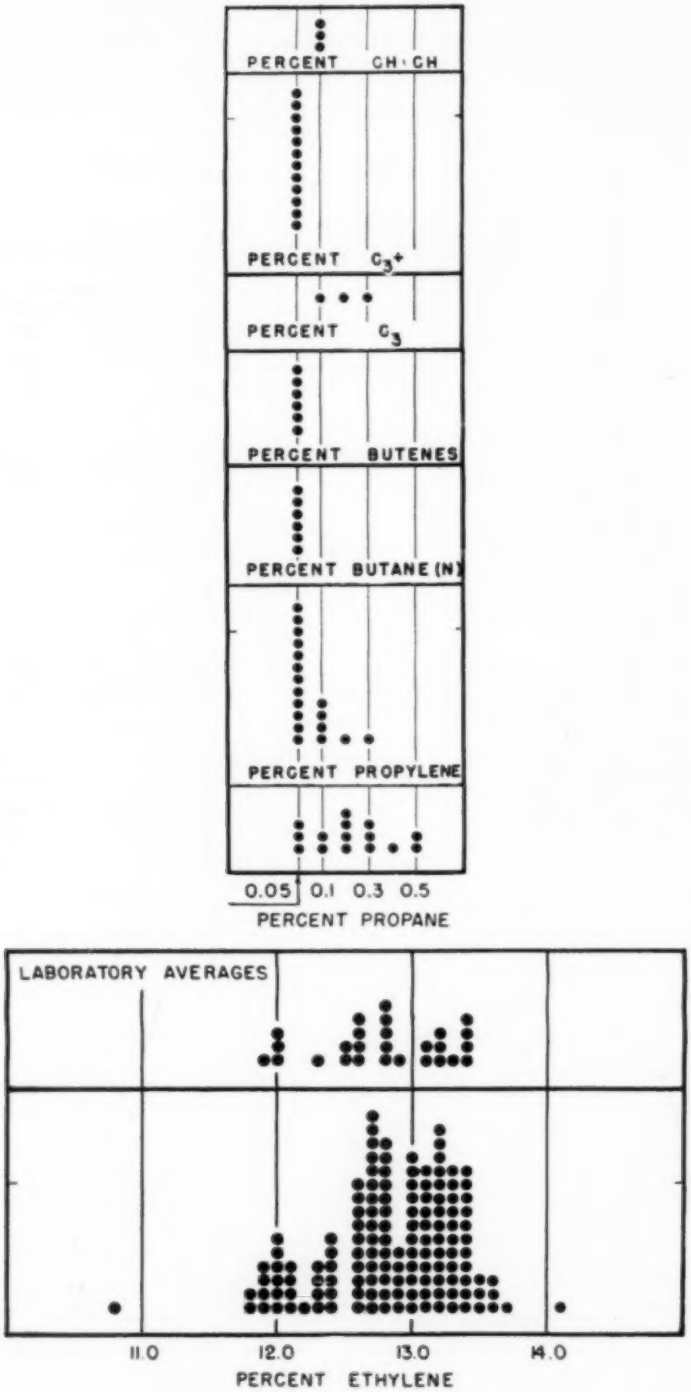

FIGURE 7. *Frequency-distribution plots for percentages of ethylene and propane.*

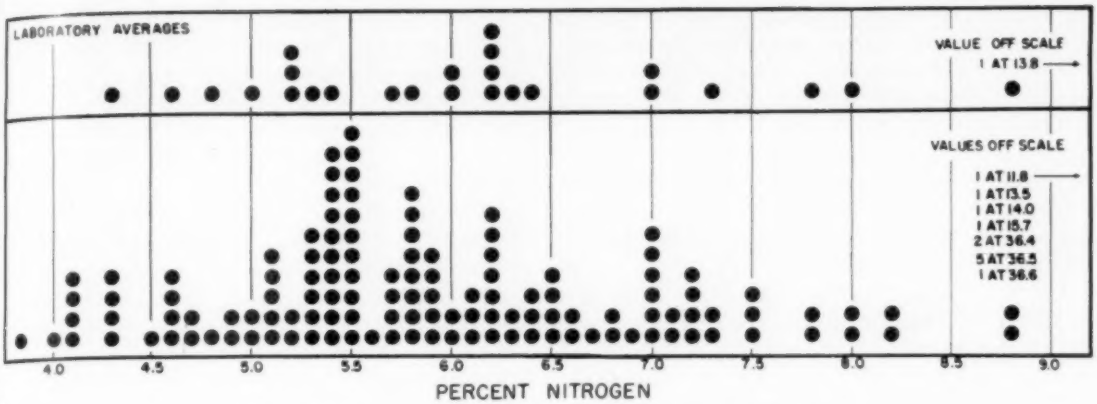

FIGURE 8. *Frequency-distribution plot for percentage of nitrogen.*

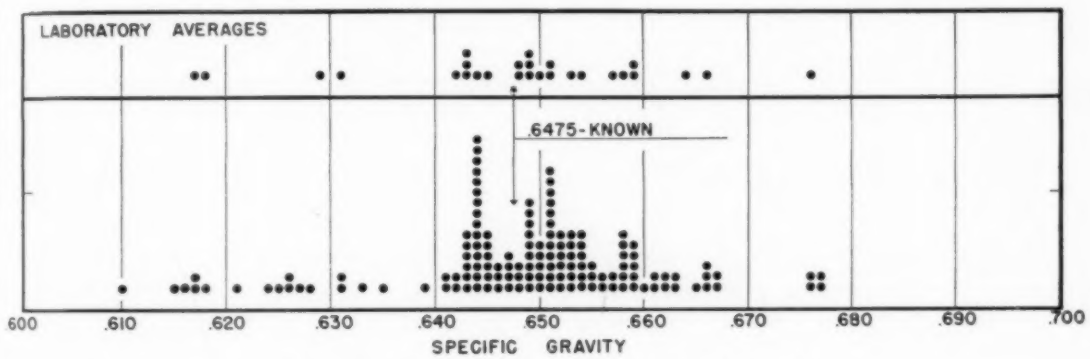

FIGURE 9. *Frequency-distribution plot for specific gravity.*

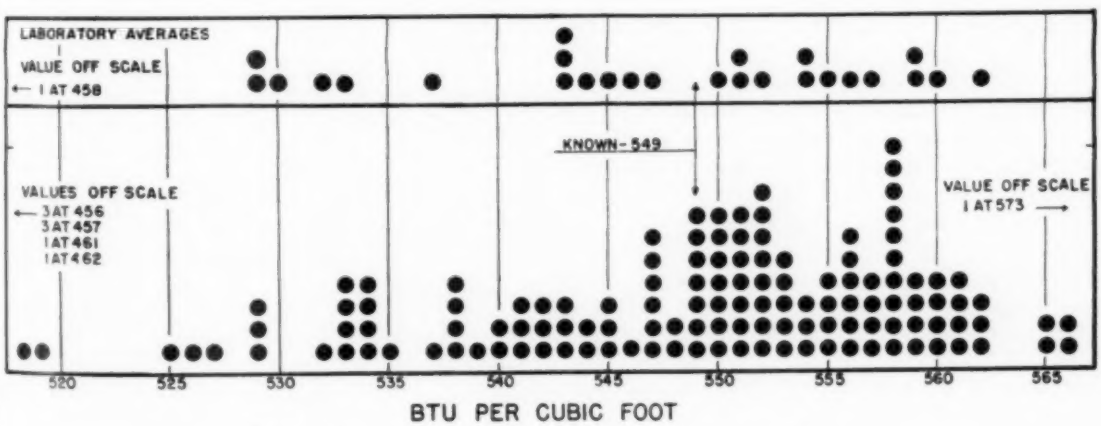

FIGURE 10. *Frequency-distribution plot for Btu per cubic foot.*

laboratories 2, 4, 8, 10, 11, 17, and 20 are examined in the instance of calculated specific gravity, which is a good over-all measure of the success of the analysis involving all components determined, these facts are evident:

(1) The differences between two calculators using the same spectrogram in the same laboratory were small. The average differences for the seven laboratories (in the order given above), expressed in thousandths, are: 1 1/2, 0, 1, 1/4, 4 1/4, 1/4, 1 1/4; the average of all the differences is 1.2. (This calculation was based on differences between O1–S1–C1 and O1–S1–C2, O1–S2–C1 and O1–S2–C2, O2–S3–C1 and O2–S3–C2, O2–S4–C1 and O2–S4–C2.)

(2) The differences between two operators using the same instrument in the same laboratory were small. The average differences for the seven laboratories are: 1 1/2, 1, 1/2, 1, 3 1/2, 1/4, 1 1/4. The average of all differences is 1. (This calculation was based on the average of all O1 measurements minus the average of all O^2 measurements for each laboratory).

(3) The differences between spectrograms were larger than between operators and calculators. For the seven laboratories, the average differences are 1 1/2, 1, 4, 4 1/4, 4 1/4, 1 3/4, 1 1/4. The average of all differences is 2.6. (This calculation was based on the differences between O1–S1–C1 and O1–S2–C1, O1–S1–C2 and O1–S2–C2, O2–S3–C1 and O2–S4–C1, O2–S3–C2 and O2–S4–C2. See O–S–C key above).

These observations agree with those made previously in the analysis of a natural gas by the mass spectrometer (see footnote 3).

In a paper given December 27, 1949 to the 109th annual meeting of the American Statistical Association, W. J. Youden remarked: "It is a fact of experience that a set of measurements made by different operators at different times or in different localities is subject to greater variation than a set of measurements made by one operator using the same apparatus on the same day." The data presented here offer no exception to this fact of experience. Thus, for example, the mean of all values of calculated specific gravity (between 0.626 and 0.677) is 0.650 $\pm$0.007; the mean of the laboratory averages is 0.648 $\pm$0.009; but the reproducibility of each laboratory varies from 0.0005 to 0.004, with an average of 0.0017—three times better than the reproducibility obtained from the laboratory averages.

The factors controlling interlaboratory differences will probably never be completely evaluated. One important factor in the present case is a difference in methods of solving spectrograms, and not enough is known about this whole subject. Particular attention is being given this phase of mass spectrometric analysis in the preparation of ASTM tentative standards.

V. Summary

As often happens, a group of values that yield a frequency plot devoid of the classical Gaussian pattern and are, from the analyst's viewpoint, inconveniently various, nevertheless have yielded a mean value very close to the most probable or the actual one. This is always a comfort if one has an abundance of data from as many sources as are necessary; but the problem remains to determine the accuracy of a single source in the absence of sufficient data from many sources. Thus, the spectrometric determination of hydrogen, and of carbon monoxide with nitrogen, has not been altogether satisfactory. However, the mass spectrometer is quite at home in the analysis of the hydrocarbon fraction of such samples as the one just studied, even though some difficulty was experienced around mass 28. In fact, the spectrometer is able to analyze actual fuel gases of this type where 20 component mixtures are not unusual. Such complicated mixtures have been difficult when analyzed by a combination of other methods.

Jean Doyle and Marthada Vaughn Kilday checked the calculations of heating value and specific gravity, and this assistance is gratefully acknowledged.

TABLE 1

Lab No.	Operator-Spectrogram-calculator key	Anal No.	Mass spectrometric analysis of sample ASTM D3VII-5 (percentage by volume)													Calculated heating value [a]	Calculated specific gravity (air = 1.000) [a]
			CO_2	O_2	N_2	H_2	CO	CH_4	C_2H_6	C_3H_8	C_4H_{10}	C_2H_4	C_3H_6	C_4H_8			
																*Btu/ft*³	
1	O1-S1-C1	1	5.2	0.1	4.8	33.1	31.6	9.2	3.4			12.6				557	0.665
	O1-S1-C2	2	5.2	.1	5.1	33.1	31.4	9.1	3.4			12.6				556	.666
	O1-S2-C1	3	5.4	.1	5.4	33.1	30.3	9.4	3.3			13.0				559	.666
	O1-S2-C2	4	5.4	.1	5.5	33.0	30.4	9.4	3.2			13.0				558	.667
	Average			.1	5.2	33.1	30.9	9.3	3.3			12.8				558	.666
2	O1-S1-C1	1	4.5		6.2	36.0	29.3	7.5	3.0	0.2		13.3				551	.643
	O1-S1-C2	2	4.6		6.2	35.9	29.3	7.5	3.1	.1		13.3		0.01		551	.645
	O1-S2-C1	3	4.6		6.2	36.0	29.2	7.5	3.3	.1		13.2	0.01	.01		551	.644
	O1-S2-C2	4	4.6		6.3	36.1	29.0	7.5	3.3	.1		13.2		.01		552	.644
	O2-S3-C1	5	4.6		6.2	35.9	29.1	7.4	3.4	.1		13.2	.03	.03		553	.644
	O2-S3-C2	6	4.6		6.2	36.1	29.0	7.4	3.3	.1		13.2	.03	.03		552	.642
	O2-S4-C1	7	4.6		6.2	36.2	29.1	7.4	3.3	.1		13.0	.01	.03		549	.641
	O2-S4-C2	8	4.6		6.3	36.1	29.2	7.4	3.3	.1		13.0	.03	.01		549	.643
	Average		4.6		6.2	36.0	29.2	7.5	3.3			13.2				551	.643
3	O1-S1-C1	1	4.4		7.0	36.2	28.4	7.4	3.5			13.1				549	.641
	O1-S2-C2	2	4.3		7.0	35.6	28.9	7.5	3.5			13.2				551	.645
	O2-S3-C1	3	4.5		7.1	35.8	29.0	7.6	3.1			12.9				541	.644
	Average		4.4		7.0	35.9	28.8	7.5				13.1				547	.643
4	O1-S1-C1	1	4.5	.1	4.6	35.4	31.3	8.0	3.4			12.7				553	.646
	O1-S1-C2	2	4.5	.1	4.6	35.4	31.3	8.0	3.4			12.7				553	.646
	O1-S2-C1	3	4.3	.1	4.3	35.5	31.6	8.0	3.4			12.8				556	.644
	O1-S2-C2	4	4.3	.1	4.3	35.5	31.6	8.0	3.4			12.8				556	.644
	O2-S3-C1	5	4.3	.1	4.6	35.5	31.3	7.9	3.5			12.8				556	.644
	O2-S3-C2	6	4.3	.1	4.6	35.5	31.3	7.9	3.5			12.8				556	.644
	O2-S4-C1	7	4.5	.1	4.7	35.7	31.1	7.8	3.3			12.8				551	.644
	O2-S4-C2	8	4.5	.1	4.7	35.7	31.1	7.8	3.3			12.8				551	.644
	Average		4.4	.1	4.5	35.5	31.3	7.9	3.4			12.8				554	.644
5	O1-S1-C1	1	4.1	.8	7.8	31.8	32.3	8.2	3.1			11.9				529	.676
	O1-S1-C2	2	4.3	.8	8.2	31.8	31.8	8.1	3.1			11.9				526	.677
	O2-S3-C1	3	4.3	.8	7.8	31.9	31.6	8.2	3.2			12.2				534	.676
	O2-S3-C2	4	4.4	.8	8.2	32.0	31.3	8.0	3.3			12.0				529	.677
	Average		4.3	.8	8.0	31.9	31.8	8.1	3.2			12.0				529	.676
6	Not specified. 1 to 4 were done 2 days before 5 to 12.	1	4.8		4.0	33.3	31.2	8.5	3.7			13.5				573	.655
		2	4.8		4.9	33.5	31.5	8.3	3.7			13.3				566	.663
		3	4.8		5.4	33.8	31.4	7.7	3.5			13.4				558	.663
		4	4.6		5.5	34.4	31.3	7.7	3.2			13.2				552	.657
		5	4.7		5.3	34.3	31.0	8.1	3.6			13.0				558	.654
		6	4.7		5.2	34.4	31.1	8.1	3.5			13.1				558	.654
		7	4.7		5.1	34.2	31.3	8.1	3.6			13.1				560	.658
		8	4.7		5.1	34.3	31.1	8.1	3.6			13.0				559	.656
		9	4.6		5.4	33.6	31.6	8.1	3.4			13.2				559	.662
		10	4.6		5.4	33.6	31.7	8.1	3.4			13.3				558	.662
		11	4.6		5.5	33.7	31.5	8.1	3.4			13.2				558	.661
		12	4.6		5.3	33.9	31.4	8.2	3.6			13.0				559	.658
	Average		4.7		5.2	34.0	31.3	8.1	3.5			13.2				560	.659
7	O1-S1-C1	1	4.0		11.8	39.2	20.6	8.0	3.4	.11		12.7	.06			535	.610
	O1-S2-C1	2	4.0		15.7	38.5	17.7	7.9	3.3	.17		12.4	.06			518	.616
	O2-S3-C1	3	4.1		13.5	38.2	19.9	8.0	3.6	.19		12.4	.19			534	.624
	O2-S4-C1	4	4.1		14.0	38.4	19.2	7.8	3.3	.16		12.7	.25			532	.621
	Average		4.1		13.8	38.6	19.3	7.9	3.4			12.6				530	.618

See footnotes at end of table.

880789—50——6

TABLE 1—Continued

Lab No.	Operator-spectrogram-calculator key	Anal No.	Mass spectrometric analysis of sample ASTMD3VII-5 (percentage by volume)													Calculated heating value [a]	Calculated specific gravity (air=1.000) [a]
			CO_2	O_2	N_2	H_2	CO	CH_4	C_2H_6	C_3H_8	C_4H_{10}	C_2H_4	C_3H_6	C_4H_8			
																Btu/ft³	
8	01-S1-C1	1	4.4	.....	36.5	34.2	.....	8.8	3.3	.....	.....	12.7	.....	.....	.....	457	0.653
	01-S1-C2	2	4.5	.....	36.6	34.1	.....	8.8	3.2	.....	.....	12.8	.....	.....	.....	456	.653
	01-S2-C1	3	4.6	.....	36.5	34.2	.....	8.8	3.3	.....	.....	12.6	.....	.....	.....	456	.653
	01-S2-C2	4	4.5	.....	36.4	34.2	.....	8.9	3.3	.....	.....	12.7	.....	.....	.....	457	.654
	02-S3-C1	5	4.5	.....	36.5	33.7	.....	9.1	3.6	.....	.....	12.6	.....	.....	.....	462	.658
	02-S3-C2	6	4.5	.....	36.5	33.7	.....	9.1	3.5	.....	.....	12.7	.....	.....	.....	461	.658
	02-S4-C1	7	4.2	.....	36.5	34.5	.....	9.2	3.3	.....	.....	12.4	.....	.....	.....	456	.650
	02-S4-C2	8	4.2	.....	36.4	34.6	.....	9.2	3.3	.....	.....	12.4	.....	.....	.....	457	.649
	Average	.....	4.4	.....	36.5	34.2	.....	9.0	3.4	.....	.....	12.6	.....	.....	.....	458	.654
9	O1-S1-C1	1	4.8	.....	5.9	34.2	30.3	8.2	3.4	.....	.....	13.1	.....	.....	.....	555	.657
	O1-S2-C1	2	4.9	.....	6.1	34.3	30.4	8.0	3.4	.....	.....	13.0	.....	.....	.....	552	.659
	O2-S3-C1	3	4.8	.....	5.9	34.4	30.0	8.2	3.4	.....	.....	13.3	.....	.....	.....	557	.656
	Average	.....	4.8	.....	6.0	34.3	30.2	8.1	3.4	.....	.....	13.1	.....	.....	.....	554	.657
10	O1-S1-C1	1	4.5	.....	6.4	35.3	28.9	8.1	3.4	0.1	.....	13.3	.....	.....	.....	558	.648
	O1-S1-C2	2	4.5	.....	6.4	35.3	28.9	8.1	3.4	.1	.....	13.3	.....	.....	.....	558	.648
	O1-S2-C1	3	4.6	0.1	5.8	35.3	29.1	8.2	3.4	.....	.....	13.5	.....	.....	.....	561	.647
	O1-S2-C2	4	4.6	.1	5.8	35.3	29.1	8.2	3.4	.....	.....	13.5	.....	.....	.....	561	.647
	O2-S3-C1	5	4.6	.1	5.8	34.8	29.5	8.4	3.4	.....	.....	13.4	.....	.....	.....	560	.650
	O2-S3-C2	6	4.6	.1	5.8	34.8	29.5	8.4	3.4	.....	.....	13.4	.....	.....	.....	560	.650
	O2-S4-C1	7	4.6	.1	6.5	35.1	28.7	8.5	3.3	.....	.....	13.2	.....	.....	.....	555	.647
	O2-S4-C2	8	4.6	.1	6.4	35.1	28.8	8.5	3.3	.....	.....	13.2	.....	.....	.....	554	.647
	Average	.....	4.6	.1	6.1	35.1	29.1	8.3	3.4	.....	.....	13.3	.....	.....	.....	559	.648
11	O1-S1-C1	1	4.1	.....	6.5	35.6	29.5	7.8	3.1	.3	.....	13.1	.....	.....	.....	555	.644
	O1-S1-C2	2	4.1	.....	6.7	35.7	29.7	7.5	3.1	.1	.....	13.1	.....	.....	.....	548	.643
	O1-S2-C1	3	4.4	.....	6.1	35.2	29.9	7.8	3.1	.1	.....	13.4	.....	.....	.....	554	.649
	O1-S2-C2	4	4.4	.....	6.2	35.2	30.1	7.8	3.0	Tr	.....	13.3	.....	.....	.....	549	.648
	O2-S3-C1	5	4.7	.....	5.9	34.8	30.0	7.8	3.2	.....	.....	13.6	.....	.....	.....	556	.653
	O2-S3-C2	6	4.7	.....	5.8	35.0	29.8	7.9	3.1	.....	.....	13.7	.....	.....	.....	557	.651
	O2-S4-C1	7	4.5	.....	6.1	35.2	29.4	7.7	3.2	.5	.....	13.3	.....	.....	.....	562	.651
	O2-S4-C2	8	4.5	.....	6.1	35.0	29.4	7.7	3.2	.5	.....	13.6	.....	.....	.....	566	.653
	Average	.....	4.4	.....	6.2	35.2	29.7	7.7	3.1	.....	.....	13.4	.....	.....	.....	556	.649
12	O1-S1-C1	1	4.0	.....	5.1	33.6	32.2	8.5	3.3	.....	.....	13.4	.....	.....	.....	565	.658
	O1-S1-C2	2	4.1	.....	5.4	33.5	32.0	8.4	3.1	.....	.....	13.4	0.1	.....	.....	561	.659
	O1-S2-C1	3	4.1	.....	5.2	33.6	32.1	8.4	3.2	.....	.....	13.4	.....	.....	.....	562	.658
	O1-S2-C2	4	4.0	.....	5.4	33.5	32.2	8.3	3.2	.....	.....	13.4	.....	.....	.....	561	.659
	Average	.....	4.0	.....	5.3	33.5	32.1	8.4	3.2	.....	.....	13.4	.....	.....	.....	562	.658
13	O1-S1-C1	1	4.7	.....	5.7	36.0	30.1	7.8	3.0	.....	.....	12.8	.....	.....	.....	542	.643
	O1-S1-C2	2	4.7	.....	5.7	36.1	30.1	7.7	3.0	.....	.....	12.7	.....	.....	.....	542	.642
	O2-S3-C1	3	4.7	.....	5.7	35.8	30.2	7.7	3.0	.....	.....	12.8	.....	.....	.....	544	.643
	O2-S3-C2	4	4.7	.....	5.8	35.8	30.2	7.7	3.0	.....	.....	12.8	.....	.....	.....	543	.644
	Average	.....	4.7	.....	5.7	35.9	30.1	7.7	3.0	.....	.....	12.8	.....	.....	.....	543	.643
[b] 14	S1	1	4.5	.....	7.3	25.7	37.8	8.1	3.3	.....	.....	12.6	.....	.....	.....	541	.617
	S2	2	4.5	.....	6.8	26.3	37.8	8.1	3.3	.....	.....	12.6	.....	.....	.....	543	.618
	S3	3	4.5	.....	5.5	27.4	37.3	8.0	3.2	.....	.....	12.7	.....	.....	.....	543	.615
	S4	4	4.6	.....	5.5	27.4	37.3	8.1	3.3	.....	.....	12.6	.....	.....	.....	545	.617
	Average	.....	4.5	.....	6.3	26.7	37.5	8.1	3.3	.....	.....	12.6	.....	.....	.....	543	.617
15	O1-S1-C1	1	4.5	.03	5.9	36.0	30.4	7.6	3.0	.....	.....	12.7	.....	.....	.....	540	.643
	O1-S2-C1	2	4.5	.03	5.8	35.6	30.3	7.8	3.0	.....	.....	13.0	.....	.....	.....	546	.645
	O2-S3-C1	3	4.5	.03	5.8	36.4	29.7	7.8	3.1	.....	.....	12.8	.....	.....	.....	545	.639
	Average	.....	4.5	.....	5.8	36.0	30.1	7.7	3.0	.....	.....	12.8	.....	.....	.....	544	.642

See footnotes at end of table.

TABLE 1—Continued

Lab No.	Operator-spectrogram-calculator key	Anal No.	Mass spectrometric analysis of sample ASTMD3VII–5 (percentage by volume)												Calculated heating value [a]	Calculated specific gravity (air = 1.000) [a]
			CO_2	O_2	N_2	H_2	CO	CH_4	C_2H_6	C_3H_8	C_4H_{10}	C_2H_4	C_3H_6	C_4H_8		
															Btu/ft [3]	
16	O1-S1-C1	1	4.2	0.55	5.0	35.5	31.4	7.0	3.4			12.9			(c)	548	0.649
	O1-S2-C1	2	4.4	.06	4.5	36.0	31.1	7.2	3.4			13.3			(c)	557	.644
	O2-S1-C2	3	4.1	.04	5.6	35.2	30.9	6.9	3.2			14.1			(c)	560	.651
	Average		4.2		5.0	35.6	31.1	7.0	3.3			13.4				555	.648
17	O1-S1-C1	1	4.5	.05	5.4	35.2	30.8	7.9	3.3			12.9			(d)	551	.649
	O1-S1-C2	2	4.5	.05	5.4	35.2	30.9	7.9	3.3			12.8			(d)	550	.649
	O1-S2-C1	3	4.5	.05	5.5	34.9	30.9	7.9	3.3			13.0			(d)	552	.651
	O1-S2-C2	4	4.5	.05	5.3	34.9	31.1	7.9	3.3			13.0			(d)	552	.651
	O2-S3-C1	5	4.6	.05	5.5	35.2	30.8	7.8	3.4			12.7			(d)	550	.650
	O2-S3-C2	6	4.6	.05	5.5	35.0	30.9	7.9	3.3			12.8			(d)	550	.651
	O2-S4-C1	7	4.5	.05	5.4	35.2	30.8	7.9	3.3			12.9			(d)	550	.649
	O2-S4-C2	8	4.5	.05	5.5	35.1	30.9	7.9	3.3			12.8			(d)	550	.649
	Average		4.5		5.4	35.1	30.9	7.9	3.3			12.9				551	.650
18	O1-S1-C1	1	4.7	.07	4.1	33.2	34.2	8.0	3.0			12.7				549	.666
	O1-S1-C2	2	4.7	.07	4.1	33.2	34.2	8.1	3.0			12.7				549	.667
	O1-S2-C1	3	4.6	.1	5.5	33.8	32.8	8.0	3.0			12.3				539	.661
	O1-S2-C2	4	4.6	.1	5.5	33.8	32.8	7.9	2.9			12.3				538	.660
	Average		4.6		4.8	33.5	33.5	8.0	3.0			12.5				543	.664
19	O1-S1-C1	1	4.4		4.3	37.6	31.1	7.6	3.1			11.9				538	.627
	O1-S1-C2	2	4.4		4.1	37.7	31.3	7.6	3.0			11.9				537	.626
	O1-S2-C1	3	4.4		5.3	37.4	30.4	7.6	3.1			11.8				533	.628
	O1-S2-C2	4	4.5		3.8	37.7	31.3	7.6	3.1			12.0				540	.626
	O2-S3-C1	5	4.7		4.3	37.1	31.2	7.6	3.1			12.0				538	.633
	O2-S3-C2	6	4.7		4.1	37.3	31.2	7.6	3.1			12.0				538	.631
	Average		4.5		4.3	37.5	31.1	7.6	3.1			11.9				537	.629
20	O1-S1-C1	1	4.7	Tr	7.2	34.8	29.0	7.6	3.5		Tr	13.2		Tr		550	.654
	O1-S1-C2	2	4.7	Tr	7.2	35.1	28.9	7.6	3.3			13.2				547	.651
	O1-S2-C1	3	4.7	Tr	7.2	35.0	29.0	7.6	3.4		Tr	13.1		Tr		547	.652
	O1-S2-C2	4	4.7	Tr	7.2	35.0	29.0	7.6	3.4		Tr	13.1		Tr		547	.652
	O2-S3-C1	5	4.7		7.3	34.6	28.6	8.2	3.5		Tr	13.1		Tr		552	.654
	O2-S3-C2	6	4.7	Tr	7.5	34.6	28.6	8.2	3.3			13.1				549	.653
	O2-S4-C1	7	4.7		7.1	34.6	28.6	8.3	3.3		Tr	13.4		Tr		554	.653
	O2-S4-C2	8	4.7		7.5	34.5	28.4	8.2	3.5		Tr	13.2		Tr		553	.654
	Average		4.7		7.3	34.8	28.8	7.9	3.4			13.2				550	.653
21	O1-S1-C1	1	4.2	.1	6.6	37.3	30.1	6.1	3.5			12.1				529	.635
	O2-S2-C1	2	4.3	Tr	6.8	37.7	29.7	6.2	3.5			11.8				525	.631
	O3-S3-C1	3	4.4	.1	5.1	38.4	30.2	6.2	3.5			12.1				534	.625
	Average		4.3		6.2	37.7	30.0	6.2	3.5			12.0				529	.631
22	O1-S1-C1	1	4.5		6.6	35.2	30.3	7.7	3.4	0.2		12.1				542	.650
	O1-S1-C2	2	4.4		6.5	35.2	30.8	7.5	3.2	.4		12.0				541	.651
	O1-S2-C1	3	4.5		6.5	35.2	30.3	7.5	3.6	.3		12.0				547	.652
	O1-S2-C2	4	4.4		6.1	35.1	30.9	7.5	3.6	.3		12.1				548	.652
	Average		4.5		6.4	35.2	30.6	7.5	3.5			12.0				544	.651
23	O1-S1-C1	1	4.5		7.0	35.8	28.7	4.5	3.5	.2		12.4	Tr			547	.644
	O1-S1-C2	2	4.5		7.0	35.6	29.1	4.5	3.5	.2		12.3	Tr			545	.646
	O1-S2-C1	3	4.5		7.0	35.7	28.8	4.5	3.5	.2		12.4	Tr			547	.645
	O1-S2-C2	4	4.5		6.9	35.7	29.1	4.5	3.5	.1		12.3	Tr			544	.644
	Average		4.5		7.0	35.7	28.9	4.5				12.3				546	.645

See footnotes at end of table.

TABLE 1—Continued

Lab No.	Operator-spectrogram-calculator key	Anal No.	Mass spectrometric analysis of sample ASTMD3VII-5 (percentage by volume)													Calculated heating value [a]	Calculated specific gravity (air=1.000) [a]
			CO_2	O_2	N_2	H_2	CO	CH_4	C_2H_6	C_3H_8	C_4H_{10}	C_2H_4	C_3H_6	C_4H_8			
																Btu/ft³ [b]	
24	O1-S1-C1	1	4.6	....	5.7	34.8	30.5	8.1	3.2	.....	.....	13.1	.....	.....	(c)	522	0.651
	O1-S1-C2	2	4.6	....	7.0	34.9	31.5	8.0	3.2	.....	.....	10.8	.....	.....	(c)	519	.651
	O1-S2-C1	3	4.5	....	5.9	35.4	30.0	8.1	3.1	.....	.....	13.0	.....	.....	(c)	550	.645
	O1-S3-C1	4	4.6	....	5.3	34.8	30.8	8.1	3.2	.....	.....	13.2	.....	.....	(c)	555	.651
	Average	.....	4.6	....	6.0	35.0	30.7	8.1	3.2	.....	.....	12.5	.....	.....	....	552	.649
25	O1-S1-C1	1	4.5	0.5	8.0	34.9	29.0	7.4	2.9	.....	.....	12.6	.....	.....	(f)	533	.632
	O1-S2-C1	2	4.4	.5	8.0	35.7	28.7	7.3	2.7	.....	.....	12.6	.....	.....	....	527	.645
	O2-S3-C1	3	4.4	.5	7.5	35.0	29.5	7.1	2.9	.....	.....	12.6	.....	.....	....	534	.649
	Average	....	4.4	.5	7.8	35.2	29.1	7.3	2.8	.....	.....	12.6	.....	.....	....	532	.649
26	O1-S1-C1	1	4.4	.4	8.8	33.9	28.8	8.0	2.8	.....	.....	12.9	.....	.....	....	533	.639
	O1-S2-C1	2	4.4	.4	8.8	33.9	28.8	8.0	3.0	.....	.....	12.7	.....	.....	....	533	.639
	Average	....	4.4	....	8.8	33.9	28.8	8.0	2.9	.....	.....	12.8	.....	.....	....	533	.639
27	S1	1	4.3	....	5.4	34.5	31.1	8.1	3.2	.....	.....	13.4	.....	.....	....	558	.652
	S2	2	4.3	....	5.3	34.6	31.2	8.1	3.2	.....	.....	13.3	.....	.....	....	557	.651
	S3	3	4.4	....	4.9	34.9	31.2	8.1	3.1	.....	.....	13.4	.....	.....	....	558	.649
	S4	4	4.4	....	5.0	34.5	31.3	8.1	3.1	.....	.....	13.6	.....	.....	....	560	.653
	Average	.....	4.3	....	5.2	34.6	31.2	8.1	3.2	.....	.....	13.4	.....	.....	....	559	.651

[a] Factors used in computations of Btu/Ft³ and sp gr:

Components	Btu/ft³	Sp Gr	Components	Btu/ft³	Sp Gr
CO_2	.....	1.5290	CH_4	997.4	0.5544
O_2	.....	1.1053	C_2H_4	1587.0	.97487
N_2	.....	.97308	C_2H_6	1759.0	1.0493
CO	316.1	.96713	C_3H_6	2339.0	1.45
H_2	319.4	.06952	C_3H_8	2528.0	1.5624

[b] Laboratories 7 and 14 used Westinghouse instruments; all others used Consolidated instruments.

[c] Reported 0.1% C_3H_8 and 0.04% C_4^+.

[d] Reported 0.05% C_4^+.

[e] Reported trace C_4^+.

[f] Reported C_4^+, 0.2, 0.1, 0.3.

WASHINGTON, December 6, 1949.

U. S. Department of Commerce
National Bureau of Standards

Research Paper RP2099
Volume 44, May 1950

Part of the Journal of Research of the National Bureau of Standards

Infrared Absorption Spectra of Hexafluoroethane and of Chloropentafluoroethane

By José R. Barcelo [1]

In the present paper the infrared absorption spectra of hexafluoroethane and chloropentafluoroethane have been studied. The spectra examined ranged from 2 to 40 microns, and for this purpose lithium fluoride, sodium chloride, potassium bromide, and thallium bromide-iodide (KRS5) prisms were used. The substances studied were in the gaseous state.

This work was undertaken to compare the spectra of two molecules of the same type of structure but with much different properties of symmetry. The spectrum of hexafluoroethane has been previously measured in the infrared to 22 microns, and only small differences are noted in the present work from the previous study. Tables are included, which classify the observed spectra of hexafluoroethane and chloropentafluoroethane as fundamental, combination, and overtone bands

I. Introduction

This paper presents the results obtained in the study of the infrared absorption spectra of two fluorocarbons, hexafluoroethane and chloropentafluoroethane, from 2 μ to 40 μ.

In spite of the interest in fluorocarbons, in view of their characteristics, no data were available on the infrared absorption spectrum of chloropentafluoroethane. The infrared absorptance of hexafluoroethane has been studied by J. R. Nielsen, C. M. Richards, and H. L. McMurry [1],[2] and the Raman shifts for this material in the liquid state have been measured by D. H. Rank and E. L. Pace [2]. In the present work, the data obtained for hexafluoroethane are in good agreement in the position of the bands with those given by Nielsen, et al. [1]. The study of the infrared absorption spectrum of chloropentafluoroethane in comparison with that of hexafluoroethane, from which it differs only slightly chemically, is of interest because, as a result of the symmetry of the latter, several of its fundamental vibrations are degenerate. Because of the asymetry of the former, however, all of the eighteen fundamental frequencies of chloropentafluoroethane are active in the infrared. Unfortunately, of the eighteen frequencies expected, seven were not observed, either because they were very low in intensity or existed in a region of long wavelengths not examined. A majority of the observed bands may be accounted for as combinations of the fundamental frequencies observed, although some difficulty in interpretation exists for three of those of lowest wave number.

II. Experimental Method

The materials used were of the group of "freons," supplied by duPont, and the spectra were obtained with these substances in the gaseous state. A gas cell of 5 cm in length with potassium bromide windows was used, except for the longest wavelengths. The initial pressure of the gas in the cell was 500 mm of mercury, but as this was too high for the observation of some of the absorption maxima, it was reduced in each case to the most suitable one. The pressure used is indicated on the curves. When measuring the long wavelength region with a thallium bromide-iodide prism, a 1-m cell with windows of polystyrene was used. On account of the lack of strength of the polystyrene windows, it was not possible to evacuate the cell. The cell was filled by allowing the gas to flow in slowly for several minutes. When the

[1] Guest worker at the National Bureau of Standards.
[2] Figures in brackets indicate the literature references at the end of this paper.

bands were too intense for observing their structure, some of the gas was removed by flowing air slowly through the cell. When the amount of gas in the cell was reduced to a level that gave a good contrast in the different parts of the band, no further removal of the gas was made. By this method of reducing the quantity of the gas, it was not possible to determine the partial pressure.

The spectra of these two substances between 2 μ and 40 μ were recorded with Perkin-Elmer spectrometers, models 12A and 12B, using lithium fluoride, sodium chloride, potassium bromide, and thallium bromide-iodide prisms. With both spectrometers scanning and slit drive were automatic. Separate motor drives were used, one for the wavelength drum and the other to open the slit continuously to achieve approximately constant background energy at different wavelengths. Further details of these devices can be found in a paper by E. K. Plyler, R. Stair, and C. J. Humphreys [3].

The detector used for the regions observed with the lithium fluoride, sodium chloride, and potassium bromide prisms was a vacuum thermocouple with potassium bromide windows. In order to detect the weak radiation in the thallium bromide-iodide region, a Golay detector was used with a window and a lens of thallium bromide-iodide to focus the energy on the receiver. In both cases the signal from the receiver was amplified and recorded automatically.

For the recording of the absorption spectra in the region beyond 15 μ the technique described by Plyler [4, 5] was followed.

III. Experimental Results

In figures 1 and 2 are shown the plots of the percentage transmission of hexafluoroethane and chloropentafluoroethane as function of the wavelength. Figure 1 shows the short wavelength region for the two substances, and figure 2 the long wavelength region. The dotted parts correspond to regions in which absorptions of water vapor and carbon dioxide appear in the background energy, and the spectra in these regions have been established with the help of the recording spectrophotometer of Baird Associates, which cancels out the atmospheric bands.

In table 1 are shown the results for hexafluoroethane, first in brackets the intensities, then the frequencies observed, and in the next column, the values for the P, Q, and R branches when observed. The intensity scale is represented by numbers that are proportional to $\log_e I_0/I$. The bands that show no transmission with a given quantity of gas are assigned the intensity 10, and the intensity number of the weaker bands are relative to this band, except that (0,0) refers to bands that have between 2- and 5-percent absorption and (0,0,0) to bands of 2 percent or less of absorption.

The experimental results obtained by observing the infrared absorption spectra of hexafluoroethane in the present work show slight variations from those reported by Nielsen, et al. [1].

The intensities of the absorption bands depend on the cell length and the pressure of the gas. Except for small changes in the transmission pro-

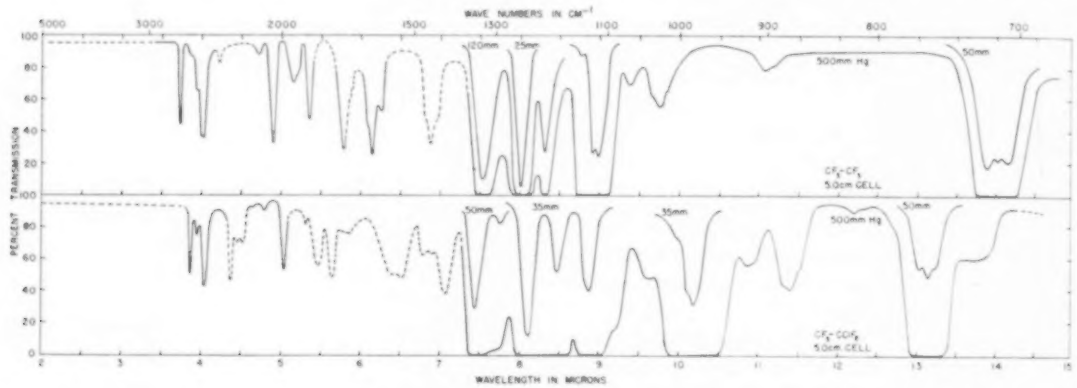

FIGURE 1. *Infrared absorption spectra of hexafluoroethane and chloropentafluoroethane in the gaseous state from 2 to 15 μ.*

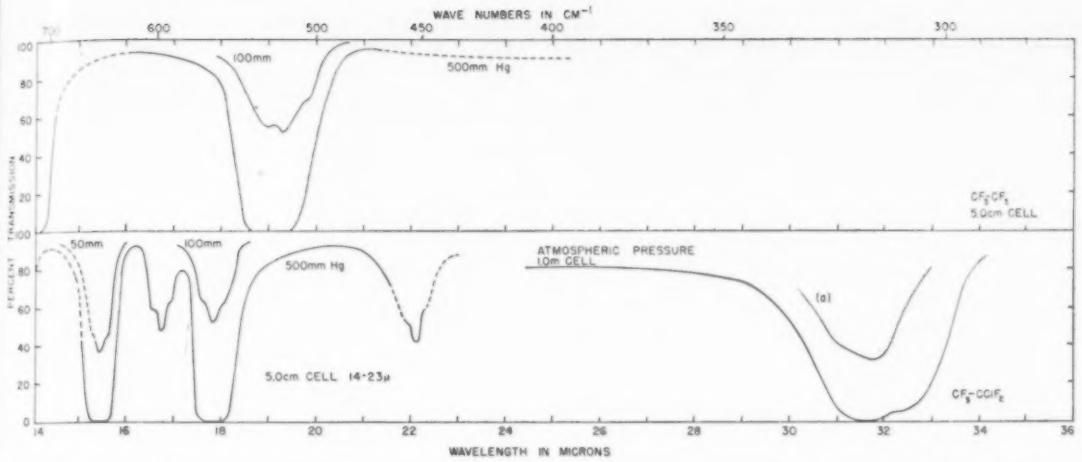

FIGURE 2. *Infrared absorption spectra of hexafluoroethane and of chloropentafluoroethane in the gaseous state from 15 to 36 μ.*

The chloropentafluoroethane insert (a) at 32 μ was observed by use of a 1-m cell with a partial pressure such that the transmittance was approximately 35 percent.

TABLE 1. *Wave numbers and relative intensities of the observed bands of hexafluoroethane*

Intensity	Observed bands		Intensity	Observed bands	
	Center	Branches		Center	Branches
	cm⁻¹	*cm⁻¹*		*cm⁻¹*	*cm⁻¹*
		505	[10]	1,247	.....
[5]	518	518	[6]	1,324	.....
		526	[3]	(1,453)	.....
		707	[2]	1,595	.....
[8]	714	714	[3]	1,626	.....
		720	[3]	1,727	.....
[0]	896	895	[2]	1,866	.....
		903	[1]	1,938	.....
[2]	1,025	.....	[3]	2,041	.....
[1]	1,065	1,063	[00]	2,115	.....
		1,067	[3]	2,483	2,475
[8]	1,117	1,112			2,493
		1,121	[1]	2,534	.....
[00]	1,142	.....	[3]	2,667	.....
[6]	1,203	.....			

duced by pressure alone when the number of molecules in the path of the radiant energy is the same, the intensities of the bands are proportional to the total number of molecules in the path. In the work of Nielsen, et al., greater absorption was obtained in the bands because they used a larger quantity of gas in the absorption path for their measurements. This may, in part, account for the differences in experimental results in the region from 10 to 13.5 μ between these two sets of data. In the present work only one band is observed in this region at 894 cm⁻¹, while several small bands are listed in the tables of Nielsen, et al. with values between 750 and 1,000 cm⁻¹.

A scanning of the region from 25 to 40 μ did not reveal any bands of sufficient intensity for detection. The absence in the 25- to 40-μ region of any bands of appreciable intensity supports the assignment of Nielsen that ν_9 is less than 250 cm⁻¹, the value 216 cm⁻¹ being used.

The band at 518 cm⁻¹ appears to have P, Q, and R branches when it is observed at a pressure of 100 mm Hg (see fig. 2). With larger amounts of gas the structure of the band is not observable, and the region of greatest absorption is at 522 cm⁻¹. The experimental results for this region are not shown by Nielsen, and it is not possible to determine the part of the band that he used in determining the value of 522 cm⁻¹.

The combination band, $\nu_1+\nu_5$, was forecast by Nielsen, et al. but does not appear in his graph of the experimental results. This band is of medium intensity and, as observed in this work, has a transmission of 40 percent at its maximum when the gas is measured with a pressure of 500 mm Hg in the 5-cm cell.

In general the two sets of data correspond closely, and in some bands the results of Nielsen, et al. show better detail. These slight differences in several parts of the spectrum are caused by observations being carried out with different amounts of hexafluoroethane in the cell.

In table 2 the values of the absorption maxima found for chloropentafluoroethane are given; the order of the wave numbers of the bands is the same as in table 1. As this substance had not been previously measured, a comparison with other experimental results is not possible. Neither in table 1 nor in table 2 are given those lateral branches not completely resolved.

TABLE 2. *Wave numbers and relative intensities of the observed bands of chloropentafluoroethane*

Intensity	Observed bands		Intensity	Observed bands		Intensity	γ
	Center	Branches		Center	Branches		
	cm^{-1}	cm^{-1}		cm^{-1}	cm^{-1}		cm^{-1}
[4]	314	.....	[6]	982	.....	[2]	(1, 828)
[3]	452	.....	[2]	1, 044	.....	[1]	(1, 883)
[5]	560	.....	[6]	1, 129	.....	[2]	1, 984
[3]	596	.....	[8]	1, 182	.....	[00]	2, 066
[8]	647	.....	[10]	1, 233	.....	[000]	2, 151
[2]	372	.....	[4]	1, 290	.....	[1]	(2, 212)
[8]	762	756 762 768	[7]	1, 346	.....	[1]	2, 252
			[2]	1, 414	.....	[2]	2, 309
[00]	808	.....	[1]	(1, 453)	.....	[2]	2, 476
[0]	820	.....	[1]	1, 473	.....	[1]	2, 531
[3]	876	868 876 884	[4]	1, 553	1, 536 1, 567	[2]	2, 591
			[00]	(1, 709)	.....	.....	.....
[2]	922	.....	[2]	(1, 776)	.....	.....	.....

IV. Discussion

1. Hexafluoroethane

The substances of this type admit two possible configurations, the alternate one with the symmetry model D_{3d} and the eclipsed one with the model D_{3h}. Nielsen, et al. [1], after a detailed discussion, preferred the alternate form, which is in accordance with the hypothesis of D. T. Hamilton and F. F. Cleveland [6] for the case of hexafluoroethane. Their analysis was made from the study of the Raman spectra.

Adopting this hypothesis, and taking into consideration the Raman data given by Rank and Pace [2], the fundamental vibrations will be those that are indicated in table 3, in which are shown the term, the wave number (cm^{-1}), the activity, and the group from which they originate.

The values given, as far as the frequencies active in the infrared are concerned, differ only from those by Nielsen, et al. [1] by a very few units for the frequencies ν_7 and ν_8. On the other hand the frequency ν_9 must be less than 250 cm^{-1}. In Nielsen's work it is supposed to be 216 cm^{-1}, and with this value concordant, numbers for the combination bands can be obtained. The region of low frequencies was examined and no absorption maximum was found, thus giving the impression

TABLE 3. *Fundamental bands of hexafluoroethane with listing of band designation, activity, wave number, and type of vibration*

Term	ν	Activity	Type of vibration	Term	ν	Activity	Type of vibration
	cm^{-1}				cm^{-1}		
ν_1	1, 420	R	ν_{CF}	ν_7	1, 247	I	ν_{CF}
ν_2	809	R	ν_{CC}	ν_8	518	I	δ_{FCF}
ν_3	349	R	δ_{FCF}	ν_9	(216)	I	δ_{CCF}
ν_4	.....	Inactive	Twist	ν_{10}	1, 237	R	ν_{CF}
ν_5	1, 117	I	ν_{CF}	ν_{11}	620	R	δ_{FCF}
ν_6	714	I	δ_{FCF}	ν_{12}	380	R	δ_{CCF}

that any possible absorption band must be in a region of an even lower frequency in accordance with the assumption by Nielsen, et al.

Considering the data obtained here, the present interpretation of the nonfundamental frequencies as combination tones has been made following the indications of Nielsen, et al. [1], and the differences between the observed and calculated values are of the same order as those of the authors mentioned, except in two cases where these values were a little larger. The combination tone corresponding to $\nu_1+\nu_2$, forecast but not found by these authors, is observed with the lithium fluoride prism at 2,534 cm^{-1}. These observed and calculated frequencies are to be found in table 4.

TABLE 4. *Observed and calculated wave numbers of the combination bands of hexafluoroethane*

ν (observed)	Term	ν (calculated)	ν (observed)	Term	ν (calculated)
cm^{-1}		cm^{-1}	cm^{-1}		cm^{-1}
896	$\nu_1-\nu_8$	902	1,727	$\nu_3+\nu_{11}$	1,737
1,025	$\nu_2+\nu_9$	1,025	1,866	$\nu_7+\nu_{11}$	1,867
1,065	$\nu_3+\nu_6$	1,063	1,938	$\nu_1+\nu_8$	1,938
1,142	$\nu_5+\nu_{11}$	1,138	2,041	$\nu_2+\nu_7$	2,056
1,203	$\nu_1-\nu_9$	1,204	2,115	$\nu_1+\nu_6$	2,134
1,324	$\nu_2+\nu_8$	1,327	2,483	$\nu_7+\nu_{10}$	2,484
1,453	$\nu_9+\nu_{10}$	1,453	2,534	$\nu_1+\nu_2$	2,537
1,595	$\nu_8+\nu_7$	1,596	2,667	$\nu_1+\nu_7$	2,667
1,626	$\nu_7+\nu_{12}$	1,627	.....	.....	.....

2. Chloropentafluoroethane

The presence of the chlorine atom destroys the symmetry, which permits the eighteen fundamental modes of vibration, all active in the infrared, to appear. Unfortunately, some frequencies are predicted to be so low that they are not in the region studied, which extends to 250 cm^{-1}. Others, which were supposed to be in the region of lowest frequencies studied, have not appeared as can be seen in the curve. The region from 25 to 40 μ shows only one absorption maximum where five were supposed to be.

With the data obtained, 11 of the 18 fundamental frequencies, which are indicated in table 5, have been established. To assign the fundamental bands, the intensities and the regions in which they appear were taken into consideration. To classify them, bringing them in relation with hexafluoroethane, "prime" frequencies have been introduced where the double degenerates of hexafluoroethane give way to two different frequencies in the chloropentafluoroethane. In table 5 the term, the value of the frequency if found, and the group from which it originates, are indicated.

TABLE 5. *Fundamental bands of chloropentafluoroethane with listing of band designation, activity, wave number, and type of vibration*

Term	ν	Type of vibration	Term	ν	Type of vibration
	cm^{-1}			cm^{-1}	
ν_1	1,346	ν_{CF}	ν_8	.....	δ_{CCLF}
ν_2	762	ν_{CC}	ν'_8	.....	δ_{CCCl}
ν_3	314	δ_{FCF}	ν_9	1,182	ν_{CF}
ν_4	.....	Twist	ν'_9	647	ν_{CCl}
ν_5	982	ν_{CF}	ν_{10}	.....	δ_{FCCl}
ν_6	596	δ_{FCF}	ν'_{11}	500	δ_{FCF}
ν_7	1,129	ν_{CF}	ν_{12}	.....	δ_{CCF}
ν'_7	1,233	ν_{CF}	ν'_{12}	.....	δ_{CCF}
ν_8	.....	δ_{FCCl}			
ν'_8	452	δ_{FCF}			

Although only a few of the fundamental frequencies are known, the remaining bands can be explained as harmonic or combination tones, with the exception of the three with lowest wave numbers. For these, surely the lowest fundamental frequencies, which have not been found, must be taken into consideration. These are given in table 6.

TABLE 6. *Observed and calculated wave numbers of the combination and overtone bands of chloropentafluoroethane*

ν (observed)	Term	ν (calculated)	ν (observed)	Term	ν (calculated)
cm^{-1}		cm^{-1}			
732	.....	.....	1,776	$\nu'_{10}+\nu_7$	1,776
808	.....	.....	1,828	$\nu'_{10}+\nu_{10}$	1,829
820	.....	.....	1,883	$\nu_2+\nu'_7$	1,891
876	$\nu'_{11}+\nu_3$	874	1,984	$\nu_2+\nu'_7$	1,995
922	$\nu_8+\nu_3$	910	2,096	$\nu_2+\nu_1$	2,108
1,044	$\nu'_8+\nu_6$	1,048	2,155	$\nu_3+\nu_{10}$	2,164
1,260	$2\nu'_{10}$	1,294	2,212	$\nu_5+\nu'_7$	2,215
1,414	$\nu'_{10}+\nu_2$	1,409	2,252	$2\nu'_7$	2,258
1,453	$\nu_3+\nu_7$	1,443	2,309	$\nu_7+\nu_{10}$	2,311
1,553	$\nu_{11}+\nu_5$	1,542	2,476	$\nu_7+\nu_1$	2,475
1,709	$\nu_6+\nu_7$	1,725	2,531	$\nu_{10}+\nu_1$	2,528
			2,591	$\nu'_7+\nu_1$	2,579

The advice and assistance given by E. K. Plyler in the course of this work are gratefully acknowledged. The suggestions of W. S. Benedict have been useful in the classification of the spectra.

V. References

[1] J. Rud Nielsen, C. M. Richards, and H. L. McMurray, J. Chem. Phys. **16,** 67 (1948).
[2] D. H. Rank, and E. L. Pace, J. Chem. Phys. **15,** 39 (1947).
[3] E. K. Plyler, R. Stair, and C. J. Humphreys, J. Research NBS **38,** 211 (1947) RP1769.
[4] E. K. Plyler, J. Opt. Soc. Am. **37,** 746 (1947).
[5] E. K. Plyler, J. Research NBS **41,** 125 (1948) RP1911.
[6] D. T. Hamilton and F. F. Cleveland, J. Chem. Phys. **12,** 249 (1944).

WASHINGTON, October 11, 1949.

U. S. Department of Commerce
National Bureau of Standards

Research Paper RP2100
Volume 44, May 1950

Part of the Journal of Research of the National Bureau of Standards

Development of Very-High-Frequency Field-Intensity Standards*

By Frank M. Greene and Max Solow

A description is given of the development of two very-high-frequency field-intensity standards, which are being used at this Bureau for the calibration of commercial field-intensity sets in the range 30 to 300 megacycles. These standards are employed to establish known values of field intensity by either of two methods: (a) the standard-antenna method in which the open-circuit voltage at the center of a receiving dipole is measured directly; (b) the standard-field method in which the current at the center of a transmitting dipole is accurately known. The techniques used for determining the antenna current and voltage are described.

The current distribution on the antenna is determined theoretically, using Schelkunoff's method, which gives the effective length. These values are compared with those obtained by measurement.

Results of field tests at 100 megacycles are presented in which the above two methods were directly intercompared using horizontal polarization. Their accuracy and limitations are discussed.

I. Introduction

For a number of years the National Bureau of Standards has maintained among its other public services, the calibration of commercial field-intensity meters. These instruments are largely used by engineering consultants and broadcast engineers, in order to determine a radio station's antenna efficiency and coverage area, acceptable values of which are specified by the Federal Communications Commission. The frequency range of this calibration service has in the past extended to approximately 30 Mc and is maintained by the Bureau's Central Radio Propagation Laboratory.

More recently, as a result of the greatly increased use of the very-high-frequency (VHF) band (30 to 300 Mc) for frequency-modulation and television broadcasting and other communication purposes, the Central Radio Propagation Laboratory has undertaken to extend the frequency range of this calibration service to include these frequencies. This necessitated the development of accurate field-intensity standards for calibration purposes. Such standards are usually employed to determine a value of field intensity in terms of either a known voltage or current in an antenna, together with certain geometrical relationships involved, such as the antenna length, distance of separation, etc. The standards developed are similar in principle to those already in use at the lower frequencies. However, it was necessary to modify the techniques employed for the measurement of antenna current and voltage as well as the over-all technique in the use of the standards in order to adapt them to use at the higher frequencies.

In many instances the accuracy with which the value of a physical quantity may be determined increases with the simplicity of the method used to make the determination. Such measurements usually involve a theoretical calculation, or an experimental observation, or both. In establishing the field-intensity standards discussed herein, the methods adopted for current and voltage measure-

*A summary of this paper was presented at the joint meeting of the International Scientific Radio Union and the Institute of Radio Engineers at Washington, D. C., on May 2, 1949.

ment were purposely made as elementary as possible for this reason. It is believed that this enables the achievement of the maximum accuracy possible or practicable at the present time. This of necessity results in some limitation of the range of measurement and flexibility of use, but the premium paid results in increased accuracy.

The standards or methods used to establish accurately known values of VHF field-intensity are (a) the standard-antenna method and (b) the standard-field method.

It is the purpose of this paper to describe two such experimental standards in some detail, the techniques involved for measuring the antenna voltage or current, as well as the propagation tests made to intercompare the field-intensity values obtained by both methods. The accuracy and limitations of the two methods are also discussed.

This work done by the authors represents one phase of a program for the development of accurate VHF field-intensity calibration standards. Although these standards were developed to cover the entire VHF band, the initial propagation tests described herein were made at a frequency of 100 Mc, using horizontal polarization only; and the standard antennas were horizontal half-wave self-resonant dipoles in all cases.

No claims are made as to the originality of the individual methods or techniques used, as most of these have been reported elsewhere. However, the standards discussed here are novel at least in their simplicity and in the accuracy obtainable. Practical rationalized mks units are used throughout this paper.

II. Standard-Antenna Method

1. Relation Between Field-Intensity and Induced Voltage

The magnitude of the electric component of VHF field-intensity existing at a given point in space may be determined in terms of the voltage, V_{oc}, induced in a standard receiving dipole immersed in the field, together with the antenna geometry. It will be assumed in the following that the antenna is a horizontal half-wave dipole oriented for maximum response, and that the voltage is referred to the center terminals. In case the antenna is not open-circuited, the voltage measured, V_L, is of course not the induced voltage but is related to it by the voltage-transfer ratio,

$$\eta \equiv \left|\frac{V_L}{V_{oc}}\right| = \left|\frac{Z_L}{Z_A + Z_L}\right|, \tag{1}$$

where Z_L is the load impedance, in ohms, connected to the antenna terminals, and Z_A the antenna input impedance in ohms.

The magnitude of the electric component of field-intensity (in volts per meter) is related to the induced voltage by

$$|E| = \frac{V_{oc}}{l_H}, \tag{2}$$

where l_H is the effective length of the antenna in meters.[1]

2. Effective Length of the Antenna

Assuming a sinusoidal current distribution on the antenna, the effective length (in meters) is

$$l_H = \frac{\lambda}{\pi} \tan \frac{\pi l}{\lambda}, \tag{3}$$

where λ is the wavelength in meters, and l the antenna half-length in meters.

For a half-wave dipole the effective length (in meters) reduces to

$$l_H = \frac{\lambda}{\pi}. \tag{4}$$

As is known, the current distribution on an antenna is not exactly sinusoidal except for an infinitely thin filament. For cylindrical antennas of radius a and half-length l, the departure from a sinusoidal distribution becomes progressively greater as the ratio $2l/a$ decreases (i. e., as the antenna gets fatter).

An approximate solution for the free-space current distribution on a cylindrical transmitting antenna [2] has been obtained by Schelkunoff [1] [3] among others, and is given by the sum of eq 34 and 35 in the appendix. The relative distribution

[1] It is assumed here (and our results seem to indicate) that the relative current distribution and hence the effective length is not (to a first approximation) a function of either the height of the antenna above the ground or the terminating impedance, Z_L.

[2] How this is handled in the case of the receiving antenna has not been made too clear in the literature, but the difference between the two cases is apparently small for moderately thin antennas. The reader is referred, for instance, to J. C. Slater, Microwave transmission, pp. 219 to 230 (McGraw-Hill Book Co., Inc., New York, N. Y., 1942).

[3] Figures in brackets indicate the literature references at the end of this paper.

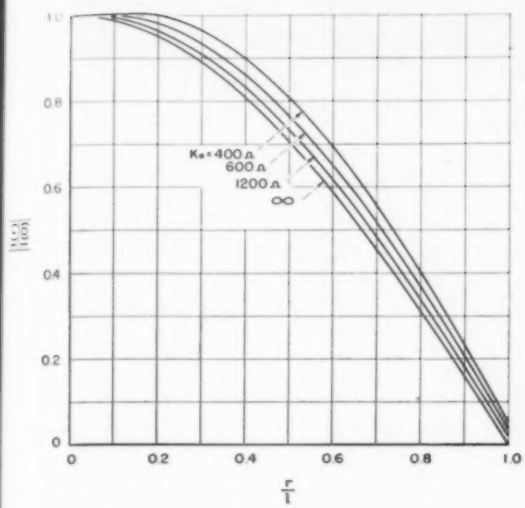

FIGURE 1. *Theoretical free-space relative current distributions on a cylindrical half-wave dipole as determined from Schelkunoff's analysis.*

The relative current $I(r)/I(0)$ is shown versus the fractional half-length r/l for several values of the average characteristic impedance, $K_0=120[\log_e(2l/a)-1]$, as determined from the sum of eq 34 and 35 in the appendix.

is a function of both the phase length $2\beta l$, and the ratio $2l/a$, and may be represented by

$$\frac{I(r)}{I(0)}=f(\beta l, K_0), \tag{5}$$

where

$I(r)$ = current in amperes at a distance r meters from the center of the antenna

$I(0)$ = current in amperes at the center of the antenna $(r=0)$

$K_0 \equiv 120\left(\log_e \frac{2l}{a}-1\right)$ ohms, and is the average characteristic impedance over the half-length l

$\beta=2\pi/\lambda$.

The relative current distributions as determined from the magnitude of the sum of eq 34 and 35 are shown in figure 1 for half-wave dipoles for several values of K_0. Because of the increasing complexity of the higher order Bessel functions in the infinite series of eq 35, only the first two terms of this series were evaluated. This accounts for the fact that the current as shown in figure 1 does not reduce quite to zero as it should at the end of the antenna, $r/l=1.0$. The contribution from the neglected terms in this series is appreciable only near the ends of the antenna, so that this approximation does not appreciably affect our results here.

The effective length of the antenna (in meters) may be determined from the relative current distribution by the relation

$$l_H=\int_{-l}^{l}\left|\frac{I(r)}{I(0)}\right| dr \tag{6}$$

The magnitude of the sum of eq 34 and 35 may be substituted in eq 6 and the integration performed either mathematically or mechanically. We preferred the latter as being less involved.

In this manner a number of values of effective length, l_H, were determined for various values of the average characteristic impedance, K_0, between 400 and 1,200 ohms. The percentage increase in l_H over that of an infinitely thin filament, $K_0=\infty$, is shown versus K_0 in figure 2 for half-wave dipoles.[4]

The agreement between calculated and observed values of l_H for the antenna used will be discussed in section IV.

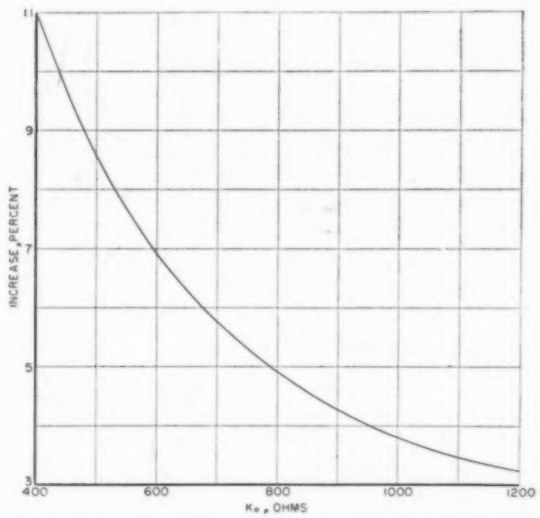

FIGURE 2. *Percentage increase in effective length of a cylindrical half-wave dipole (over that of an infinitely thin filament) versus the average characteristic impedance, K_0, as determined by substituting the sum of eq 34 and 35 in 6.*

[4] The percentage increase in l_H for the case of thin self-resonant dipole antennas was found to be very nearly the same as that for full half-wave dipoles for the values of K_0 usually encountered.

In order to operate a half-wave dipole at self-resonance it is necessary, as is known, to shorten its length somewhat from a full half-wavelength.

Schelkunoff [2] and King [3] have obtained independent approximate solutions yielding the required shortening for self-resonant operation of thin cylindrical antennas. Although obtained by radically different methods, the value of the required shortening as determined from Schelkunoff's solution is in substantial agreement with that obtained from King's second-order solution, and is given by

$$\frac{4l}{\lambda}=1-\frac{60Si(2\pi)}{\pi K_0}=1-\frac{27.08}{K_0}, \qquad (7)$$

where $Si(x)\equiv\int_0^x(\sin t/t)dt$ and $Si(2\pi)=1.41815$.

Values of the percentage shortening determined from eq 7 are shown versus the average characteristic impedance of the antenna K_0, in figure 3.

3. Antenna Voltmeter

The standard receiving antenna used was a self-resonant (half-wave) dipole shortened approximately 4 percent from a full half-wavelength (f= 100.0 Mc) (as determined from fig. 3) to make it self-resonant. Dural tubing $\frac{3}{16}$ in. in diameter was used, giving a ratio $2\,l/a\cong600$, and an average characteristic impedance $K_0=120\ [\log_e(2l/a)-1]\cong650$ ohms. The induced voltage referred to the center terminals of the antenna was measured directly by means of a relatively high-impedance balanced voltmeter connected across the gap at the center. In this manner the necessity for a separate measurement of the antenna input impedance was eliminated, which greatly simplified the problem. The voltmeter consisted of a modified type 1N28 silicon-crystal rectifier built into the gap as shown in figure 4. The crystal output was filtered by means of a balanced resistance-capacitance network, and the d-c output voltage was measured directly against a standard cell on a special precision slide-wire potentiometer. The central portion of an experimental receiving antenna assembly minus the antenna rods is shown in figure 5. The input impedance of the resistance-capacitance filter was approximately 10,000 ohms in shunt with 0.05 $\mu\mu$f. High-frequency resistors were employed, which were available commercially.

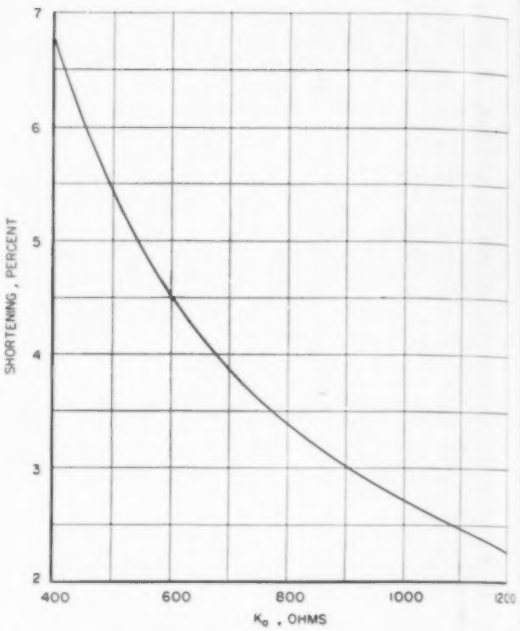

FIGURE 3. *Percentage shortening of a cylindrical half-wave dipole required for self-resonant operation versus the average characteristic impedance, K_0, as determined from eq 7.*

The effective shunt capacity of the crystal diode was less than 0.75 $\mu\mu$f. However, since the resulting reactance of some 2,000 ohms was in quadrature with the radiation resistance of the antenna, the resulting shunting error from this source was a small fraction of 1 percent.

In selecting the crystal rectifier it was necessary to consider both its r-f (input) resistance and its

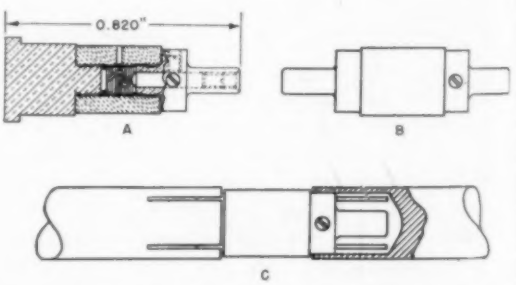

FIGURE 4. *Method used to mount the type 1N28 silicon crystal rectifier in the gap at the center of the half-wave standard receiving antenna.*

A, Western Electric 1N28 silicon crystal rectifier; B, 1N28 as modified; C, modified 1N28 as mounted in the antenna gap.

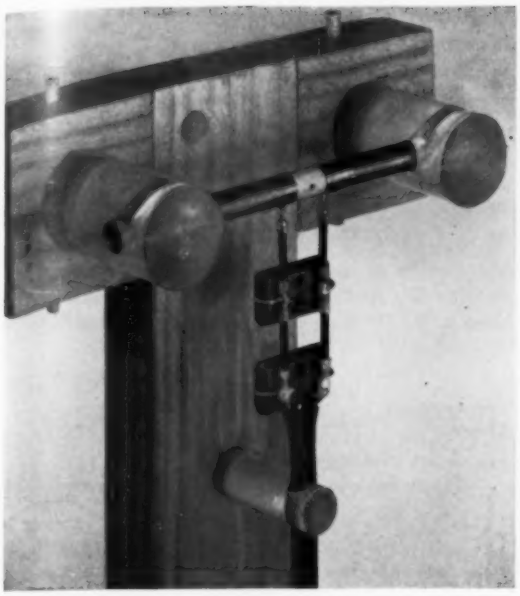

FIGURE 5. *View of the central portion of an experimental standard receiving antenna minus the antenna rods showing the crystal rectifier and resistance-capacity filter network.*

(internal) d-c-output resistance. Both are a function of the applied r-f-voltage level, decreasing with increasing level, although not necessarily at the same rate.

In order to limit the shunting caused by the presence of the crystal voltmeter in determining the open-circuit antenna voltage, it was necessary to select a crystal having as high a value of r-f resistance as possible. On the other hand, to maintain as high a sensitivity as possible in measuring the d-c-output voltage of the crystal, it was necessary to select a crystal with a relatively low value of d-c-output resistance.

A satisfactory compromise was obtained by selecting a crystal having an r-f resistance between 8,000 and 10,000 ohms when measured at an r-f level of 0.1 v and self-biased. This resulted in a shunting error of less than 2 percent in determining the induced antenna voltage. It was found in general that the type 1N28 crystals came closest to meeting these requirements.

The variation of both the r-f resistance and the d-c-output resistance versus applied r-f voltage at 100 Mc is shown in figure 6 for the 1N28 crystal selected when operated self-biased. These crystal characteristics are not representative of the 1N28 crystals in general, as it was possible to find many with considerably higher or lower values of r-f and d-c resistance than the values shown. The variation among other crystals of types 1N21 to 1N27 was found to be even greater.

The r-f input resistance of the 1N28 crystal was measured by a resistance-variation method [4] using several high-frequency resistors having widely separated values as cross checks in determining each value of crystal resistance. The crystal was connected in series with a 200-$\mu\mu$f d-c-blocking condenser across an antiresonant circuit during these measurements. The d-c-output voltage acting as self-bias on the crystal was developed across this condenser.

The d-c-output resistance of the crystal is the equivalent internal dynamic source resistance of the d-c-output circuit. This is sometimes referred to as the d-c, or video, impedance [5] and may be defined (in ohms) as

$$R_i \equiv \frac{\Delta e}{\Delta i}, \tag{8}$$

where Δe=a small change in the d-c balancing voltage of the slidewire potentiometer and Δi= the resulting change in the d-c current in the output circuit. If Δe is kept smaller than about 5 mv, when measuring R_i, either a positive or a negative value of Δe will result in very nearly the same value of R_i.

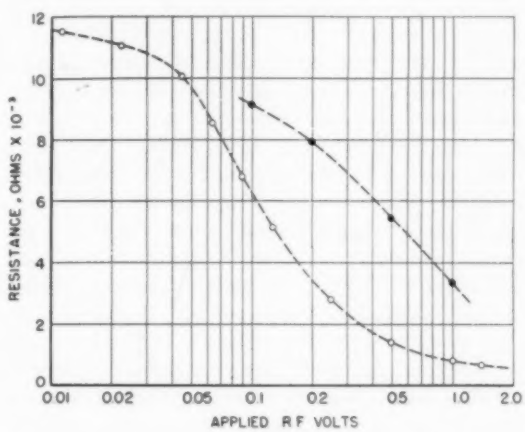

FIGURE 6. *Variation of the r-f input resistance and dynamic d-c output resistance as a function of the applied r-f voltage level for a selected type 1N28 silicon crystal rectifier.*

The measurements were made at 100 Mc with full self d-c bias applied to the crystal. These curves are not representative of the type 1N28 crystals in general. ○, d-c output resistance; ●, r-f resistance.

The d-c output resistance of the crystal was determined in this manner for a number of r-f voltage levels. The crystal was removed from the antenna and placed in a coaxial mount fed by a 25-ohm r-f source. The d-c output voltage was measured across a 200- $\mu\mu$f blocking condenser in the ground-return circuit.

As the d-c output voltage of the crystal was measured on a precision slidewire potentiometer, it is necessary to define the sensitivity of this instrument. This determined the useful range of d-c output voltages that could be measured, and hence the resulting range of applied r-f voltages that could be determined.

The voltage sensitivity of the potentiometer (in volts) is

$$\Delta e = R\Delta i \tag{9}$$

where

Δe=smallest change in the balancing voltage that can be set on the slidewire dial of the potentiometer.

Δi=smallest unbalance current readable on the galvanometer.

R=total series d-c resistance of the measuring circuit and crystal.

The potentiometer used in these experiments was a commercially available portable type, weighing approximately 15 lb. It housed a standard cell, dry cells for comparison purposes, and a sensitive light-beam galvanometer, together with the slidewire dial and standard resisters all in a portable carrying case. The instrument had a useful measuring range of 0.5 to 161 mv. Other instruments were available having a range up to 1.6 v.

The most sensitive portable light-beam galvanometer available was used for measuring the output voltage of the crystal. Its sensitivity was approximately 0.03 μa per scale division (1 mm). Assuming that one could detect a change of current, Δi, of 0.1 division, and that the total series d-c resistance of the crystal, filter, and potentiometer was approximately 20,000 ohms, the voltage sensitivity was $\Delta e = R\Delta i = 2\times10^{4}\times3\times10^{-9} = 60\times10^{-6}$ v. Thus, neglecting the other errors in the instrument, which were small, d-c output voltages of the crystal could be determined to an accuracy of better than 2 percent from something less than 3 mv to over 1 v (the safe upper voltage limit of the crystal). This corresponded to a range of r-f input voltage to the crystal of roughly 0.02 to 1.0 v as will be shown.

The silicon crystal voltmeter was calibrated in terms of a standard voltmeter. One type used at 100 Mc comprised a quarter-wavelength balanced transmission line of accurately known characteristic impedance terminated in a previously calibrated VHF vacuum thermocouple.[4] As is known, the magnitude of the transfer impedance of a quarter-wave length uniform low-loss transmission line is equal to its characteristic impedance [6], i. e.,

$$|Z_T| \cong \left|\frac{V_s}{I_R}\right| \cong Z_0, \tag{10}$$

where

V_s=sending-end voltage

I_R=receiving-end current

Z_0=characteristic impedance.

Thus the sending-end voltage may be determined in terms of the receiving-end current and the characteristic impedance of the transmission line. This relationship is independent of the magnitude or phase-angle of the terminating impedance (in this case the heater of the VHF vacuum thermocouple). The line losses involved were found to be small enough so as not to appreciably affect the results.

The frequency error of the thermocouple was determined in terms of small bead-type thermistors used as current standards. These are known to maintain their d-c value of resistance up to frequencies well above the VHF band when biased to low values of resistance. The circuit used to determine the frequency error is shown in figure 7. The bridge circuit measured the d-c resistance of the series combination of the thermistors and thermocouple heater biased with either d-c or r-f current. A measure of the r-f current was thus provided in terms of a known d-c current. A negligibly small d-c measuring current was used in the presence of the r-f current so as not to appreciably alter the thermistor resistance. Two matched thermistors were used to preserve the symmetry, as the frequency correction of the thermocouple will in general be considerably different if used in an unbalanced circuit.

The desired value of direct current was first established in the thermocouple heater. Resist-

[4] The VHF thermocouple referred to herein has a separate heater insulated from the couple by means of a small glass bead.

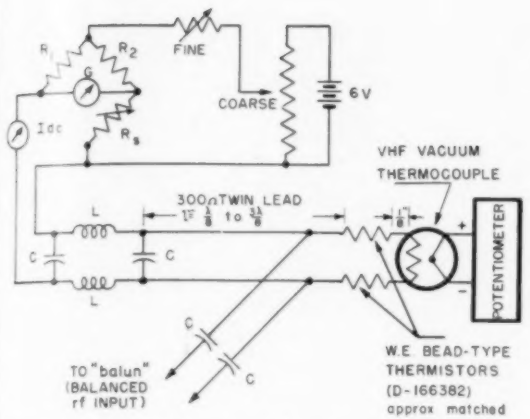

FIGURE 7. *Circuit diagram of the apparatus used to determine the frequency correction of VHF vacuum thermoelements when used in a balanced circuit arrangement.*

L≃1/4μh; C≃200μμf(f=100Mc).

ance R_s was then adjusted to balance the bridge, at the same time maintaining the value of current by readjusting the battery voltage if necessary. After measuring the d-c voltage output of the thermocouple, the direct current was reduced in value to 5 percent or less. The r-f voltage of desired frequency was then applied, adjusted in value until the bridge was rebalanced, and the d-c voltage output of the thermocouple measured. The r-f voltage was then removed and the value of direct current determined to reproduce this value of thermocouple output. The frequency correction was obtained from the two values of direct current. With sufficient sensitivity in the bridge and associated controls, it was found possible to reproduce these frequency corrections to a small fraction of a percent.

Generally speaking, for a given accuracy, a current standard is somewhat easier to provide at these frequencies than is a voltage standard. Fortunately, the relation given by eq 10 enables one to provide an r-f voltage standard having an accuracy approximating that of the current standard used. The difficulty, however, in this case is in the restricted frequency range over which the standard may be used. Normally a continuous voltage calibration is not required over the frequency range of the standard antenna. A number of individual calibrations spaced at frequency intervals of approximately 25 or 50 percent over the desired range is usually sufficient when the response is broadband.

Probably one of the most accurate methods of determining the characteristic impedance of the balanced low-loss transmission line used in this voltage standard is from the relation

$$Z_0 = \frac{1}{V_p C} \tag{11}$$

where

Z_0 = characteristic impedance in ohms,
V_p = velocity of propagation in meters per second, and
C = mutual capacity between conductors in farads per meter.

The type of transmission line used was commercially available unshielded twin-lead having a nominal characteristic impedance of 75 ohms. The velocity of propagation was determined to an accuracy of better than 0.25 percent at 100 Mc by measuring the resonant frequency of a half-wavelength section of line short circuited at both ends. The length of the short circuit used was such as to introduce a negligible error in the measurement. The calculated effect of the line loss on the velocity of propagation was also found to be negligible. The balanced mutual capacity, C, per unit length was determined on a special precision Schering bridge at a frequency of 1,000 cycles to the same order of accuracy. There is no reason to suspect that the capacity per unit length should change with frequency, at least up to frequencies of several hundred megacycles. Thus the characteristic impedance was probably determined to better than 0.5 percent. The characteristic impedance of a number of samples 1 m in length cut from the same piece of twin-lead varied less than ± 0.1 percent from the average value of the lot. This would seem to indicate the exceedingly small departure from uniformity existing within a given sample of the line. The average value of Z_0 for the lengths measured was 83.0 ohms. The variations between samples of different production-runs of twin-lead was quite large, being as high as 10 to 15 percent, as might be expected. The aging of the twin-lead seems to be negligible if not exposed to the weather or undue stress. This was indicated by having a value of the velocity of propagation of a particular sample repeat to within 0.1 percent after several months.

Another type of balanced voltage standard used consisted simply of a sensitive thermocouple previously calibrated in a manner similar to that already described and shown in figure 7. However, in this case a single thermistor was used in shunt with the thermocouple heater. A 1,000-$\mu\mu$f ceramic disk condenser was used in series with each thermocouple heater lead to provide dc isolation and preserve the symmetry. The leads were kept as short as physically possible (⅛ in. in most cases).

The voltage standards described above were used at only one voltage level (approximately 1 v), that corresponding to the rated current through the terminating thermocouple. The voltage range was extended downward by means of a precision piston (mutual inductance) attenuator [6a] having an accuracy better than 0.1db (approximately 1.0%) over a range of 60 db. The total rms harmonic content of the r-f generator output was less than 1 percent, so that any resulting error in the voltage standard from this cause was negligible. Pi matching networks were used in both the input and output circuits of the standard attenuator to decrease the insertion loss.

Figure 8 is a block diagram showing the equipment and its arrangement for one of the methods used to calibrate the balanced crystal voltmeter. The antenna rods were removed during calibration. A broadband balun [7] was used to transform from the unbalanced output of the standard attenuator to the balanced circuit of

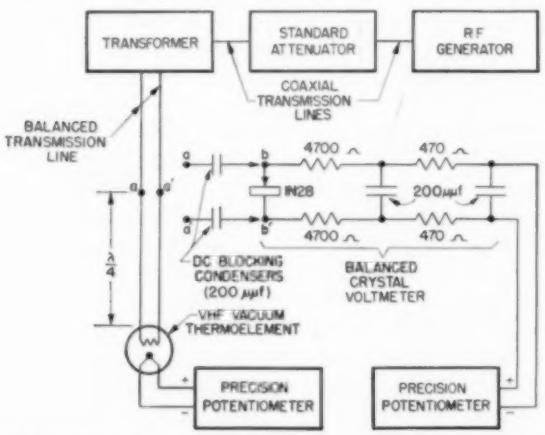

FIGURE 8. *Diagram showing the equipment and method used to calibrate the balanced crystal voltmeter used in the standard receiving antenna.*

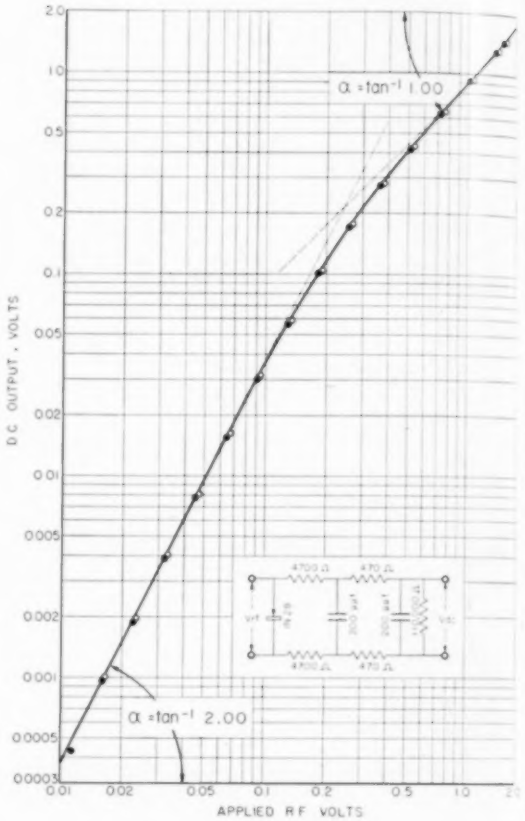

FIGURE 9. *Typical calibration curves of the crystal voltmeter, showing the variation in d-c output voltage versus applied r-f voltage for the circuit shown.*

Calibrations "A" and "B" were made 2 days apart at approximately the same ambient temperature. ●, Calibration A; ○, calibration B. *f*-100 Mc

the antenna and voltmeter. The "Pi" matching networks are not shown. Two 200-$\mu\mu$f d-c blocking condensers were used to prevent short-circuiting the d-c output of the antenna crystal.

Typical calibration curves of the antenna voltmeter made at 100 Mc are shown in figure 9. The usable range of r-f input voltage was from 0.02 to 1.0 v and the probably accuracy about ±2 percent over most of the range. The solid points and curve joining them represent the first of two calibrations. The circles represent a repeat calibration 2 days later at a temperature 1 deg C lower.

The data of figure 9 show the order of reproducibility possible with such a crystal voltmeter under partially controlled temperature conditions. The

diameter of the individual points represents approximately 5 percent of the voltage, so that any point touching the curve is in agreement to within ±2½ percent.

It was usually possible to repeat a crystal calibration to within 1 percent if made within a few hours at the same ambient temperature. In no case was the calibration relied on for more than a day.

In making the field-intensity measurements described in section IV, using this standard-antenna, the crystal voltmeter was always calibrated in the field within an hour of the time the tests were completed. A record of the temperature was kept and usually did not vary more than 2 deg C during any test. Thus all that was required of the crystal voltmeter was a good short-time stability.

Although the effect of variations in temperature and the accompanying hysteresis are known to contribute largely to the instability in a crystal voltmeter, no data were accumulated on the exact magnitude of these effects. We have so far avoided this by operating under as small a temperature variation as possible. Thus it would probably not be feasible to calibrate the crystal in a laboratory and use it for measurements outside at a temperature as much as 10 or 15 deg C different.

The response of the antenna crystal voltmeter was found to be essentially independent of frequency up to 200 Mc with a rising response beyond (output indication high) due to series resonance within the crystal and mount. The series-resonant frequency for this voltmeter was of the order of 2,000 Mc.

III. Standard-Field Method

1. Theory

A predetermined value of field intensity may be established at a given point in space in terms of the current distribution in a transmitting antenna, the effect of the ground, and the geometry involved.

In the development of the standards being reported here, only horizontally polarized transmission over plane homogeneous earth having finite values of relative dielectric constant, ϵ_r, and conductivity, σ, was considered. The distance of separation used between the transmitting and receiving antennas was from 2 to 20 wavelengths. These conditions simplify the resulting formulas somewhat and for the accuracy desired are quite justified. This range of distances is usually of little interest to the propagationist, at these frequencies, and many of the transmission vagaries of concern to him are ignored here. At these smaller separations a more exact knowledge of the actual angle of incidence and ground reflection coefficient is usually needed in order to produce the required degree of accuracy in predicting the actual value of field intensity existing. The geometry of the transmission system is shown in figure 10.

The root-mean-square value of the electric component of field intensity produced by a horizontal transmitting dipole at distances greater than about 2λ over plane homogeneous earth is [8, 9, 10] (in volts per meter)

$$E \simeq -j\frac{60\pi l_H I}{\lambda}\left[\underbrace{\frac{e^{-jkR_1}}{R_1}}_{\substack{\text{Direct}\\ \text{wave}}} + \underbrace{\frac{\Gamma e^{-jkR_2}}{R_2}}_{\substack{\text{Ground-}\\ \text{reflected}\\ \text{wave}}} + \underbrace{\frac{(1-\Gamma)}{R_2}A(R)e^{-jkR_2}}_{\substack{\text{Surface}\\ \text{wave}}}\right]. \tag{12}$$

in which

l_H = effective length of the antenna in meters
λ = wavelength in meters
R_1 = direct-ray path length in meters
R_2 = ground-reflected-ray path-length in meters
$\Gamma = \rho\epsilon^{-j\phi}$ = complex plane-wave reflection coefficient (horizontal polarization)
$A(R)$ = complex surface-wave attenuation factor
I = rms current in amperes at the center of the transmitting antenna
$k = 2\pi/\lambda$
$j = \sqrt{-1}$

The first term of eq 12 represents the field intensity that would exist if the transmitting and receiving antennas were located in free space. The remaining terms take into account the presence of the earth. The second term represents the ground-reflected wave which, when added vectorially to the first term of eq 12, comprises the space wave. The third term of eq 12 represents the surface wave associated with the r-f currents actually flowing in the ground.

The total field given by eq 12 is usually referred to as the ground wave. Propagation via the

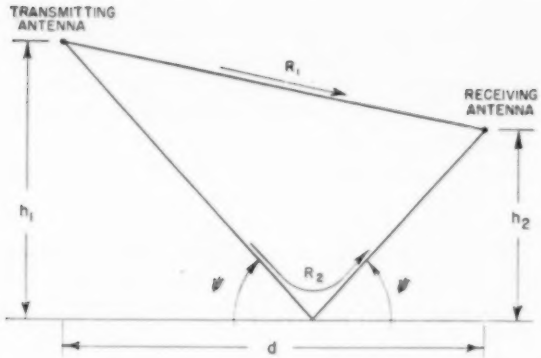

FIGURE 10. *Ray-path diagram showing: (a) direct ray along R_1; (b) ground-reflected ray along R_2 making an angle $\psi = \tan^{-1}(h_1+h_2)/d$ with the earth.*

Heights of the transmitting and receiving antennas are h_1 and h_2, respectively, and d is the horizontal distance of separation.

ionosphere or troposphere, which is subject to changing solar or meteorological conditions is being ignored here.

The magnitude of the surface wave is usually negligibly small for horizontally polarized transmission at these frequencies [11], and in the remaining formulas used herein we shall neglect its presence entirely.

The complex reflection coefficient of the ground, Γ, may be expressed in terms of the angle $\psi = \tan^{-1}(h_1+h_2)/d$ and a complex dielectric constant ϵ_0, as follows, for horizontal polarization [12],

$$\Gamma = \frac{\sin\psi - \sqrt{\epsilon_0 - \cos^2\psi}}{\sin\psi + \sqrt{\epsilon_0 - \cos^2\psi}}, \tag{13}$$

where

$$\epsilon_0 \equiv \epsilon_r\left(1 - j\frac{\sigma}{\epsilon\omega}\right) = \epsilon_r - j60\lambda\sigma$$

ϵ_r = relative dielectric constant of the ground (referred to free space as unity)

$\epsilon \equiv \epsilon_r\epsilon_r$, where ϵ_r is the permittivity of evacuated free space

$\epsilon_r \cong \frac{1}{36\pi} \times 10^{-9}$ farad per meter

σ = ground conductivity, in mhos per meter

$\omega = 2\pi f$

λ = wavelength, in meters

f = frequency, in cycles per second

Values of the magnitude of eq 13, ρ, are shown versus $\tan\psi = (h_1+h_2)/d$ in figure 11 for various values of the relative dielectric constant, ϵ_r, for low-loss dielectrics ($\sigma/\epsilon\omega \ll 1$). Many types of ground may be treated as low-loss dielectrics over a large portion of the VHF band as far as their reflecting properties are concerned. This is particularly true at the higher frequencies above 50 or 75 Mc.

In this case the phase shift on reflection ϕ, is very nearly 180° for horizontal polarization, so that the value of the reflection coefficient is given approximately by

$$\Gamma \cong -\rho. \tag{14}$$

Ignoring the surface wave altogether, the magnitude of eq 12 may be written (in volts per meter)

$$|E| \cong \frac{60\pi l_H I}{\lambda}\left|\frac{1}{R_1} + \frac{\Gamma e^{-jk(R_2-R_1)}}{R_2}\right|. \tag{15}$$

Equation 15 may be expanded without further approximation, giving (in volts per meter)

$$|E| \cong \frac{60\pi l_H I}{\lambda} \left\{\left(\frac{1}{R_1} + \frac{\rho}{R_2}\right)^2 - \frac{4\rho}{R_1R_2}\sin^2\left[\frac{k(R_2-R_1)+\phi}{2}\right]\right\}^{\frac{1}{2}}, \tag{16}$$

where ρ is the magnitude of the reflection coefficient, Γ, and ϕ is its phase lag in radians. Equation 16 is in a form somewhat more suitable for computation, since no loss of accuracy is involved as a result of the taking of small differences between large computed quantities.

In case the approximation given by eq 14 applies, eq 16 may be written (in volts per meter)

$$|E| \cong \frac{60\pi l_H I}{\lambda}\left\{\left(\frac{1}{R_1} - \frac{\rho}{R_2}\right)^2 + \frac{4\rho}{R_1R_2}\sin^2\left[\frac{k(R_2-R_1)}{2}\right]\right\}^{\frac{1}{2}}. \tag{17}$$

The quantity $[(1/R_1)-(\rho/R_2)]^2$ within the radical becomes negligibly small when $d \gg (h_1+h_2)$, since $R_1 \to R_2 \to d$, $\rho \to 1$, and $R_2 - R_1 \cong 2h_1h_2/d$. Under these conditions, eq 17 becomes (in volts per meter)

$$|E| \cong \frac{120\pi l_H I}{\lambda d}\left|\sin\left(\frac{2\pi h_1 h_2}{\lambda d}\right)\right|. \tag{18}$$

Equation 18 is obviously not valid in the vicinity of the zeros of the sine term, since the first term of eq 17 is not then negligible. Therefore use of eq 18 should preferably be restricted to values of $h_1h_2/\lambda d < 0.5$. If either the wavelength, λ, or the distance, d, is increased, eq 18 will reach its last maximum value when $h_1h_2/\lambda d = 0.3229\ldots$, after which it will steadily decrease. If the antenna

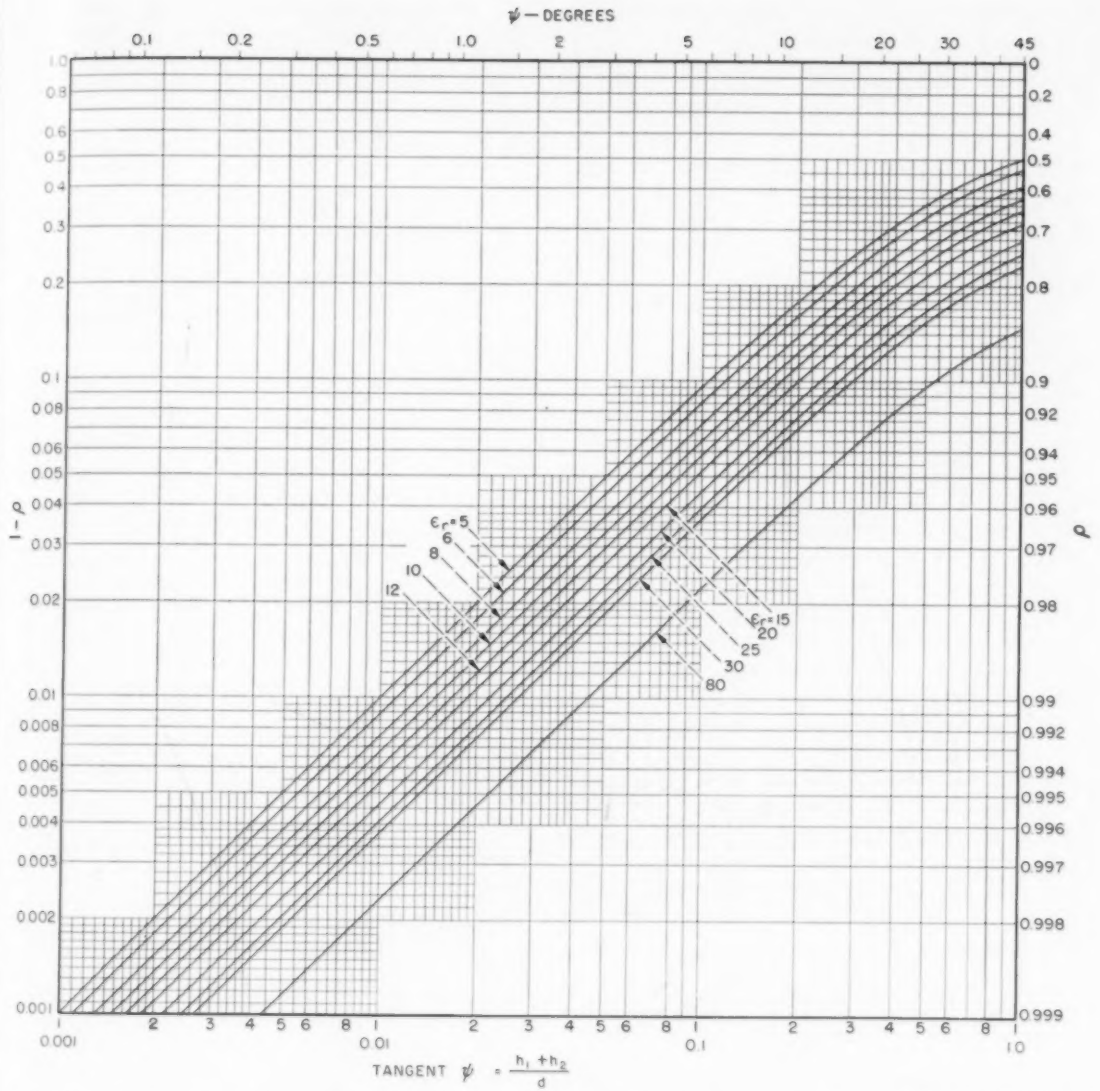

FIGURE 11. *Variation of the magitude, ρ, of the complex plane-wave reflection coefficient, Γ, versus tan ψ = (h₁+h₂)/d for several values of relative dielectric constant, εr.*

The curves apply to low-loss dielectrics, $(\sigma/\epsilon\omega \ll 1)$, and horizontal polarization only and were determined from eq 13.

heights h_1 or h_2 above are varied, this maximum will occur when $h_1h_2/\lambda d = 0.25$.

When $2\pi\, h_1h_2/\lambda d \leqq 1/4$ the field intensity is given (in volts per meter) to within 1 percent by

$$|E| \simeq \frac{240\pi^2 l_H I}{d^2}\left(\frac{h_1h_2}{\lambda^2}\right), \qquad (19)$$

since $\sin\theta \simeq \theta$ to within the stated accuracy for $\theta \leq 1/4$ radian.

When attempting to establish values of standard field intensity, however, one should rely on eq 16 or 17 until the assumptions applying to eq 18 and 19 are found to be fully justified.

2. Description of the Standard Transmitting Antenna

The transmitting antenna used was similar in many respects to the standard receiving antenna described in section II. A horizontal half-wave dipole was used shortened 4 percent for self-resonant operation at 100.0 Mc. Dural tubing $\frac{3}{16}$ in. in diameter was used, giving a ratio $2l/a \simeq 600$ and an average characteristic impedance $K_0 = 120\ [\log_e (2l/a) - 1] \simeq 650$ ohms.

The current at the center of the antenna was measured by means of a previously calibrated VHF vacuum thermocouple and a section of balanced twin-lead transmission line one-half wavelength long. The antenna and thermocouple terminated the transmission line at opposite ends, and a balanced feed-line from the r-f generator was tapped in at the midpoint. Thus the currents flowing at the opposite ends of the half-wave line were identical in value. The magnitude of the antenna current was thus indicated by the thermocouple $\lambda/2$ distant and was entirely independent of the magnitude and phase angle of the terminations, namely, the antenna input impedance, and the impedance of the thermocouple heater. A broadband balun [7] was used to transform the unbalanced output of the r-f generator to the balanced transmission system. A block diagram of the equipment and its arrangement are shown in figure 12. The thermocouple was calibrated in a similar manner to that described earlier for the receiving antenna voltmeter, and was found to have a frequency error of 0.5 percent at 100 Mc.

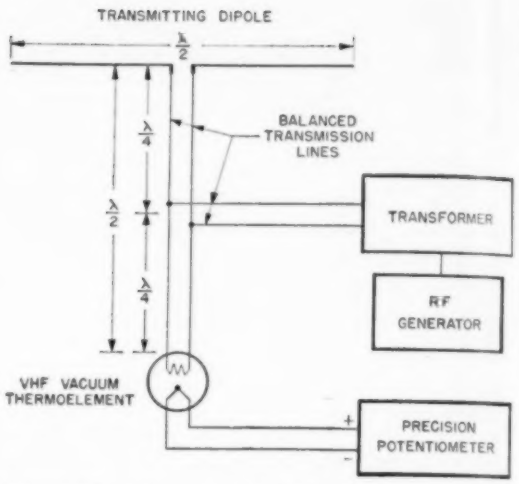

FIGURE 12. *Diagram showing the method used for determining the r-f current at the center of the transmitting dipole.*

IV. Propagation Tests

1. General

In order to determine the probable accuracy of the VHF field-intensity determinations made by the standard-antenna and standard-field methods previously described, actual propagation tests were made at a frequency of 100.0 Mc, using horizontal polarization only. The purpose was to actually intercompare values of field-intensity determined with the two standards.

For instance, a predetermined value of field intensity was established by means of the standard-field method, and simultaneously measured using the standard (receiving)-antenna method, and the results compared. However, instead of relying on isolated pairs of such measurements to determine the probable accuracy of the two methods, more or less complete propagation runs were made involving some 15 or 20 pairs of determinations in each, in order to determine the trend with varying antenna height or distance of separation. In this manner it was possible to determine the range of antenna heights and distances of separation between the antennas over which the previous assumptions applying to the earth were valid, and to what extent we were dealing with a uniform field.

Three general types of tests were made as follows:

(a) *Vertical-incidence standing-wave measurements,* in which the standard field beneath the horizontal transmitting antenna was probed vertically using the standard (receiving) antenna.

(b) *Variable-height runs,* in which the heights of the transmitting and receiving antennas were varied separately for a fixed horizontal distance of separation.

(c) *Variable-distance runs,* in which the horizontal distance between the transmitting and receiving antennas was varied for several fixed antenna heights.

In order to conduct these tests it was necessary to select a special site. The usual requirements specify that the location be relatively flat and free of such reflecting objects as trees, buildings, wires,

etc. in order to approximate the conditions assumed to exist in deriving the standard field formulas in section III.

A site of approximately 100 acres was made available at the Beltsville, Md. Airport for these tests. The land had been cleared and graded and met the above requirements. Interference from aircraft was negligible, inasmuch as the airport was officially closed and used only for emergency landings.

One other requirement, dictated by the lack of selectivity in the standard antenna, made it necessary to conduct such tests at a location where the field intensity of frequency-modulation and television broadcast stations was negligible compared to the standard field being used. Such interference was further minimized (since the test site was sufficiently free of reflecting objects) by properly orienting the two antennas. This was possible in our case since the interfering stations, some 20 miles distant, were all approximately in the same direction from the test site.

2. Vertical-Incidence Standing-Wave Measurements

This run was originally intended to be used for determining the reflection coefficient and hence the apparent dielectric constant, and conductivity of the ground at the test site. However, it was also found to be useful later in determining the effective length of the transmitting and receiving antennas, as will be shown.

For this test the horizontal transmitting dipole was located at the top of an all-wood ladder-mast at a fixed height $h_1 = 9.27$ m. The balanced unshielded 75-ohm r-f transmission line ran at right angles to the antenna and approximately 10 deg below the horizontal. The unshielded balanced d-c output lead from the thermocouple paralleled the r-f line and was spaced approximately 3 ft with negligible r-f pickup. The r-f power generator and associated equipment were located on the ground approximately 200 ft distant. The transmitting-antenna current was continuously monitored by an operator at the generator and was held constant to within ± 0.1 percent. The d-c output of the thermocouple was measured on a portable precision potentiometer. The probable accuracy of the antenna-current measurement was about 1 percent. The frequency of the r-f generator was also continuously monitored by means of a calibrated heterodyne frequency meter, and held to 100.0 Mc ± 0.1 percent.

The standard (receiving) antenna (oriented parallel to the transmitting antenna), was mounted on a movable carriage on the same mast, and was readily adjustable in height by means of a continuous rope passing through nonmetallic pulleys at the base and top of the mast. Certain predetermined heights were marked directly on the side of the mast and read by a second operator located at some distance off the end of the antenna in a null. The actual height of the antenna above ground could be thus measured to better than 0.5 cm. The balanced d-c output of the receiving antenna crystal-rectifier was carried over rubber-covered lamp cord, which passed vertically down the mast to the ground. From this point the d-c line went directly to the operator's position where the voltage was measured on the precision slide-wire potentiometer previously mentioned. Tests were made for r-f pickup on the d-c line, and in the resistance-capacitance filter at the antenna, with the antenna rods removed, but was found to be negligible even with the d-c line running the entire height of the mast.

Tests were made for stray radiation from the transmitting system caused by any slight unbalance in the feed line to the antenna or by leakage. The transmitting antenna rods were removed and a 65-ohm high-frequency resistor substituted to terminate the transmission line. With the normal r-f current of 0.1 amp flowing, the resulting field was too small to be measured for any height of the receiving antenna. The vertical component of field existing at the receiving antenna was more than 40 db below the main field, with the horizontal transmitting antenna excited.

Returning to the description of the vertical-incidence measurements, the resulting interference between the direct and ground-reflected waves, set up a standing-wave in the space beneath the transmitting antenna, as shown in figure 13. The standard (receiving) antenna was moved vertically up or down the mast to measure the resulting value of field intensity. The reflection coefficient was accurately determined from the standing-wave ratio, as will be shown. Once this was known, the expressions for the field intensity for the standard-antenna and standard-field methods, eq 2 and 15, were equated and solved for the remaining unknown, the effective length of the

antennas. This was deemed permissible since both antennas were physically identical.

The field intensity as determined by the standard-field method was obtained by substituting $R_1=h_1-h_2$, $R_2=h_1+h_2$, $d=0$ in eq 15, giving (in volts per meter)

$$|E|\cong\frac{60\pi l_H I}{\lambda}\left|\frac{1}{h_1-h_2}+\frac{\Gamma e^{-j2kh_2}}{h_1+h_2}\right|. \tag{20}$$

If $h_1\gg h_2$, the value of field intensity given by eq 20 will have a maximum value if $(2kh_2+\phi)=2n\pi$, and a minimum value if $(2kh_2+\phi)=(2n-1)\pi$, where $n=1, 2, 3, \ldots$. The magnitude of the ratio of the maximum to minimum values of field intensity is then

$$SWR=\left|\frac{E_{\max}}{E_{\min}}\right|\cong\frac{\dfrac{1}{h_1-h_{2\max}}+\dfrac{\rho}{h_1+h_{2\max}}}{\dfrac{1}{h_1-h_{2\min}}-\dfrac{\rho}{h_1+h_{2\min}}}. \tag{21}$$

The magnitude, ρ, of the complex reflection coefficient, Γ, of the ground may be determined from the SWR and the heights, h_2, of the receiving antenna corresponding to the maximum and the minimum values of field intensity measured plus the height of the transmitting antenna, thus

$$\rho\cong\frac{SWR\left(\dfrac{1}{h_1-h_{2\min}}-\dfrac{1}{h_1-h_{2\max}}\right)}{\dfrac{SWR}{h_1+h_{2\min}}+\dfrac{1}{h_1+h_{2\max}}}. \tag{22}$$

The angle of phase lag, ϕ, of the reflection coefficient may be determined from the shift in the positions of the maxima or minima from the positions corresponding to $\phi=0$. For the maxima this gives

$$\phi=2\left[\frac{2\pi h_{2\max}}{\lambda}-(n-1)\,\pi\right], \tag{23}$$

where $n=1, 2, 3, \ldots$ is the number of the maximum used to calculate ϕ, counting from the ground upward.

In using the minima to determine ϕ, the expression is

$$\phi=2\left[\frac{(2n-1)\,\pi}{2}-\frac{2\pi h_{2\min}}{\lambda}\right], \tag{24}$$

$h_{2\min}$ and $h_{2\max}$ are the actual heights, in meters, at which the particular minimum or maximum occurs.

In determining the value of the reflection coefficient of the ground at the test site, the heights, h_2, of the various maxima and minima were carefully measured. It was found possible to determine these to within ± 1.0 cm. To within this accuracy the positions corresponded to a phase shift, ϕ, on reflection of 180 deg. The possible error in determining ϕ thus amounts to approximately 2 deg. It is interesting to note that the calculated phase shift, ϕ, for average ground ($\epsilon_r=15$, $\sigma=5\times10^{-3}$ mho per meter) at 100 Mc is very nearly 179 deg at normal incidence. An error of 2 deg in determining ϕ usually has a negligible effect on the magnitude, ρ, of the reflection coefficient, and on the resulting value of field intensity calculated.

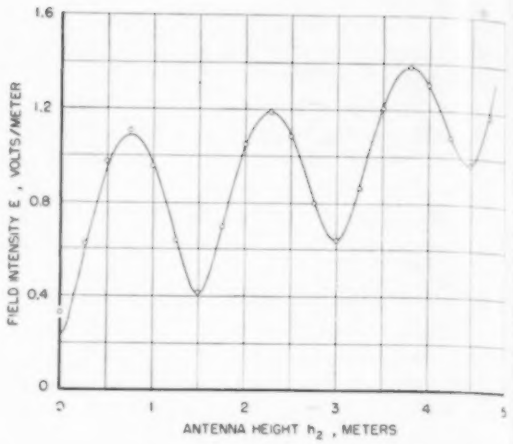

FIGURE 13. *Variation of the observed and calculated values of electric field intensity, $|E|$ in volts per meter, versus the height, h_2, in meters, of the standard receiving antenna.*

The transmitting antenna was located above and parallel to the receiving antenna at a fixed height, $h_1=9.27$ m, $d=0$, $f=100.0$ Mc, $I=0.100$ amp.
○, observed, ——, calculated.

Although the standing-wave method cannot be used to determine even approximately the ground conductivity at these frequencies, such information is usually not required if the reflection coefficient can be accurately determined.

An example will be given of the method of determining the magnitude, ρ, of the reflection coefficient, and the dielectric constant, ϵ_r, of the ground from the observed data presented in figure 13. Three different values of standing-wave ratio were determined from the three maxima and the three succeeding minima. The minimum occurring at the ground ($h_2=0$) was ignored because of its questionable value.

The value of ρ corresponding to each SWR was then determined from eq 22, and the resulting value of the relative dielectric constant ϵ_r determined from the relation

$$\epsilon_r=\left(\frac{1+\rho}{1-\rho}\right)^2, \tag{25}$$

which was obtained from eq 13 by substituting $\psi=\pi/2$, and $\Gamma=-\rho$ and solving for ϵ_r, $(\sigma/\epsilon\omega\ll 1)$. The results are given in table 1.

TABLE 1. *Values of ρ and ϵ_r, as determined from standing-wave measurements*

SWR	ρ	ϵ_r
2. 67	0. 648	21. 9
1. 85	. 635	20. 1
1. 42	. 636	20. 2
Average...	. 640	20. 7

The values of ρ and ϵ_r measured are determined largely by the moisture content of the ground. Consequently, their values fluctuate somewhat from day to day with changing moisture content. Four values of ϵ_r obtained in a similar manner over a period of a few months are shown in figure 14, together with values of daily rainfall. It can be seen that the variation in the dielectric constant is quite large. Normally, this is not of much concern to the propagationist, who is usually interested in grazing incidence, but it is apt to affect the accuracy of standard-field measurements at very short distances if the incident angle is large. Near the surface the moisture content and consequently the ground constants themselves may vary with depth. Since the skin depth in turn varies with frequency and angle of incidence (among other factors), the (apparent) values determined for these constants may also depend on these parameters.

If desired, the reflection coefficient of the ground for vertical incidence may be calculated from eq 13 upon substituting $\psi=\pi/2$, giving

$$\Gamma=\frac{1-\sqrt{\epsilon_r\left(1-j\,\frac{\sigma}{\epsilon\omega}\right)}}{1+\sqrt{\epsilon_r\left(1-j\,\frac{\sigma}{\epsilon\omega}\right)}}. \tag{26}$$

Values of the magnitude of eq 26 are plotted versus ϵ_r in figure 15 for low-loss dielectrics, $(\sigma/\epsilon\omega\ll 1)$, remembering that $\Gamma\cong-\rho$ for this condition.

Determining the value of the reflection coefficient, Γ, of the ground from the observed data of figure 13 actually required only relative values of the measured field intensity. With the value of Γ now accurately determined, the only remaining unknown in eq 20 is the effective length, l_H, of the transmitting antenna. Since the standard transmitting and receiving antennas used are geometrically identical, the assumption is made that their effective lengths are equal. There has been some indication in the works of King [13] that such is not exactly the case, and further that the value of l_H is also somewhat dependent upon the antenna termination. However, it is shown that for self-resonant antennas these differences are small. Shelkunoff does not elaborate on these points, but our experimental values of

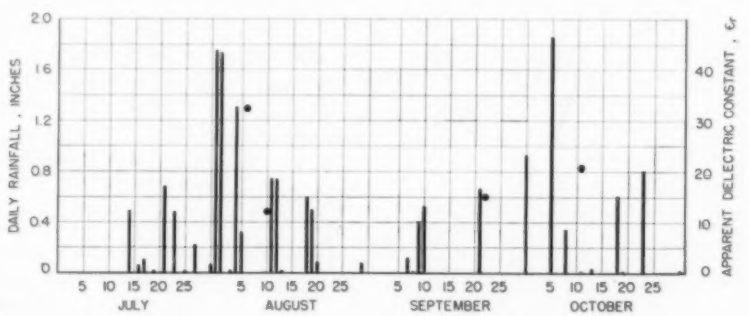

FIGURE 14. *Chart showing four measured values of the apparent relative dielectric constant, ϵ_r, of the ground at one particular site, as affected by rainfall. $f=100.0$ Mc.*

●, Dielectic constant; ▌, daily rainfall.

880789—50——7

effective length agree well with those calculated from his analysis of cylindrical antennas, as will be shown. The value of the effective length, l_H, may be determined by equating eq 2 and 20, and solving for l_H.

The data shown in figure 13 provide 19 separate determinations of l_H (ignoring the observed value corresponding to $h_2=0$ because of its questionable value). The average of these gives a measured value of $l_H=0.960$ m for the self-resonant antennas used.

Figure 16 shows the percentage difference between each pair of determinations as presented in figure 13, versus the height, h_2, of the receiving antenna. In this information is included experimental error, differences caused by changes in the receiving antenna current distribution due to the presence of the ground, and differences caused by the proximity of the transmitting and receiving antennas, of which the latter should be small in view of the fact that the receiving antenna was operated open-circuited. These differences, in general, are less than 3 percent, and give a good indication of the agreement possible between the standard-antenna and standard-field methods at least for the case of normal incidence where the reflection coefficient of the ground could be accurately determined.

It is also indicated that any varying effect (with antenna height) of the presence of the ground on the receiving antenna current distribution and hence upon its effective length is negligible, at least for the present purpose for antenna heights in excess of 0.1 wavelength.

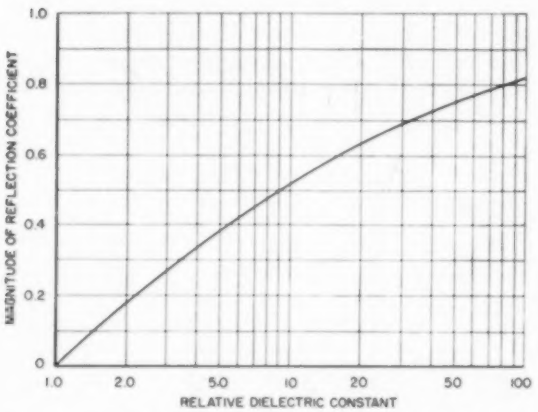

FIGURE 15. *Calculated variation of the magnitude, ρ, of the complex plane-wave reflection coefficient of the ground Γ, versus the relative dielectric constant, ϵ_r, for vertical incidence, $\psi=\pi/2$.*

The curve applies to low-loss dielectrics only ($\sigma/\omega\epsilon \ll 1$), and was determined from eq 26.

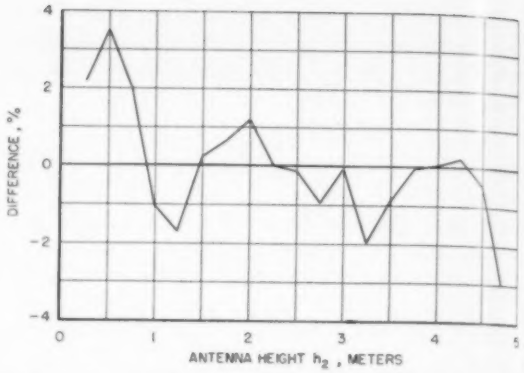

FIGURE 16. *Variation of the percentage difference between the observed and calculated values of field intensity of figure 13, with height, h_2, of the receiving antenna.*

The calculated value of the effective length is obtained from the product of the following values: (a) the classical value of effective length for a half-wave dipole given by eq 4; (b) the percentage shortening for self-resonant operation from figure 3; and (c) the percentage increase for cylindrical antennas from figure 2. The resulting value is $l_H \cong \lambda/\pi \times 0.96 \times 1.06 \cong 0.97$ m for operation at 100 Mc, and agrees to within about 1 percent with the above measured value.

3. Variable Height Runs

The purpose of the tests described in this section was to determine the probable measurement error existing in the two field-intensity standards under discussion. Determinations made by the two standards were directly intercompared, the maximum probable error (in the absence of other reference standards) being evaluated as one-half the percentage difference between the two measurements. Parallel horizontal self-resonant dipoles were used at a frequency of 100.0 Mc.

Values of field intensity established by means of the standard-field method were measured using the standard (receiving)-antenna method and the results compared.

These runs consisted of varying separately the heights of either the receiving or transmitting antennas for a fixed height of the other antenna, and for a fixed distance of separation.

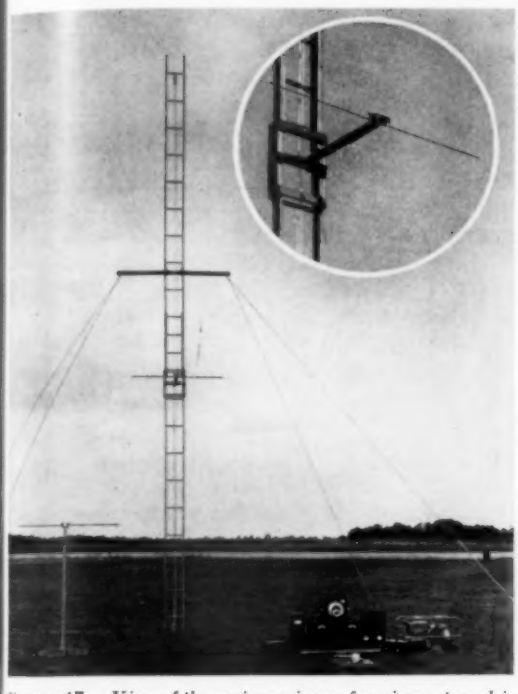

FIGURE 17. *View of the various pieces of equipment used in obtaining the measured data of figures 13, 14, 18, 19, and 20.*

In the background and insert are shown the ladder mast and carriage for the receiving dipole. The transmitting antenna, r-f generating equipment, and an engine-driven alternator are shown in the foreground. The location is the Beltsville (Md.) Airport.

In the first two runs the receiving antenna was varied in height, h_2, from 0.265 to 9.0 m, using the ladder-mast assembly shown in figure 17. The heights, h_1, of the transmitting antenna were 1.58 and 3.05 m, respectively, and the horizontal distance of separation, d, was 30.5 m. The measured value of the effective length of the antennas determined in the standing-wave test was used, namely, $l_H \cong 0.96$ m.

The results are shown in figure 18. In determining the field by the standard-antenna method, eq 2 was used (in volts per meter)

$$|E| = \frac{V_{oc}}{l_H}, \tag{2}$$

where V_{oc} is the measured value of open-circuit voltage.

The value of field determined by the standard-field method was obtained (in volts per meter) from eq 17,

$$|E| \cong \frac{60\pi l_H I}{\lambda}\left\{\left(\frac{1}{R_1}-\frac{\rho}{R_2}\right)^2+\frac{4\rho}{R_1R_2}\sin^2\left[\frac{k(R_2-R_1)}{2}\right]\right\}^{1/2}, \tag{17}$$

where

$l_H = 0.96$ m
$I = 0.100$ amp
$\lambda = 3.00$ m
$k = 2\pi/\lambda$
$R_1 = [(h_1-h_2)^2+d^2]^{1/2}$
$R_2 = [(h_1+h_2)^2+d^2]^{1/2}$.

Values of the magnitude, ρ, of the reflection coefficient were determined by taking the magnitude of eq 13, assuming low-loss dielectrics, $(\sigma/\epsilon\omega \ll 1)$. Values of ρ may also be taken from figure 11.

It was not found practical to measure the dielectric constant of the ground before each run because of the special setup required and the time consumed. Previous measurements showed that on the average the dielectric constant had a value around 15, except after a rain or after a prolonged dry spell. This value of ϵ_r was therefore used in calculating ρ from eq 13.

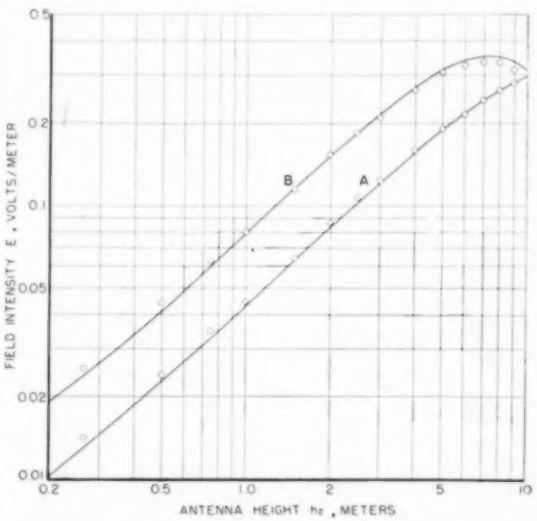

FIGURE 18. *Variation of the magnitude of the electric component of field intensity, $|E|$ in volts per meter as determined by the standard-antenna and standard-field methods vs the height, h_2 in meters, of the standard receiving antenna.*

Fixed heights $h_1 = 1.58$ m (A), and 3.05 m (B) of the transmitting antenna were used, and $d = 30.5$ m. $f = 100.0$ Mc, $I = 0.100$ amp, $\epsilon_r = 15$, $\sigma = 0$. Horizontal self-resonant half-wave dipoles were used having effective lengths of 0.960 m. ○, Standard-antenna method; ——, standard-field method.

880789—50——8

The diameter of the circles representing the standard-antenna data in figure 18 is approximately 5 percent of the value of field intensity. Thus the difference is 2.5 percent or less for those points that touch the solid curves. Over most of the range of heights, h_2, the agreement is within about 5 percent.

A similar run is shown in figure 19, except that the height of the transmitting antenna was varied for a fixed height of the receiving antenna. The antenna current, I, was maintained constant at 0.100 amp. The other conditions are the same as those applying to figure 18. The agreement between the two standards is about the same as in the two previous runs.

4. Variable-Distance Runs

In these last tests the field intensity versus the horizontal distance of separation, d, was determined for fixed heights of the transmitting and receiving antennas.

The receiving antenna was maintained at a fixed height h_2=3.05 m, and the distance, d, varied from 6 to 60 m for each of two heights of the transmitting antenna h_1=1.58 and 3.05 m, respectively.

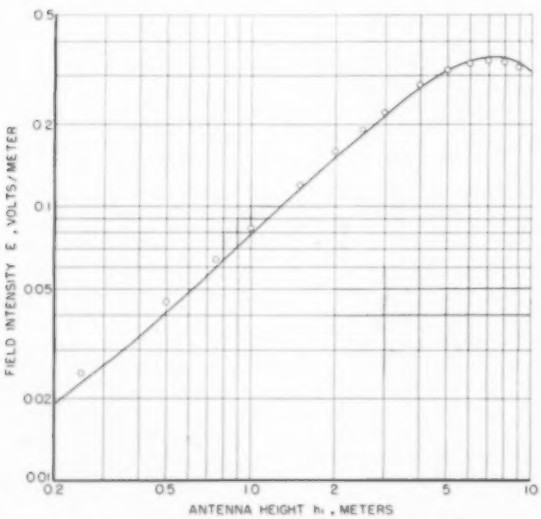

FIGURE 19. *Variation of the magnitude of the electric component of field intensity, $|E|$ in volts per meter, as determined by the Standard-Antenna and Standard-Field methods versus the height, h_1 in meters, of the transmitting antenna.*

A fixed height, h_2=3.05 m, of the receiving antenna was used. The remaining conditions are identical to those applying to figure 18. ○, Standard-antenna method; —, standard-field method.

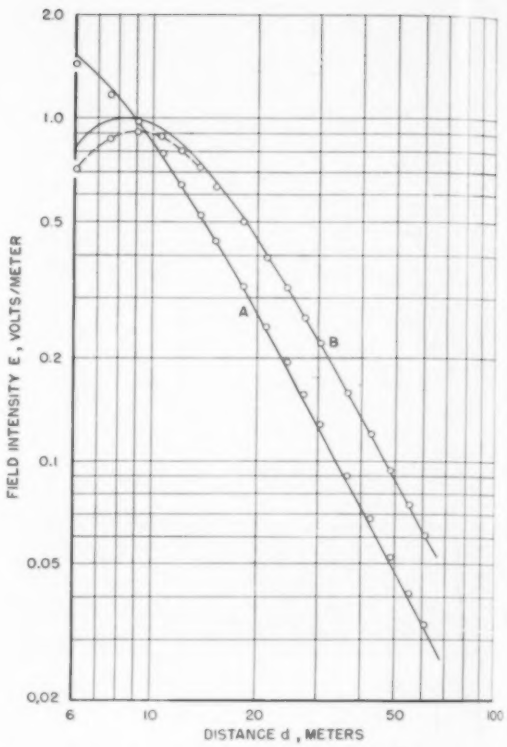

FIGURE 20. *Variation of the magnitude of the electric component of field intensity, $|E|$ in volts per meter, as determined by the Standard-Antenna and Standard-Field methods versus the horizontal distance of separation, d in meters, between the antennas.*

Fixed heights of the transmitting antenna h_1=1.58 m (A), and 3.05 m (B), and a fixed height of the receiving antenna, h_2=3.05 m were used. The remaining conditions are identical to those applying to figure 18. ○, Standard-antenna method; —, standard-field method.

Horizontal self-resonant half-wave dipoles were used as before. The field intensity was determined for various distances of separation using both the standard-antenna and standard-field methods. The remaining conditions are the same as those in the previous section. The results are shown in figure 20.

The values of field intensity determined by both the standard-antenna and standard-field methods (figs. 13, 18, 19, and 20) seem to be in fairly good agreement over most of the range of antenna heights or distance of separation involved. It is reasonable to assume that the effective length of both antennas remains fixed throughout the entire

range. The larger disagreements noted are therefore probably a result of errors in calculating the standard field because of the accuracy with which the actual ground constants are known for the various incident angles involved.

V. Conclusions

A description has been given of two standard methods of establishing known values of VHF field intensity used at the National Bureau of Standards for the calibration of commercial field-intensity meters. Methods and techniques used to calibrate and verify the accuracy of the standards were described. Values of standard field intensity can be established in the range from 20 mv/m to 1v/m at 100 Mc. This range can be considerably increased by varying the transmitting-antenna current in known amounts by means of the standard attenuator previously mentioned. The propagation tests described indicate that the probable accuracy of the standards is about 5 percent under most of the conditions used.

The limitations in the use of the standards lie in the somewhat restricted range of field intensity available, the temperature effect of the crystal rectifier, and for some uses the lack of selectivity in the standard receiving antenna. However, for the purposes reported here and under the conditions used these factors presented little difficulty.

The initial work described in this report was confined to the use of horizontal polarization at a frequency of 100 Mc. Further tests are in progress to verify the accuracy of these calibration standards at frequencies up to 300 Mc under conditions normally used in the field. The additional use of vertical as well as circular polarization will be included in this program.

Under most conditions normally employed for calibrating VHF field-intensity meters, the value of the antenna constant[6] as determined by means of horizontally polarized transmission would probably be substantially the same if vertical polarization were employed. This would be approximately true provided the antenna were immersed in a uniform field in both instances, and that its height above ground was greater than about a half wavelength. The antenna constant can be shown to be influenced by the effect of the presence of the ground on the current distribution along the antenna, as well as on its input impedance. Although, these effects are different for horizontal polarization than for vertical, they are probably relatively small for antenna heights above approximately a half wavelength.

Results presented herein indicate that for the case of horizontal polarization any possible effect of the ground on the antenna current distribution probably results in less than about a 2-percent change in the antenna constant for antenna heights greater than 0.1 wavelength.

The effect of the presence of the ground on the antenna constant as caused by changes in the antenna input impedance has been shown to be less than about 5 percent for antenna heights greater than 0.65 wavelength above average ground ($\epsilon_r=15$, $\sigma=5\times10^{-3}$ mho/m) [14].

In the calibration of commercial VHF field-intensity meters the accuracy of calibration as certified by this Bureau at the present time would probably be from twice to several times the accuracy of the standards described, depending upon the merits of the individual meter under test.

VI. Appendix. A Summary of Schelkunoff's Analysis of the Current Distribution on a Thin Cylindrical Antenna

Schelkunoff [1] obtained an approximate solution for the free-space current distribution on a hollow cylindrical antenna by analogy with a thin biconical antenna, together with the theory of the nonuniform transmission line.

The antenna region and the space beyond are considered as two multiple transmission lines or waveguides in tandem, each with its own distinct set of transmission modes.

In the antenna region (that space within a geometrical boundary sphere passing through the ends of the antenna) the field is composed of a principal or dominant mode plus a complementary set of an infinite number of higher order modes. The principal mode or wave, is that usually associated with a two-conductor transmission line. The complementary waves are generated in order to match the field (at the boundary sphere) to the field in the external region where no principal mode of transmission exists. Because of the nonexistence of physical conductors in the external region, the field consists solely of an infinite set of higher-order transmission modes. While these sets

[6] The antenna constant may be defined as $K=1/\eta l_{\mathrm{eff}}$, where η is the voltage-transfer ratio defined by eq 1.

are distinct in their respective regions, they approach equality at the boundary, thus preserving the continuity of the field.

Associated with the principal and complementary waves in the antenna region are the principal current $I_0(r)$, and the complementary current flowing on the antenna given by

$$\bar{I}(r)=I_1(r)+I_3(r)+I_5(r)\ \ldots\ , \tag{27}$$

where the even-order modes vanish because of the symmetry involved.

At the ends of the hollow cylindrical doublet antenna ($r=l$) the total current is essentially zero or

$$I(l)=I_0(l)+\bar{I}(l)=0. \tag{28}$$

Therefore,

$$I_0(l)=-\bar{I}(l). \tag{29}$$

Since it can be shown that the total voltage associated with any complementary wave is zero,

$$V(r)=V_0(r). \tag{30}$$

It can be seen that the presence of the complementary waves affect the amplitudes of the principal waves as would an impedance

$$Z_t=\frac{V_0(l)}{I_0(l)}, \tag{31}$$

terminating the antenna.

As far as the principal waves are concerned, then, the antenna may be considered as a nonuniform transmission line terminated by an impedance $Z_t=R_t+jX_t$. The real part, R_t, is the radiation resistance of outer space as seen from the ends of the antenna, and the imaginary part, X_t, represents the reactive field associated with the complementary waves. These two components represent the end effect usually associated with radiation from an antenna.

The current distribution on the antenna is therefore determined by the actual distribution of L and C along the antenna and by the presence of the complementary currents generated by reflection at the ends.

In a uniform parallel-wire transmission line, L and C per unit length, and consequently Z_0, are constant throughout. In a transmission line composed of a straight wire of length $2l$, driven at the center, L and C vary continuously along its length. The potential difference between any two points equidistant from the center is simply the integral of the electric field intensity along a line of constant intensity terminating at the two points. The cylindrical doublet may be compared to such a nonuniform transmission line. L and C usually vary only slowly with r in such a line, and by analogy to a thin biconical antenna with slowly varying cone angle, ψ, the characteristic impedance as a function of r can be expressed approximately as

$$K(r)\cong 120\log_e\frac{2r}{a}\quad (r\gg a). \tag{32}$$

The average characteristic impedance over length l is

$$K_0\cong\frac{1}{l}\int_0^l K(r)dr\cong 120\left(\log_e\frac{2l}{a}-\ \right). \tag{33}$$

From the theory of the nonuniform transmission line, the relative distribution of the principal current is given for the case in which the variation in $K(r)$ is small

$$\frac{I(r)}{I(0)}=\left[\cos\beta r-\frac{M(r)}{K_0}\cos\beta r+\frac{N(r)}{K_0}\sin\beta r\right]$$
$$-\frac{jZ(0)}{K_0}\left[\sin\beta r+\frac{M(r)}{K_0}\sin\beta r+\frac{N(r)}{K_0}\cos\beta r\right], \tag{34}$$

where

$\beta=2\pi/\lambda$, and $Z(0)$ is the input impedance of the antenna

$$M(r)=\beta\int_0^r[K_0-K(r)]\sin 2\beta r\,dr$$
$$=60(1-\cos 2\beta r)[\log_e(l/r)-1]+60\,(\log_e 2\beta r-Ci2\beta r+C)$$

$$N(r)=\beta\int_0^r[K_0-K(r)]\cos 2\beta r\,dr$$
$$=60\left(\log\frac{l}{r}-1\right)\sin 2\beta r+60Si\ 2\beta r,$$

$$Si(x)\equiv\int_0^x\frac{\sin t}{t}dt$$

$$Ci(x)\equiv\int_\infty^x\frac{\cos t}{t}dt$$

$C=0.5772\ \ldots$ (Euler's constant).

The relative complementary current for a biconical antenna and to a second approximation for any thin antenna is given by

$$\frac{\bar{I}(r)}{I_0}=\frac{60}{K_0}\sum_{m=0}^{\infty}\frac{4m+3}{(m+1)(2m+1)}[\hat{N}_{2m+1}(\beta l)+j\hat{J}_{2m+1}(\beta l)]\hat{J}_{2m+1}(\beta r). \tag{35}$$

I_0 is the principal current amplitude on the transmission line, and m is an integer. For $(2n+1)$ $\lambda/2$ doublets in which we are interested (where $n=0, 1, 2, 3, \ldots$), $I_0 \simeq I(0)$. $\hat{J}_{2n+1}(\beta l)$ and $\hat{N}_{2n+1}(\beta l)$ are special functions related to J and N Bessel functions of order $n+1/2$ [1, p. 52].

The total relative current on the antenna is given by the sum of eq 34 and 35. For an antenna composed of an infinitely thin filament ($K_0=\infty$) the relative current distribution reduces to cos βr, as is usually assumed for such a case.

VII. References

[1] S. A. Schelkunoff, Electromagnetic waves, p. 290 to 292 and 441 to 479 (D. Van Nostrand Co., Inc., New York, N. Y., 1943).

[2] S. A. Schelkunoff, Theory of antennas of arbitrary size and shape, Proc. IRE **29,** 508 (Sept. 1941).

[3] R. King, Graphical representation of the characteristics of cylindrical antennas, Cruft Laboratory, Tech. Rept. No. 20 (ONR) (Oct. 1, 1947).

[4] L. S. Nergaard, A survey of ultra-high-frequency measurements, RCA Rev. **3,** 183 (Oct. 1938).

[5] MIT Radiation Laboratory Series—Crystal rectifiers, Louis N. Ridenour, editor, p. 333 to 360 (McGraw-Hill Book Co., New York, N. Y., 1948).

[6] Ernst A. Guillemin, Communication Networks II, 64 (John Wiley & Sons Inc., New York, N. Y., 1935).

[6a] R. E. Grantham, and J. J. Freeman, A Standard of Attenuation for Microwave Measurements, Trans. A. I. E. E., **67,** p. 535, 1948.

[7] Nathand Marchand, Transmission-line conversion transformers, Electronics p. 142 to 145 (Dec. 1944).

[8] K. A. Norton, The propagation of radio waves over the earth and in the upper atmosphere, Proc. IRE **25,** 1217 (Sept. 1937).

[9] K. A. Norton, The calculation of ground-wave field intensity over a finitely-conducting spherical earth, Proc. IRE **29,** 623 to 639 (Dec. 1941).

[10] C. R. Burrows, Radio propagation over plane earth—Field strength curves, Bell System Tech. J. **16,** 45 to 75 (Jan. 1937).

[11] K. Bullington, Radio propagation at frequencies above 30 megacycles, Proc. IRE **35,** 1122 to 1136 (Oct. 1947).

[12] J. A. Stratton, Electromagnetic theory, p. 493 (McGraw-Hill Book Co., Inc., New York, N. Y., 1941).

[13] R. King, H. R. Mimno, A. H. Wing, Transmission lines, antennas, and waveguides, p. 160 (McGraw-Hill Book Co., Inc., New York, N. Y., 1945).

[14] Frank M. Greene, The influence of the ground on the calibration and use of VHF field-intensity meters, J. Research NBS **44,** 123 (1950) RP2062.

Washington, October 3, 1949.

U. S. Department of Commerce
National Bureau of Standards

Research Paper RP2101
Volume 44, May 1950

Part of the Journal of Research of the National Bureau of Standards

Note on the Runge-Kutta Method[1]

By W. E. Milne

A comparison is made between the standard Runge-Kutta method of solving the differential equation $y'=f(x,y)$ and a method of numerical quadrature. By examples it is shown that the Runge-Kutta method may be unfavorable even for simple functions f.

One of the most celebrated methods for the numerical solution of differential equations is the one originated by Runge[2] and elaborated by Heun,[3] Kutta,[4] Nyström,[5] and others. This method is usually given considerable prominence in texts where numerical methods are discussed.

In contrast to step-by-step procedures based on formulas for numerical quadrature the Runge-Kutta method (as it is usually called) enjoys two conspicuous advantages:

(1) No special devices are required for starting the computation.

(2) The length of the step can be modified at any time in the course of the computation without additional labor.

On the other hand it is open to two major objections:

(1) The process does not contain in itself any simple means for estimating the error or for detecting computation mistakes. It is true that Bieberbach[6] has found an expression which provides an upper bound for the error at a given step of the Runge-Kutta process (or more accurately, the Kutta process). However this estimate depends on quantities which do not appear directly in the computation, and therefore requires some additional separate calculation.

(2) Each step requires four substitutions into the differential equation. For the case of complicated equations this may demand an excessive amount of labor per step.

By accident or design it happens that examples usually chosen in textbooks to illustrate the Runge-Kutta method are such that the method appears in a very favorable light.

It is the purpose of this note to exhibit examples where the Runge-Kutta method does not make a very good showing when compared with a method based on numerical quadrature. For the comparison we employ the commonly used form of the Runge-Kutta method (actually due to Kutta). If the differential equation is

$$\frac{dy}{dx}=f(x,y),$$

the step from x_n to $x_{n+1}=x_n+h$ is made by the formulas

$$y_{n+1}=y_n+(k_1+2k_2+2k_3+k_4)/6,$$

where

$$k_1=hf(x_n, y_n),$$
$$k_2=hf(x_n+\tfrac{1}{2}h, y_n+\tfrac{1}{2}k_1),$$
$$k_3=hf(x_n+\tfrac{1}{2}h, y_n+\tfrac{1}{2}k_2),$$
$$k_4=hf(x_n+h, y_n+k_3).$$

These formulas yield an approximation of the fourth degree in h, that is, the expansion in powers of h of y_{n+1} defined by these formulas agrees through terms of the fourth degree with the expansion of y_{n+1} obtained directly from the differential equation.

[1] The preparation of this paper was sponsored (in part) by the Office of Naval Research.

[2] C. Runge, Ueber die Numerische Auflösung von Differentialgleichungen, Math. Ann. **46,** 167 (1895).

[3] K. Heun, Zeitschrift Math. Phys. **45,** 23 (1900).

[4] W. Kutta, Zeitschrift Math. Phys. **46,** 435 (1901).

[5] E. J. Nyström, Acta Societatis Scientiarum Fennicae **50,** No. 13, 1 to 55, (1925).

[6] L. Bieberbach, Theorie der Differentialgleichungen, Berlin (1946) (now Dover Publications, New York, N. Y.), page 54.

This is to be compared with the method [7] that makes the step from x_n to x_{n+1} by using

$$\bar{y}_{n+1}=y_{n-3}+4hy'_{n-1}+\frac{8h}{3}\delta^2y'_{n-1}$$

to obtain a trial value $\bar{y}_{n+1}$ of y_{n+1}, then calculating y'_{n+1} approximately from the differential equation, and finally computing a corrected value of y_{n+1} by

$$y_{n+1}=y_{n-1}+2hy'_n+\frac{h}{3}\delta^2y'_n.$$

This method is also of fourth degree in h in the sense that the error terms are proportional to h^5. The difference

$$\bar{y}_{n+1}-y_{n+1}=E_{n+1}$$

serves as a control, since it may be shown that the error of y_{n+1} (ignoring rounding errors and errors accumulated from previous steps) is approximately $E_{n+1}/29$. In actual calculation it is customary to tabulate E_n and to correct the trial value by estimating E_{n+1} from the trend of the E_n already known. When this is done and when the number of places retained in y is kept such that $E_{n+1}/29$ is not significant, it will not be necessary to recompute y'_{n+1} after y_{n+1} has been corrected. Thus after the computation is well under way we need only *one* substitution per step.

Thus this method has two advantages:

1. By internal evidence the computation shows how many places in y can be accepted as reliable (of course accumulation of rounding errors, etc., excepted).

2. Except at the beginning, only one substitution is required per step.

Two disadvantages may be cited:

1. Special devices are necessary to get started.

2. Change of the interval h in the course of a computation is somewhat troublesome.

Now let us consider a particular example

$$\frac{dy}{dx}=\frac{5y}{1+x},\ y=1 \text{ when } x=0.$$

In each case take $h=0.1$ and carry the computation to $x=1$.

[7] Milne, W. E., Numerical integration of ordinary differential equations, Am. Math. Monthly **33**, 455 (1926). (The formulas of the present paper are expressed in terms of central differences but are actually identical with those of the above reference.)

In Kutta's method, without making some independent investigation, we have no idea how many places in y to retain. In the comparison below, we arbitrarily retained four decimal places.

The results obtained by the two methods are given in table 1 and are compared with those obtained from the actual solution $y=(1+x)^5$.

TABLE 1. *Solution of* $dy/dx=5y/(1+x)$, $y=1$, *at* $x=0$.

x	Kutta	Error	Milne	Error	$(1+x)^5$
0	1.0000	.....	1.0000	.....	1.0000
.1	1.6103	0.0002	1.6105	.....	1.6105
.2	2.4878	.0005	2.4883	.....	2.4883
.3	3.7119	.0010	3.7129	.....	3.7129
.4	5.3765	.0017	5.3782	.....	5.3782
.5	7.5911	.0027	7.5937	0.0001	7.5938
.6	10.4819	.0039	10.4857	.0001	10.4858
.7	14.1931	.0055	14.1985	.0001	14.1986
.8	18.8882	.0075	18.8956	.0001	18.8957
.9	24.7509	.0101	24.7609	.0001	24.7610
1.0	31.9867	.0133	31.9999	.0001	32.0000

For this simple differential equation a comparison of the times required by the two methods is not very significant. However, since in this example Kutta requires 40 substitutions while the second method requires 15 or so (depending on exactly how the start is made), the difference would obviously be significant for more difficult equations.

It is of some interest to make the comparison for the equations

$$\frac{dy}{dx}=\frac{4y}{1+x}$$

and

$$\frac{dy}{dx}=\frac{2y}{1+x},$$

with $y=1$ at $x=0$, and $h=0.1$.

For the first of these Kutta is in error at $x=1$ by 0.00242, and for the second by 0.0000205. In both of these cases the second method gives *exact* values.

The foregoing examples serve to show that even for very innocent looking differential equations the Runge-Kutta method may give very bad results. Since the accuracy is in any case difficult to ascertain, the possibility of such errors occurring is a serious indictment of the Runge-Kutta method.

LOS ANGELES, June 16, 1949.

U. S. Department of Commerce
National Bureau of Standards

Research Paper RP2102
Volume 44, May 1950

Part of the Journal of Research of the National Bureau of Standards

A Sampling Method for Determining the Lowest Eigenvalue and the Principal Eigenfunction of Schrödinger's Equation[1]

By M. D. Donsker and M. Kac

This is a preliminary report on a sampling method for finding the lowest eigenvalue and the corresponding eigenfunction of Schrödinger's equation. The theory underlying the procedure is explained and two cases treated numerically. Although the initial results are encouraging, more experimentation will be needed to fully test the practicality of the method.

I. Introduction

Certain problems leading to complicated partial or integro-differential equations have recently been approached and some actually solved by utilizing various probability techniques and sampling methods. Collectively these methods have become known as the "Monte Carlo" method.

The problems to which Monte Carlo techniques have been applied seem to be divided into two types. Typical of the first type is the problem of neutrons diffusing in material media in which the particles are subjected not only to certain deterministic influences but to random influences as well. In such a problem, the Monte Carlo approach consists in permitting a "particle" to play a game of chance, the rules of the game being such that the actual deterministic and random features of the physical process are step by step exactly imitated by the game. By considering very large numbers of particles, one can answer such questions as the distribution of the particles at the end of a certain period of time, the number of particles to escape through a shield of specified thickness, etc. One important characteristic of the preceding approach is that the functional equation describing the diffusion process is bypassed completely, the probability model used being derived from the process itself.

A more sophisticated application of Monte Carlo methods is to the problem of finding a probability model or game whose solution is related to the solution of a partial differential equation, or, as in the present paper, to determine the least eigenvalue of a differential operator by means of a sampling process. As an example of how the latter problem might be attacked, we quote from a paper of Metropolis and Ulam:[2]

"For example, as suggested by Fermi, the time independent Schrödinger equation

$$\Delta\phi(x,y,z)=(\lambda-V)\phi(x,y,z),$$

could be studied as follows. Reintroduce time dependence by considering

$$u(x,y,z,t)=\phi(x,y,z)e^{-\lambda t};$$

then, u will obey the equation

$$\frac{\partial u}{\partial t}=\Delta u-Vu.$$

This last equation can be interpreted, however, as describing the behavior of a system of particles each of which performs a random walk, i. e., diffuses isotropically and at the same time is subject to multiplication, which is determined by the value of the point function V. If the solution of the latter equation corresponds to a spatial

[1] The preparation of this paper was sponsored (in part) by the Office of Naval Research.

[2] N. Metropolis and S. Ulam, The Monte Carlo method, J. Am. Stat. Assn. 44, 247, pp. 335 to 341 (Sept. 1949).

mode multiplying exponentially in time, the examination of the spatial part will give the desired $\phi(x,y,z)$—corresponding to the lowest 'eigenvalue' λ." [3]

The main purpose of the present paper is to present an alternative method for finding the lowest eigenvalue and corresponding eigenfunction of Schrödinger's equation. The chief difference between the two approaches is that ours involves only a random walk eliminating entirely the multiplicative process. This alteration in the model seems to simplify the numerical aspects of the problem, especially if punched card equipment is to be used. Apart from the possible numerical simplification, the method is based on a mathematical theory that in itself is of some interest.

II. Mathematical Theory

Let $X_1, X_2, X_3, \ldots$ be independent identically distributed random variables each having mean 0 and standard deviation 1 and let $S_k = X_1 + X_2 + \ldots + X_k$. Under certain general assumptions on $V(x)$, the most severe of which is that $V(x)$ be nonnegative, it can be shown [4] that the limiting distribution function $\sigma(\alpha,t)$ of the random variable

$$\frac{1}{n}\sum_{k<nt} V\left(\frac{S_k}{\sqrt{n}}\right) \tag{1}$$

is such that

$$\int_0^\infty \int_0^\infty e^{-\alpha - st} d_\alpha \sigma(\alpha,t)\, dt = \int_{-\infty}^\infty \psi(x)\, dx, \tag{2}$$

where $\psi(x)$ is the fundamental solution of the differential equation

$$\frac{1}{2}\frac{d^2\psi}{dx^2} - (s + V(x))\psi = 0, \tag{3}$$

subject to the conditions

$$\psi(x) \to 0 \qquad x \to \pm\infty$$

$$|\psi'(x)| < M \qquad x \neq 0$$

$$\psi'(+0) - \psi'(-0) = -2.$$

The fundamental solution $\psi(x)$ of (3) is expressible in terms of the normalized eigenfunction $\{(\psi_j(x)\}$ and eigenvalues λ_j of the one-dimensional Schrödinger eigenvalue problem [5]

$$\frac{1}{2}\frac{d^2\psi}{dx^2} - V(x)\psi(x) = -\lambda\psi \qquad \lambda > 0 \tag{4}$$

as

$$\psi(x) = \sum_j \frac{\psi_j(0)\psi_j(x)}{s + \lambda_j}. \tag{5}$$

Thus from (5 and 2)

$$\int_{-\infty}^\infty \psi(x)\, dx = \int_0^\infty \int_0^\infty e^{-\alpha - st} d_\alpha \sigma(\alpha,t)\, dt$$

$$= \sum_j \frac{\psi_j(0) \int_{-\infty}^\infty \psi_j(x)\, dx}{s + \lambda_j}. \tag{6}$$

Inverting (6) with respect to s we get,

$$\int_0^\infty e^{-\alpha} d_\alpha \sigma(\alpha,t) = \sum_j e^{-\lambda_j t} \psi_j(0) \int_{-\infty}^\infty \psi_j(x)\, dx, \tag{7}$$

and therefore we obtain the expression for λ_1,

$$\lambda_1 = \lim_{t\to\infty} -\frac{1}{t} \log \int_0^\infty e^{-\alpha} d_\alpha \sigma(\alpha,t). \tag{8}$$

If in (7) we neglect all terms in the expansion but the first, we obtain

$$\log \int_0^\infty e^{-\alpha} d_\alpha \sigma(\alpha,t) \sim \log\left\{\psi_1(0) \int_{-\infty}^\infty \psi_1(x)\, dx\right\} - \lambda_1 t,$$

or

$$\lambda_1 \sim \frac{\log\left\{\psi_1(0) \int_{-\infty}^\infty \psi_1(x)\, dx\right\}}{t} - \frac{1}{t} \log \int_0^\infty e^{-\alpha} d_\alpha \sigma(\alpha,t). \tag{9}$$

Thus, if, by choosing a finite t, we attempt to calculate λ_1 from (8), we have two sources of error. The first, usually a small source of error, is from the exponentials neglected in the expansion (7). The second, and more important, is from neglecting the term $(1/t)\log\left\{\psi_1(0)\int_{-\infty}^\infty \psi_1(x)\, dx\right\}$. This latter source of error is especially significant, since, as will be apparent shortly, it is impractical from other points of view to take t very large. All of this difficulty may be obviated by considering (7) for two distinct values of t, say t_1 and t_2, then, if

[3] We have since learned that Dr. G. W. King has made similar calculations using a closely related method.

[4] M. Kac, On distributions of certain Wiener functionals, Trans. Am. Math. Soc. **65**, 1 to 13 (1949).

[5] From here on all the steps are formal. In all cases of physical interest they can be justified rigorously.

we neglect the exponentials after the first as before, we get on dividing

$$\lambda_1 \sim \frac{1}{t_2-t_1} \log \frac{\int_0^\infty e^{-\alpha} d_\alpha \sigma(\alpha,t_1)}{\int_0^\infty e^{-\alpha} d_\alpha \sigma(\alpha,t_2)}. \tag{10}$$

The Monte Carlo process consists in the calculation of $\sigma(\alpha,t_1)$ and $\sigma(\alpha,t_2)$ by a sampling process.

If instead of $\sigma(\alpha,t)$ we consider the limiting distribution $\sigma_\xi(\alpha,t)$ of the random variable

$$\frac{1}{n} \sum_{k \le nt} V\left(\xi + \frac{S_k}{\sqrt{n}}\right), \tag{11}$$

then $\sigma_\xi(\alpha,t)$ also satisfies (2 and 3), but now the condition $\psi'(+0)-\psi'(-0)=-2$ is replaced by $\psi'(\xi+)-\psi'(\xi-)=-2$. Therefore, repeating steps (4 to 7), we get

$$\int_0^\infty e^{-\alpha} d_\alpha \sigma_\xi(\alpha,t) = \sum_j e^{-\lambda_j t} \psi_j(\xi) \int_{-\infty}^\infty \psi_j(x)\,dx. \tag{12}$$

Thus

$$\frac{\psi_1(\xi)}{\psi_1(0)} = \lim_{t\to\infty} \frac{\int_0^\infty e^{-\alpha} d_\alpha \sigma_\xi(\alpha,t)}{\int_0^\infty e^{-\alpha} d_\alpha \sigma(\alpha,t)}, \tag{13}$$

so that we are also able to calculate the principal eigenfunction.

The extension of the preceding method to multidimensional Schrödinger equations is immediate. It is in these cases that the method will probably prove to be most useful since, unlike the standard variational procedures, the extension to several dimensions seems to cause comparatively little difficulty. For illustrative purposes we will consider Schrödinger's equation in three dimensions. Here we must consider three independent sequences

$$X_1, X_2, X_3, \ldots,$$

$$Y_1, Y_2, Y_3, \ldots,$$

$$Z_1, Z_2, Z_3, \ldots,$$

of independent identically distributed random variables each having mean 0 and standard deviation 1. Let $S_{xk}=X_1+X_2+\cdots+X_k$, and S_{yk}, S_{zk} have the obvious meanings. We consider the limiting distributions $\sigma(\alpha,t)$ and $\sigma(\alpha,\xi,\eta,\zeta,t)$ of the random variables

$$\frac{1}{n} \sum_{k \le nt} V\left(\frac{S_{xk}}{\sqrt{n}}, \frac{S_{yk}}{\sqrt{n}}, \frac{S_{zk}}{\sqrt{n}}\right),$$

and

$$\frac{1}{n} \sum_{k \le nt} V\left(\xi + \frac{S_{xk}}{\sqrt{n}}, \eta + \frac{S_{yk}}{\sqrt{n}}, \zeta + \frac{S_{zk}}{\sqrt{n}}\right),$$

respectively.

In exactly the same way as in the one dimensional case, we arrive at

$$\lambda_1 \sim \frac{1}{t_2-t_1} \log \frac{\int_0^\infty e^{-\alpha} d_\alpha \sigma(\alpha,t_1)}{\int_0^\infty e^{-\alpha} d_\alpha \sigma(\alpha,t_2)},$$

and

$$\frac{\psi_1(\xi,\eta,\zeta)}{\psi_1(0,0,0)} = \lim_{t\to\infty} \frac{\int_0^\infty e^{-\alpha} d_\alpha \sigma(\alpha,\xi,\eta,\zeta,t)}{\int_0^\infty e^{-\alpha} d_\alpha \sigma(\alpha,t)}.$$

So far, the theory was carried out under the assumption that the potential function V was nonnegative. In most cases of physical interest this is not so. For the hydrogen atom, for instance

$$V(x,y,z) = -\frac{\text{const.}}{\sqrt{x^2+y^2+z^2}}.$$

However, the modification is easy, although we have not as yet cleared up all the points of mathematical rigor.

The formula for the lowest eigenvalue now becomes

$$\lambda_1 \sim \frac{1}{t_2-t_1} \log \frac{\int_{-\infty}^0 e^{-\alpha} d_\alpha \sigma(\alpha,t_1)}{\int_{-\infty}^0 e^{-\alpha} d_\alpha \sigma(\alpha,t_2)},$$

and a corresponding modification needs to be made in the formula for the principal eigenfunction. We have not yet tested numerically any case with a negative potential function, but we hope to be able to report on this in the near future.

III. Numerical Examples and Discussion

The Monte Carlo procedure used here consists in the calculation of the distribution function $\sigma(\alpha,t)$ by a sampling process; the principal eigenvalue is then calculated from (10). For the purposes of numerical illustration we consider two examples, $V(x)=x^2$ and $V(x)=|x|$. In both of

these cases the eigenvalues are known, and hence we have a check on the accuracy of our procedure. In order to calculate $\sigma(\alpha,t)$, say when $V(x)=x^2$, we see from (1) that we must consider the limiting distribution as $n\to\infty$ of

$$\frac{1}{n^2}\sum_{k\leq nt} S_k^2. \tag{14}$$

This means from our point of view that we must (a) choose a distribution for the X's, (b) choose a sufficiently large n, (c) select an appropriate t, (4) calculate for nt X's the normalized sum (14), (5) repeat (4) many times, so that the empirical distribution may be obtained from these many samples.

Although, under the conditions mentioned previously, the distribution function $\sigma(\alpha,t)$ is independent of the distribution of the X's, the actual numerical calculation of $\sigma(\alpha,t)$ is expedited by choosing the distribution of the X's to be the Bernoulli distribution, i. e.,

$$P(X=1)=P(X=-1)=\frac{1}{2}.$$

The sequence of random variables X_1, X_2, X_3, . . . is then a sequence of $+1$'s and -1's, such as might be obtained in coin tossing. This is conveniently and rapidly achieved on a calculating machine by considering sequences of random digits, counting even digits $+1$ and odd digits -1.

The value of n to be used must be large enough so that the empirical distribution function calculated is close to the theoretical limiting distribution function $\sigma(\alpha,t)$. From (10) we see that the two values of t, t_1, and t_2, to be used in the calculation of λ must be large enough so that the exponential terms neglected are sufficiently small. However, since the sample size is nt, the desire to make both n and t large must be tempered by practical considerations. The number of samples to be used must be large enough so that the empirical distribution adequately represents $\sigma(\alpha,t)$. Before discussing these points in more detail we consider an actual numerical computation. The following data for $V(x)=x^2$ and $V(x)=|x|$ were calculated from a certain set of random digits [6] on the IBM Electronic Calculating Punch, Type 604. For both x^2 and $|x|$ n was selected to be 400, $t_1=5$, $t_2=3.75$, and 100 samples were used. In table 1 is tabulated

$$A_1=\frac{1}{8000}\sum_{k=1}^{1500}|S_k|, \quad A_2=\frac{1}{8000}\sum_{k=1}^{2000}|S_k|,$$

$$B_1=\frac{1}{160000}\sum_{k=1}^{1500}S_k^2, \quad B^2=\frac{1}{160000}\sum_{k=1}^{2000}S_k^2.$$

Since each RAND random number card contains 50 random digits, and 2,000 digits are needed to form one sample, a set of 4,000 RAND cards was sufficient for this experiment. It takes 20 minutes on the IBM 604 to calculate A_1 and A_2 for one sample (similarly for B_1 and B_2), so that it takes approximately 35 hours to secure the following data.

TABLE 1. *Experimental data for lowest eigenvalue*

	A_1	A_2	B_1	B_2
1	1.332	2.101	0.738	1.290
2	3.808	5.707	5.295	8.502
3	2.795	5.545	3.460	9.610
4	8.723	13.917	30.722	52.616
5	4.169	4.766	6.123	6.602
6	1.195	2.136	.598	1.453
7	6.674	12.112	15.258	39.058
8	4.103	5.242	5.826	7.004
9	5.751	8.840	10.440	18.143
10	4.250	4.981	6.069	6.679
11	2.909	5.643	3.844	10.044
12	2.834	3.416	3.602	4.097
13	1.888	2.194	1.595	1.700
14	2.022	2.337	1.510	1.638
15	1.680	3.908	1.184	5.289
16	7.700	12.712	24.760	44.936
17	3.228	4.973	3.563	6.145
18	1.844	2.654	1.523	2.183
19	2.376	5.275	2.017	8.854
20	4.533	5.640	6.380	7.616
21	4.209	7.543	7.735	16.703
22	3.847	5.590	6.666	9.204
23	5.206	6.314	9.148	10.600
24	1.962	2.698	1.859	2.923
25	3.523	4.807	5.084	6.482
26	3.605	5.397	5.014	7.680
27	9.168	13.692	27.973	44.461
28	5.625	7.898	11.528	16.010
29	3.215	4.152	3.362	4.170
30	3.293	3.972	4.136	4.677
31	2.710	3.683	3.006	4.025
32	3.638	7.386	6.114	17.413
33	7.928	11.567	25.084	36.001
34	3.475	3.846	4.396	4.550
35	1.958	2.594	1.457	1.948
36	5.356	7.216	8.888	11.781
37	3.297	6.395	3.800	11.555
38	1.883	2.682	1.387	1.995
39	4.849	10.020	8.396	30.233
40	2.282	3.067	2.258	2.882

[6] This set of random digits was prepared by the RAND Corporation, Santa Monica, Calif.

TABLE 1. *Experimental data for lowest eigenvalue*—Con.

	A_1	A_2	B_1	B_2
41	4.253	6.957	6.744	13.502
42	7.559	8.834	17.143	18.702
43	1.122	2.587	.500	2.634
44	1.433	3.602	.869	4.855
45	2.984	3.477	2.851	3.161
46	1.677	3.158	1.025	3.341
47	5.145	9.697	11.941	28.826
48	4.982	9.140	9.201	23.092
49	1.675	2.152	1.129	1.472
50	1.580	3.375	1.147	3.807
51	2.606	3.621	2.254	3.247
52	4.303	5.883	7.987	10.104
53	7.553	12.092	19.632	36.427
54	3.138	5.703	3.968	9.325
55	3.343	4.327	4.264	5.380
56	1.423	2.315	0.770	1.533
57	7.996	11.458	21.405	31.585
58	1.916	2.744	1.253	1.959
59	1.490	2.161	0.789	1.404
60	3.536	5.382	4.125	7.461
61	6.278	11.060	16.187	34.779
62	1.174	1.709	0.573	0.919
63	5.272	9.919	10.463	27.825
64	3.576	5.277	6.021	8.707
65	2.686	5.081	3.577	8.307
66	6.166	8.785	14.056	19.627
67	4.412	5.548	6.095	7.182
68	1.732	4.664	1.170	8.720
69	2.730	4.970	2.440	6.639
70	1.331	2.772	0.765	2.642
71	3.668	5.318	5.730	8.001
72	2.948	3.801	3.248	4.104
73	5.279	8.931	12.455	23.513
74	11.284	15.784	41.684	58.525
75	2.183	2.787	2.086	2.455
76	4.288	7.427	9.139	17.157
77	1.412	2.893	0.894	3.490
78	2.002	2.567	1.602	2.024
79	2.619	3.780	2.981	4.205
80	2.695	4.616	2.974	6.077
81	4.706	6.672	8.330	11.487
82	5.517	7.981	9.846	14.805
83	1.755	2.099	1.066	1.207
84	2.084	2.876	1.735	2.504
85	1.574	2.743	0.993	2.256
86	5.818	10.444	13.322	30.522
87	4.387	7.844	9.037	18.695
88	3.666	5.244	4.416	6.541
89	7.111	13.311	19.834	50.822
90	6.280	8.548	13.403	17.587
91	4.872	5.836	9.230	10.023
92	3.035	3.323	2.865	2.973
93	3.608	4.697	4.256	5.357
94	3.977	4.964	5.215	6.242
95	3.614	7.867	5.757	20.434
96	9.193	11.183	27.789	31.075
97	4.108	5.282	5.918	7.374
98	4.355	5.744	7.774	10.223
99	1.898	2.661	1.507	2.013
100	9.683	17.154	35.833	80.543

In order to calculate λ_1 from (10) we need the values of $\int_0^\infty e^{-\alpha} d_\alpha \sigma(\alpha,t_1)$ and $\int_0^\infty e^{-\alpha} d_\alpha \sigma(\alpha,t_2)$. Both of these integrals were calculated numerically from the data in table 1 by adding the exponentials of the entries in appropriate columns. For the case $V(x)=|x|$, the values of the integrals were obtained from $1/100 \sum_{i=1}^{100} e^{-A_{1i}}$ and $1/100 \sum_{j=1}^{100} e^{-A_{2i}}$ and for $V(x)=x^2$ from $1/100 \sum_{j=1}^{100} e^{-B_{1i}}$ and $1/100 \sum_{j=1}^{100} e^{-B_{2i}}$. In the case $V(x)=|x|$ the true lowest eigenvalue to two places is 0.81, and in the case $V(x)=x^2$ it is $\sqrt{2}/2=0.71$.

	First 50 samples	Second 50 samples	All 100 samples
$\|x\|$	0.83	0.79	0.81
x^2	.80	.69	.75

An interesting feature of the data is that column B_2, for example, may be thought of as arising from $n=2000$, $t=1$; $n=1000$, $t=2$, etc., as well as from $n=400$, $t=5$. The larger we take n, the closer will be the empirical distribution to $\sigma(\alpha,t)$. The value of $\int_0^\infty e^{-\alpha} d_\alpha \sigma(\alpha,t)$ in the case $t=1$, and $V(x)=x^2$ can be calculated exactly and, to three places, is 0.678. Calculating this integral from column B_2 with $n=2000$, $t=1$, we get 0.685.

Instead of using Bernoulli distributed variables, one might use other distributions. One definite advantage of Bernoulli distributed variables is that the computation utilizes only the crudest properties of the random digits, i. e., whether they are even or odd. One possible advantage for certain other distributions is that n might not have to be taken so large. In particular this should be true if we use Gaussian distributed variables. RAND Gaussian deviates were used in constructing table 2. Here we chose $t_1=3.75$, $t_2=5$ as before, but now $n=100$. This means samples of size 500 instead of 2000 and therefore a total machine computation time of 9 hours for 100 samples.

Envisaging the possibility of calculating the second eigenvalue, we considered the quantities

$$10^{-4} \sum_{k=1}^{375} (S_k+5)^2 \text{ and } 10^{-4} \sum_{k=1}^{500} (S_k+5)^2, \quad (15)$$

TABLE 2. *Experimental data for second eigenvalue*

	C_1	C_2		C_1	C_2
1	3.963	13.997	61	49.929	84.307
2	2.348*	2.721	62	3.095	6.220
3	1.889*	2.251	63	2.585*	3.867*
4	3.817*	4.372*	64	1.318*	1.906*
5	2.395	2.802*	65	2.241*	9.102*
6	12.467	27.683	66	9.737	12.185
7	1.068*	1.115*	67	9.738*	11.347*
8	0.578*	0.967*	68	4.604	5.589
9	1.504*	1.760	69	20.364	29.707
10	4.249	9.787	70	1.097*	1.895*
11	1.751*	3.316*	71	5.891	13.391
12	9.922	13.975	72	9.019*	12.815*
13	5.680	6.649	73	1.843	6.280
14	3.348	4.684	74	7.961	11.431
15	13.431	24.769	75	1.109	1.926
16	1.473*	2.615*	76	2.417*	3.037
17	45.262	74.304	77	2.402*	2.797*
18	1.157*	3.109	78	2.043*	4.214*
19	0.906*	3.644*	79	0.582*	0.752
20	4.601	12.641	80	2.429	4.381
21	8.356*	13.084*	81	8.584	13.054
22	0.308*	1.874*	82	2.793*	4.659*
23	2.111*	4.428*	83	1.557	5.023
24	2.035*	2.726	84	1.006*	1.677*
25	1.625*	3.898	85	5.327*	15.531*
26	1.879*	5.713	86	2.058	7.307
27	1.333	8.961	87	12.481	12.803*
28	1.799	2.319*	88	0.925*	2.403
29	1.906*	2.417*	89	15.519	19.879
30	7.522	7.979*	90	1.456*	4.009*
31	14.934	15.493*	91	5.244	10.047
32	4.282*	13.747*	92	2.497	2.931
33	1.356*	2.718	93	16.700	17.382
34	4.448	8.329	94	4.471*	8.156*
35	1.306*	2.112*	95	2.139*	2.580*
36	5.465*	12.398*	96	1.196*	2.273*
37	2.918	9.006	97	23.014	28.420
38	35.821	56.626	98	6.959*	7.022*
39	9.814*	11.707*	99	3.374*	8.651*
40	1.811	4.628	100	1.600*	2.259*
41	3.374	6.460	101	4.626*	7.794*
42	1.633	6.578	102	5.195*	10.215*
43	6.976	8.705	103	6.837*	12.160*
44	7.595	13.096	104	1.913	4.412*
45	2.336	2.862	105	2.276*	2.770
46	1.931*	2.579*	106	1.935*	3.983*
47	4.507*	8.294*	107	3.560	5.808
48	8.581*	11.301*	108	2.857*	7.384*
49	4.698*	8.220*	109	3.399*	4.484*
50	10.154	16.884	110	6.917*	27.107*
51	8.828	15.387	111	38.661	56.479
52	0.997*	1.604*	112	1.891	2.000*
53	8.582	12.838	113	8.506	9.646*
54	2.730*	3.249*	114	4.209	10.461
55	10.471	13.140	115	33.194	44.247
56	1.456*	1.845*	116	0.869*	1.289
57	8.230*	11.924*	117	3.946	15.204
58	5.515*	8.146*	118	1.680*	2.985*
59	2.202*	3.182*	119	8.178*	9.056
60	2.129*	9.650*	120	27.621	51.650

TABLE 2. *Experimental data for second eigenvalue*—Con.

	C_1	C_2		C_1	C_2
121	8.444*	15.836*	161	3.546	4.040*
122	13.254	16.467	162	1.238*	2.304*
123	1.755*	5.246*	163	0.975*	1.283
124	36.902	70.134	164	1.980	3.659*
125	7.567*	18.553*	165	14.620*	17.565*
126	14.725	38.551	166	2.378*	2.865
127	0.983*	2.572	167	2.279	6.279
128	24.529	31.660	168	10.846	13.754
129	2.042*	2.385*	169	1.341*	3.673*
130	3.587*	9.858*	170	1.861*	2.729*
131	1.335*	1.755	171	28.588*	53.358*
132	2.142*	3.801*	172	2.943	3.087*
133	16.361	27.759	173	1.694	2.568
134	8.193	9.301	174	1.729	2.516*
135	2.719*	5.141*	175	0.844*	1.449*
136	4.767*	12.737*	176	3.441*	5.380*
137	42.230	108.038	177	0.712	0.838*
138	41.236	78.423	178	1.222*	3.469*
139	8.243	9.911*	179	20.852*	42.263*
140	31.522	36.393	180	7.575*	16.552*
141	2.600	2.881*	181	2.042*	3.058
142	1.932	2.055*	182	6.797	7.343*
143	8.562	10.813	183	1.536	4.499
144	1.421*	3.652*	184	1.235	1.472*
145	2.669*	3.889*	185	3.541*	4.272
146	1.125*	2.071	186	5.394*	6.149*
147	3.439*	5.824*	187	18.589	28.787
148	1.269*	5.651	188	8.372	12.628
149	7.949	14.252	189	13.470*	23.775*
150	2.808*	4.434*	190	1.196*	2.851*
151	6.413	12.573	191	3.507	7.712
152	5.936*	10.432*	192	21.489	43.372
153	9.788	18.093	193	1.038*	1.109*
154	1.251	2.707	194	3.591*	3.864
155	34.799	63.494	195	2.295*	2.529*
156	0.841*	1.742*	196	1.044*	2.320
157	1.461*	1.615*	197	4.865*	6.759*
158	7.220	21.125	198	1.184	11.852
159	1.275*	2.359*	199	1.228*	1.969*
160	9.355	19.565	200	9.346*	22.204*

which correspond to taking $\xi=0.5$ in (11). This should not make any difference in the calculation of the lowest eigenvalue, and consequently table 2 can be utilized in the same way as table 1. It should however be borne in mind that columns C_1 and C_2 of table 2 represent experimental values of the quantities (18) with the S_k's being sums of Gaussian deviates. Asterisks on the entries of table 2 indicate that S_{375} or S_{500} was negative. Although this information is unnecessary for the purpose of calculations of the lowest eigenvalue, it is used in the calculation of the next eigenvalue. How this can be done is explained briefly in section IV.

Using the data in table 2 and again (10) we computed the following approximations to λ_1 (actual value=0.71)

	First 50 samples	Second 50 samples	Third 50 samples	Fourth 50 samples	All 200 samples
λ_1	0.82	0.72	0.83	0.64	0.74

For both $V(x)=|x|$ and $V(x)=x^2$, all the eigenvalues are known so that in the two illustrative examples above it was easy to choose appropriate values for t_1 and t_2. The proper value for n and the appropriate number of samples was determined experimentally. In general when all eigenvalues are unknown the following "rule of thumb" procedure seems to be feasible. Having first made a guess at an appropriate n and t, and a certain number of samples, compute λ_1. Repeat the computation now for the same n, the same number of samples and successively larger t's until the calculated values of λ_1 become stable to the desired number of places. If they do not become stable, the number of samples must be increased. Keeping two values of t, for which the calculated λ's had the stable value, increase n and see if the calculated value of λ changes. If not, n is sufficiently large. If it does change, increase n until a new stability appears. This stable value is then the appropriate approximation to λ_1. The mere fact that stability is observed means the number of samples is sufficiently large.

The Second Eigenvalue

If the principal eigenfunction is even, then it is possible to extend the theory of section II in such a way that the calculation of the second eigenvalue becomes feasible. Without going into any details we just state the pertinent result: Let

$$E_t^+(\xi)=\lim_{n\to\infty} E\left\{e^{-\frac{1}{n}\sum_{k\le nt} V\left(\xi+\frac{S_k}{\sqrt{n}}\right)} \mid S_{nt}>0\right\}, \quad (16)$$

and

$$E_t^-(\xi)=\lim_{n\to\infty} E\left\{e^{-\frac{1}{n}\sum_{k\le nt} V\left(\xi+\frac{S_k}{\sqrt{n}}\right)} \mid S_{nt}<0\right\}, \quad (17)$$

the mathematical expectations on the right hand sides being *conditional* expectations under the conditions $S_{nt}>0$ and $S_{nt}<0$, respectively.
We then have

$$\frac{1}{2}\left\{E_t^+(\xi)-E_t^-(\xi)\right\}=\sum_{j=2}^{\infty} e^{-\lambda_j t}\psi_j(\xi)\int_{-\infty}^{\infty}\rho(x)\psi_j(x)dx, \quad (18)$$

where

$$\rho(x)=\begin{cases}+1, & x>0\\ -1, & x<0.\end{cases}$$

If t_1 and t_2 are sufficiently large, we get

$$\lambda_2\sim-\frac{1}{t_2-t_1}\log\frac{E_{t_2}^+(\xi)-E_{t_2}^-(\xi)}{E_{t_1}^+(\xi)-E_{t_1}^-(\xi)}. \quad (19)$$

From the discussion of section III it should be clear how one applies (19) when the data of table 2 are available. One must see to it that ξ is so chosen that $\psi_2(\xi)\neq 0$, otherwise a higher eigenvalue may have been calculated. From the data of table 2 we obtain

$$\lambda_2\sim 1.1,$$

whereas the exact value is $3/2\sqrt{2}=2.12$. The poor agreement could have been expected in view of low accuracy in the calculation of λ_1.

In conclusion, we thank E. C. Yowell, of the National Bureau of Standards, for wiring the boards and for excellent supervision of all the punched card work.

Los Angeles, September 12, 1949.